New Optical Materials Containing Isobenzofuran
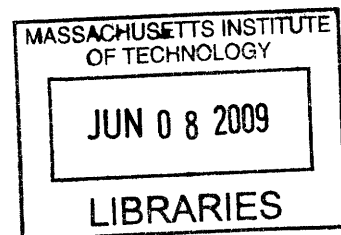
by

Scott Thomas Meek

B.A. (High Honors) Chemistry
Dartmouth College, 2003

Submitted to the Department of Chemistry in Partial Fullfillment of the
Requirements for the Degree of

Doctor of Philosophy

at the

Massachusetts Institute of Technology

June 2009

Signature of Author:_____

Department of Chemistry
May 15, 2009

Certified by:_____

Timothy M. Swager
Thesis Supervisor

Accepted by:_____

Robert W. Field
Chairman, Departmental Committee on Graduate Studies

This doctoral thesis has been examined by a Committee of the Department of Chemistry as follows:

Professor Timothy F. Jamison:_____   _____
                                                        Thesis Committee Chair

Professor Timothy M. Swager:_____   _____
                                                        Thesis Supervisor

Professor Sarah E. O'Connor:___   _____
                                                        Department of Chemistry

Dedicated to my Grandfathers

New Optical Materials Containing Isobenzofuran

by

Scott Thomas Meek

Submitted to the Department of Chemistry on May 22, 2009
in Partial Fulfillment of the Requirements for the Degree of
Doctor of Philosophy in Chemistry.

ABSTRACT

Isobenzofuran, a member of the benzo[c]heterocycles, is an extremely reactive molecule with unusual electronic properties. In this thesis we investigate the integration of isobenzofuran subunits into conjugated optical materials.

We discuss the properties of isobenzofuran, its role in organic chemistry, and the synthesis of isobenzofuran containing materials in the context of the other well known benzo[c]heterocycle, isothianaphthene. Isothianaphthene has been used in conducting polymers and organic fluorophores as a proquinoid unit, and we posit that isobenzofuran, due to its intrinsic instability, would display greater proquinoid character. To study this effect, we developed a synthetic route to integrate isobenzofuran into near-infrared donor-acceptor type fluorophores. These dyes, the **IBF-NIADs,** exhibit red-shifted absorption and emission over corresponding isothianaphthene containing dyes, thus highlighting the effective proquinoid nature of isobenzofuran.

With the fundamentals of the **IBF-NIAD** dyes developed, we then expanded the series into a library of fluorophores for near-infrared fluorescence imaging application. Due to low absorption, autofluorescence, and scattering in the near-infrared region, near-infrared fluorescence imaging has the potential to provide non-invasive diagnostic techniques. In particular, our interest lay in imaging β-amyloid plaques, a hallmark pathology of Alzheimer's disease. We tailored our dye series by modifying the conjugated backbone and the electron-donating group in order to optimize their photophysical properties, minimize their aggregation in aqueous solution, and maximize their optical response on binding to β-amyloid fibrils. Through these efforts we developed several fluorophores that exhibit large bathochromic shifts on binding, with concomitant increases in fluorescence intensity and lifetime, and absorption and emission spectra that extend well into the near-infrared. With the Backskai group at MGH, we found that most of these dyes stain β-amyloid plaques in transgenic APP/PS1 mouse brain tissue, and efforts are underway to test their in vivo imaging potential.

Finally, we present our initial synthetic work in integrating isobenzofuran into donor-acceptor-donor oligomers for nonlinear optical applications.

Thesis Supervisor: Timothy M. Swager
Title: John D. MacArthur Profesor and Head of the Chemistry Department

Table of Contents

List of Figures

List of Schemes

List of Tables

17

Chapter 1

Introduction to Fluorescence Imaging

1.1 Introduction to Fluorescence

1.1.1 Preface

With the 2008 Nobel Prize in Chemistry awarded to Osamu Shimomura, Martin Chalfie, and Roger Tsien for the discovery and development of Green Fluorescence Protein (GFP),[1] this has been an auspicious year for fluorescence imaging. GFP was first isolated from *Aequorea victoria*, a jellyfish, by Shimomura, who later identified the chemical structure of the fluorophore subunit (Figure 1.1).[2] The gene for GFP was cloned, and then recombinantly expressed in model organisms *E. coli* and *C. elegans* by Chalfie.[3] Tsien determined the mechanism of fluorophore formation, and demonstrated that it occurs autocatalytically in the presence of oxygen.[4] In the intervening years, the spectrum of fluorescent proteins has been broadened to include blue, cyan, yellow, and red variants.[5] The great strength of this technology lies in ability of the GFP gene to
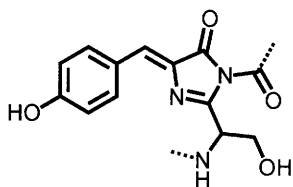
Figure 1.1 The fluorescent unit of GFP

be spliced into an organism's genome, thus giving rise to fluorescent fusion proteins which can be viewed in living cells and tissue by fluorescence microscopy. This innovation has opened numerous protein interactions and other biological events to visual inspection,[6] revolutionizing the way cellular processes are viewed. The example of GFP beautifully illustrates the inherent power of fluorescence imaging: illuminating and elucidating the processes of life that were previously invisible and unknown.

1.1.2 History of Fluorescence

Fluorescence is a form of photoluminescence by which a molecule, after having been promoted to an excited state by absorption of a photon, emits a photon as it relaxes to its ground state. Nicolás Monardes, a Spanish botanist and physician, reported the first observation of

fluorescence in 1595,[7] when he noted the blue color at surface of water steeped with *Pterocarpus indicus*, a tropical hardwood. Both Sir Isaac Newton and Robert Boyle also studied this effect. In 1833 David Brewster observed that, when view from the side, leaf extracts appear red when the solution is illuminated with white light. The name "fluorescence" was not bestowed on this phenomenon until it was investigated by George Gabriel Stokes in 1852. Stokes split the solar spectrum with a prism, and then passed a glass containing a solution of quinine sulfate through the refracted light.[8] In the visible spectrum, the solution remained colorless. However, when the glass was moved into the invisible ultraviolet region, the quinine solution emitted a "beautiful celestial blue colour" (Figure 1.1). In his original manuscript, Stokes named this effect *dispersive reflexion*, but later coined the term *fluorescence*, invoking fluorspar, a fluorescent mineral.[9]
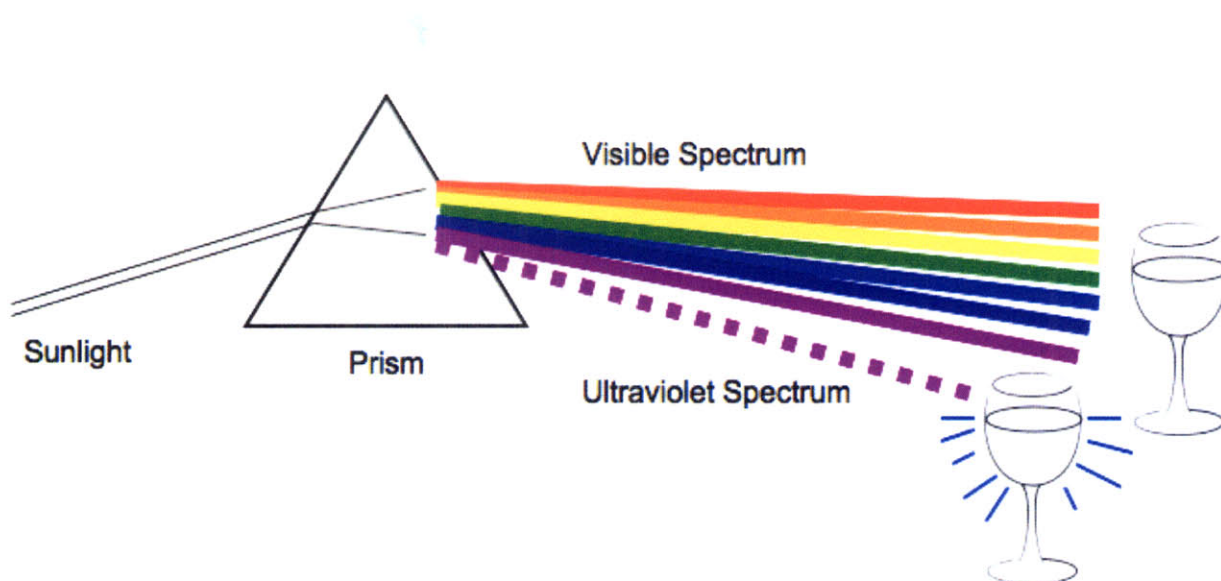
Figure 1.2 A diagram of Stokes' experiment. In the visible region, the quinine sulfate solution is colorless. In the UV region, it glows blue.

1.1.3 Basic Principles of Fluorescence
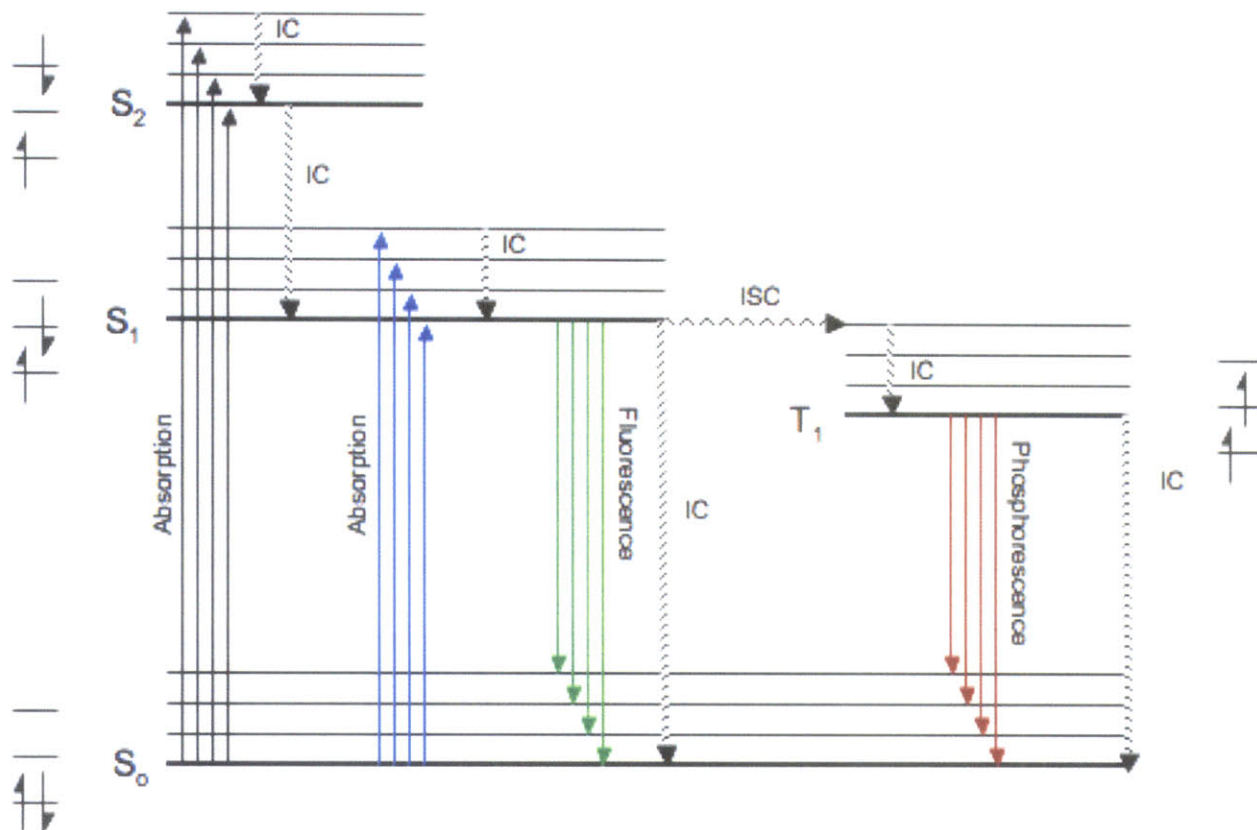
Figure 1.3 A Jablonski diagram. IC stands for internal conversion. ISC stands for intersystem crossing

As fluorescence will be a central theme of this thesis, we will first lay out its basic principles. The Jablonski diagram (Figure 1.2) was constructed for the purpose of visualizing the possible processes surrounding the interaction of molecules and light. Absorption of a photon promotes a molecule from the ground state (S_0) to an excited state, typically one of the vibrational levels of S_1 or S_2. The excited state may then relax back to the ground state via several different pathways. Non-radiative transition between two electronic states of the same spin multiplicity (i.e. $S_2 \rightarrow S_1$) is termed *internal conversion* and is accompanied by a loss of vibrational or rotational energy, typically to the solvent. Emissive relaxation from the $S_0 \rightarrow S_1$ is called *fluorescence*. It should be noted that fluorescence is almost always an $S_1 \rightarrow S_0$ transition (Kasha's Rule),[10] with a notable exception being azulene, which exhibits an emissive $S_2 \rightarrow S_0$

transition.[11] As the absorption from S_0 can be to higher vibrational levels than S_1, and as the decay from S_1 can be to higher vibrational levels than S_0, energy is lost in the subsequent internal conversion processes, and the fluorescence emission spectrum is typically at lower energies and longer wavelengths. The difference between the absorption maximum and the fluorescence emission maximum is termed the *Stokes' Shift*. The third possible fate of the excited state is *intersystem crossing*, in which the S_1 state transitions to the first triplet excited state, T_1. From T_1, de-excitation can occur by non-emissive internal conversion or by a radiative process called *phosphorescence*. As the $T_1 \rightarrow S_0$ transition is forbidden, the rate constant for phosphorescence is substantially slower than that for fluorescence. T_1 is lower in energy than S_1, and thus phosphorescent emission is red shifted from fluorescent emission.

Apart from Stokes' Shift, there exist other characteristics of fluorescence emission that are pertinent to the work presented herein. Quantum yield is defined as the ratio of excited molecules that relax to the ground state with emission of a photon via fluorescence, or more simply, the ratio of the number of photons emitted to the number of photons absorbed. Quantum yield can also be defined as the ratio of the rate of radiative decay from $S_1 \rightarrow S_0$ (k^r_s) to the sum of the rate of radiative decay from $S_1 \rightarrow S_0$ and the rate of none radiative decay from $S_1 \rightarrow S_0$ (k^s_{nr}) (Equation 1.1).

$$\Phi_F = \frac{k^s_r}{k^s_r + k^s_{nr}} \qquad (1.1)$$

The excited state lifetime τ_s is defined in Equation 1.2.[12]

$$\tau_s = \frac{1}{k^s_r + k^s_{nr}} \qquad (1.2)$$

Thus fluorescence quantum yield can be proportional to the fluorescence lifetime (Equation 1.3).

$$\Phi_F = k^s_t \tau_s \qquad (1.3)$$
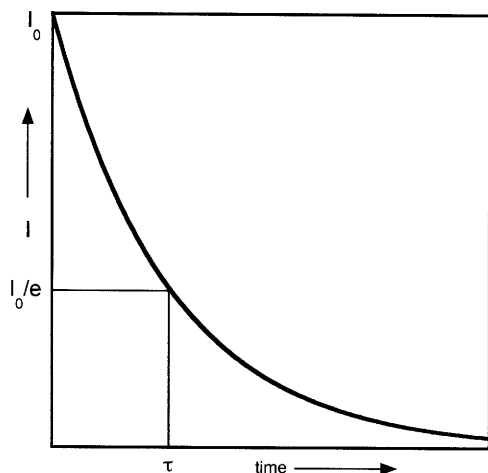
Figure 1.4 Single exponential decay of a fluorescence signal. I_0 is the intensity at time 0

Fluorescence lifetime is the average time a molecule spends in the excited state. If the exited state experiences single exponential decay (Figure 1.3, Equation 1.4), then the lifetime can be defined as the time it takes for the fluorescence signal intensity to reach I_0/e.

$$I = I_0 e^{\frac{-t}{\tau}}$$

(1.4)

1.2 Fluorescent Probe Mechanisms

There are several mechanisms by which a fluorophore may be integrated into a sensory scheme. The most basic is staining, wherein a dye accumulates in a certain structure, such as a cellular component, and that structure can then be viewed by fluorescence. DAPI (4',6-diamidino-2-phenylindole) is a well known stain for DNA which exhibits blue fluorescence.[13] A dyes may also be covalently bound to molecules, such as a protein, so that the location and interactions of that molecules can be viewed by fluorescence. GFP and other fluorescent proteins are commonly employed for labeling studies as genetically engineered organisms can express the labeled protein in situ. Both of these methods depend on the local concentration of fluorophores as a method of obtaining contrast.

A responsive probe, on the other hand, experiences a physical change that modulates its optical properties, and thus provides a mechanism for contrast. This response can take several different forms. An analyte can covalently modify a dye, and thereby change its photophysical

properties. This sensory mechanism may function by disrupting an aromatic system, thereby extinguishing its fluorescence signal, as observed in the interactions between squaraines and thiols (Figure 1.5).[14] Cleavage of a functional group that is quenching fluorescence signal, such as cleavage of a peptide group by a protease, yields a "turn-on" response.[15] Similarly, cleavage of one of a pair of FRET molecules can change the wavelengths of absorption or emission.[16] Chemical modification by an analyte can also build conjugation, and form a fluorescent system.[17]
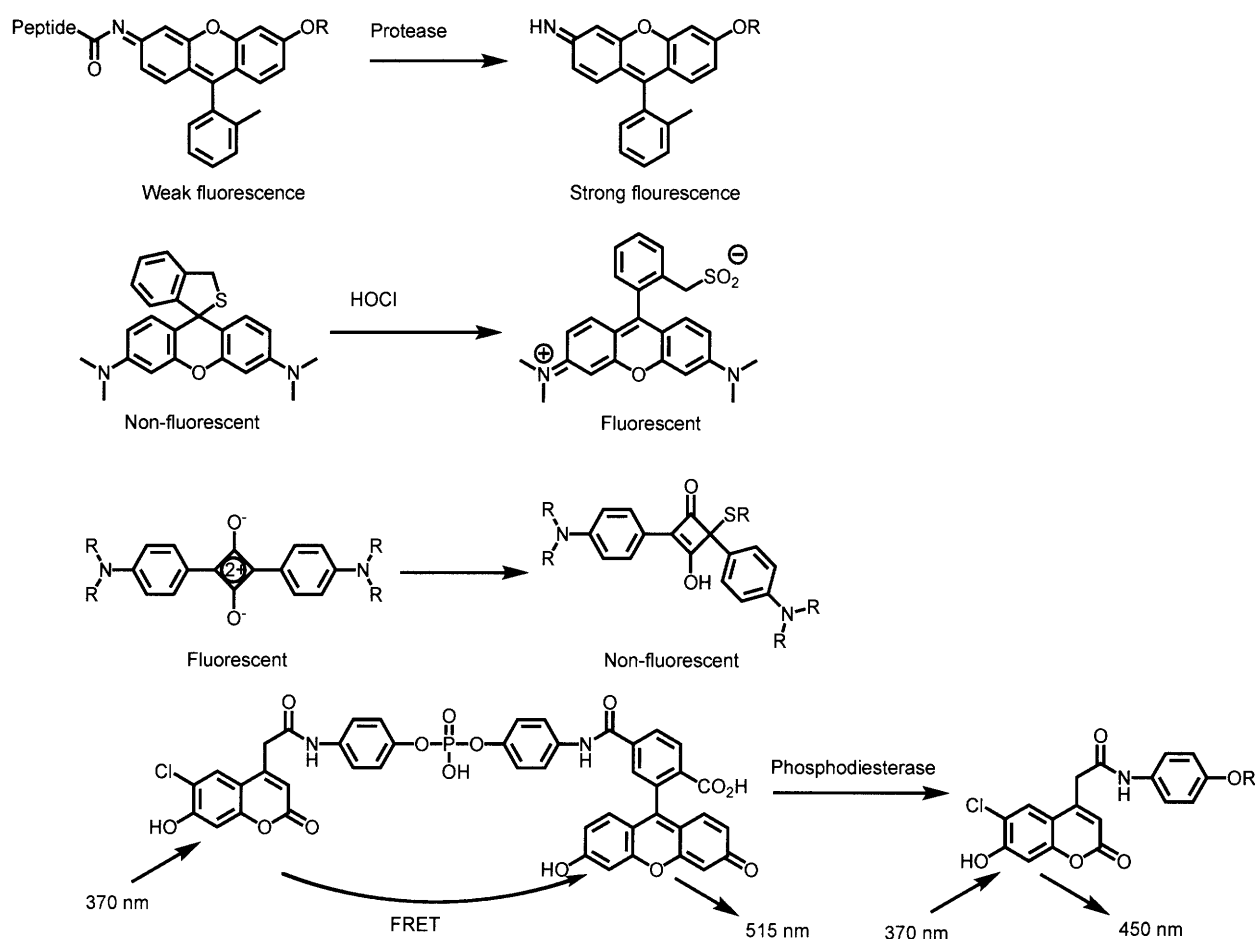
Figure 1.5 Fluorescent probes that undergo covalent modification. See text for discussion

Fluorescent probes may also be constructed with molecular recognition units. In this design, non-covalent binding of the analyte to the fluorophore modulates the fluorescence response. The response can be quenching, turn-on, or wavelength change, depending on the nature of the electronic interaction between the molecular recognition element and the fluorophore. The most common electronic interaction, photoinduced electron transfer (PET), has been studied extensively for cation sensing.[18] In PET an electron from the HOMO of the receptor is transferred to the HOMO of the fluorophore in its excited state, thus quenching its fluorescence. On binding, the HOMO of the donor group is lowered, PET is disrupted, and fluorescence is activated (Figure 1.6).[19] Crown ethers, cryptands, cyclodextrins, and calixarenes have all been used as cation recognition elements. If the recognition unit is linked to a donor-acceptor pair, binding can modulate the wavelengths of absorption and emission. Cation interaction with a donor will reduce the electron-donating character, and thus blue shift the spectrum,[20] while contact with the acceptor will enhance its electron withdrawing properties, resulting in a red shifted spectrum.
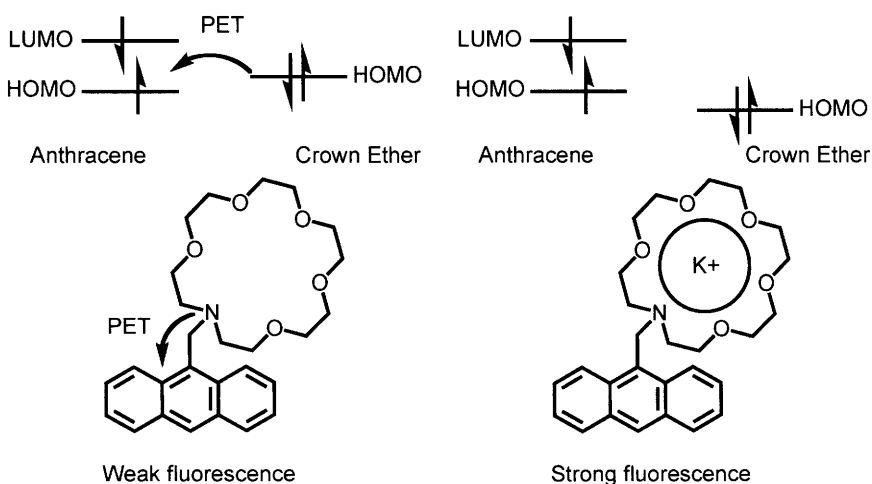
Figure 1.6 Example of a PET fluorescent cation sensor.

A probe's interaction with its environment can also alter its photophysical properties, and this type of response will be most relevant to this thesis. For many organic fluorophores, the molecule becomes more polarized in the excited state, thus gaining a larger dipole moment. The more polar excited state will interact more strongly with its molecular environment.
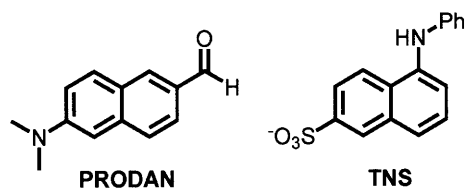
Figure 1.7 Donor-acceptor polarity probes **PRODAN** and **ANS**

Consequentially, the excited state is stabilized, the energy gap between the ground and excited states is decreased, and the spectra are shifted to the red. In more polar solvents or environments, this effect, termed *solvatochromism* is more pronounced. If the polarity of the probe is increased by addition of a donor-acceptor pair, then the dye will experience larger solvatochromic shifts (Figure 1.6).[21] Typically, the shift to longer wavelengths is associated with a decrease in quantum yield, due to increased environmental quenching.[22] The rigidity of a dye's environment can also affect its photophysical properties, especially if the conjugated system of the dye is flexible. In a rigid medium, rotational and vibrational processes that couple the ground and excited states and promote internal conversion are minimized, and thus quantum yield is increased.[23] A flexible molecule can also be planarized by interaction with a rigid environment, thus increasing conjugation in the dye backbone, decreasing the HOMO-LUMO gap, and red shifting the absorption spectrum.[24]

1.3 Near-Infrared Fluorescence Imaging

1.3.1 Basic Principles

In recent years, fluorescence imaging exploiting near-infrared (NIR) light has attracted much attention, as it affords the opportunity for non-invasive, in vivo imaging.[25,26] In the NIR region of the spectrum (650-900 nm) the main biological chromophore, hemoglobin, experiences a dramatic decrease in extinction coefficient (Figure 1.7), thus photon absorption in tissue is greatly decreased. A simple demonstration may serve to illustrate this concept: the light from red laser pointer applied to the thumb will transmit through the tissue, while the light from a green laser pointer will not. Tissue autofluorescence is also low in this region, thus minimizing background signal,[27] as is photon scattering.[28] These characteristics allow NIR light to penetrate several centimeters[29] into tissue, thus enabling non-invasive imaging of biological structures.

Figure 1.8 Absorption spectra of (red) oxy-hemoglobin and (black) hemoglobin

1.3.2 Available Fluorophores

n= 1, 2, 3
X, Y= O, S, C(CH$_2$)
R= substituted alkyl, aryl
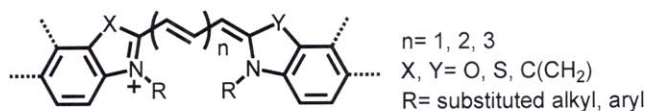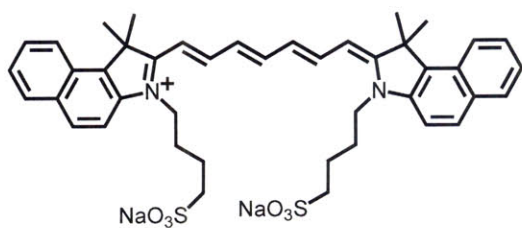
Cyanines

Indocyanine Green

Figure 1.9 Cyanine dyes

The most common NIR fluorophores are the cyanine dyes. Structurally, these dyes consist of two heterocycles linked by a polymethine chain (Figure 1.9). Numerous derivatives of these dyes have been synthesized, spanning a broad spectrum of wavelengths, and many are commercially

available, including indocyanine green (ICG), which has been approved by the FDA for use in human subjects. While cyanines may exhibit good quantum yields (up to 50%),[30] they have small Stokes' shifts and are formally charged, thus limiting access to certain biological environments, like the blood brain barrier.

Another common class of NIR fluorophores is BODIPY dyes, which are comprised of a dipyrromethane complexed with a difluorinated boron atom (Figure 1.10). BODIPY dyes also span a broad spectrum of wavelengths, with several derivatives absorbing and emitting in the NIR region.[31] Due to the conformational rigidity of the central unit, BODIPY fluorophores enjoy high quantum yields.[32] Water solubility of these compounds has proved problematic, though recent work has started addressing this compatibility issue.[20]
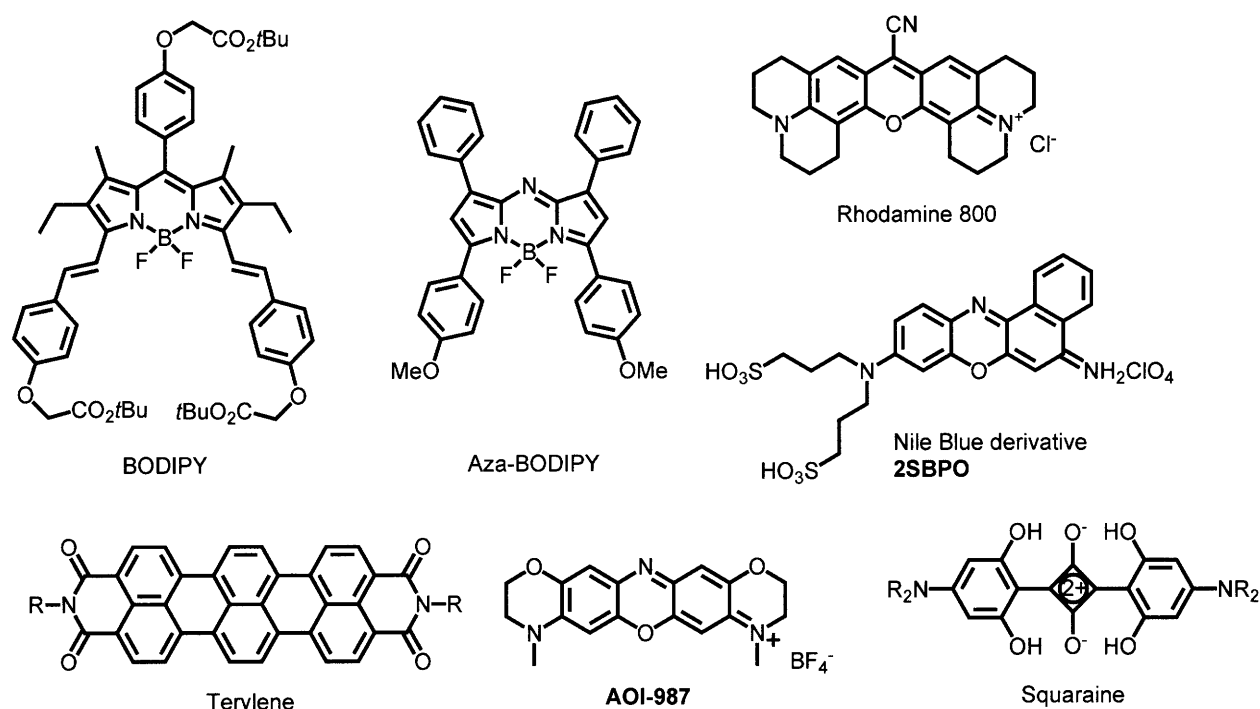
Figure 1.10 Examples of NIR dyes. See text for discussion.

Other classes of dyes that extend into the NIR include benzo[a]phenoxazines such as Nile blue and its derivatives,[33] Oxazine dyes such as **AOI-987**,[34] and rhodamines (Figure 1.10).[35] These compounds all exhibit modest quantum yields, and moderate Stokes' shifts. As charged compounds, these dyes face similar biological limitations to cyanine dyes, except for **AOI-987**, which can penetrate the blood brain barrier. Terylenes, rigid NIR dyes with high quantum yields have been studied primarily for optoelectronic devices, such as fluorescence solar collectors,[36] but they have also recently been explored in our group as emissive components of organic nanoparticles. Squaraines are built on a donor-acceptor-donor zwitterionic framework, and have been implemented into various NIR ion sensors.[37] Tsien and coworkers have recently reported NIR fluorescent proteins.[38] Quantum dots, fluorescent inorganic semiconducting nanocrystals, can also absorb and emit in the NIR region,[39] though organic coatings are required for biocompatibility.[40] In Chapter 2, we will discuss the synthesis of a new class of NIR fluorophores based on a donor-acceptor framework.

1.3.4 Applications of NIRF Imaging

NIR fluorescence (NIRF) imaging has been applied to many types of tissues and pathologies, a brief review of which we will provide here. Vasculature mapping was one of the earliest applications of NIRF, and, as ICG is FDA approved, is feasible for use with human subjects. ICG has been used clinically to detect posterior uveitis, a swelling in the back of the eye.[41] It has also been employed to image brain vasculature to locate aneurysms in humans[42] and heart vascular to locate myocardial perfusion in pigs.[43] Atherosclerosis in living mice has been imaged using a cyanine based probe activated by cathepsin B.[44] A cyanine-folic acid conjugate has been explored for imaging inflammatory joint disease.[45] Numerous examples of tumor

imaging have been reported, including methods exploiting protease detection,[46] albumin-activated indocyanines,[47] quantum dots,[48] and cyanine labeled angiogenesis inhibitors[49] and antibodies.[50] Oxazine derivative **AOI-987** has been used to detect β-amyloid plaques,[34] along with donor-acceptor dye, **NIAD-4**.[24] The later, while providing excellent contrast with significant changes in its spectroscopic properties on binding, does not absorb and emit far enough in the NIR for true non-invasive imaging. Chapter 2 of this thesis will discuss modification to the **NIAD-4** framework to shift it into the NIR, and Chapter 3 will integrate the resulting dyes in detection schemes for β-amyloids.
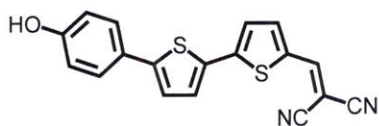
Figure 1.11 NIAD-4

1.3.5 Imaging Techniques
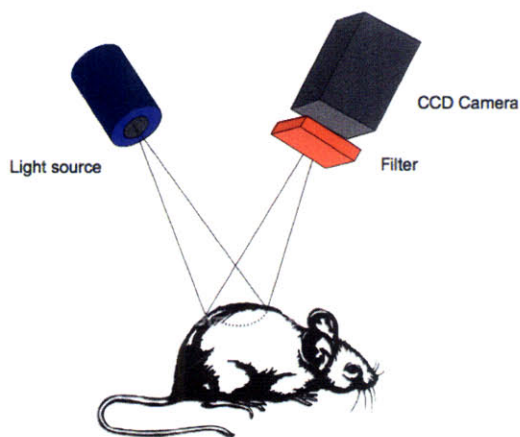
Figure 1.12 Fluorescence reflectance imaging apparatus

Several techniques exist by which NIR fluorescence images may be obtained, including fluorescence reflectance imaging (FRI), fluorescence molecular tomography (FMT), and fluorescence lifetime imaging (FLIM). The most basic of these methods, FRI, uses a light source with a defined bandwidth, often a laser, to excite contrast agents in the tissue. These fluorophores then emit light, typically at a longer wavelength, which is then collected by a filtered CCD camera located on the same side of the tissue as the light source (Figure 1.12). Often an image is also obtained without fluorescence filters for calibration purposes. While FRI provides a

relatively straightforward, inexpensive method for imaging, it is limited in its depth of tissue penetration to a few millimeters, as reflectance at the surface dominates the background signal.[51]

In order to detect fluorophores at depths more the a few millimeters, and in order to create a composite 3D image, fluorescence molecular tomography must be employed. In this technique, light is directed at the target from multiple points in a cylindrical optical imaging bore (Figure 1.13), and both fluorescence and absorption measurements are obtained. This data is then compiled[52] to form a 3D reconstruction of fluorophore concentration in the analyzed tissue. FMT data can be combined with high-resolution FRI to correlate the tomographic data with biological features.
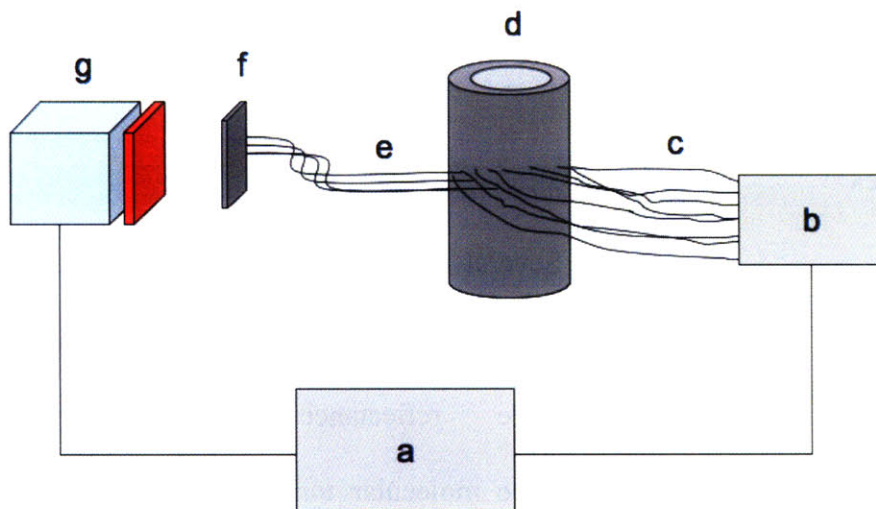
Figure 1.13 Diagram of an FMT apparatus. (a) computer (b) optical controller (c) input fiber optic cables (d) optical bore (e) output fiber optic cables (f) fiber optic array (g) CCD camera

Both FRI and FMT depend largely on fluorophore concentration to obtain contrast, though, as previously discussed, responsive probes help mitigate this effect. Fluorescence lifetime, however, is a characteristic of a fluorophore and its environment, and is thus independent of concentration. Scattered light and tissue autofluorescence typically have relatively short lifetimes, thus longer lifetime probes, especially those with longer lifetimes in the

bound state, can provide high contrast, even in the absence of weak fluorescent signal.[53] Fluorescence lifetimes can be measured by phase-modulation, in which the excited light is modulated with a frequency between 100-200 MHz, and the modulated fluorescence signal is detected. The phase shift between it and the frequency of excited light, along with the modulation depth of the fluorescence signal, are used to calculate the lifetime. Single photon counting may also be used to calculate lifetime. In this technique, the fluorophore is excited by a short pulse, and then single photons are detected and timed, and this data is used to reconstruct the decay curve. FLIM may be used in conjugation with tomographic techniques for 3D lifetime imaging.[54]

Another technique that exploits absorption of long-wavelength light is multiphoton microscopy. In this method, a fluorophore is excited by two low energy photons that would not, under normal circumstances, promote the molecule to an excited state (Figure 1.14) For two-photon absorption to occur, the photons must arrive with 10^{-18} seconds of each other in and with precise spatial overlap, thus necessitating the use of an ultra-fast laser.[55] As the intensity of the laser drops off as the square of the distance from the focal plane, only the fluorophores at the focal point are excited, and thus minimizing "out of focus" fluorescent signal. Because longer wavelength are used for excitation, fluorophores with absorption energies outside the NIR can be imaged with NIR light, thus allowing for deeper tissue penetration.

Figure 1.14 Diagram of (blue) single photon absorption and (red) two-photon absorption

1.4 References

(1)   Nienhaus, G. U. *Angew. Chem. Int. Ed.* **2008**, *47*, 8992.

(2)   Shimomura, O. *FEBS Lett.* **1979**, *104*, 220.

(3)   Chalfie, M.; Tu, Y.; Euskirchen, G.; Ward, W. W.; Prasher, D. C. *Science* **1994**, *263*, 802.

(4)   Tsien, R. Y.; *Annu. Rev. Biochem.* **1998**, *67*, 509.

(5)   Shaner, N. C.; Campbell, R. E.; Steinbach, P.A.; Giepmans, B. N. G.; Palmer, A. E., Tsien, R. Y. *Nat. Biotechnol.* **2004**, *22*, 1567.

(6)   Yuste, R. *Nat. Methods.* **2005**, *2*, 902.

(7)   Muyskens, M. J. *J. Chem. Ed.* **2006**, *83*, 765.

(8)   Stokes, G. C. *Phil. Trans.* **1852**, *142*, 463.

(9)   Stokes, G. C. *Phil. Trans.* **1853**, *143*, 385.

(10)   Kasha, M. *Discuss. Faraday Soc.* **1950**, *9*, 14.

(11)   Beer, M.; Longuet-higgins, H. C. *J. Chem. Phys.* **1955**, *23*, 1390.

(12)   Valeur, Bernard *Molecular Fluorescence: Principles and Applications*; Wiley & Sons: New York, 2001.

(13)   Silverstein, T. P. *J. Chem. Ed.* **2008**, *85*, 1192.

(14)   Ros-Lis, J. V.; Garcia, B.; Jimenez, D.; Martinez-Manez, R.; Sancenon, F.; Soto, J.; Gonzalvo, F.; Valldecabres, M. C. *J. Am. Chem. Soc.* **2004**, *126*, 4064.

(15)   Li, J.; Yao, S. Q. *Org. Lett.* **2009**, *11*, 1671.

(16)   Takakusa, H.; Kikuchi, K.; Urano, Y.; Sakamoto, S.; Yamaguchi, K.; Nagano, T. *J. Am. Chem. Soc.* **2002**, *124*, 1653.

(17)   Kenmoku, S.; Urano, Y.; Kojima, H. Nagano, T. *J. Am. Chem. Soc.* **2007**, *129*, 7313.

(18)   Bissell, R. A.; De Silva, A. P.; Gunaratne, H. Q. N.; Lynch, P. L. M.; Maguire, G. E. M.; McCoy, C. P.; Sandanayake, K. R. A. S. *Top. Curr. Chem.* **1993**, *168*, 223.

(19)   De Silva, A. P.; De Silva, S. A. *J. Chem. Soc. Chem. Commun.* **1986**, 1709.

(20)   Atilgan, S.; Ozedmir, T.; Akkaya, E. U. *Org. Lett.* **2008**, *10*, 4065

(21)   Demchenko, Alexander P. *Introduction to Fluorescence Sensing*; Springer Science + Business Media, New York, 2009

(22)   Demchenko, A. P. *Anal. Biochem.* **2005**, *343*, 1.

(23)   Willets, K. A.; Ostroverkhova, O.; He, M.; Twieg, R. J.; Moerner, W. E. *J. Am. Chem. Soc.* **2003**, *125*, 1174.

(24)   Nesterov, E. E.; Skoch, J.; Hyman, B. T.; Klunk, W. E.; Bacsckai, B. J.; Swager, T. M. *Angew. Chem. Int. Ed.* **2005**, *44*, 5452.

(25)   Rao, J.; Dragulescu-Andrasi, A.; Yao, H. *Curr. Opin. In Biotechnol.* **2007**, *18*, 17.

(26)   Weissleder, R.; Ntziachristos, V. *Nat. Biotechnol.* **2003**, *9*, 123.

(27)   Sevick-Muraca, E. M.; Houston, J. P.; Gurfinkel, M. *Curr. Opin. Chem. Biol.* **2002**, *6*, 642.

(28)   Lim, Y. T.; Kim, S.; Nakayama, A.; Stott, N. E.; Bawendi, M. G.; Frangioni, J. V. *Mol. Imaging* **2003**, *2*, 50.

(29)   Ntziachristos, V.; Ripoll, J.; Weissleder, R. *Opt. Lett.* **2002**, *27*, 527.

(30)   Mujumdar, R. B.; Ernst, L. A.; Mujumdar, S. R.; Lewis, C. J.; Waggoner, A. S. *Bioconjugate Chem.* **1993**, *4*, 105.

(31)   Loudet, A.; Burgess, K. *Chem. Rev.* **2007**, *107*, 4891.

(32)   Weili, Z.; Carreira, E. M. *Angew. Chem. Int. Ed.* **2005**, *44*, 1677.

(33)   Ho, N.; Weissleder, R.; Tung, C. *Tetrahedron* **2006**, *62*, 578.

(34)   Hintersteiner, M.; Enz, A.;, Frey, P.; Jaton, A. L.; Kinzy, W.; Kneuer, R.; Neumann, U.; Rudin, M.; Staufenbiel, M.; Stoeckli, M.; Wiederhold, K-H.; Gremlich, H-U. *Nat. Biotechnol.* **2005**, *23*, 577

(35)   Sakanoue, J.; Ichikawa, K.; Nomura, Y. Tamura, M. *J. Biochem.* **1997**, *121*, 29.

(36)   Holtrup, F. O.; Muller, G. R. J.; Quante, H.; Feyter, S.; Schryver, F. C.; Mullen, K. *Chem. Eur. J.* **1997**, *3*, 219.

(37)   Ajayaghosh, A. *Acc. Chem. Res.* **2005**, *38*, 449.

(38) Shu, X.; Royant, A.; Lin, M. Z.; Aguilera, T. A.; Lev-Ram, V.; Steinbach, P. A.; Tsien, R. Y. *Science* **2009**, *324*, 804.

(39) Dubertret, B.; Skourides, P.; Norris, D. J.; Noireaux, V.; Brivanlou, A. H.; Libchaber, A. *Science*, **2002**, *298*, 1759.

(40) Mattoussi, H.; Mauro, J. M.; Goldman, E. R.; Anderson, G. P.; Sundar, V. C.; Mikulec, F. V.; Bawendi, M. G. *J. Am. Chem. Soc.* **2000**, *122*, 12142.

(41) Herbort, C. P.; LeHoang, P.; Guex-Croiser, Y. *Ophthalmology*, **1998**, *105*, 432.

(42) Raabe, A.; Beck, J.; Gerlach, R.; Zimmermann, M.; Seifert, V. *Neurosurgery* **2003**, *52*, 132.

(43) Frangioni, J. V. *Curr. Opin. Chem. Biol.* **2003**, *7*, 625.

(44) Chen, J.; Tung, C. H.; Mahmood, U.; Ntziachristos, V.; Gyurko, R.; Fishman, M. C.; Huang, P. L.; Weissleder, R. *Circulation*, **2002**, *105*, 2766.

(45) Che, W. T.; Mahmood, U.; Weissleder, R.; Tung, C. H. *Arthritis Res. Ther.* **2005**, *7*, R310.

(46) Weissleder, R.; Tung, C. H.; Mahmood, U.; Bogdanov, A. *Nat. Biotechnol.* **1999**, *17*, 375

(47) Montet, X.; Rajopadhye, M.; Weissleder, R. *ChemMedChem.* **2006**, *1*, 66.

(48) Gao, X. H.; Cui, Y. Y.; Levenson, R. M.; Chung, L. W. K. Nie, S. M. *Nat. Biotechnol.* **2004**, *22*, 969.

(49) Citrin, D.; Lee, A. K.; Scott, T.; Sproull, M.; Menard, C.; Tofilon, P. J.; Camphausen, K. *Mol. Cancer Ther.* **2004**, *3*, 481.

(50) Bailou, B.; Fisher, G. W.; Hakala, T. R.; Farkas, D. L. *Biotechnol. Prog.* **1997**, *13*, 649.

(51) Ntziachristos, V.; Bremer, C. Weissleder, R. *Eur. Radiol.* **2003**, *13*, 195.

(52) Ntziachristos, V.; Ripoll, J.; Weissleder, R. *Optics Lett.* **2002**, *27*, 333.

(53) Raymond, S. B.; Skoch, J.; Hills, I. D.; Nesterov, E. E.; Swager, T. M.; Bacski, B. J. *Eur. J. Nucl. Med. Mol. Imaging.* **2008**, *35*, S93.

(54) Godavarty, A.; Sevick-Muraca, E. M.; Eppstein, M. J.; *Med. Phys.* **2005**, *32*, 992.

(55) Helmchen, F.; Denk, W. *Nat. Methods* **2005**, *2*, 932.

Chapter 2

Benzo[c]heterocyle Based Donor-Acceptor Near-Infrared Fluorophores

2.1 Introduction

2.1.1 Isothianaphthene

A unique group of compounds, the benzo[c]heterocycles are bicyclic aromatic structures composed of a five-membered heterocycle perched symmetrically atop a six-membered ring (Figure 2.1). The proclivity of the six membered ring to attain its stable, aromatic benzene form drives the reactivity and electronic properties of these molecules. Isothianaphthene (1) and isobenzofuran (2), the sulfur and oxygen containing moieties respectively, have received the most attention in the literature, and a comparison of the two as components in conjugated materials will be the central theme of this chapter.
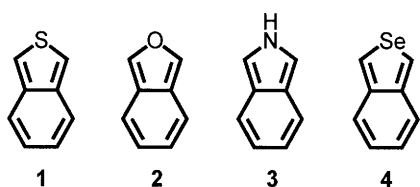
Figure 2.1 Benzo[c]heterocycles

Isothianaphthene (**ITN**), first synthesized in 1963,[1] was first integrated into a material in 1984 when Wudl and coworkers achieved its electropolymerization.[2] Poly(isothianaphthene) (**PITN**) proved to have unusual electronic properties, with a bandgap of 1-1.2 eV, about 1.0 eV less than poly(thiophene).[3] Thus, **PITN** originated a group of materials known as low bandgap polymers, which are of particular interest in organic electronics due to their high intrinsic conductivity and increased optical transparency in a doped state.[4] In the intervening years, new synthetic methods for **PITN** and its derivatives have been reported, along with other low bandgap polymers, a full discussion of which an interested reader may find in several reviews.[5,6] Other than transparent conductors, **PITN** has been explored as a component material for a variety of applications, including photovoltaics[7] and materials with nonlinear optical properties.[8]

After **PITN**'s initial report, its electronic properties were studied both theoretically and experimentally in order to ascertain the root of its decreased bandgap. Polyaromatic compounds have two resonance structures: aromatic and quinoid. In the case of polythiophene and its derivatives, the HOMO of the aromatic form resembles the LUMO of the quinoid form, and the LUMO of the aromatic form resembles the HOMO of the quinoid form. With increasing contribution of the quinoid structure, the HOMO is destabilized, the LUMO stabilized, and the gap between them diminished (Figure 2.2).[9] In the case of isothianaphthene, the aromatization of the six membered ring stabilizes the quinoid resonance structure, thus

Figure 2.2 A diagram of the HOMO and LUMO structures of the aromatic and quinoid forms of **PITN** and poly(thiophene)

increasing its contribution, and decreasing the band gap. The structure of PITN has been shown by ^{13}C NMR[10] and Raman[11] spectroscopy to be largely quinoidal, though its end units have more aromatic character.[12]

Apart from PITN, isothianaphthene has also been employed in controlling the bandgap of oligomeric materials. Several groups have reported the synthesis of ITN and ITN-thiophene mixed oligomers[13] for OLED applications. In the area of fluorescent compounds, the integration of ITN red-shifts both the absorption and emission of donor-acceptor type fluorophores.[14] The proquinoid nature of ITN stabilizes the charge-separated form of these dyes, thus disrupting their aromaticity and decreasing their bandgaps. In earlier work, our group demonstrated the utility of this principal with myelin contrast agents **NIM-1** and **NIM-2** (Figure 2.3).[15] **NIM-2** experiences

40 nm and 150 nm red-shifts in its λ_{max} absorbance and emission respectively. ITN was also integrated into the **NIAD-4** (see chapter 1) framework, with similar effects. The ITN analogue of **NIAD-4**, **NIAD-6**, exhibits a 50 nm red-shift in λ_{max} absorbance and a 16 nm red-shift in λ_{max} emission.[16]

NIM 1

λ_{max} abs. : 650 nm

λ_{max} em. : 670 nm

NIM 2

λ_{max} abs. : 690 nm

λ_{max} em. : 820 nm

NIAD-4

λ_{max} abs. : 475 nm

λ_{max} em. : 621 nm

NIAD-6

λ_{max} abs. : 545 nm

λ_{max} em. : 684 nm

NIAD-15

λ_{max} abs. : 579 nm

λ_{max} em. : 785 nm
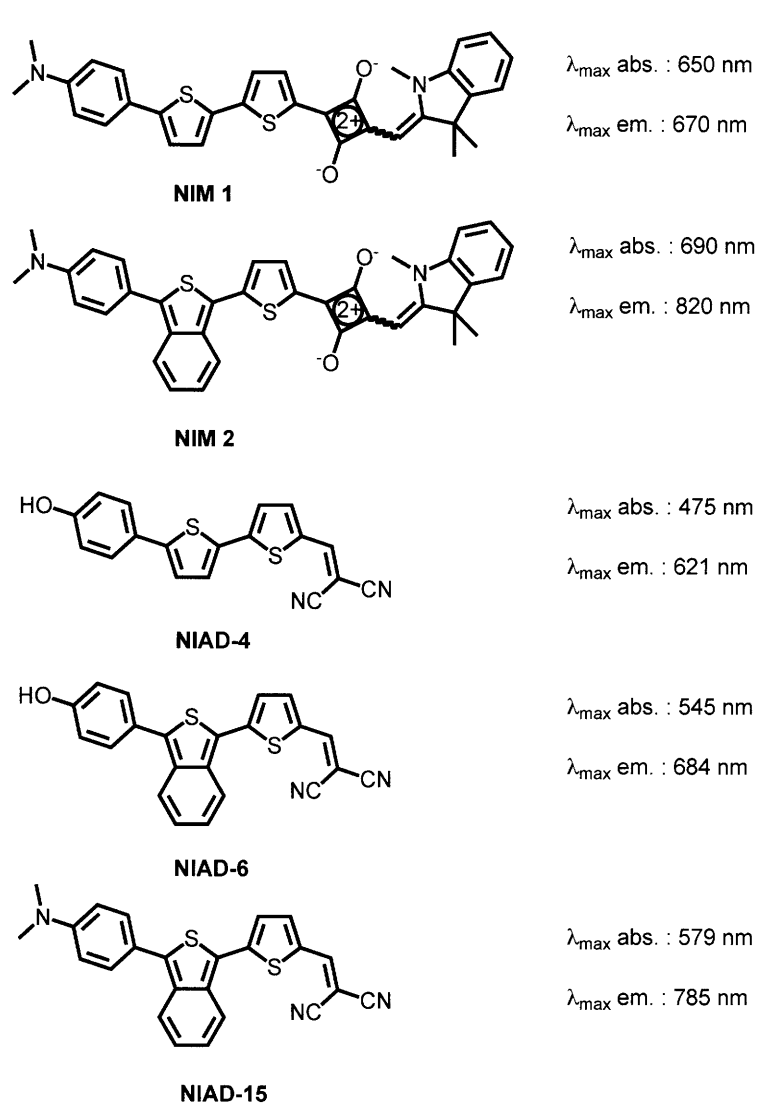
Figure 2.3 The structures and spectroscopic properties of **NIM 1**, **NIM 2**, **NIAD-4**, **NIAD-6**, **NIAD-15**

The synthesis of ITN oligomeric materials may be achieved in several different ways (Scheme 2.1). ITN dimers and trimers have been formed via retro diels-alder reaction of thiophenes annulated with bicylco[2.2.2]octadiene rings.[17] Recently, 1,3-ditrimethylstannyl and 1,3-dipinacolborane ITN derivatives were synthesized and utilized in the construction of fluorene-ITN and thiophene-ITN copolymers and oligomers.[18] However, the most common method for ITN synthesis employs Lawesson's reagent to convert a ketone to a thioketone, which then participates in a ring closure to form the ITN unit. This transformation has been reported for 1,2-diaryl ketones[19] and the ketone-alcohol products of grignard condensations with aryl-phthalides.[20] Diaryl-

isobenzofurans have also be converted directly to isothianaphthenes with Lawesson's reagent,[21] and this reaction will be discussed in greater detail later in this chapter.

Scheme 2.1 Synthetic Pathways for ITN Oligomers
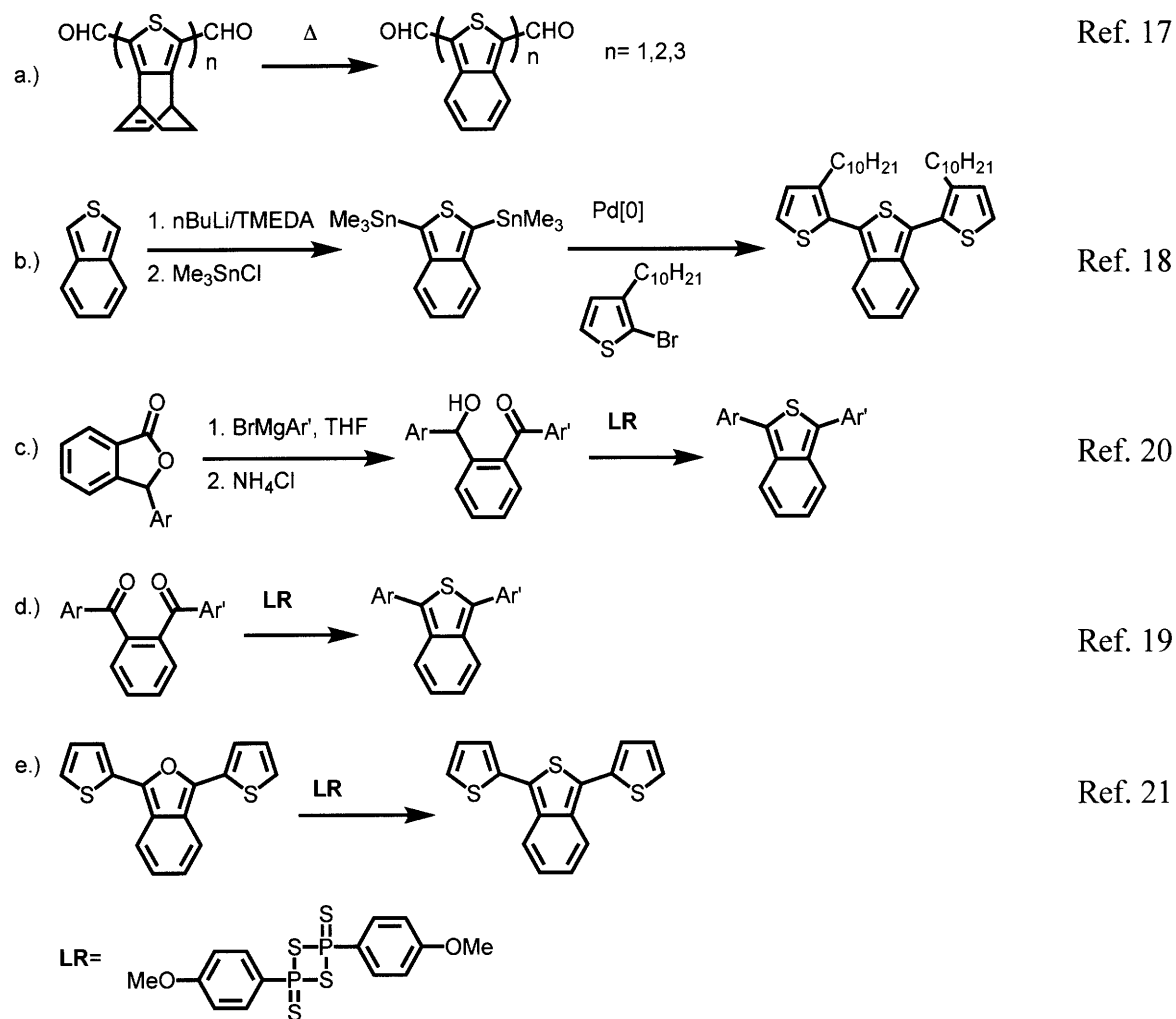
2.1.2 Isobenzofuran

Isobenzofuran (IBF), the oxygen containing member of the benzo[c]heterocycles, is both useful and notorious for its instability. While 1,3-diphenylisobenzofuran was reported in 1905,[22] a synthesis of the parent compound was not achieved until 50 years later by Wittig and Pohmer,

Scheme 2.2 Wittig's Synthesis of Isobenzofuran
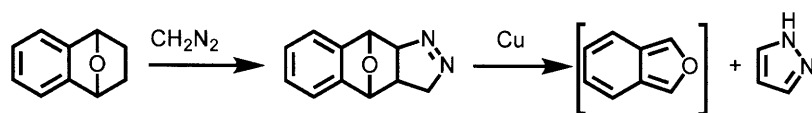
and was then only observed as a transient intermediate that polymerized spontaneously upon isolation (Scheme 2.2).[23] In the past 50 years, IBF and its derivatives have been studied extensively, both as compounds of theoretical interest, and as reactive intermediates in organic synthesis. While we will review some of this chemistry here, we direct the interested reader to two excellent reviews by Friedrichsen.[24]

Much of the theoretical debate revolving around IBF has focuses on its aromaticity, or lack thereof. Early calculations of the heat of atomization predict a slight resonance energy of 2.4 kcal/mol.[25] These results are corroborated by AM1 FMO calculations[26] which also indicate a low level of aromaticity.[27] A similar conclusion is reached by comparison of magnetic susceptible anisotropies calculated with DFT methods.[28] On the other hand, initial NMR studies[29] of IBF show that the furan protons are shifted considerably downfield, implying the presence of a diamagnetic ring current characteristic of a degree of aromaticity. NMR and crystallographic investigation of 1-cyano IBF derivative **5** (Figure 2.4), a rare stable IBF compound, suggests that IBF may be viewed as a 6π aromatic system perched atop a *cis*-butadiene
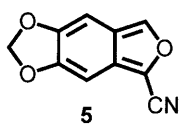
Figure 2.4 A stable IBF derivative.

fragment based on bond lengths and ^{13}C chemical shifts.[30] Aromaticity has also been implicated in one ring of IBF by calculations of Nucleus Independent Chemical Shift (NICS), though reports differ as to which ring.[31,32] While diverse opinions about the aromaticity of IBF and its derivatives abound, views on its general lack of stability and lower comparative stability to ITN, aromatic or otherwise, are uniform in the aforementioned reports.

42

In organic synthesis, the intrinsic instability of IBF has proved to be a valuable asset. Indeed, IBF garners most of its fame as a very reactive diene for Diels-Alder reactions,[33] with many IBF derivatives only ever isolated as Diels-Alder adducts. This property of IBF has been exploited in the synthesis of natural products, including 7-deoxydauntonmycinon[34] and resistomycin **6** (Scheme 2.3).[35] When reacted with an alkyne or benzyne intermediate, IBF forms epoxynaphthalenes, which can undergo dehydration to form extended polycyclic aromatic scaffolds.[36] IBF is even known to undergo Diels-Alder reactions with C_{60}.[37]

Scheme 2.3 Synthesis of Resistomycin

Ref. 35

6
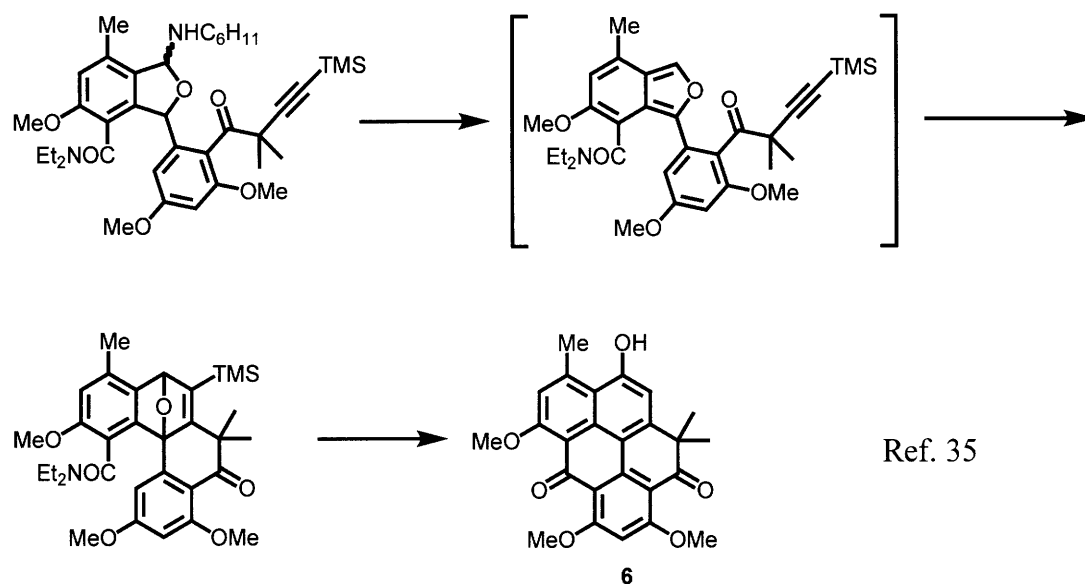
The synthesis of isobenzofuran and its derivatives may be achieved by numerous pathways, a sample of which is included in Scheme 2.4. The archetypal synthesis employs the elimination of either acetylene with the aid of dipyridyl tetrazine,[38] or ethylene under flash vacuum pyrolysis conditions.[39] LDA induced elimination of methoxy compound **7** forms IBF, and further addition of LDA lithiates the 1- and 3- positions.[40] Condensation of aryl-lithium or

aryl-grignard reagents with aryl-phthalides followed by dehydration with acetic anhydride (or HCl) yields diaryl-IBF compounds,[41] which may also be synthesized from aryl-aldehyes and ketamines using a rhenium catalyst.[42] Finally, IBF dimers have been formed by photochemical exocyclic [2+2+2] cycloaddition.[43]

Scheme 2.4 Synthetic Pathways for IBF and its Derivatives
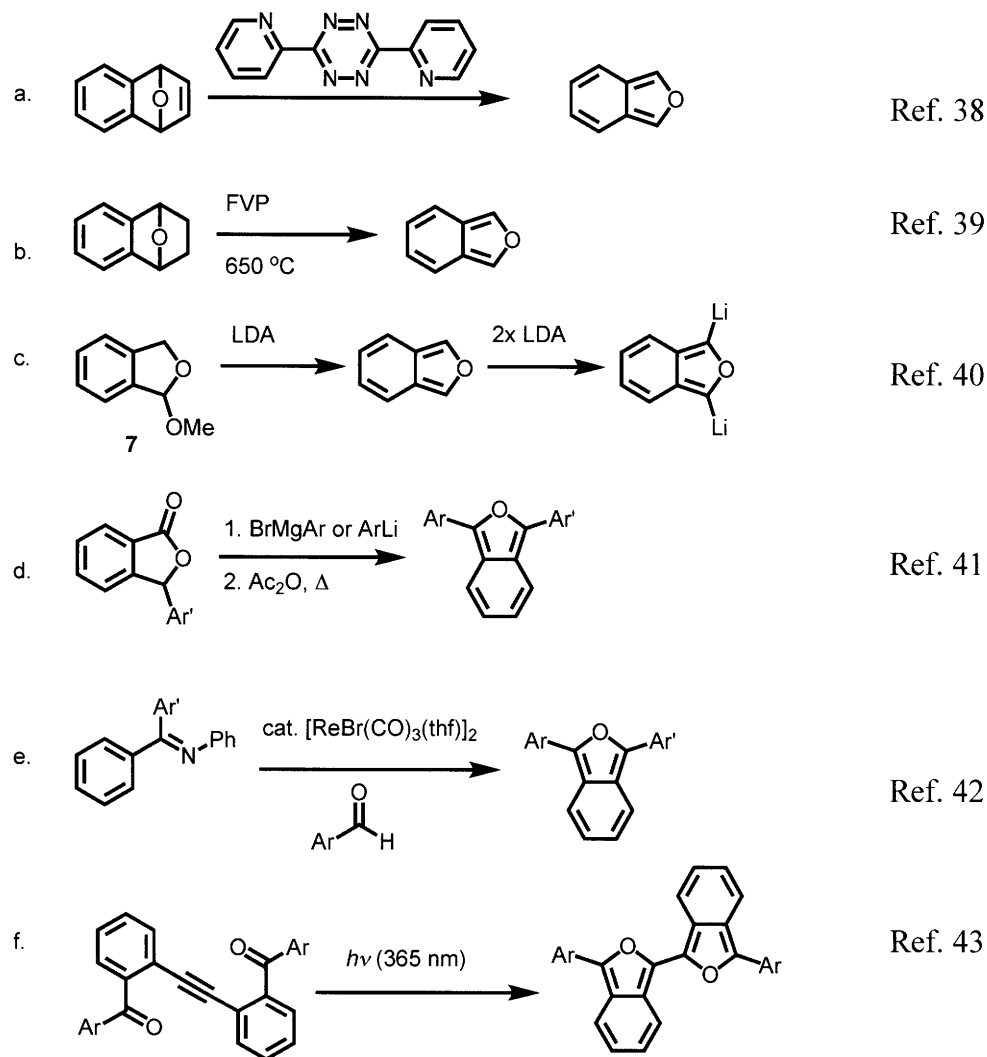
In contrast with the numerous reports that make use of IBF's interesting electronic properties in organic synthesis, few reports exist that integrate IBF into functional materials,

44

presumably due to synthetic difficulties stemming from their instability.[44] The most famous IBF

based material is 1,3-diphenylisobenzofuran, a fluorescent probe that reacts with singlet oxygen

to form a non-fluorescent complex.[45] In the field of OLEDS, 1,3-di-p-anisylisobenzofuran **8**[46]

and hexaphenylisobenzofuran **9**[47] have been used as a dopant and an electron transport material

respectively. Coatings of Poly(dihydroisobenzofuran)[48] and its functionalized derivatives[49] have

been synthesized by chemical vapor deposition. While poly(isobenzofuran) has been studied

theoretically,[50] no synthesis of this conjugated material has yet been reported, though

photochemically produced IBF-dimers have been recently reported.[43]
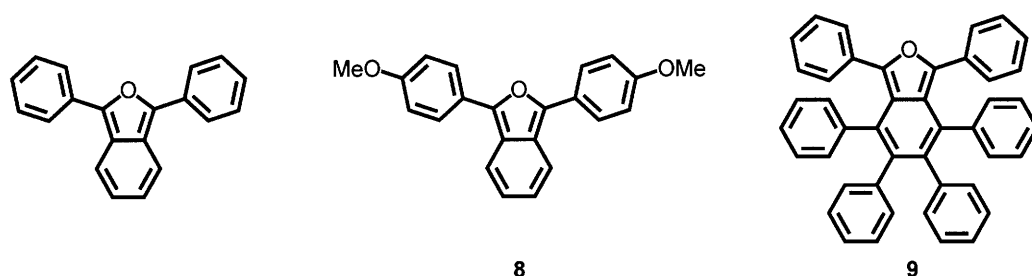
Figure 2.5 Isobenzofuran containing conjugated materials. From left to right, 1,3-diphenylisobenzofuran, a singlet oxygen probe, 1,3-di-p-anisyl-isobenzofuran, an OLED dopant, and hexaphenylisobenzofuran, an OLED electron transport material. See text for references

The paucity of IBF containing conjugated materials in the literature inspired us to explore

its properties as a component in oligomeric systems. In particular, we believed that IBF would

induce a larger proquinoid effect than ITN due to its lower stability, and would thus provide

materials with reduced band gaps. As we wished to further red-shift the NIAD dye series for

NIRF imaging applications, we deemed the incorporation of IBF subunits a worthwhile pursuit.

This chapter will focus on controlling the band gaps of near-infrared donor-acceptor

fluorophores using ITN and IBF.

2.2 Results and Discussion

2.2.1 Synthesis and Spectroscopic Properties of IBF-NIAD Dyes

After surveying the possible reactions in the literature, we decided upon a route (Scheme 2.5) in which the isobenzofuran core is constructed by condensation of 3-lithiothiophene with an aryl-phthalide followed by dehydration with acetic anhydride. Phthalides were commercially available or produced from acid catalyzed condensation of carboxybenzaldehyde 10 with appropriately substituted benzenes. Lithiation followed by quenching with DMF would produce aldehydes 13a-d, which would be converted into corresponding dyes 14a-d via the Knoevenagel condensation with malonitrile.

Scheme 2.5 Initial Synthesis of IBF-NIAD 0-3

11a: R= H- : NA[a]
11b: R= MeO- : 58%
11c: R= Me$_2$N- : 48%
11d: R= TIPSO- : 73%

12a-d

Unstable

13a-d

14a-d
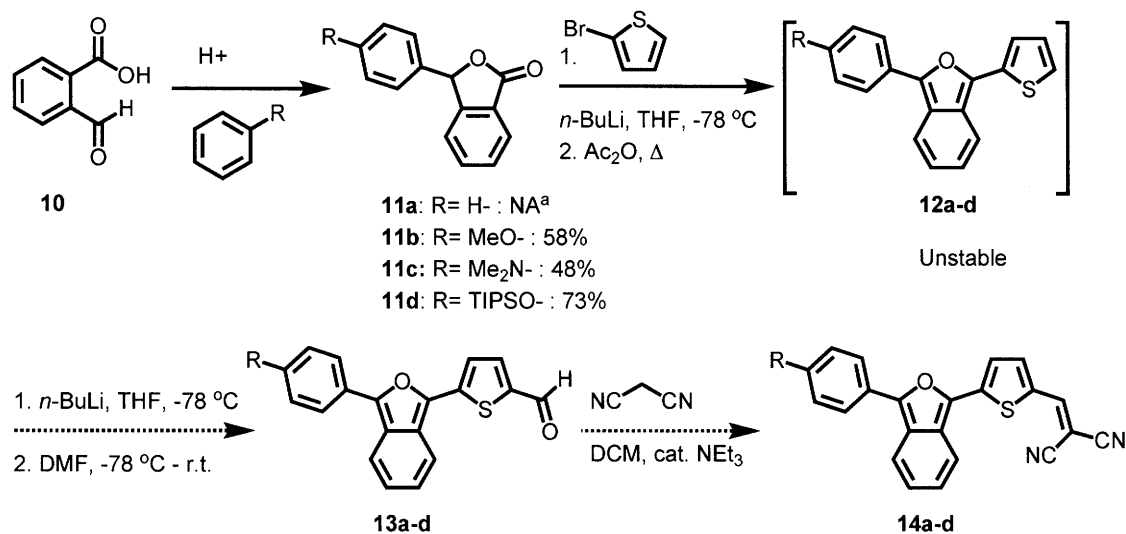
[a] 11a is commercially available
a. R= H- b. R= MeO- c. R= Me$_2$N- d. R= TIPSO-

This route proved impractical due the poor stability of 12a-d, which were prone to spontaneous decomposition upon purification by column chromatography and concentration.

Attempts to install a bromide in the 5-position of the thiophene were similarly unsuccessful. Small amounts of aldehydes **13a-d** were synthesized from crude **12a-d**, and proved more amenable to isolation; thus, we sought to bypass the troublesome unsubstituted thiophenes with acetal protected aldehyde **15** (Scheme 2.6). This method afforded adehydes **13a-d** and **IBF-NIADs 0-3** (**14a-d**) in fair yields. TIPS protection was employed in the synthesis of **IBF-NIAD 3**, though the susceptibility of the dicyanomethylene group to cleavage by fluoride necessitated the use of strong acid for deprotection.

Scheme 2.6 Improved Synthesis of IBF-NIAD 0-3

11a: R= H- : NA[a]
11b: R= MeO- : 58%
11c: R= Me₂N- : 48%
11d: R= TIPSO- : 73%

13a: R= H- : 41%
13b: R= MeO- : 33%
13c: R= Me₂N- : 61%
13d: R= TIPSO- : 47%

IBF-NIAD 0: R= H- : 78%
IBF-NIAD 1: R= MeO- : 67%
IBF-NIAD 2: R= Me₂N- : 38%
14d: R= TIPSO- : 55%

16

93%

11d

78%

14d

IBF-NIAD 3

88%

48
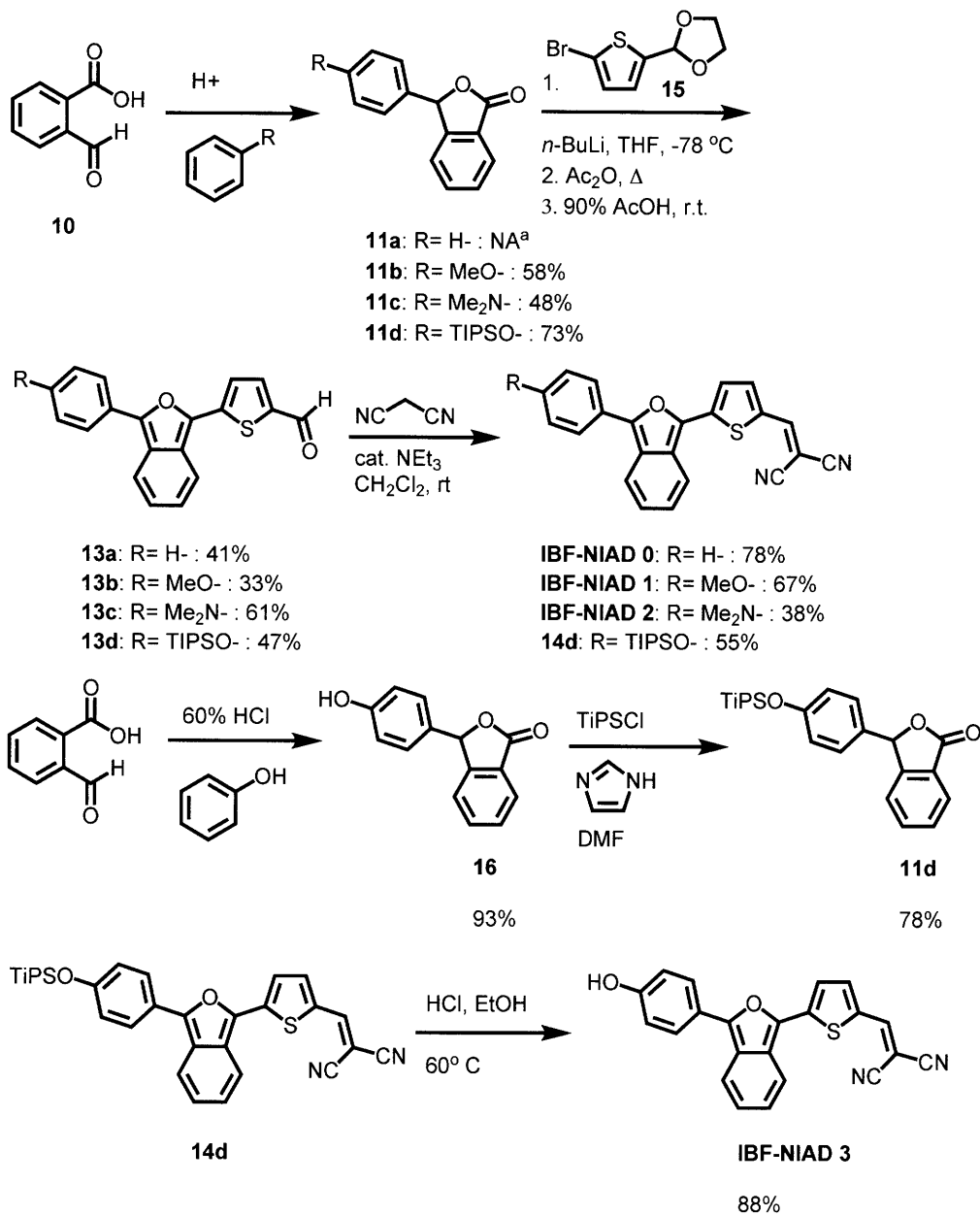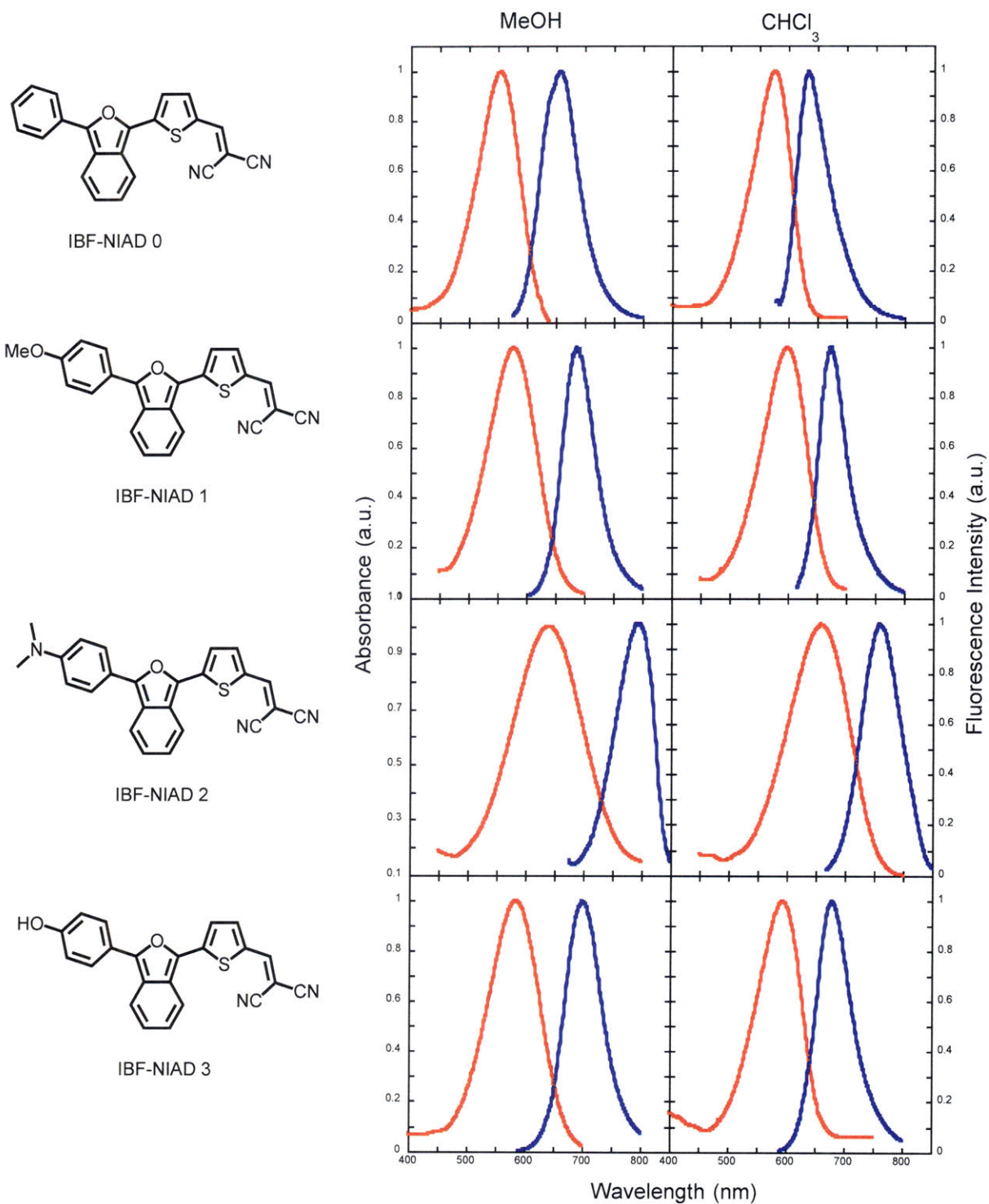
Figure 2.6 Absorption (red) and normalized fluorescence spectra (blue) of IBF-NIADs 0-3 in MeOH and CHCl₃.

Table 2.1 Spectroscopic Properties of Dyes 0-3

Dye	λ_{max} Abs. (nm)		λ_{max} Emission (nm)		Φ		ε (M^{-1} cm^{-1})	
	MeOH	CHCl$_3$	MeOH	CHCl$_3$	MeOH	CHCl$_3$	MeOH	CHCl$_3$
IBF-NIAD 0	556	578	658	635	0.077	0.075	34500	46300
IBF-NIAD 1	578	599	686	675	0.078	0.16	13500	37700
IBF-NIAD 2	637	656	790	762	0.0055	0.046	29700	29800
INF-NIAD 3	584	600	696	679	0.049	0.12	41900	35300

The UV-vis and fluorescence spectra of **IBF-NIAD 0-3** are shown in Figure 2.6 and their spectroscopic properties are summarized in Table 2.1. These dyes absorb in the far-red or NIR region and emit in the NIR region. Stoke shifts range between 102 and 153 nm in MeOH and 57 and 106 nm in CHCl$_3$. Quantum yields range from 0.046 to 0.16 in CHCl$_3$ and 0.0055 and 0.078 in MeOH. Compared to the absorption λ_{max} (MeOH) of **NIAD-6** and **NIAD-15**, **IBF-NIAD-3** and **IBF-NIAD-2** show 39 and 58 nm red-shifts respectively, demonstrating that IBF is a more efficacious proquinoidal unit. This result led us to synthesize the ITN containing versions of **IBF-NIAD 0** and **IBF-NIAD 1** in order to complete the series for a full comparison.

2.2.2 Synthesis and Spectroscopic Properties of ITN-NIADs

With the IBF dyes in hand, we decided to explore methods by which a corresponding set of ITN dyes could be obtained. **NIAD-6** and **NIAD-15** had been previously synthesized by the route in Scheme 2.7. We sought to expedite this process by converting the IBF dyes directly into their ITN counterparts. As mentioned above, the transformation of diaryl-isobenzofurans to diaryl-isothianaphthenes with Lawesson's reagent has been reported in the literature. When we

exposed **IBF-NIAD 0** to excess Lawesson's reagent under air and moisture free conditions, no reaction was observed, even after 24h at room temperature.

Scheme 2.7 Synthesis of NIAD-6 and NIAD-15
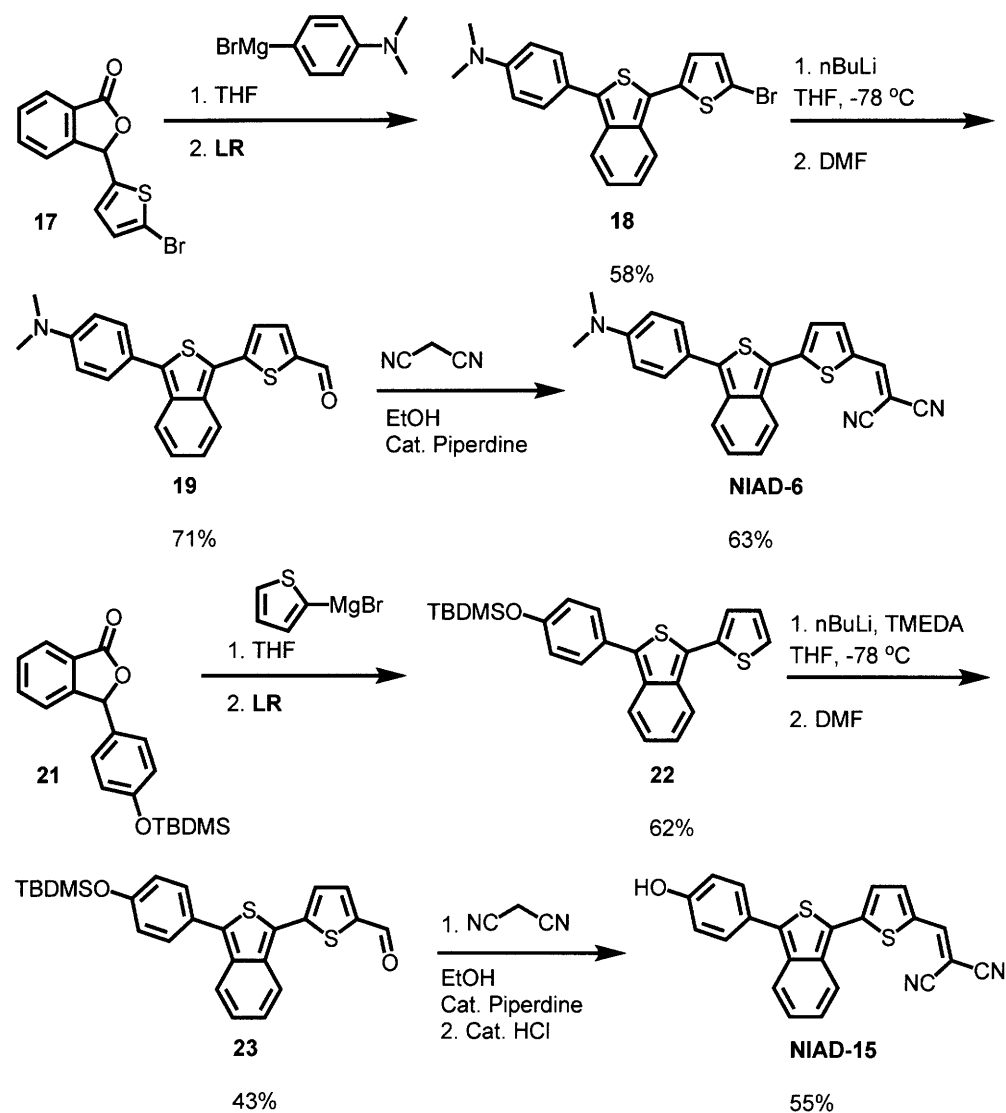
However, when the reaction mixture was exposed to air, the reaction proceeded to completion in 7 hours and furnished the desired product in 87% yield (Scheme 2.8). For **IBF-NIAD 1-3**, an anhydrous oxygen atmosphere was required. In the case of **IBF-NIAD 2**, the dicyanomethylene

acceptor group was cleaved by Lawesson's reagent, presumably to a thioaldehyde. The strength of the dimethylamino donor group is apparently sufficient to polarize the double bond to the point at which it is sensitive to Lawesson's reagent. Addition of excess malonitrile and triethylamine after the completion of the **LR** conversion reinstalled the acceptor group in good yield.

Scheme 2.8 Synthesis of ITN-NIAD 0-3
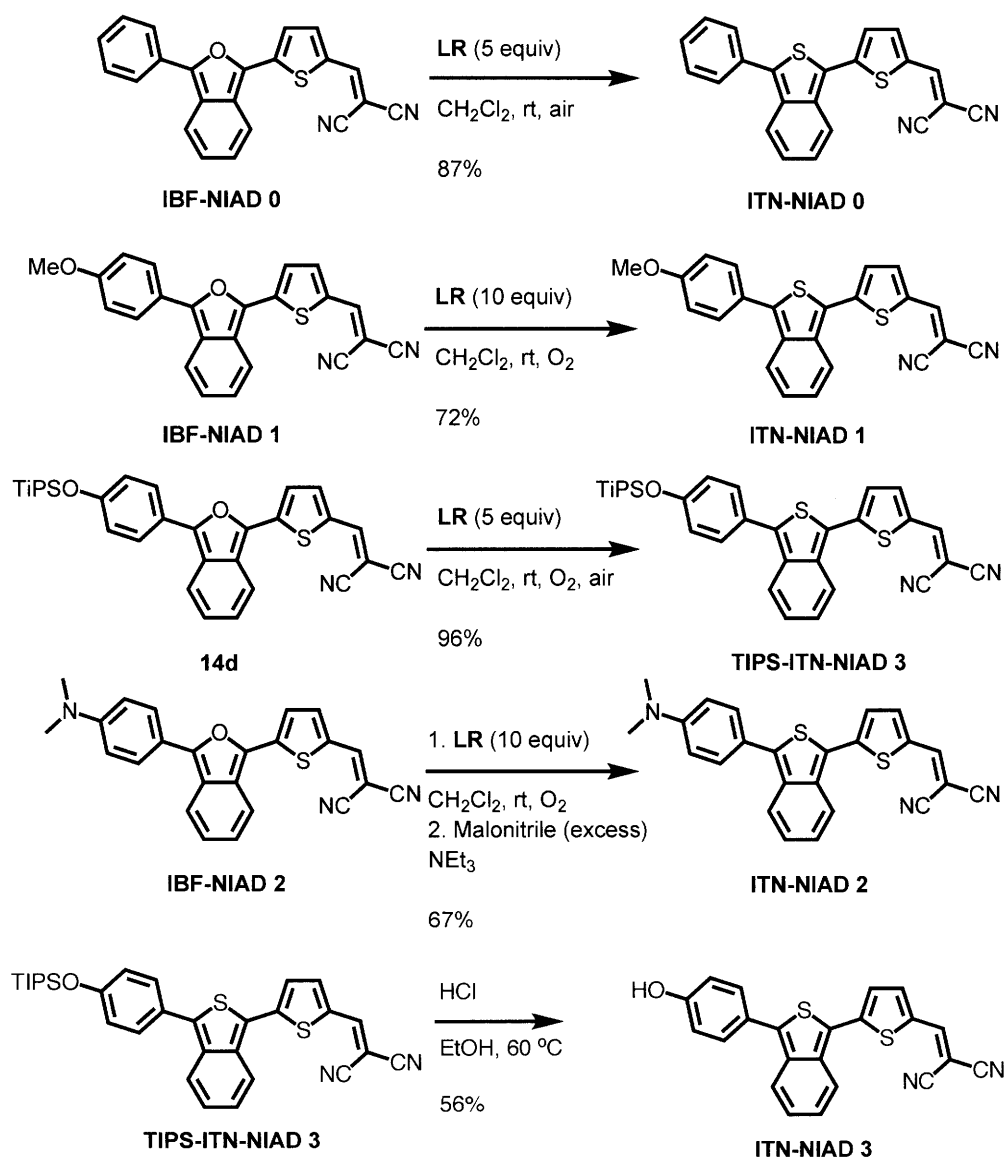
Although the direct conversion of IBF to ITN has been previously reported, the role of oxygen has never been studied. As mentioned previously, diarylisobenzofurans are sensitive to singlet oxygen and to a limited extent, triplet oxygen.[51] This reaction results in an endoperoxide, which in turn rearranges into a diketone,[52] though the mechanism of this particular rearrangement is not well understood.[53] We propose that this conversion occurs for **IBF-NIAD** dyes, and that the diketone is then cyclized to the isothianapthene with Lawesson's Reagent (Scheme 2.9).

Scheme 2.9 The Proposed Mechanism for the IBF to ITN Conversion
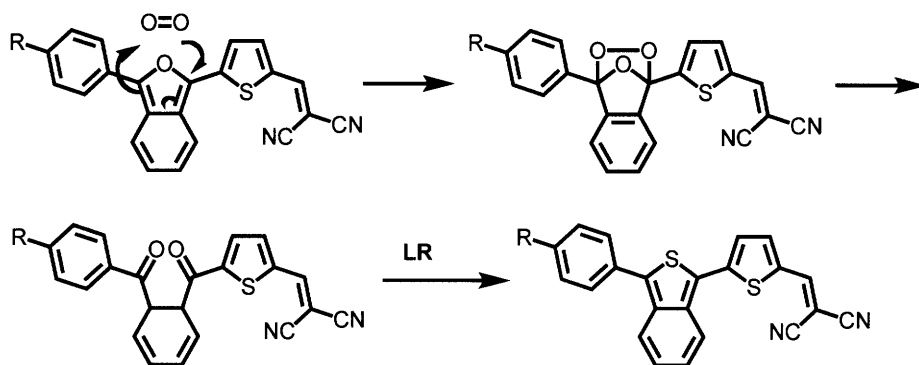
The UV-vis and fluorescence spectra of **ITN-NIAD 0-3** are shown in Figure 2.7 and their spectroscopic data is summarized in Table 2.2. The red-shifts in λ_{max} of absorbance and emission are listed in Table 2.3, and represented in an esthetically pleasing manner in Figure 2.8. In general, the red-shifts in absorbance increased with the efficacy of the electron donating group, with 31 nm for H-, 40 nm for MeO-, 41 nm for HO-, and 58 nm for Me_2N-. The red-shifts in emission were far more modest, between 5 nm and 21 nm, suggesting that the quinoid resonance structure might not factor heavily in the excited-state energies of these molecules. In general, the
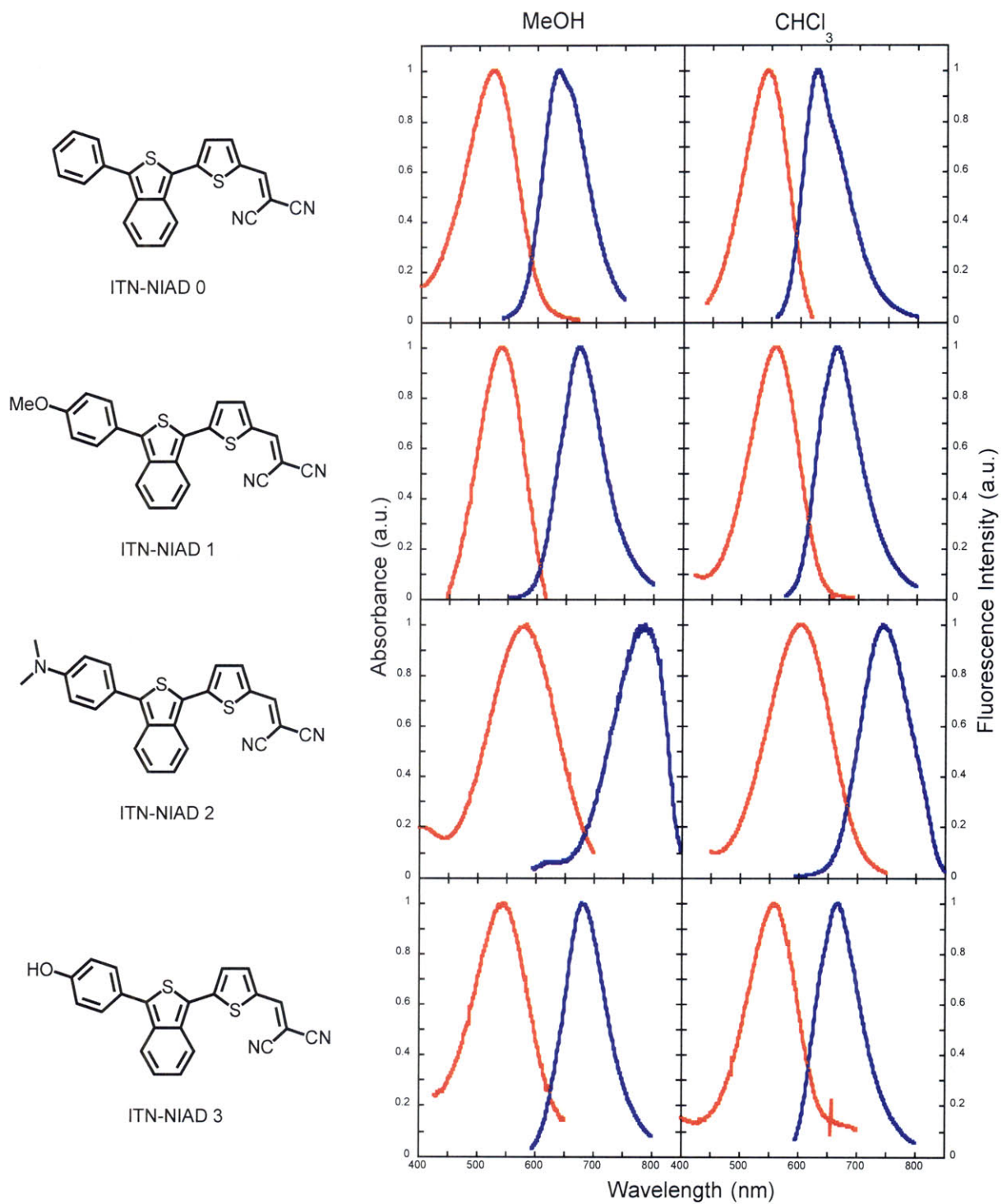
Figure 2.7 Absorbance (red) and normalized fluorescence intensity (blue) spectra of ITN-NIAD 0-3 in CHCl₃ and MeOH.

quantum yields for the IBF dyes were higher than their corresponding ITN counterparts, a trend

that we will discuss in the next chapter.

Table 2.2 Spectroscopic Properties of ITN-NIAD dyes

Dye	λ_{max} Abs. (nm)		λ_{max} Emission (nm)		Φ		ε (M^{-1} cm^{-1})	
	MeOH	CHCl$_3$	MeOH	CHCl$_3$	MeOH	CHCl$_3$	MeOH	CHCl$_3$
ITN-NIAD-0	525	544	637	629	0.061	0.079	20300	24700
ITN-NIAD-1	537	559	672	663	0.046	0.099	15600	17000
ITN-NIAD-2 (NIAD-15)	579	604	785	743	0.0015	0.021	17200	11800
ITN-NIAD-3 (NIAD-6)	545	559	684	667	0.023	0.071	36700	16500

Table 2.3 Red shifts for S-O conversion

Solvent	ITN-IBF 0 (nm) R= H-		ITN-IBF 1 (nm) R= MeO-		ITN-IBF 2 (nm) R= Me$_2$N-		ITN-IBF 3 (nm) R= HO-	
	Abs.	Em.	Abs.	Em.	Abs.	Em.	Abs.	Em.
MeOH	31	21	41	14	58	5	39	12
CHCl$_3$	34	6	40	12	52	19	41	12
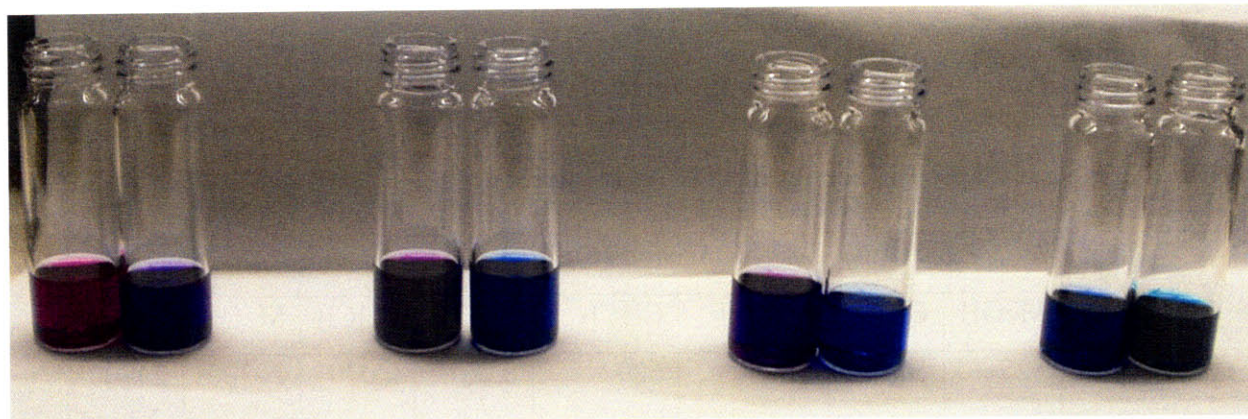
Figure 2.8 IBF-NIAD 0-3 and **ITN-NIAD 0-3** in MeOH. From left to right, **ITN-NIAD 0**, **IBF-NIAD 0**, **ITN-NIAD 1**, **IBF-NIAD 1**, **ITN-NIAD 3**, **IBF-NIAD 3**, **ITN-NIAD 2**, **IBF-NIAD 2.**

2.3 Conclusions

In summary, a series of new isobenzofuran containing near-infrared, donor-acceptor type fluorophores was synthesized. A corresponding set of isothianaphthene containing dyes was synthesized via direct conversion with oxygen and Lawesson's Reagent. Comparison of the photophysical properties of both dye sets revealed the greater effectiveness of IBF over ITN as a red-shifting component in this class of dyes, an effect attributable to the strongly pro-quinoidal nature of IBF. Subsequent chapters will describe the expansion of the IBF dye series and its use as a near-infrared fluorescence contrast agent.

2.4 Experimental Section

Materials. Commercial reagents were purchased from Sigma Aldrich, Alfa Aesar, or GFS Chemicals, and used as received. Dry solvents were obtained using a solvent purification system (Innovative Technologies, Inc.) and handled under an argon atmosphere, unless otherwise noted. Flash chromatography was performed using SiliaFlash F60 (230-400 mesh) from Silicycle.

Instrumentation. Melting points were determined in open capillaries using a Mel-Temp II apparatus and are uncorrected. Proton nuclear magnetic resonance (1H NMR) spectra and carbon nuclear magnetic resonance (^{13}C NMR) spectra were recorded on a Varian Mercury-300 (300 MHz) or an Inova-500 (500 MHz) NMR spectrometer. Chemical shifts for protons are reported in parts per million downfield from tetramethylsilane and are referenced to residual protium in the NMR solvent (CHCl$_3$: δ 7.27). Chemical shifts for carbon are reported in parts per million downfield from tetramethylsilane and are referenced to the carbon resonances of the solvent (CDCl$_3$: δ 77.0). Data are represented as follows: chemical shift, integration, multiplicity (br = broad, s = singlet, d = doublet, t = triplet, q = quartet, sp = septet, m = multiplet), and coupling constants in Hertz (Hz). High-resolution mass spectra (HRMS) were obtained at the MIT Department of Chemistry Instrumentation Facility using a peak-matching protocol to determine the mass and error range of the molecular ion, employing either electron impact or electrospray as the ionization technique. Fluorescence spectra were measured on a SPEX Fluorolog-τ3 fluorimeter (model FL-321, 450 W Xenon lamp) using right-angle detection. Ultraviolet-visible absorption spectra were measured with an Agilent 8453 diode array spectrophotometer and corrected for background signal with a solvent-filled cuvette. Fluorescence quantum yields were determined by the optically dilute method[54] using cresyl violet perchlorate in methanol (Φ=0.54)

or zinc phthalocyanine in 1% pyridine in toluene (Φ=0.30) as standards and were corrected for solvent refractive index and absorption differences at the excitation wavelength.

Synthetic Procedures
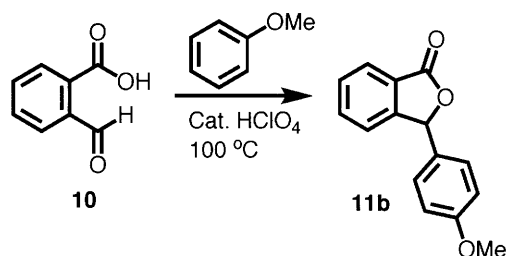
To a solution of **10** (5.0 g, 33 mmol) in anisole (10 ml, 92 mmol) were added 8 drops of 70% $HClO_4$, and the solution was stirred at 100 °C for 2 hours. After cooling, the reaction mixture was poured into water and stirred for 30 minutes. The sticky white product was collected by suction filtration and was washed with water and saturated sodium bicarbonate. Recrystalization from methanol afforded **11b** as white crystals (4.5 g, 19 mmol, 58% yield, Mp=117-118 °C). ^{1}H NMR (300 MHz, CDCl$_3$): 7.97 (1H, d, 7.6 Hz), 7.67 (1H, td, 7.4 Hz, 1.2 Hz), 7.57 (1H, t, 7.6 Hz), 7.32 (1H, d, 7.6 Hz), 7.19 (2H, dm, 8.8 Hz), 6.90 (2H, dm, 8.8 Hz), 6.39 (1H, s), 3.82 (3H, s). ^{13}C NMR (125 MHz, CDCl$_3$): 170.5, 160.3, 149.7, 134.2, 129.2, 128.7, 128.1, 125.8, 125.4, 122.9, 114.2, 82.6, 55.2. HRMS (ESI): 241.0853 [calc'd for M+H$^+$: 241.0859]. These values are consistent with data reported in the literature.[55]
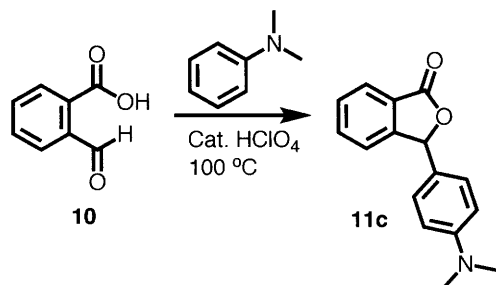
To a solution of **10** (4.0 g, 27 mmol) in *N,N*-dimethylaniline (8.2 ml, 65 mmol) were added 6 drops of 70% HClO₄, and the solution was stirred at 100 °C for 2 hours. After cooling, the reaction mixture was poured into water and stirred for 30 minutes. The light blue product was collected by suction filtration and was washed with water and saturated sodium bicarbonate. Recrystalization from acetone afforded **11c** as white crystals (3.4 g, 13 mmol, 48% yield, Mp= 193-195 °C) ¹H NMR (300 MHz, CDCl₃): 7.96 (1H, d, 7.6 Hz), 7.65 (1H, td, 7.5 Hz, 1.2 Hz), 7.55 (1H, t, 7.5 Hz), 7.33 (1H, d, 7.6 Hz), 7.10 (2H, dm, 8.8 Hz), 6.90 (2H, dm, 8.8 Hz), 6.37 (1H, s), 2.97 (6H, s). ¹³C NMR (125 MHz, CDCl₃): 170.7, 151.1, 150.0, 134.0, 129.0, 128.7, 126.2, 125.4, 123.04, 123.02, 83.5, 40.3. HRMS (ESI): 254.1176 [calc'd for M+H⁺: 254.1176].
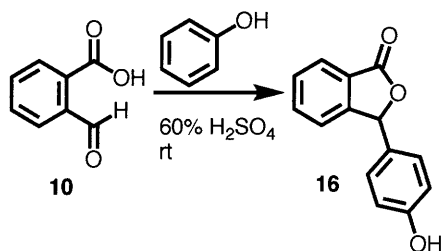
10 (2.2 g, 15 mmol) was dissolved in 12 ml of 60% H₂SO₄ and stirred for 10 min at room temperature. Phenol (1.4 g, 15 mmol) was added in one portion, and the reaction mixture was stirred for an additional 2 hours at room temperature. The reaction mixture was then poured onto ice and stirred for 30 minutes. The white product was collected by suction filtration and washed with water and saturated sodium bicarbonate solution. Recrystalization from 20% aqueous ethanol afforded **16** as white crystals (3.1 g, 14 mmol, 93% yield, Mp = 161-163 °C). ¹H NMR (300 MHz, CDCl₃): 7.97 (1H, d, 7.6 Hz), 7.67 (1H, td, 7.5 Hz, 1.2 Hz), 7.57 (1H, t, 7.2 Hz), 7.32 (1H, dq, 7.6 Hz, 0.9 Hz), 7.13 (2H, dm, 8.4 Hz), 6.90 (2H, dm, 8.6 Hz), 6.38 (1H, s), 5.13 (1H, s). ¹³C NMR (125 MHz, CDCl₃): 170.9, 156.7, 149.7, 134.4, 129.4, 129.0, 128.1, 125.8, 125.6,

123.0, 115.9, 82.9. HRMS (ESI): 249.0526 [calc'd for M+Na$^+$: 249.0522]. These values are consistent with data reported in the literature.[56]
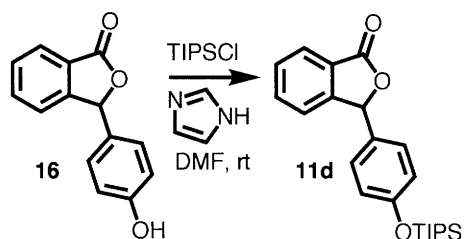
16 (5.1 g, 23 mmol) was dissolved in DMF (94 ml) along with imidazole (6.8 g, 0.10 mol) and triisopropylsilyl chloride (9.4 ml, 44 mmol), and the solution was stirred overnight at room temperature. The reaction mixture was then poured onto ice and stirred for one hour. The white solid was collected by suction filtration. Recrystalization from methanol afforded **11d** as a white crystalline solid (6.4 g, 18 mmol, 78% yield, Mp= 102-103 °C). ^{1}H NMR (300 MHz, CDCl$_3$): 7.97 (1H, d, 7.6 Hz), 7.66 (1H, td, 7.5 Hz, 1.2 Hz), 7.56 (1H, tt, 7.4 Hz, 0.8 Hz), 7.33 (1H, dq, 7.6 Hz, 1.1 Hz), 7.11 (2H, dm, 8.4 Hz), 6.87 (2H, dm, 8.7 Hz), 6.37 (1H, s), 1.26 (3H, sp, 6.8 Hz), 1.09 (18H, d, 6.7 Hz). ^{13}C NMR (125 MHz, CDCl$_3$): 170.5, 157.0, 149.7, 134.2, 129.2, 128.7, 128.5, 125.9, 125.5, 122.9, 120.2, 82.8, 17.8, 12.6. HRMS (ESI): 405.1855 [calc'd for M+Na$^+$: 405.1856].
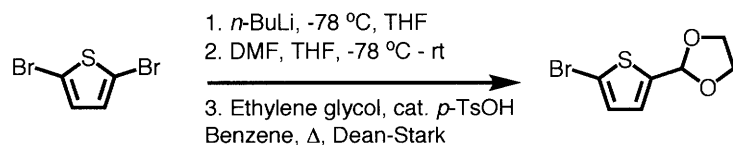
2,5-Dibromothiophene (6.0 g, 25 mmol) and dry THF (50 ml) were added to a vacuum dried Schlenk flask under argon and the solution was cooled to -78 °C. n-BuLi (15.6 ml 1.6M solution in hexanes, 25 mmol) was added dropwise and the solution was stirred at -78 °C for 90 minutes.

A solution of dry DMF (2.5 ml, 32 mmol, distilled from NaH) in dry THF (10 ml) was added, and the reaction mixture was warmed to room temperature and stirred overnight. The reaction mixture was then poured onto saturated sodium bicarbonate and extracted with ethyl acetate. The organic fraction was washed with saturated sodium bicarbonate, water, and brine, dried over magnesium sulfate, and concentrated in vacuo. The resulting dark, viscous liquid was then dissolved in benzene (100 ml) along with ethylene glycol (3.2 ml, 57 mmol) and p-toluenesulfonic acid monohydrate (0.060 g, 0.32 mmol), and this solution was refluxed overnight in a flask equipped with a Dean-Stark trap. The reaction mixture was then cooled to room temperature, concentrated in vacuo, taken up in ethyl acetate and washed with saturated sodium bicarbonate and brine. The organic layer was dried over magnesium sulfate and concentrated in vacuo. The residue was purified by flash chromatography on silica gel (2:1 hexane:ethyl acetate) and then vacuum distillation (66-70 °C, 190 mtorr) to afford **6** as a clear liquid (2.2 g, 9.4 mmol, 38% yield) ^{1}H NMR (300 MHz, CDCl$_3$): 6.95 (1H, d, 3.8 Hz), 6.92 (1H, d, 3.8 Hz), 6.02 (1H s), 4.15-3.95 (4H, m). ^{13}C NMR (125 MHz, CDCl$_3$): 143.3, 129.4, 126.5, 113.5, 65.2 HRMS (ESI): 234.9417 [calc'd for M+H$^+$: 234.9423]. These values are consistent with data reported in the literature.[57]

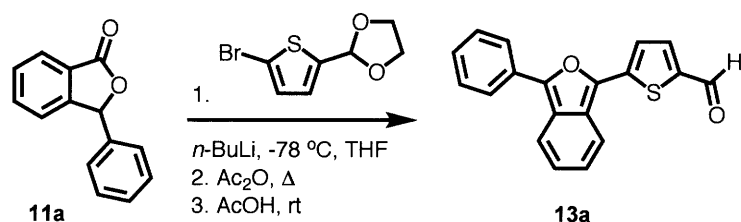General procedure for synthesis of aldehydes **13a-d**

n-BuLi (1.4 ml of 1.6M solution in hexanes) was added to a solution of **15** (0.5 g, 2.1 mmol) in dry THF (7 ml) in a vacuum dried Schlenk flask at -78 °C under argon, and the solution was stirred at -78 °C for 2 hours. A solution of 3-phenylphthalide **11a** (0.45 g, 2.1 mmol) in dry THF (7 ml) was added dropwise, and the reaction mixture was stirred at -78 °C for an additional hour. Acetic anhydride (0.23 ml, 2.4 mmol) was added, and the solution was warmed to room temperature, and was then refluxed for 10 minutes. The reaction mixture was cooled to room temperature, and was then diluted with ethyl acetate and washed with saturated aqueous sodium bicarbonate and brine. The organic layer was dried over magnesium sulfate and concentrated in vacuo. Acetic acid (15 ml of 90% aqueous solution) was then added to the residue, and this solution was stirred under argon for 2 hours, and then poured into water and stirred for 30 minutes. The red solid was collected by suction filtration and washed with saturated aqueous sodium bicarbonate and water. Recrystallization from 5% aqueous methanol afforded **13a** as red crystals (0.26 g, 0.86 mmol, 41% yield, Mp = 150-152 °C) ^{1}H NMR (300 MHz, CDCl$_3$): 9.92 (1H, s), 7.99-7.92 (2H, m), 7.90 (1H, dt, 8.8 Hz, 1.2 Hz), 7.82-7.76 (2H, m), 7.58-7.49 (3H, m), 7.38 (1H, tt, 7.4 Hz, 1.2 Hz), 7.23-6.99 (2H, m). ^{13}C NMR (125 MHz, CDCl$_3$): 182.3, 146.3, 142.3, 140.5, 137.4, 130.6, 129.1, 128.1, 127.2, 125.9, 125.3, 124.5, 122.4, 122.0, 120.6, 119.6, 99.8. HRMS (ESI): 305.0641[calc'd for M+H$^+$: 305.0631]
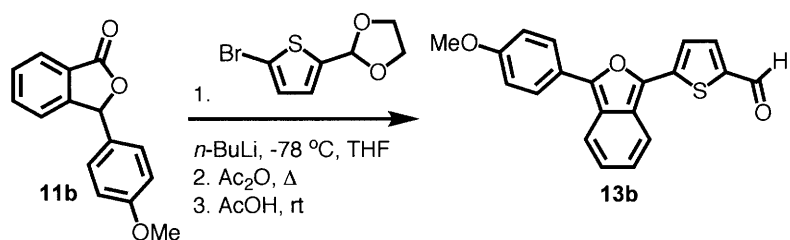
The reaction was carried out on a 2.1 mmol scale, and **13b** was obtained as a rusty red powder after recrystallization from ethanol (0.23 g, 0.69 mmol, 33% yield, Mp = 79-81 °C) ^{1}H NMR (300 MHz, CDCl$_3$): 9.90 (1H, s), 7.90 (2H, dt, 9.1 Hz, 2.2 Hz), 7.84 (1H, dt, 8.8 Hz, 1.0 Hz), 7.79-7.75 (2H, m), 7.51 (1H, d, 4.1 Hz), 7.18 (1H, ddd, 8.8 Hz, 3.0 Hz, 0.8 Hz), 7.11-7.02 (3H, m), 3.90 (3H, s). ^{13}C NMR (125 MHz, CDCl$_3$): 182.0, 159.5, 146.5, 142.4, 139.7, 137.9, 137.4, 127.0, 126.7, 125.2, 124.5, 123.4, 121.24, 121.20, 120.6, 119.3, 114.5, 55.3. HRMS (ESI): 335.0741 [calc'd for M+H$^+$: 335.0736]
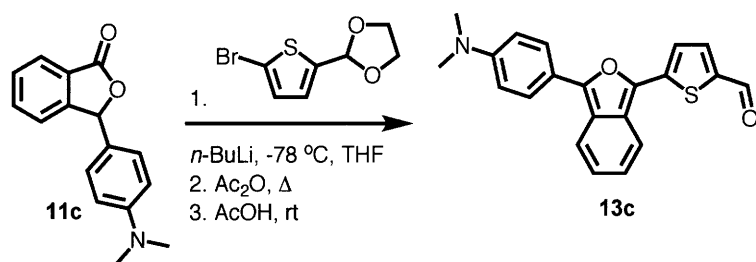
The reaction was carried out with 2.1 mmol of **15** and 1.8 mmol of **11c** in dry THF (40 ml), and 20 ml of 90% aqueous acetic acid were used in the work up. The acetic acid solution was poured into water, and then small portions of saturated aqueous sodium bicarbonate were carefully added. The dark product was collected by suction filtration, and was washed with sodium bicarbonate and brine. Flash chromatography on silica gel (dichloromethane) afforded **13c** as a dark solid (0.38 g, 1.1 mmol, 61% yield) ^{1}H NMR (300 MHz, CDCl$_3$): 9.87 (1H, s), 7.88-7.82 (3H, m), 7.76-7.72 (2H, m), 7.46 (1H, d, 4.2 Hz), 7.17 (1H, ddd, 8.8 Hz, 6.5 Hz, 0.9 Hz), 7.04 (1H, ddd, 8.8 Hz 0.9 Hz), 6.83 (2H, dm, 8.8 Hz), 3.07 (6H, s). 182.0, 150.1, 148.2, 143.0, 139.1, 137.7, 137.2, 127.2, 126.7, 125.0, 124.6, 121.3, 120.7, 120.6, 119.4, 118.7, 112.3, 40.2. HRMS (ESI): 348.1051 [calc'd for M+H$^+$: 348.1053]
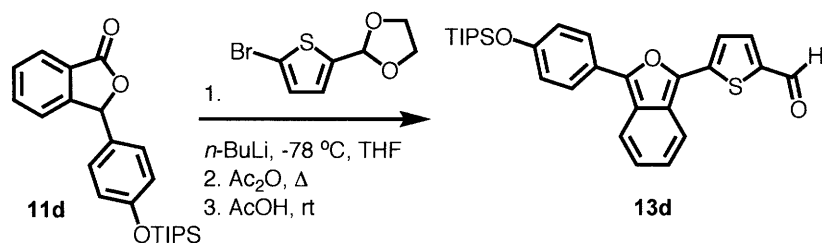
The reaction was carried out on a 2.1 mmol scale. After acetic acid workup, the reaction mixture was poured into water, stirred for 30 minutes, and then extracted with ethyl acetate. The organic layer was washed with saturated aqueous sodium bicarbonate and brine, and was then dried over magnesium sulfate and concentrated in vacuo. Flash chromatography on silica gel (2:1 hexane:ethyl acetate) afforded **13d** as a viscous red oil (0.47 g, 0.99 mmol, 47% yield) ^{1}H NMR (300 MHz, CDCl$_3$): 9.90 (1H, s), 7.88-7.82 (3H, m), 7.79-7.74 (2H, m), 7.52 (1H, d, 4.1 Hz), 7.18 (1H, ddd, 8.7 Hz, 6.3 Hz, 0.9 Hz), 7.12-7.00 (3H, m), 1.30 (3H, sp, 6.9 Hz), 1.15 (18H, d, 6.9 Hz). ^{13}C NMR (125 MHz, CDCl$_3$): 182.0, 156.4, 146.7, 142.5, 139.8, 137.9, 137.4, 127.0, 126.7, 125.2, 124.5, 123.7, 121.3, 121.2, 120.7, 120.6, 119.4, 17.9, 12.6. HRMS (ESI): 499.1733 [calc'd for M+Na$^+$: 499.1734]

General Procedure for synthesis of dyes **IBF-NIAD 0**
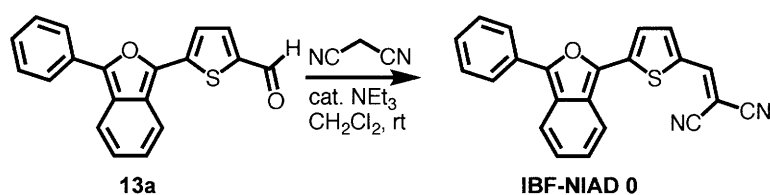
13a (70 mg, 0.23 mmol) was dissolved in a solution of malonitrile (15 mg, 0.23 mmol) in dry dichloromethane (10 ml) and then 3 drops of triethylamine were added and the resulting solution was stirred overnight, under argon, at room temperature. The reaction mixture was then diluted with ethyl acetate, washed with water and brine, dried over magnesium sulfate, and concentrated

in vacuo. Flash chromatography over silica gel (dichloromethane) afforded **IBF-NIAD 0** as a purple solid (62 mg, 0.18 mmol, 78% yield). ^{1}H NMR (300 MHz, CDCl$_3$): 7.97-7.88 (3H, m), 7.72 (1H, d, 8.7 Hz), 7.66 (1H, s), 7.59 (1H, d, 4.3 Hz), 7.53 (2H, t, 7.2 Hz), 7.48 (1H, d, 4.3 Hz), 7.41 (1H, tt, 7.2 Hz, 1.3 Hz), 7.26-7.14 (2H, m). ^{13}C NMR (125 MHz, CDCl$_3$): 149.1, 148.2, 144.0, 140.2, 138.5, 132.5, 130.0, 129.2, 128.8, 128.3, 126.4, 125.9, 125.6, 122.8, 122.2, 121.0, 119.6, 114.9, 114.1, 73.3. HRMS (ESI): 353.0753 [calc'd for M+H$^+$: 353.0743]
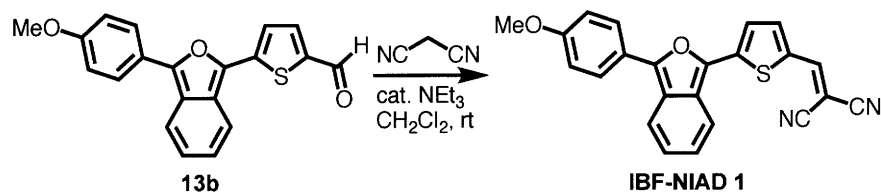
13b → **IBF-NIAD 1**

The reaction was carried out on a 0.18 mmol scale with 10 ml of dry dichloromethane. Flash chromatography over silica gel (dichloromethane) afforded **IBF-NIAD 1** as a purple solid (45 mg, 0.12 mmol, 67% yield). ^{1}H NMR (300 MHz, CDCl$_3$): 7.96-7.87 (3H, m), 7.78 (1H, d, 8.7 Hz), 7.73 (1H, s), 7.66 (1H, d, 4.4 Hz), 7.52 (1H, d, 4.4 Hz), 7.31-7.24 (1H, m), 7.16 (1H, ddd, 8.8 Hz, 6.5 Hz 0.9 Hz), 7.07 (2H, dm, 8.9 Hz), 3.92 (3H, s). ^{13}C NMR (125 MHz, CDCl$_3$): 160.3, 149.0, 148.9, 144.4, 140.4, 137.9, 132.1, 128.5, 127.4, 126.3, 126.0, 123.0, 122.0, 121.6, 121.2, 119.6, 115.2, 114.8, 114.4, 72.5, 55.5. HRMS (ESI): 383.0845 [calc'd for M+H$^+$: 383.0849]
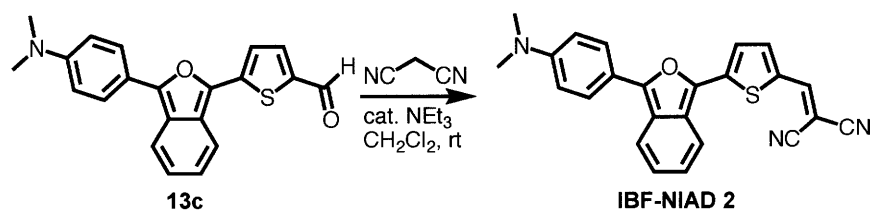
13c → **IBF-NIAD 2**

The reaction was carried out on a 0.25 mmol scale with 15 ml of dry dichloromethane. Flash chromatography over silica gel (dichloromethane) afforded **IBF-NIAD 2** as a green solid (38 mg, 0.096 mmol, 38% yield). ^{1}H NMR (300 MHz, CDCl$_3$): 7.94-7.86 (3H, m), 7.76 (1H, dt, 8.9 Hz, 0.9 Hz), 7.66 (1H, s), 7.61 (1H, d, 4.0 Hz), 7.44 (1H, d, 4.3 Hz), 7.31-7.24 (1H, m, obscured by solvent), 7.12 (1H, ddd, 8.8 Hz, 6.5 Hz, 0.9 Hz), 6.83 (2H, dm, 9.2 Hz), 3.10 (6H, s). ^{13}C NMR (125 MHz, DMF-d$_7$): 152.2, 151.8, 151.5, 144.8, 144.2, 138.1, 132.8, 130.2, 128.3, 127.8, 126.8, 123.2, 122.7, 122.3, 120.4, 118.4, 116.9, 116.3, 113.6, 70.9, 40.5. HRMS (ESI): 396.1170 [calc'd for M+H$^+$: 396.1170]

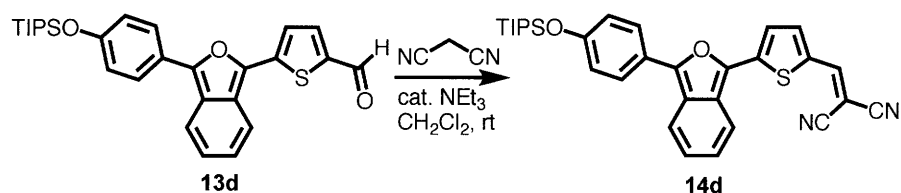The reaction was carried out on a 0.38 mmol scale with 15 ml dry dichloromethane. Flash chromatography over silica gel (dichloromethane) afforded **14d** as a purple solid (0.11 g, 0.21 mmol, 55% yield). ^{1}H NMR (300 MHz, CDCl$_3$): 7.92-7.85 (3H, m), 7.78 (1H, d, 8.9 Hz), 7.73 (1H, s), 7.66 (1H, d, 4.4 Hz), 7.51 (1H, d, 4.3 Hz), 7.31-7.24 (1H, m), 7.15 (1H, ddd, 8.9 Hz, 6.3 Hz 0.9 Hz), 7.05 (2H, dm, 8.9 Hz), 1.30 (3H, sp, 7.0 Hz), 1.15 (18H, d, 7.0 Hz). ^{13}C NMR (125 MHz, CDCl$_3$): 157.2, 149.0, 148.9, 144.3, 140.4, 137.8, 132.0, 128.4, 127.3, 126.3, 125.9, 123.1, 122.0, 121.5, 121.3, 120.8, 119.5, 115.2, 114.3, 17.9, 12.7. HRMS (ESI): 547.1837 [calc'd for M+Na$^+$: 547.1846]
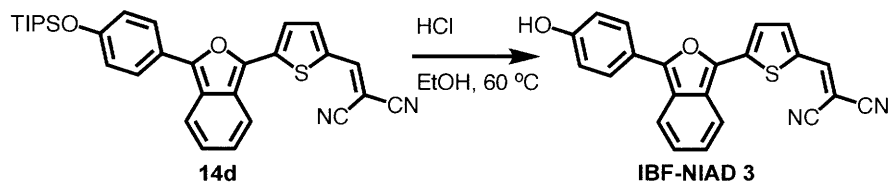
8d (13.5 mg, 0.026 mmol) was dissolved in ethanol (12 ml, 200 proof) at 60 °C. Hydrochloric acid (1.3 ml, 36%) was added and the solution was stirred at 60 °C under argon for 18 hours. The reaction mixture was cooled to room temperature, diluted with ethyl acetate, and washed with water, saturated aqueous sodium bicarbonate, and brine, and was then dried over magnesium sulfate and concentrated in vacuo. Flash chromatography over silica gel (9:1 methylene chloride: ethyl acetate, then 2:1 ethyl acetate: hexane) afforded **IBF-NIAD 3** as a blue solid (8.4 mg, 0.023 mmol, 88% yield). ^{1}H NMR (500 MHz, DMSO-d_6): 9.03 (1H, bs), 6.85 (1H, s), 6.53 (1H, d, 8.5 Hz), 6.42 (2H, d, 8.5 Hz), 6.32 (1H, d, 4.4 Hz), 6.22 (1H, d, 8.9 Hz), 6.08 (1H, d, 4.3 Hz), 5.88 (1H, t, 7.5 Hz), 5.77 (1H, t, 8.0 Hz), 5.65 (2H, d, 8.5 Hz). ^{13}C NMR (125 MHz, DMSO-d_6): 158.9, 150.6, 148.9, 143.2, 143.1, 137.2, 131.9, 129.0, 127.6, 126.3, 125.9, 122.0, 121.7, 121.3, 121.0, 119.3, 116.8, 115.8, 115.0, 70.2. HRMS (ESI): 367.0539 [calc'd for M-H⁻: 367.0547]

IBF-NIAD 0 → Lawesson's Reagent (5 equiv) DCM, rt, air → **ITN-NIAD 0**
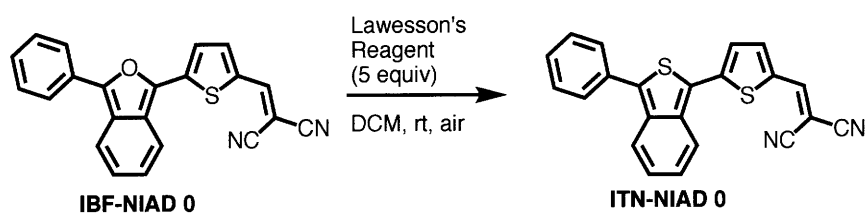
Lawesson's reagent (7.5 mg, 0.019 mmol) was added to a solution of **IBF-NIAD 0** (11 mg, 0.031 mmol) in dry dichloromethane (10 ml) and the reaction was stirred open to air for 3 hours. Another portion of Lawesson's reagent (52 mg, 0.13 mmol) was added and the reaction mixture was stirred for an addition 4 hours, monitored by thin later chromatography (dichloromethane). When the starting material had been consumed, the reaction mixture was purified by flash chromatography over silica gel (dichloromethane) to afford **ITN-NIAD 0** as a purple solid (10 mg, 0.027 mmol, 87% yield) ^{1}H NMR (300 MHz, CDCl$_3$): 8.08 (1H, dt, 8.9 Hz, 0.9 Hz), 7.88 (1H, dt, 8.9 Hz, 0.9 Hz), 7.78 (1H, s), 7.74-7.67 (3H, m), 7.59-7.44 (4H, m), 7.37 (1H, ddd, 8.9

Hz, 6.5 Hz, 0.9 Hz), 7.23 (1H, ddd, 8.9 Hz, 6.5 Hz, 0.9 Hz). ^{13}C NMR (125 MHz, CDCl$_3$): 149.5, 148.9, 140.2, 139.7, 136.9, 136.0, 133.2, 132.9, 129.4, 129.3, 128.8, 127.4, 125.2, 125.0, 124.6, 122.1, 121.3, 114.7, 113.9, 74.6. HRMS (EI): 368.0429 [calc'd for M$^+$: 368.0436]
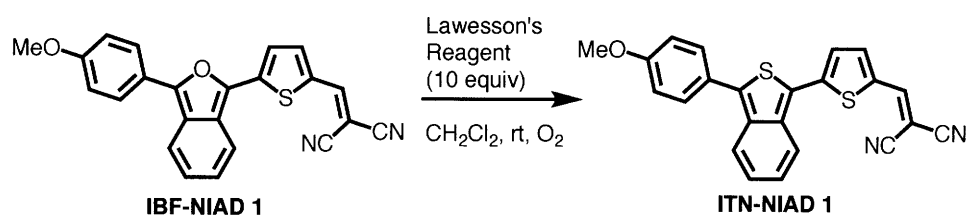
IBF-NIAD 1 (11 mg, 0.029 mmol) was dissolved in 10 ml of dry dichloromethane (10 ml) in a Schlenk flask along with Lawesson's reagent (55 mg, 0.14 mmol), and the solution was cooled to -78 °C. Anhydrous oxygen was bubbled through the solution for 5 minutes, after which the flask was sealed, and the reaction mixture was allowed to warm to room temperature and was stirred at room temperature for 3 hours. A second portion of Lawesson's reagent (55 mg, 0.14 mmol) was added and the reaction mixture was stirred at room temperature for 6 hours under an oxygen atmosphere. The reaction mixture was purified by flash chromatography over silica gel (dichloromethane) to afford **ITN-NIAD 1** as a purple solid (8.3 mg, 0.021 mmol, 72% yield). ^{1}H NMR (300 MHz, CDCl$_3$): 8.07 (1H, dt, 8.9 Hz, 0.9 Hz), 7.84 (1H, dt, 8.8 Hz, 0.9 Hz), 7.77 (1H, s), 7.71 (1H, d, 4.3 Hz), 7.63 (2H, d, 8.9 Hz), 7.48 (1H, d, 4.2 Hz), 7.36 (1H, ddd, 8.9 Hz, 6.5 Hz, 0.9 Hz), 7.21 (1H, ddd, 8.8 Hz, 6.5 Hz, 0.9 Hz), 7.08 (2H, dm, 8.9 Hz), 3.91 (3H, s). ^{13}C NMR (125 MHz, CDCl$_3$): 160.2, 149.4, 149.2, 140.7, 139.8, 136.9, 135.6, 132.9, 130.6, 127.4, 125.3, 125.3, 124.9, 124.7, 123.6, 122.2, 121.3, 114.8, 114.0, 74.0, 55.5. HRMS (EI): 398.0544 [calc'd for M$^+$: 398.0542]
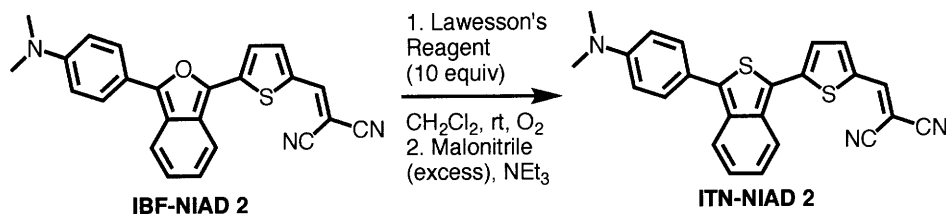
IBF-NIAD 2 (7.0 mg, 0.018 mmol) and Lawesson's reagent (70 mg, 0.17 mmol) were dissolved in dry dichloromethane (7 ml) in a Schlenk flask and the solution was cooled to -78 °C. Anhydrous oxygen was bubbled through the reaction mixture for 5 minutes, after which the flask was sealed, and the reaction mixture was allowed to warm to room temperature and was stirred at room temperature for 7 hours. Malonitrile (80 mg, 2.4 mmol) was then added along with triethylamine (0.1 ml) and the solution was stirred at room temperature under argon for 30 minutes. The reaction mixture was purified by flash chromatography over silica gel (dichloromethane) to afford **ITN-NIAD 2** as a blue solid (4.9 mg, 0.012 mmol, 67% yield). ^{1}H NMR (300 MHz, CDCl$_3$): 8.07 (1H, d, 8.9 Hz), 7.90 (1H, d, 8.8 Hz), 7.74 (1H, s), 7.68 (1H, d, 4.5 Hz), 7.59 (2H, d, 9.0 Hz), 7.45 (1H, d, 4.5 Hz), 7.35 (1H, ddd, 8.9 Hz, 6.3 Hz, 0.9 Hz), 7.18 (1H, ddd, 8.9 Hz, 6.5 Hz, 0.9 Hz), 6.85 (2H, d, 8.9 Hz), 3.08 (6H, s). ^{13}C NMR (125 MHz, DMF-d$_7$): 152.4, 152.2, 149.3, 143.6, 143.4, 138.1, 135.9, 134.0, 131.2, 128.8, 126.2, 125.9, 123.9, 123.0, 122.2, 121.0, 116.3, 115.8, 113.8, 73.5, 40.6. HRMS (EI): 411.0863 [calc'd for M^{+}: 411.0858]
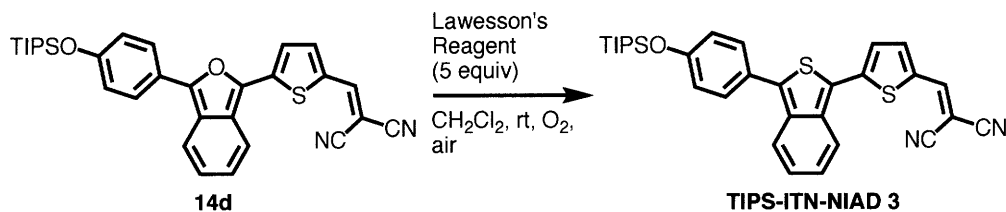

14d (13.7 mg, 0.026 mmol) and Lawesson's reagent (53 mg, 0.13 mmol) were dissolved in dry dichloromethane (10 ml) in a Schlenk flask and the solution was cooled to -78 °C. Anhydrous

oxygen was bubbled through the reaction mixture for 5 minutes, after which the flask was sealed, and the reaction mixture was allowed to warm to room temperature and was stirred at room temperature for 4 hours. The solution was then opened to air and stirred for an additional 3 hours at room temperature. The reaction mixture was purified by flash chromatography over silica gel (dichloromethane) to afford **TIPS-ITN-NIAD 3** as a blue solid (13.3 mg, 0.025 mmol, 96% yield). ^{1}H NMR (300 MHz, CDCl$_3$): 8.06 (1H, d, 8.9 Hz), 7.85 (1H, d, 8.9 Hz), 7.76 (1H, s), 7.70 (1H, d, 4.3 Hz), 7.55 (2H, d, 8.7 Hz), 7.47 (1H, d, 4.3 Hz), 7.35 (1H, ddd, 8.9 Hz, 6.5 Hz, 0.9 Hz), 7.20 (1H, ddd, 8.9 Hz, 6.3 Hz, 0.9 Hz), 1.31 (3H, sp, 7.0 Hz), 1.16 (18H, d, 7.1 Hz). ^{13}C NMR (125 MHz, CDCl$_3$): 157.1, 149.4, 149.2, 141.0, 139.8, 136.9, 135.6, 132.9, 130.5, 127.4, 125.5, 124.8, 124.7, 123.5, 122.3, 121.2, 120.7, 114.8, 114.0, 74.0, 17.9, 12.7. HRMS (EI): 540.1719 [calc'd for M$^+$: 540.1720]

TIPS-ITN-NIAD 3   →   **ITN-NIAD 3**

HCl
EtOH, 60 °C
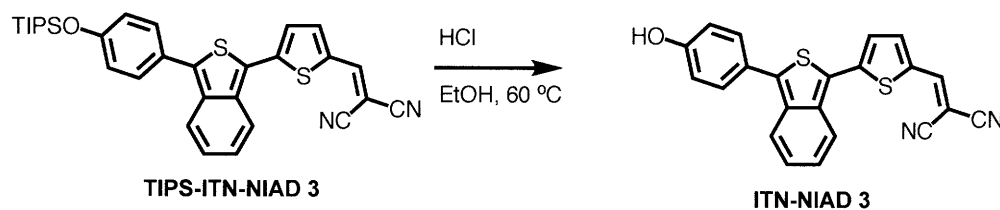
TIPS-ITN-NIAD 3 (34 mg, 0.063 mmol) was dissolved in ethanol (16 ml, 200 proof) at 60 °C. Hydrochloric acid (1.66 ml, 36%) was added and the reaction was stirred at 60 °C under argon for 18 hours. The reaction mixture was cooled to room temperature, diluted with ethyl acetate, and washed with water, saturated aqueous sodium bicarbonate, and brine, and was then dried over magnesium sulfate and concentrated in vacuo. Flash chromatography (2:1 ethyl acetate:hexane) afforded **ITN-NIAD 3** as a purple solid (13.5 mg, 0.035 mmol, 56% yield). ^{1}H NMR (500 MHz, DMSO-d$_6$): 9.17 (1H, s), 7.70 (1H, s), 7.10 (1H, dd, 8.9 Hz, 0.8 Hz), 7.04 (1H, d, 4.1 Hz), 6.95 (1H, dd, 8.9 Hz, 0.8 Hz), 6.83 (1H, dd, 4.1 Hz, 0.9 Hz), 6.67 (2H, d, 8.7 Hz),

6.54 (1H, dd, 8.9 Hz, 6.3 Hz), 6.38 (1H, dd, 8.9 Hz, 6.3 Hz), 6.09 (2H, d, 8.7 Hz). ^{13}C NMR (125 MHz, DMSO-d$_6$): 158.6, 151.7, 147.4, 142.3, 140.6, 136.2, 134.6, 132.8, 130.6, 127.7, 125.4, 125.11, 122.9, 122.5, 122.3, 120.8, 116.5, 115.1, 114.4, 72.4. HRMS (ESI): 383.0310 [calc'd for M-H$^-$: 383.0318]

2.5 References

(1)   Meyer, R.; Kleinert, H.; Richter, S.; Gewald, K. *J. Prakt. Chem.* **1963**, *20*, 244.

(2)   Wudl, F.; Kobayashi, M.; Heeger, A. J. *J. Org. Chem.* **1984**, *49*, 3382.

(3)   Brédas, J. L.; Heeger, A. J.; Wudl, F. *J. Chem. Phys.* **1986**, *85*, 4673.

(4)   Polec, I.; Henckens, A.; Goris, L.; Nicolas, M.; Loi, A.; Adriaensens, P. J.; Lutsen, L.; Manca, J. V.; Vanderzande, D.; Sariciftci, N. S. *J. Polym. Sci, Part A: Polym. Chem.* **2003**, *41*, 1034.

(5)   (a) *Handbook of Conducting Polmyers*, 2nd Ed.; Skotheim, T. A.; Elsenbaumer, R. L.; Reynolds, J. R., Eds.; CRC Press, New York, 1998. (b) *Handbook of Conducting Polmyers*, 3rd Ed.; Skotheim, T. A.; Elsenbaumer, R. L.; Reynolds, J. R., Eds.; CRC Press, New York, 2007.

(6)   Roncali, J. *Chem. Rev.* **1997**, *97*, 173

(7)   Vangeneugden, D. L.; Vanderzande, D. J. M.; Salbeck, J.; van Hal, P. A.; Janssen, R. A. J.; Hummelen, J. C.; Brabec, C. J.; Shaheen, S. E.; Sariciftci, N. S. *J. Phys. Chem. B,* **2001**, *105* , 11106.

(8)   Fein, A.; Shaier, P.; Zinger, B. Kotler, Z. *Proc. of SPIE* **1994**, *2285*, 394.

(9)   Hoogmartens, I.; Adriaensens, P.; Vanderzande, D.; Gelan, J.; Quattrocchi, C.; Lazzaroni, R.; Bredas, J. L. *Macromolecules* **1992**, *25*, 7347.

(10)   Hoogmartens, I.; Adriaensens, P.; Carleer, R.; Vanderzande, D., Martens, H.; Gelan, J. *Synth. Met.* **1992**, *51*, 219

(11)   Zerbi, G.; Magnoni, M. C.; Hoogmartens, I.; Kiebooms, R.; Carleer, R.;Vanderzande, D.; Gelan, J. *Adv. Mater.* **1995**, *7*, 1027

(12)   Kürti, J.; Surjan, P. R. *J. Chem. Phys.* **1990**, *92*, 3247.

(13)   Mitschke, U.; Bauerle, P. *J. Chem. Soc., Perkin Trans. 1* **2001**, *7*, 740.

(14)   Mohanakrishnan, A. K.; Lakshmikantham, M. V.; McDougal, C. D.; Cava, M. P.; Baldwin, J. W.; Metzger, R. M. *J. Org. Chem.* **1998**, *63*, 3105–3112.

(15)   Xiang, Z.; Nesterov, E. E.; Skoch, J.; Lin, T.; Hyman, B. T.; Swager, T. M.; Bacskai, B. J.; Reeves, S. A. *J. Histochem. Cytochem.* **2005**, *53*, 1511.

(16)   Nesterov, E. E., Unpublished results.

(17)   Shimizu, Y.; Shen, Z.; Ito, S.; Uno, H.; Daub, J.; Ono, N. *Tetrahedron Lett.*, **2002**, *43*, 8485.

(18)   Qin, Y.; Kim, J. Y.; Frisbie, C. D.; Hillmyer, M. A. *Macromolecules*, **2008**, *41*, 5563.

(19)   Lorcy, D.; Cava, M. P. *Adv. Mater.* **1992**, *4*, 562.

(20)   Mohanakrishnan, A. K.; Amaladass, P. *Tetrahedron Lett.* **2005**, *46*, 4225.

(21)   Baüerle, P.; Götz, G.; Emerle, P.; Port, H. *Adv. Mater.* **1992**, *4*, 564.

(22)   Guyot, A.; Catel, J. *Bull. Soc. Chim. Fr.* **1906**, *35*, 1124.

(23)   Wittig, G.; Pohmer, L. *Chem. Ber.* **1956**, *89*, 1334.

(24)   Friedrichsen, W. *Adv. Heterocycl. Chem.* **1999**, *73*, 1.

(25)   Dewar, J. S.; Harget, A. J.; Trinajstic, N.; Worley, S. D. *Tetrahedron* **1970**, *26*, 4505

(26)   Jursic, B. S. *THEOCHEM* **1999**, *468*, 171.

(27)   Zhou, Z.; Parr, R. G. *J. Am. Chem. Soc.* **1989**, *111*, 7371.

(28)   Jursic, B. S. *J. Heterocycl. Chem.* **1996**, *33*, 1079.

(29)   Warrener, R. N. *J. Am. Chem. Soc.* **1971**, *93*, 2346.

(30)   Rodrigo, R.; Knabe, S. M.; Taylor, N. J.; Rajapaksa, D.; Chernishenko, M. *J. Org. Chem.* **1986**, *51*, 3973.

(31)   Subramanian, G.; Schleyer, P. R.; Jiao, H. *Angew Chem. Int. Ed.* **1996**, *35*, 2638.

(32)   Martinez, A.; Vazquez, M.; Carreon-Marcedo, J. L.; Sansores, L. E.; Salcedo, R. *Tetrahedron* **2003**, *59*, 6415.

(33)   Jursic, B. S. *THEOCHEM* **1998**, *427*, 165

(34)   Kende, A. S.; Curran, D. P.; Tsay, Y.; Mills, J. E. *Tet. Lett.* 1977, 3537

(35)   Keay, B. A.; Rodrigo, R.; *J. Am. Chem. Soc.* **1982**, *104*, 4725

(36)   Hunger, J.; Wolff, C.; Tochtermann, W.; Peters, E. M.; Peters, K.; von Schnering, H. G. *Chem. Ber.* **1986**, *119*, 2698.

(37)   Prato, M.; Suzuki, T.; Foroudian, H.; Li, Q.; Khemani, K.; Wudl, F.; Leonetti, J.; Little, R. D.; White, T.; Rickborn, B., Yamago, S.; Nakamura, E. *J. Am. Chem. Soc.* **1993**, *115*, 1594

(38)   Warrener, R. N. *J. Am. Chem. Soc.* **1971**, *93*, 2346.

(39)   Wiersum, U.E.; Mijs, W. J.; *J. Chem. Soc., Chem. Commun.* **1972**, 347.

(40)   Crump, S. L.; Rickborn, B. *J. Org. Chem.* **1984**, *49*, 304.

(41)   Dodge, J. A.; Bain, J. D.; Chamberlin, A. R. **1990**, *55*, 4190.

(42)   Kuninobu, Y.; Nishina, Y.; Nakagawa, C.; Takai, K. *J. Am. Chem. Soc.* **2006**, *128*, 12376.

(43)   Zhang, H.; Wakamiya, A.; Yamaguchi, S. *Org. Lett.*, **2008**, *10*, 3591.

(44)   Amaladass, P.; Clement, J. A.; Mohanakrishnan, A. K. **2008**, 3798.

(45)   Haugen, C. M.; Bergmark, W. R.; Whitten, D. G. *J. Am. Chem. Soc.* **1992**, *114*, 10293.

(46)   Li, J. Y.; Hong, Z. R.; Wang, P. F.; Lee, C. S.; Wong, N. B.; Kwong, H. L.; Lee, S. T. *Thin Solid Films* **2004**, *446*, 111.

(47)   Maindron, T.; Dodelet, J. P.; Lu, J.; Hlil, A. R.; Hay, A. S.; D'Iorio, M. *Synth. Met.* **2002**, *130*, 247

(48)   Choi, H.; Amara, J. P.; Martin, T. P.; Gleason, K. K.; Swager, T. M.; Jensen, K. F. *Chem. Mater.* **2006**, *18*, 6339.

(49)   Ollsen, Ylva, M.S. Thesis, Massachusetts Institute of Technology, Cambridge, MA, 2003.

(50)   Lagerstedt, I.; Wennerstroem, O. *Synth. Met.* **1987**, *20*, 269

(51)   Friedrichsen, W. *Adv. Heterocycl. Chem.* **1980**, *26*, 135.

(52)   Haynes, R. K.; Peters, J. M.; Wilmot, I. D. *Aust. J. Chem.* **1980**, *33*, 2653.

(53)   *Encyclopedia of Reagents for Organic Synthesis, Online Ed.*; Kierkus, P. C.; John Wiley & Sons, Ltd., 2001.

(54)   Demas, J. N.; Crosby, G. A. *J. Phys. Chem.* **1971**, *75*, 991.

(55)   Barili, P. L.; Scartoni, V. *J. Heterocycl.Chem.* **1985**, *22*, 1199.

(56)   Al-Hamdany, R.; Al-Rawi, J. M.; Ibrahim, S. *J. Prakt. Chem.* **1987**, *329*, 126.

(57)   Johnson, A. L. *J. Org. Chem.* **1976**, *41*, 1320.
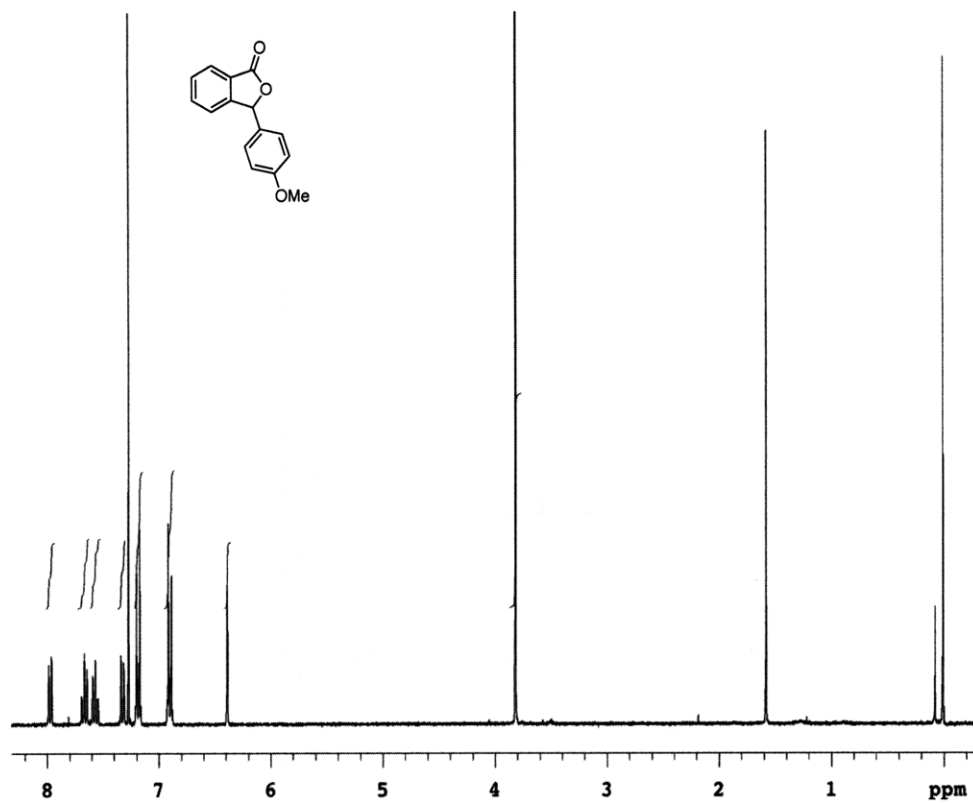
2.A Appendix

^{1}H NMR and ^{13}C NMR Spectra
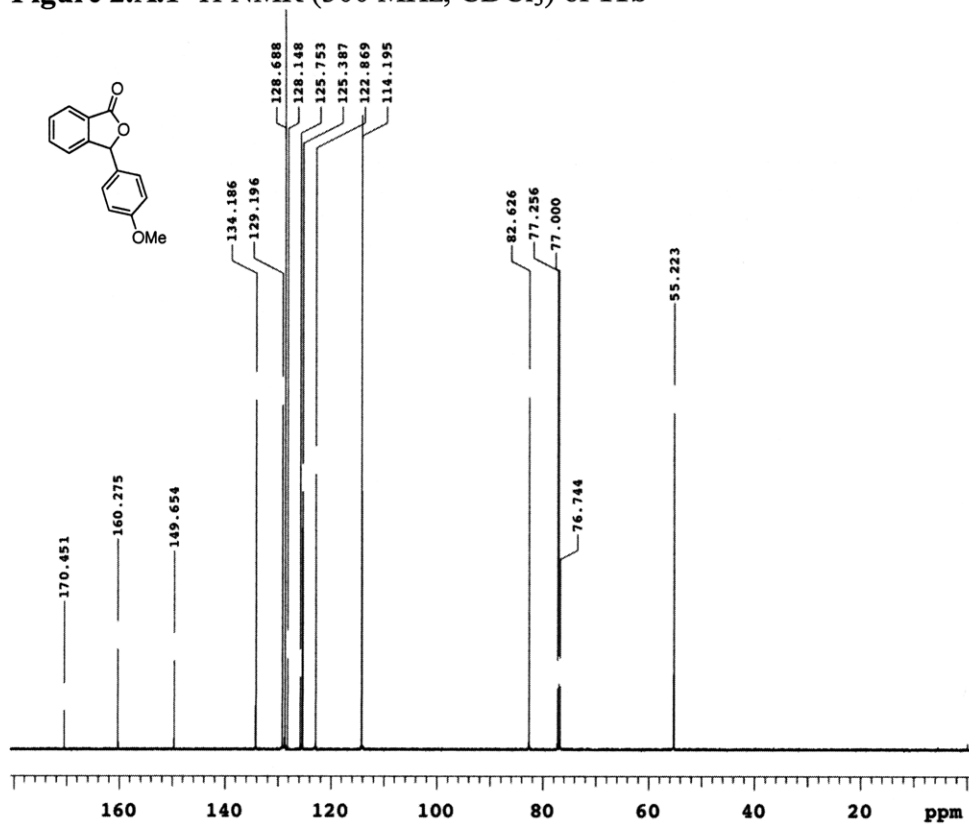
Figure 2.A.1 ^{1}H NMR (300 MHz, CDCl$_3$) of **11b**

Figure 2.A.2 ^{13}C NMR (125 MHz, CDCl$_3$) of **11b**

76

Figure 2.A.3 ^{1}H NMR (300 MHz, CDCl$_3$) of **11c**
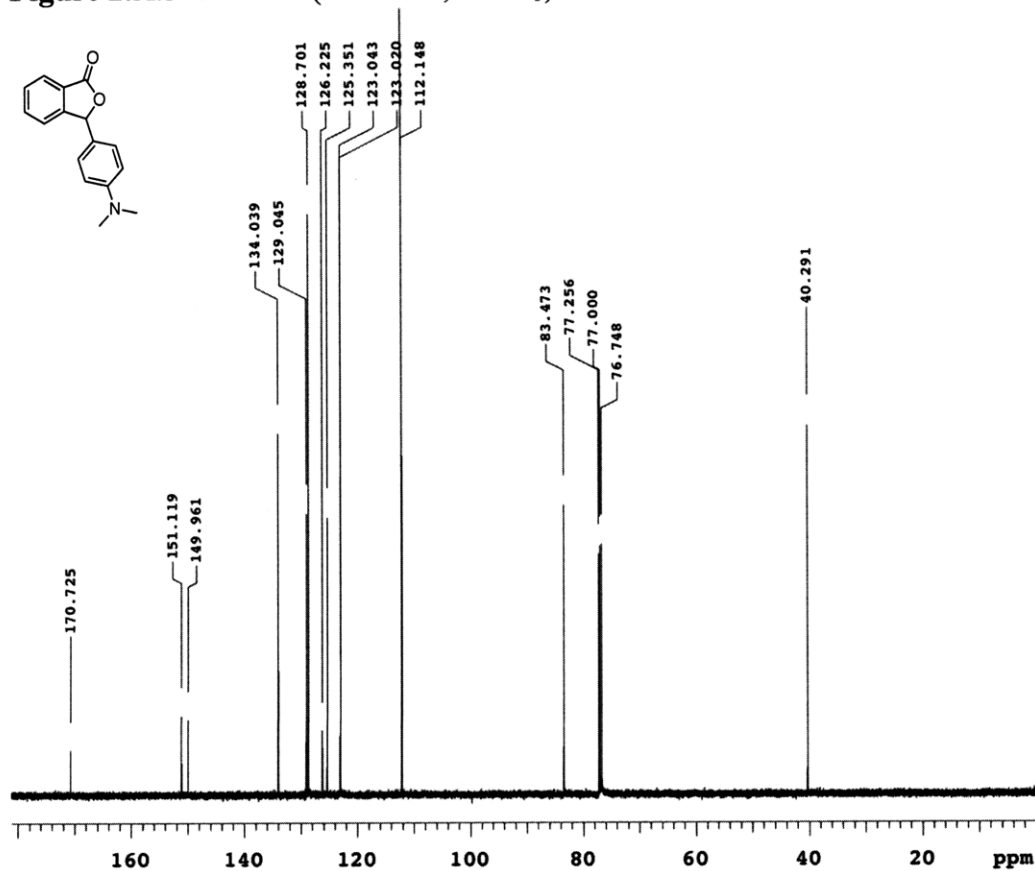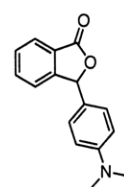
Figure 2.A.4 ^{13}C NMR (125 MHz, CDCl$_3$) of **11c**

Figure 2.A.5 ^{1}H NMR (300 MHz, CDCl$_3$) of **16**
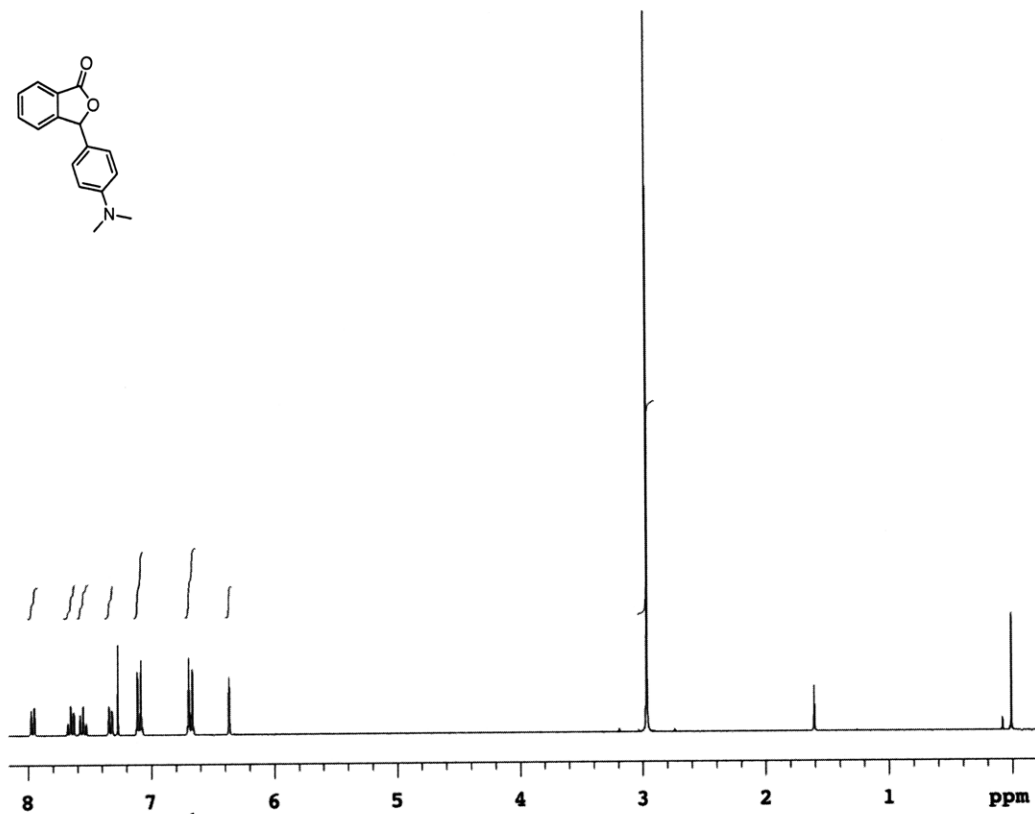

Figure 2.A.6 ^{13}C NMR (125 MHz, CDCl$_3$) of **16**

Figure 2.A.7 ^{1}H NMR (300 MHz, CDCl$_3$) of **11d**

Figure 2.A.8 ^{13}C NMR (125 MHz, CDCl$_3$) of **11d**

79

Figure 2.A.9 ^{1}H NMR (300 MHz, CDCl$_3$) of **15**

Figure 2.A.10 ^{13}C NMR (125 MHz, CDCl$_3$) of **15**
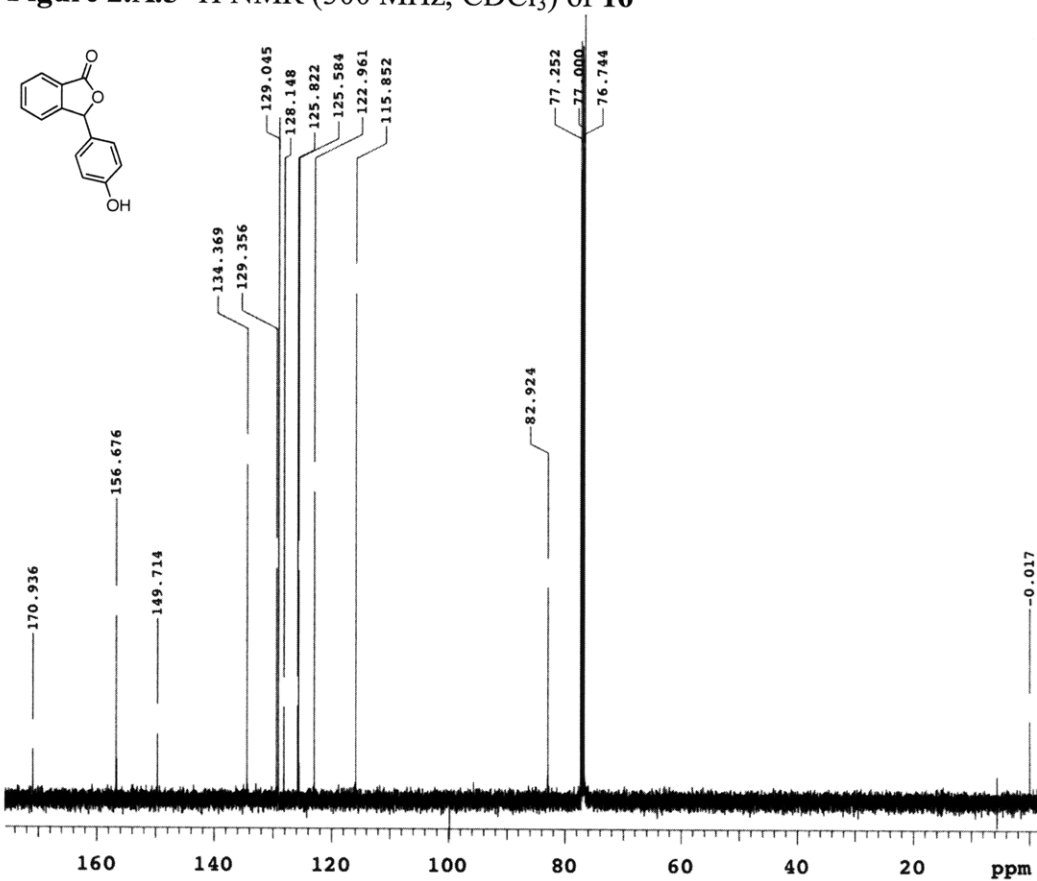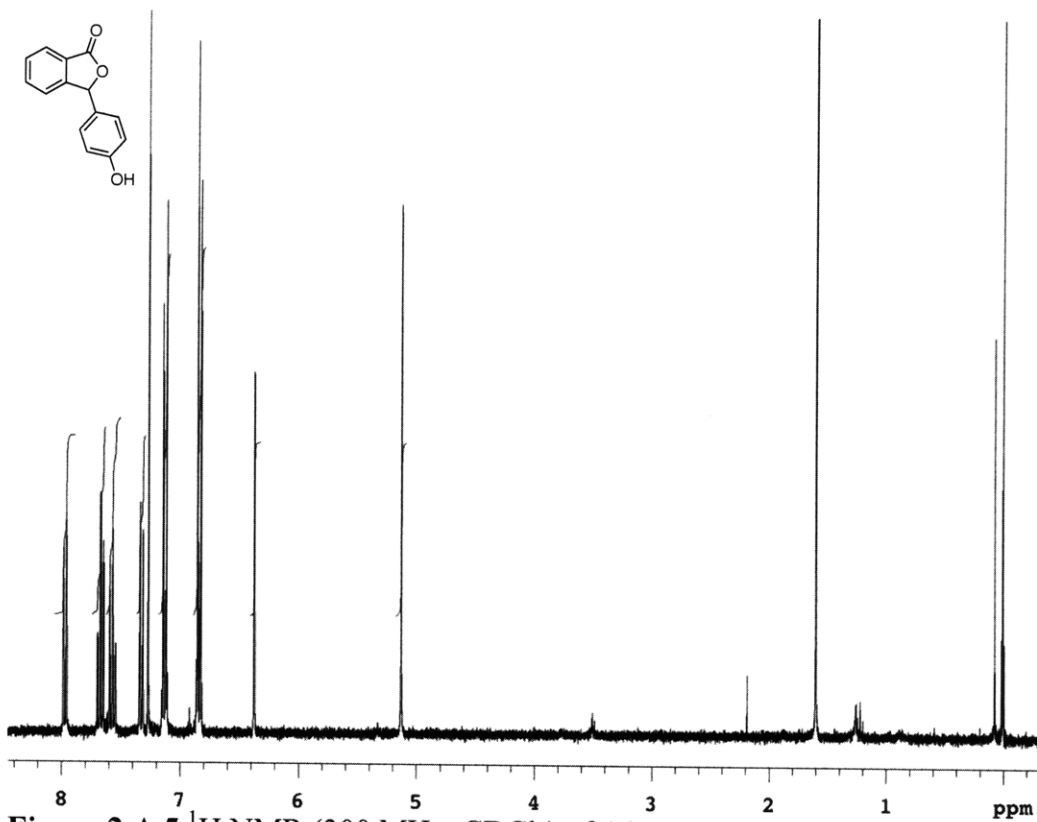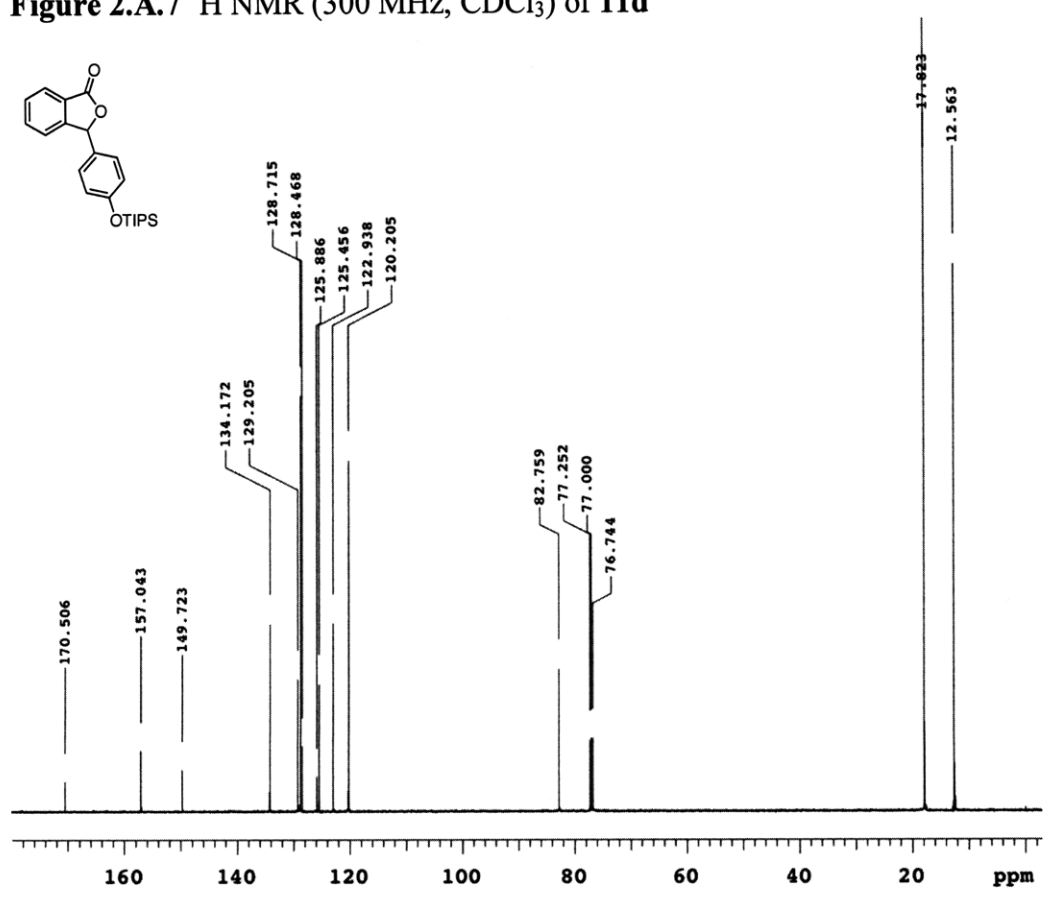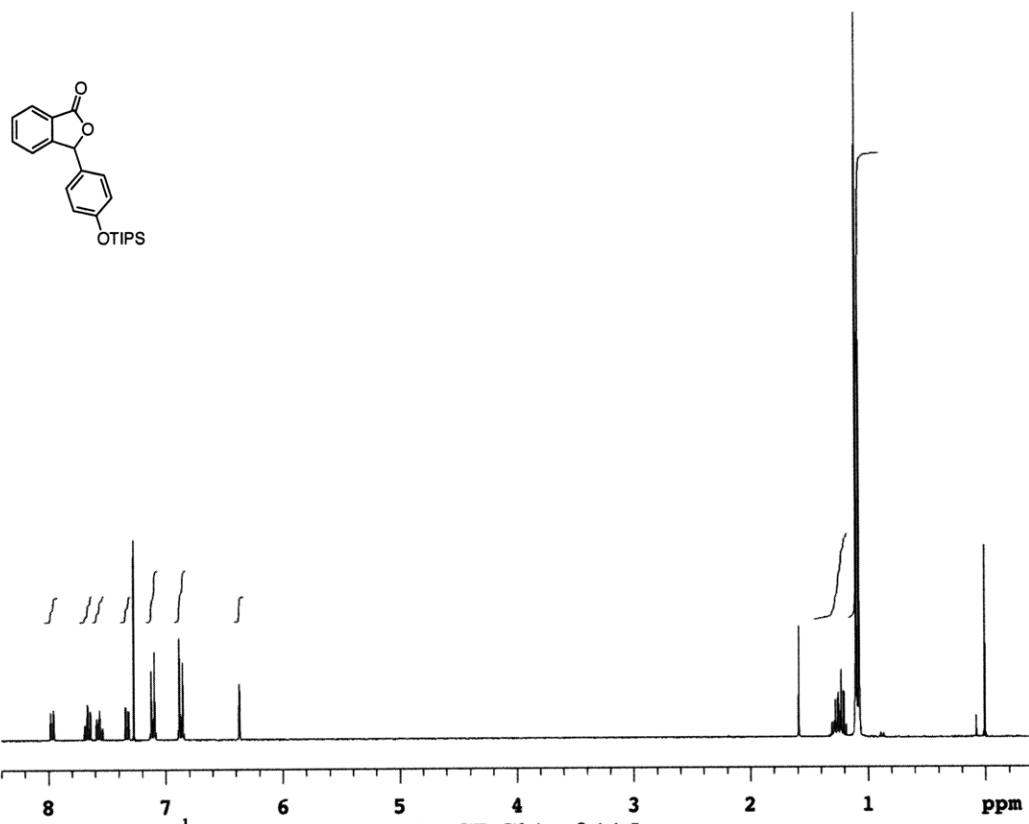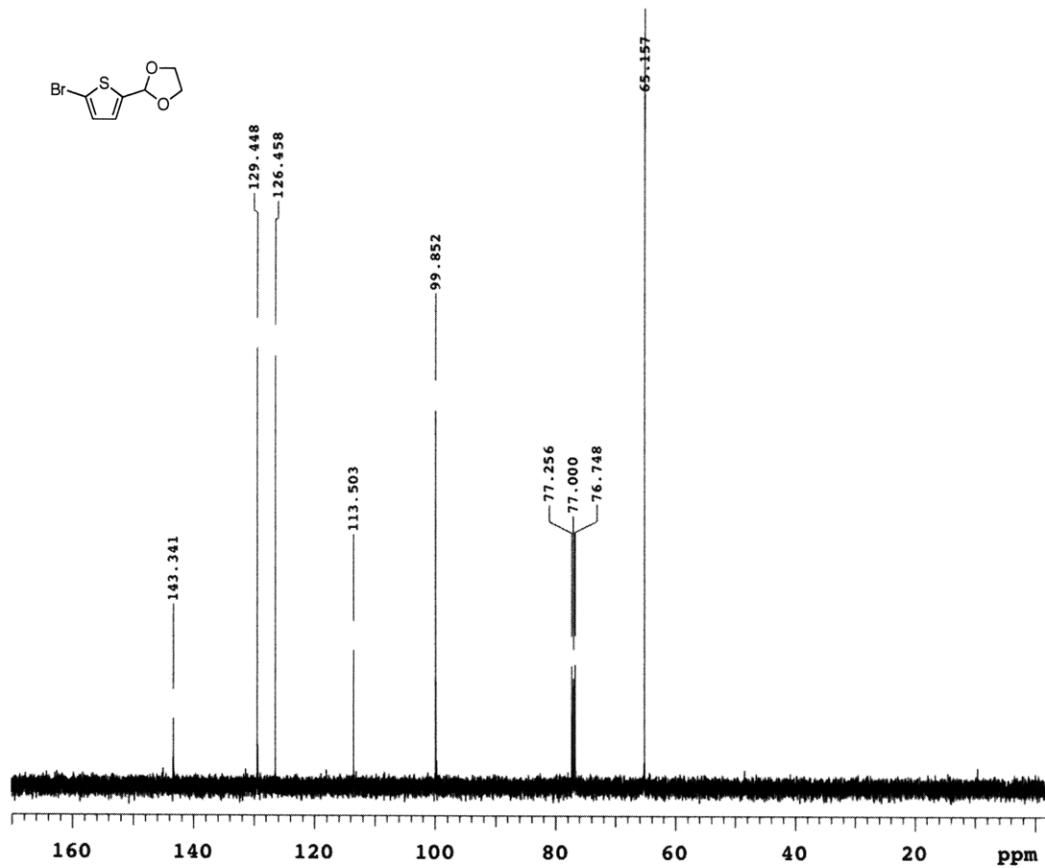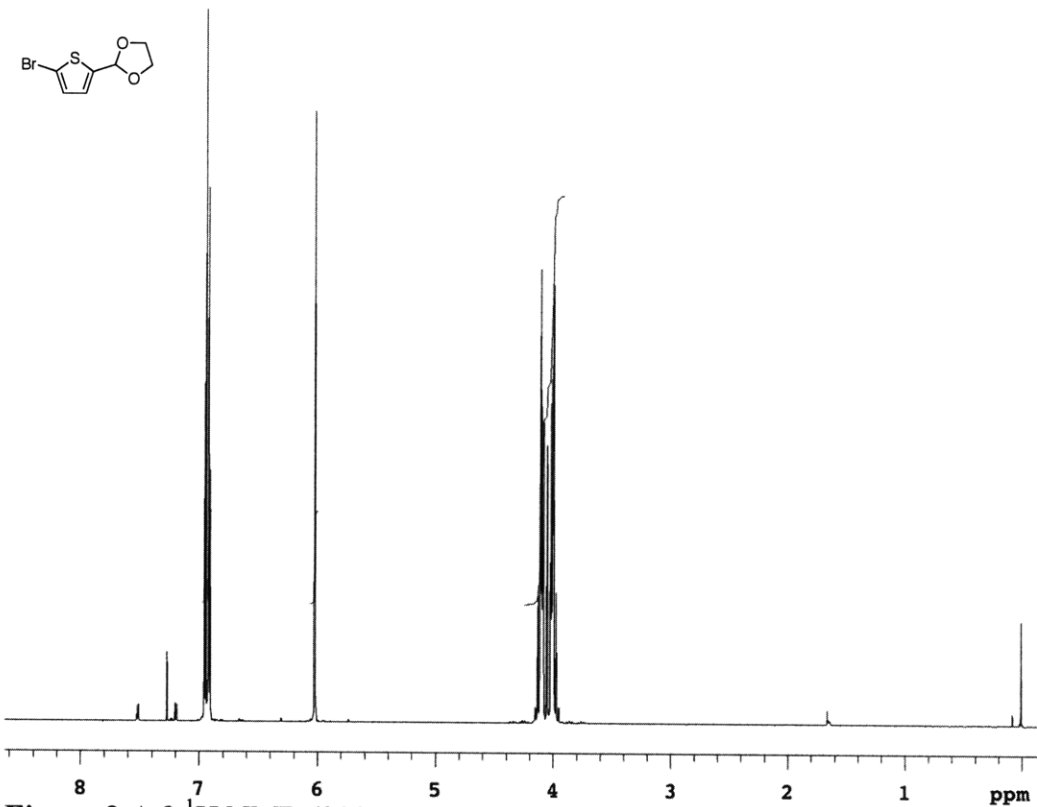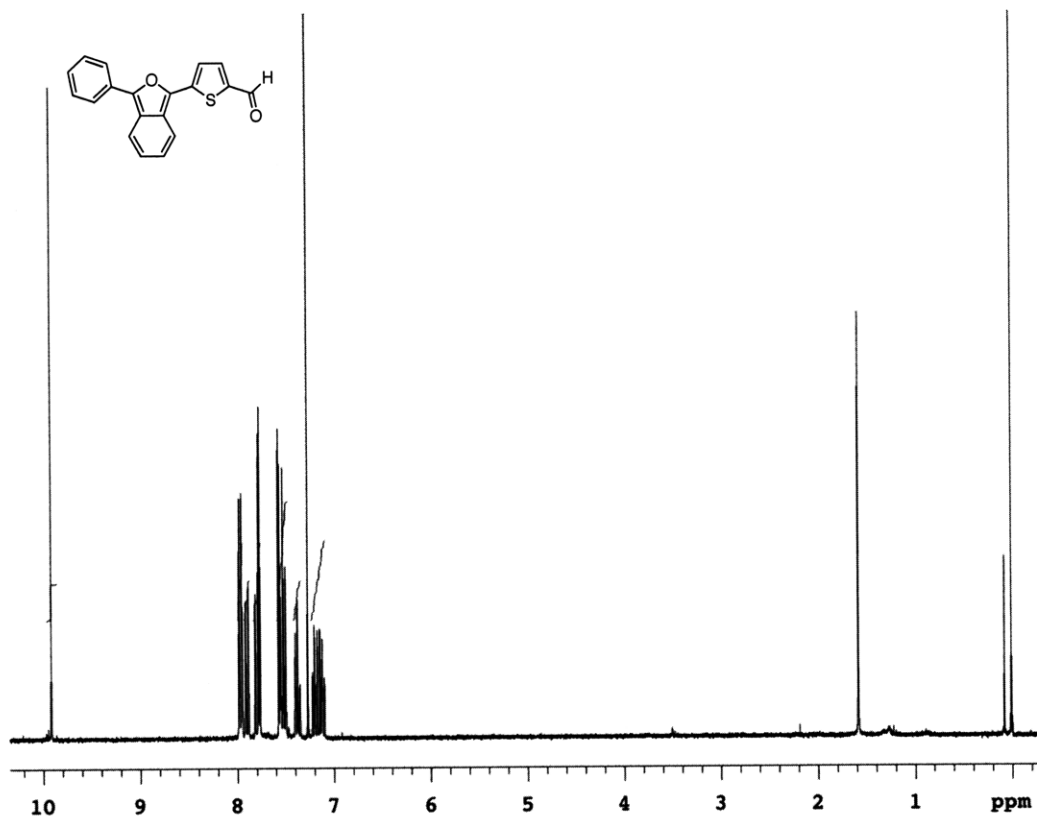
Figure 2.A.11 ^{1}H NMR (300 MHz, CDCl$_3$) of **13a**
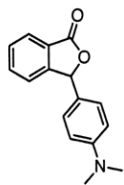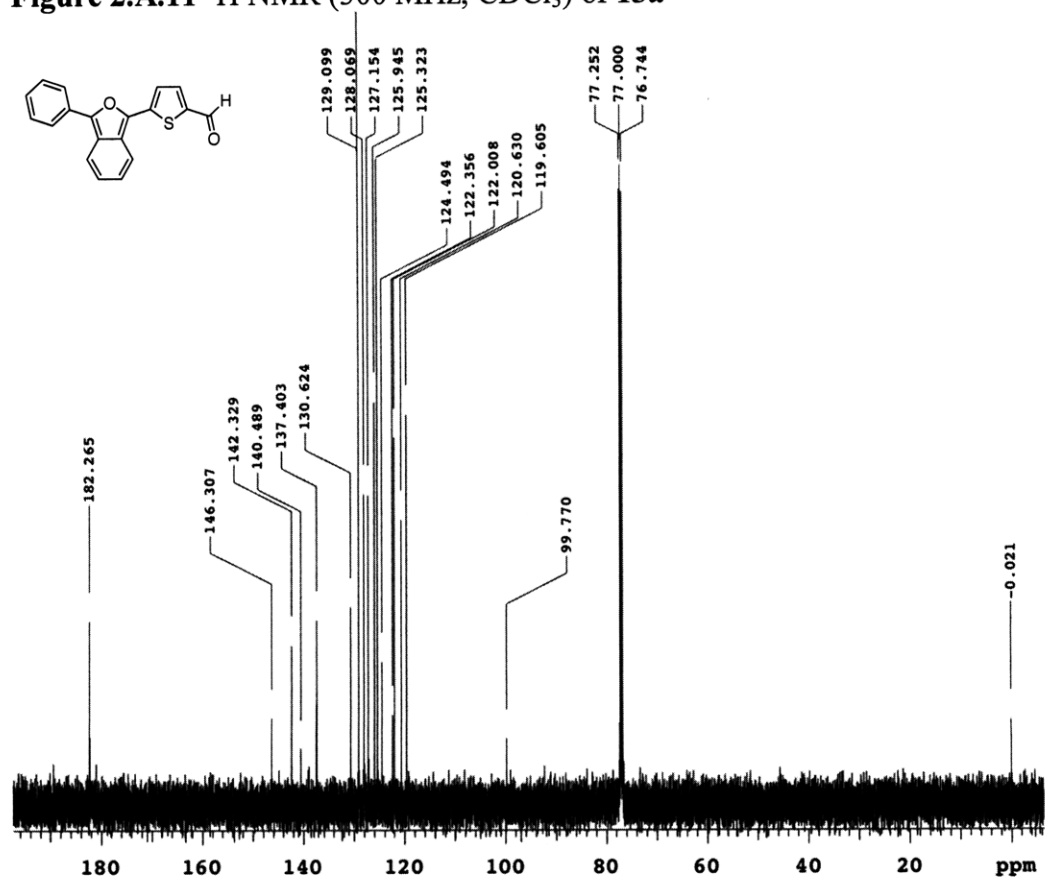

Figure 2.A.12 ^{13}C NMR (125 MHz, CDCl$_3$) of **13a**

81
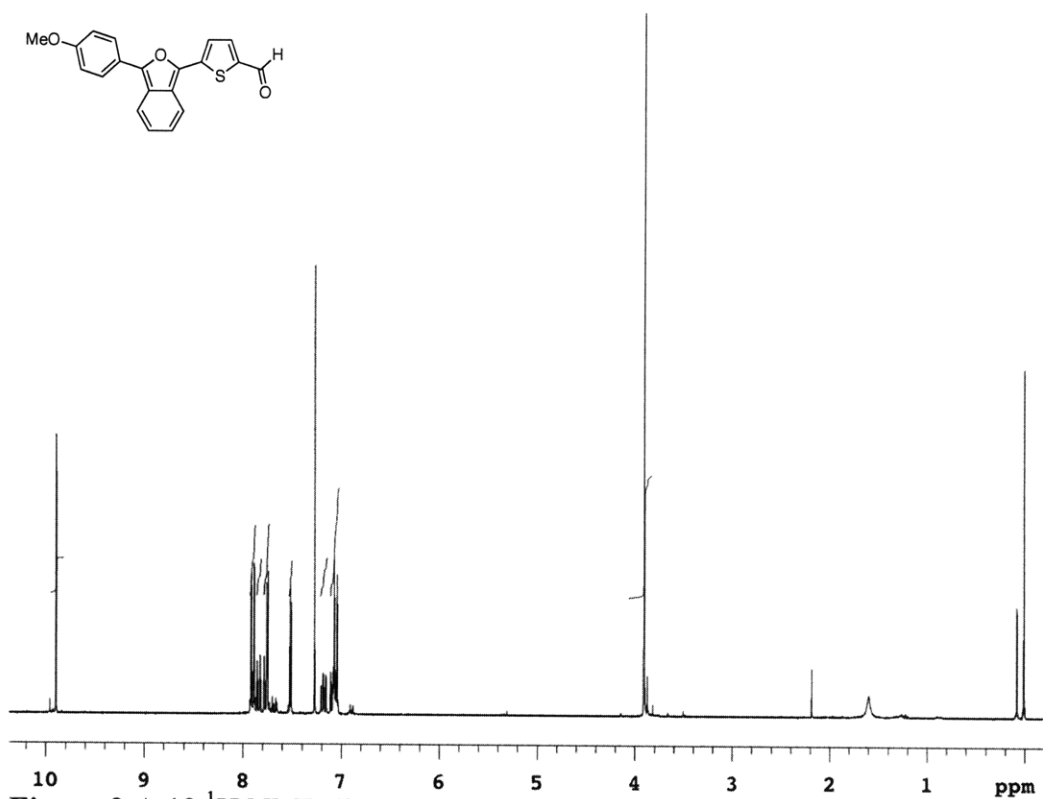
Figure 2.A.13 ^{1}H NMR (300 MHz, CDCl$_3$) of **13b**
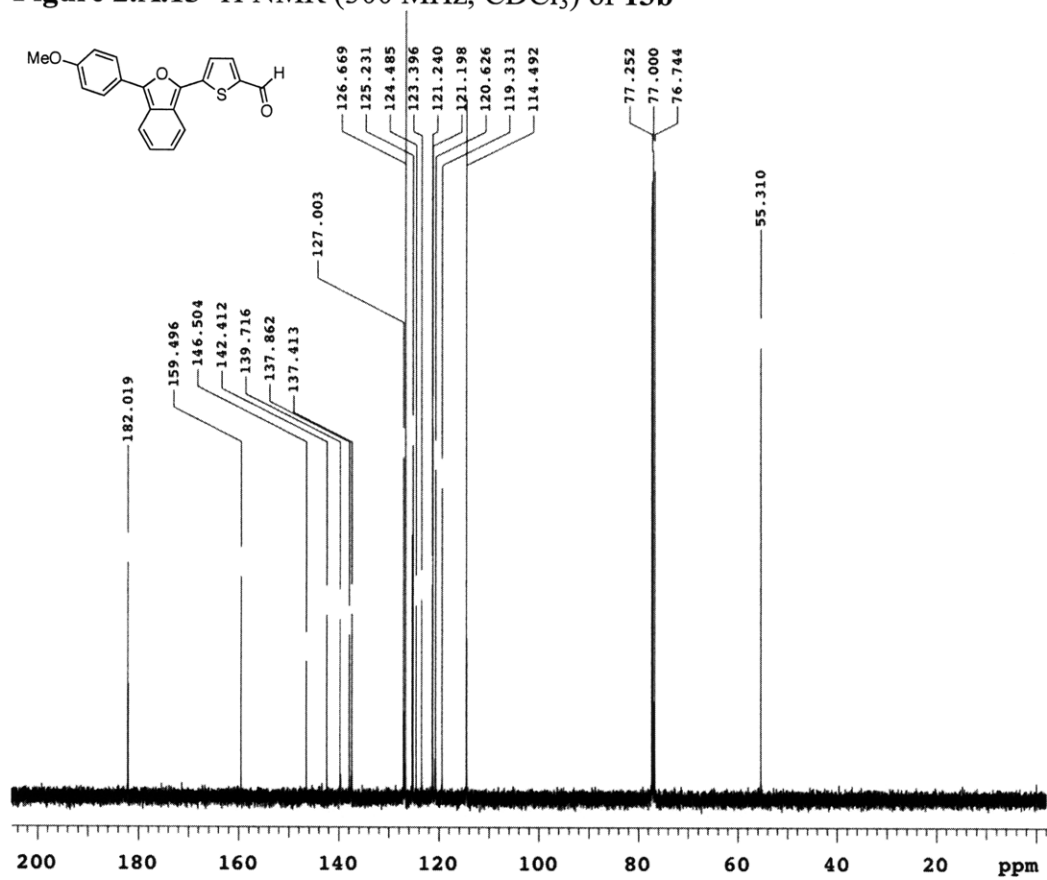
Figure 2.A.14 ^{13}C NMR (125 MHz, CDCl$_3$) of **13b**
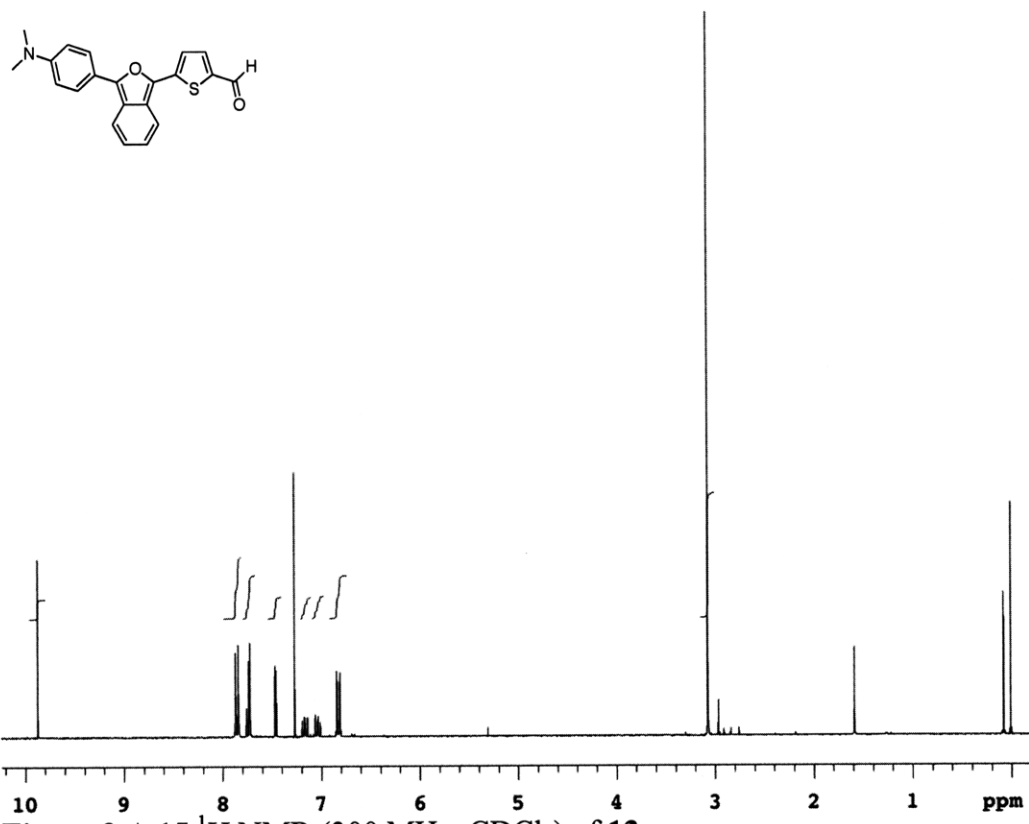
Figure 2.A.15 ^{1}H NMR (300 MHz, CDCl$_3$) of **13c**
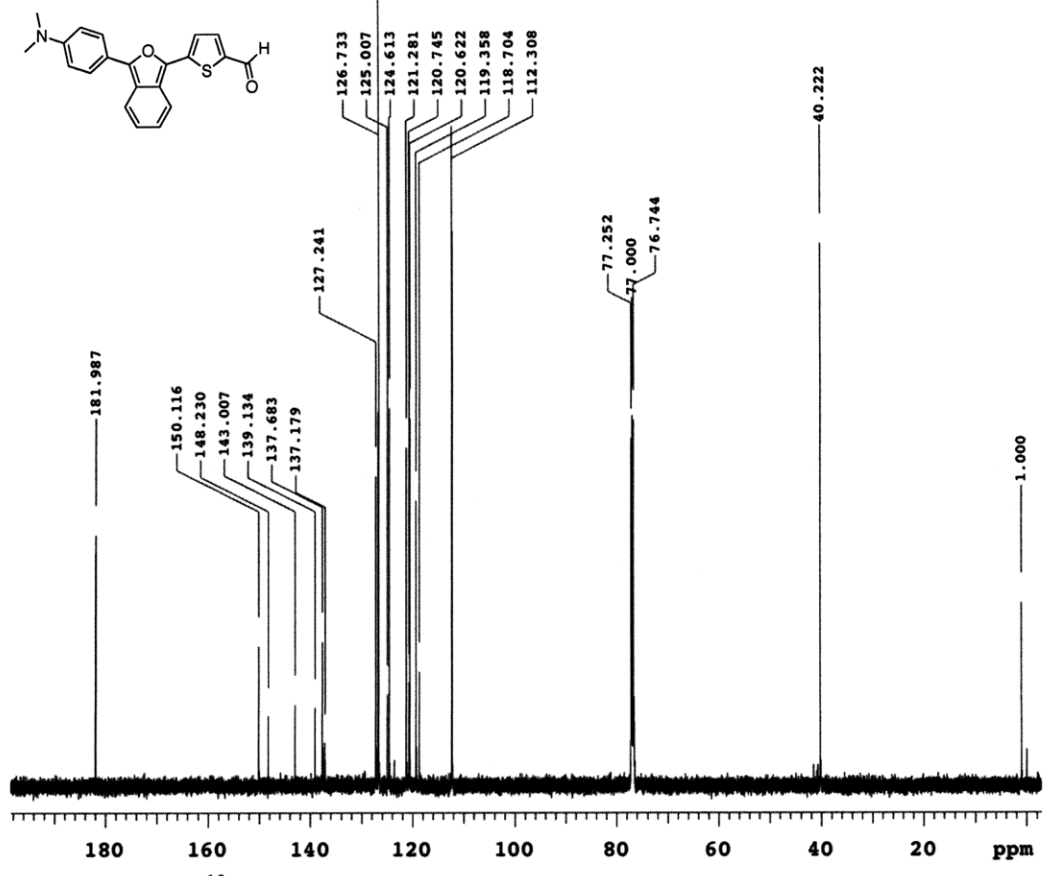
Figure 2.A.16 ^{13}C NMR (125 MHz, CDCl$_3$) of **13c**

Figure 2.A.17 ¹H NMR (300 MHz, CDCl₃) of **13d**

Figure 2.A.18 ¹³C NMR (125 MHz, CDCl₃) of **13d**
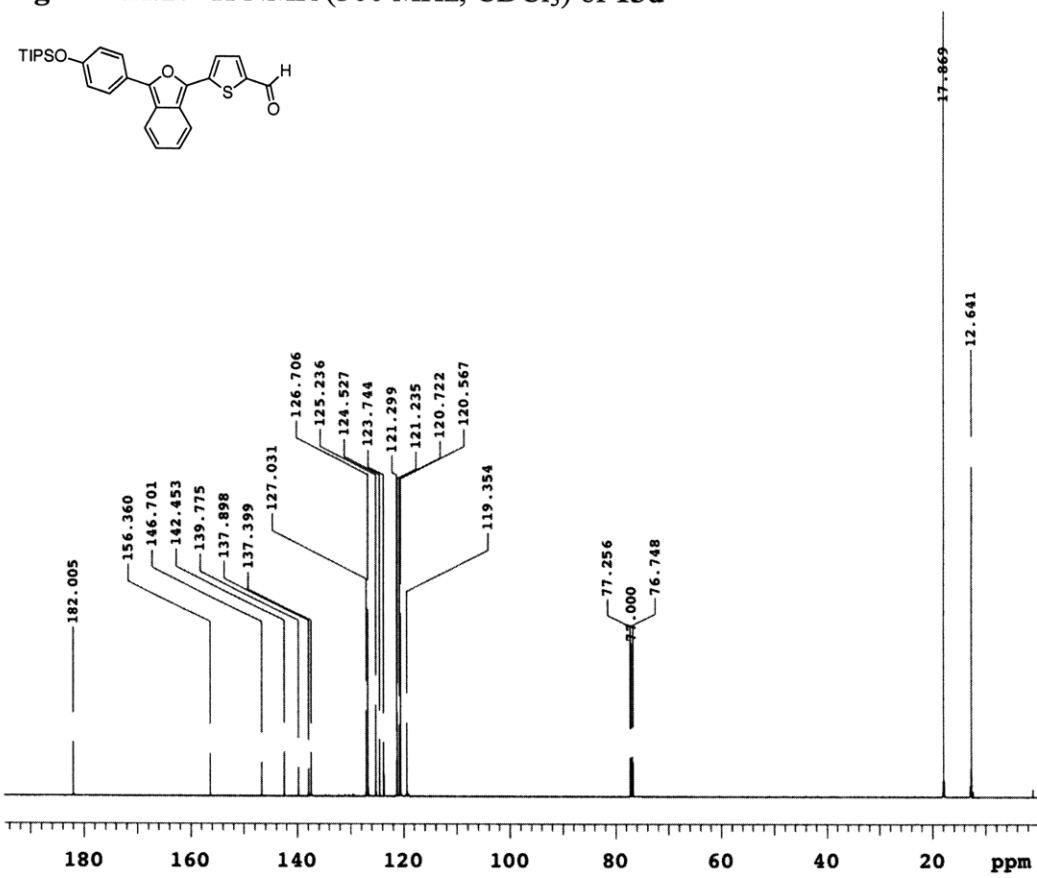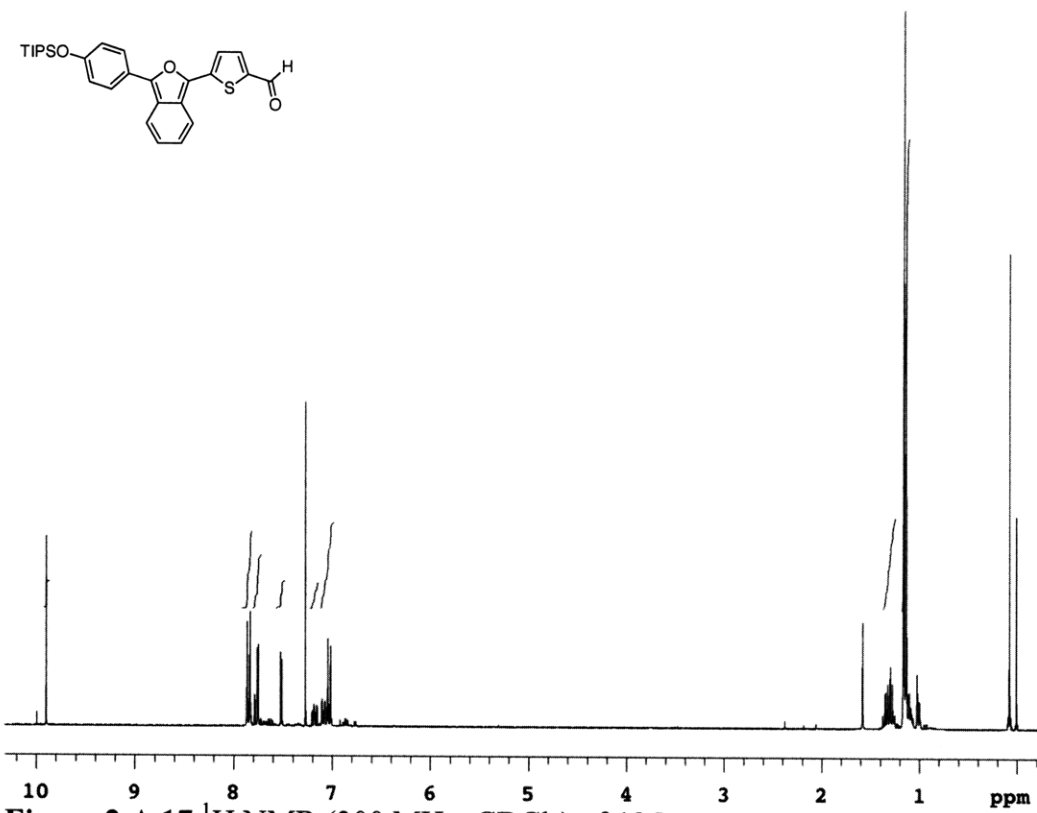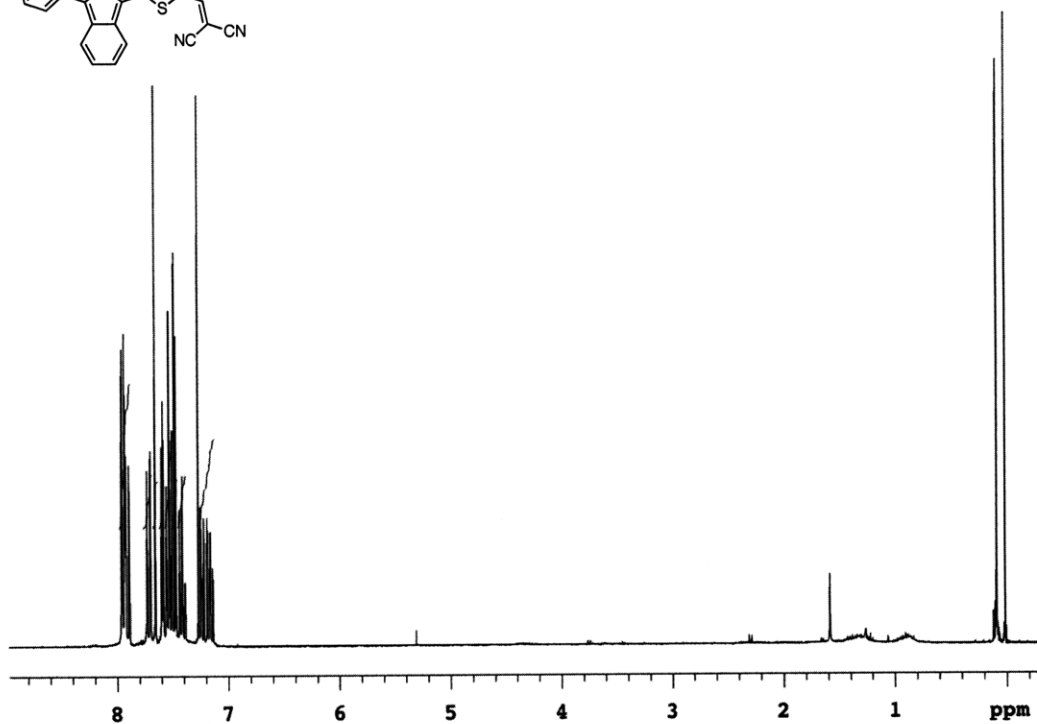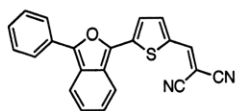
Figure 2.A.19 ^{1}H NMR (300 MHz, CDCl$_3$) of **IBF-NIAD 0**
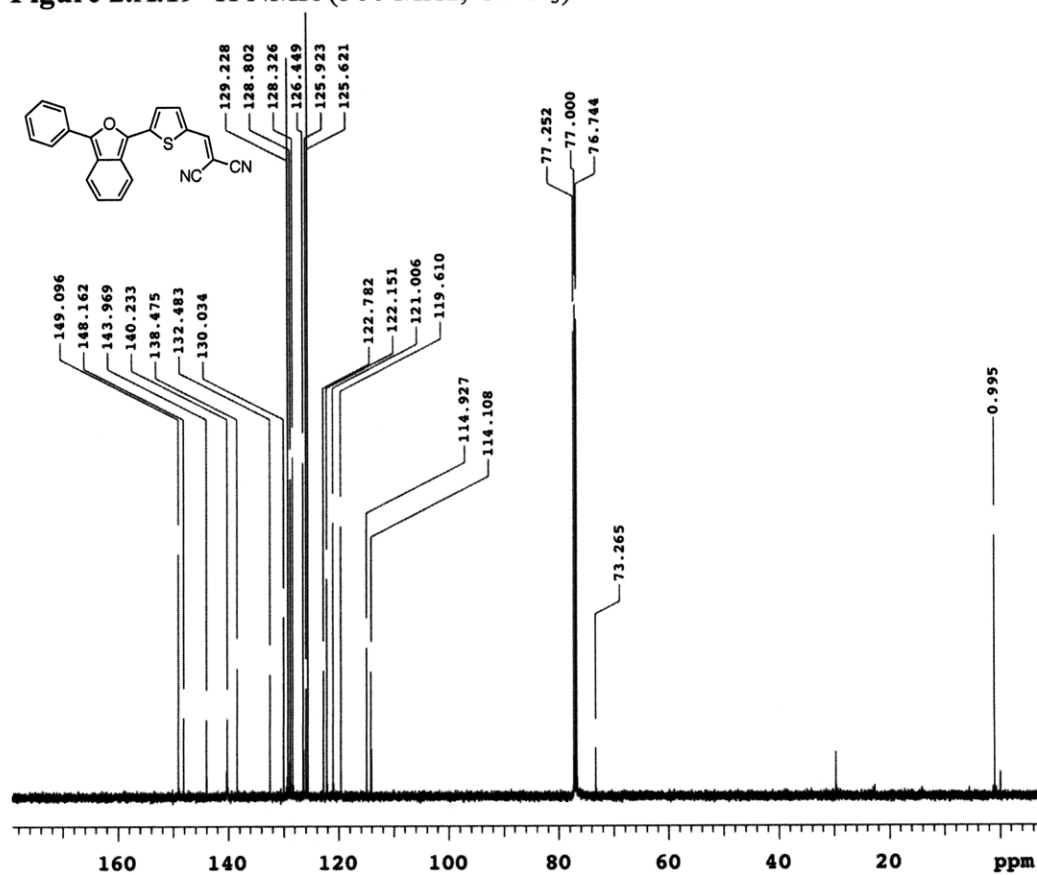
Figure 2.A.20 ^{13}C NMR (125 MHz, CDCl$_3$) of **IBF-NIAD 0**
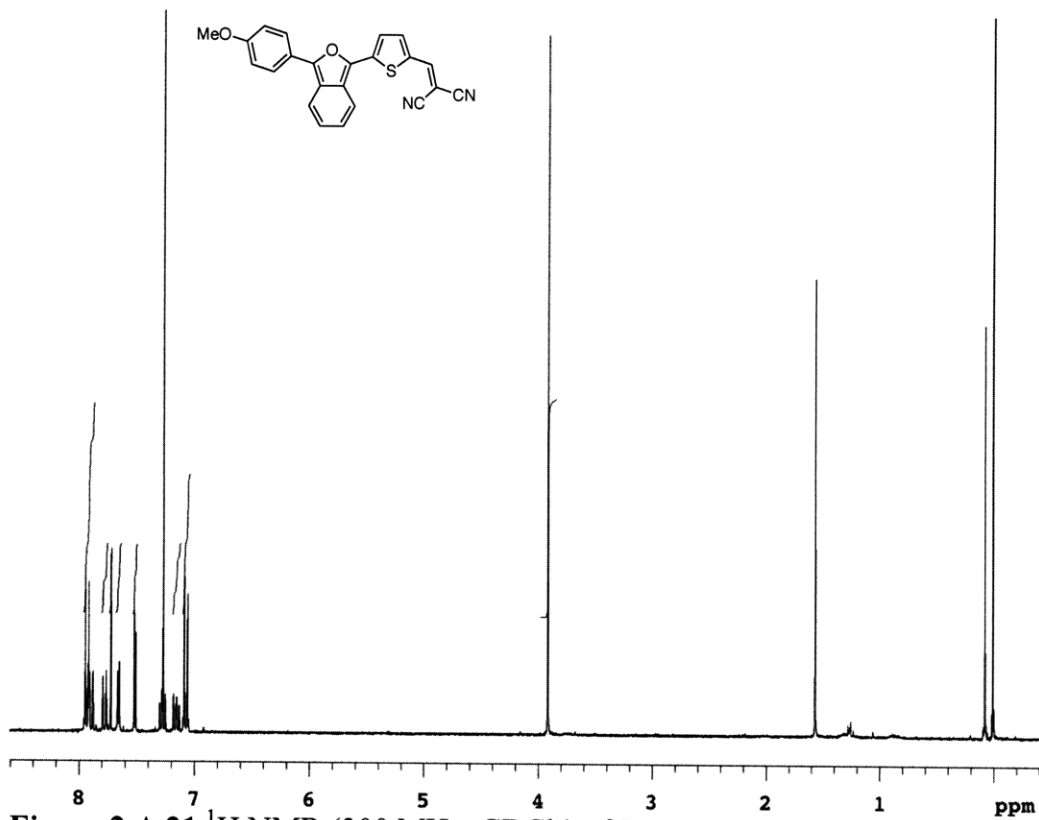
Figure 2.A.21 ^{1}H NMR (300 MHz, CDCl$_3$) of **IBF-NIAD 1**
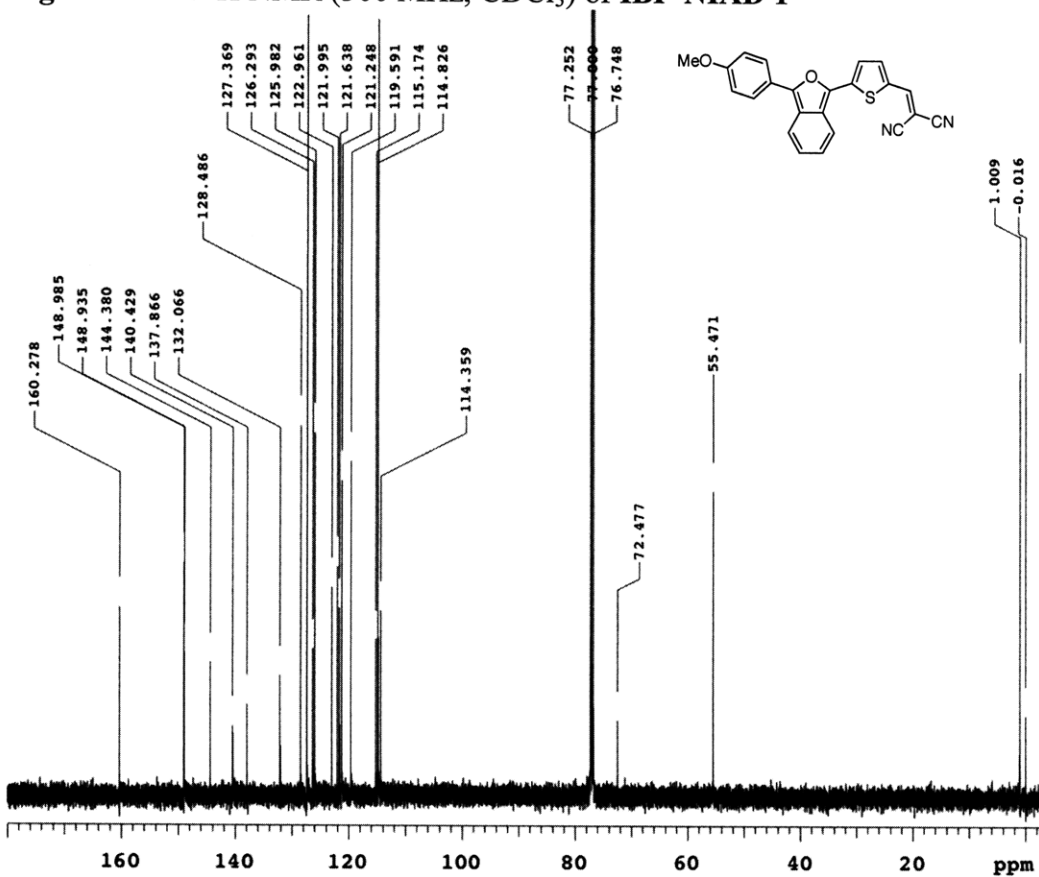
Figure 2.A.22 ^{13}C NMR (125 MHz, CDCl$_3$) of **IBF-NIAD 1**

Figure 2.A.23 ^{1}H NMR (300 MHz, CDCl$_3$) of **IBF-NIAD 2**
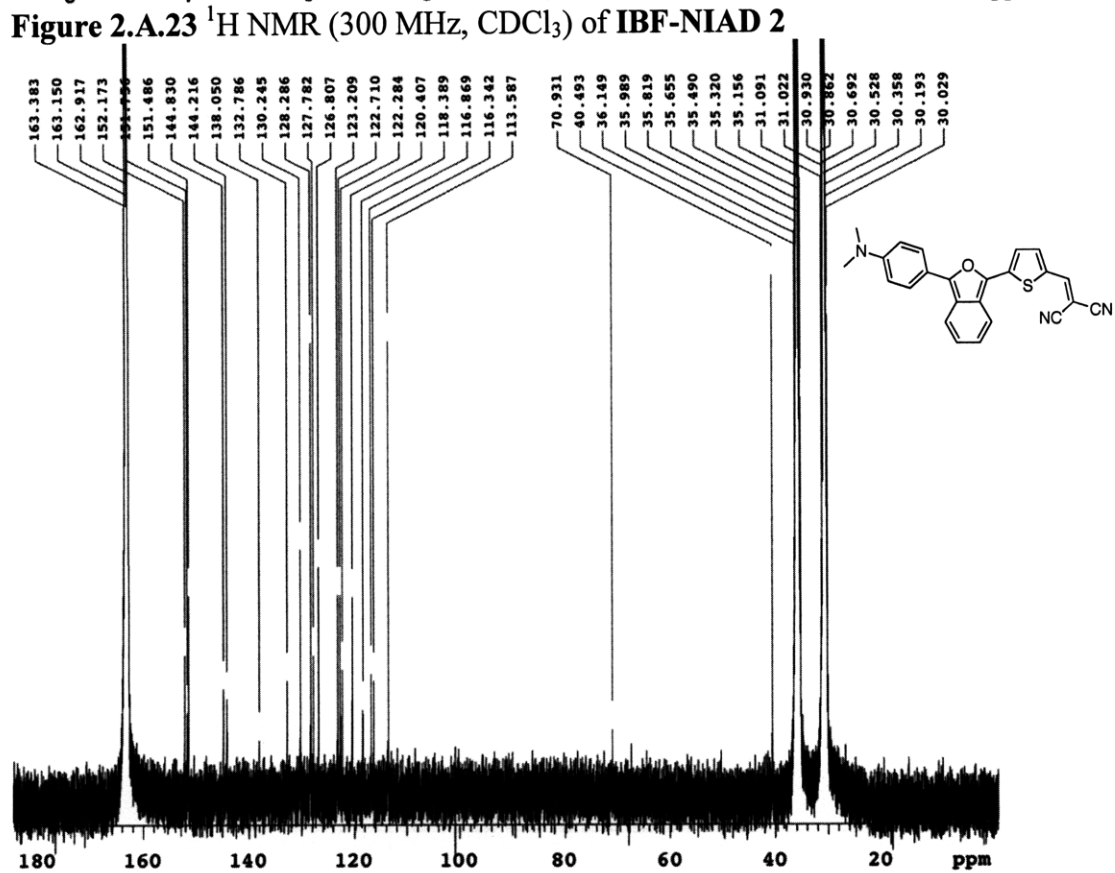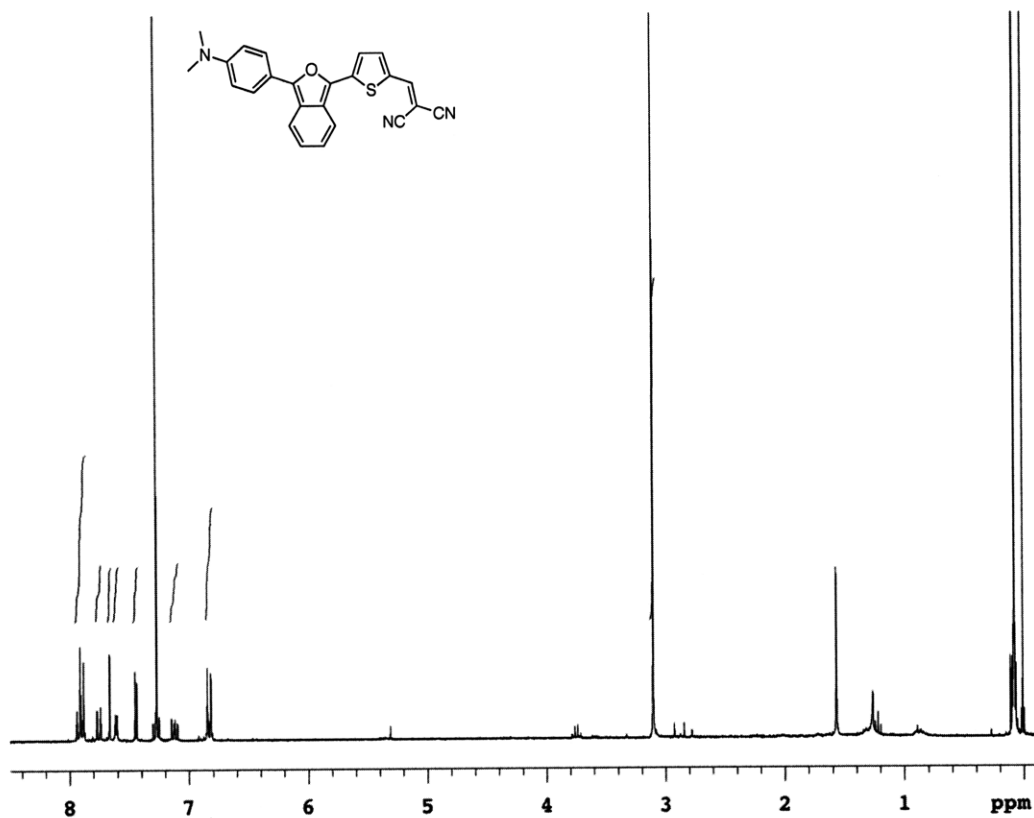
Figure 2.A.24 ^{13}C NMR (125 MHz, DMF-d$_7$) of **IBF-NIAD 2**
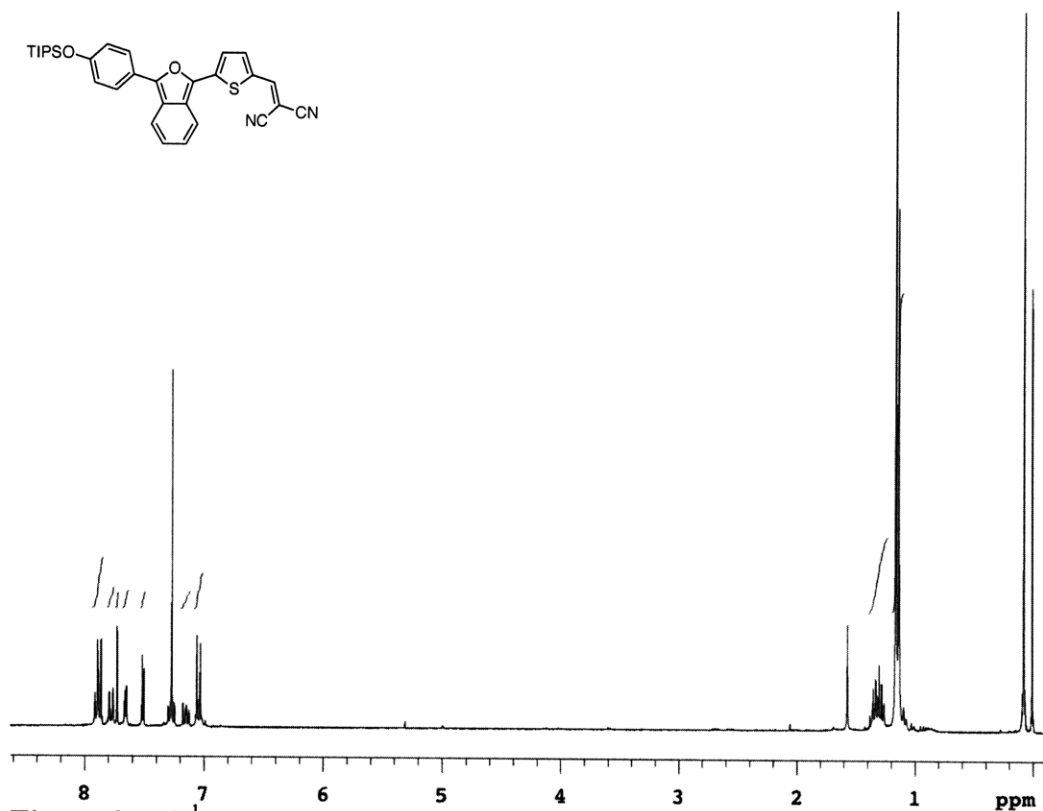
Figure 2.A.3 ^{1}H NMR (300 MHz, CDCl$_3$) of **14d**
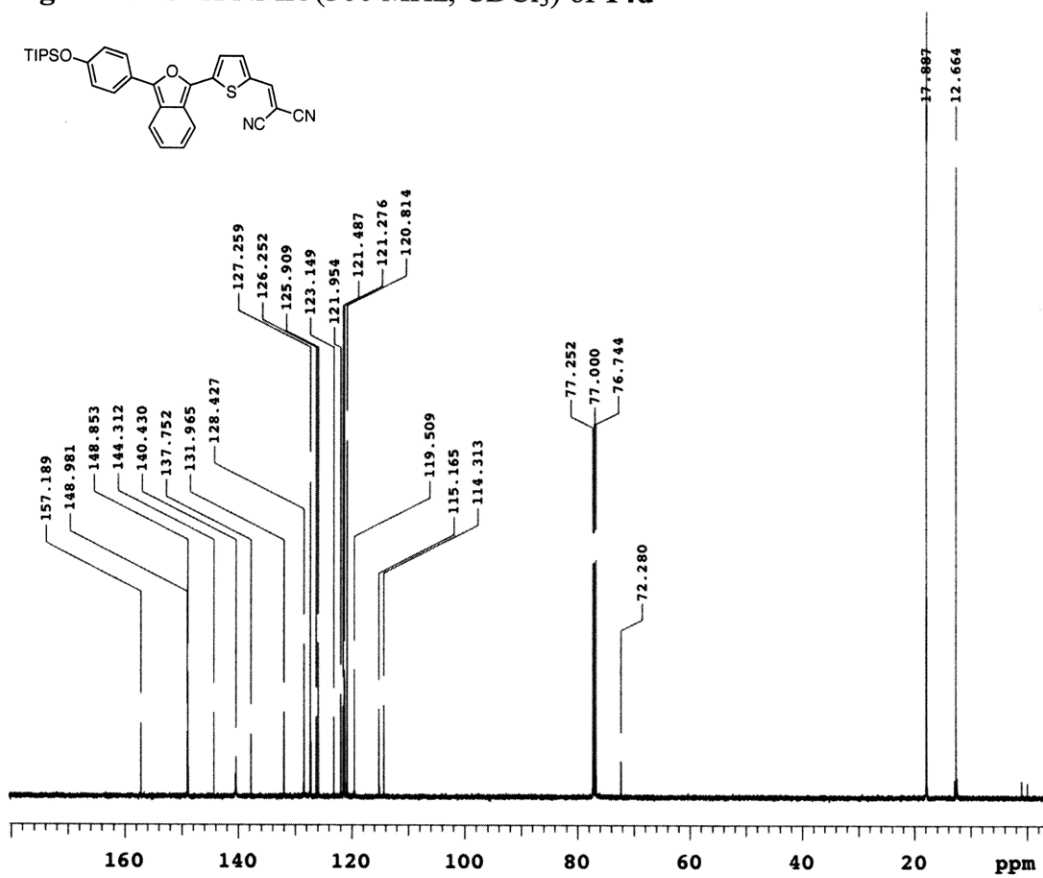
Figure 2.A.26 ^{13}C NMR (125 MHz, CDCl$_3$) of **14d**
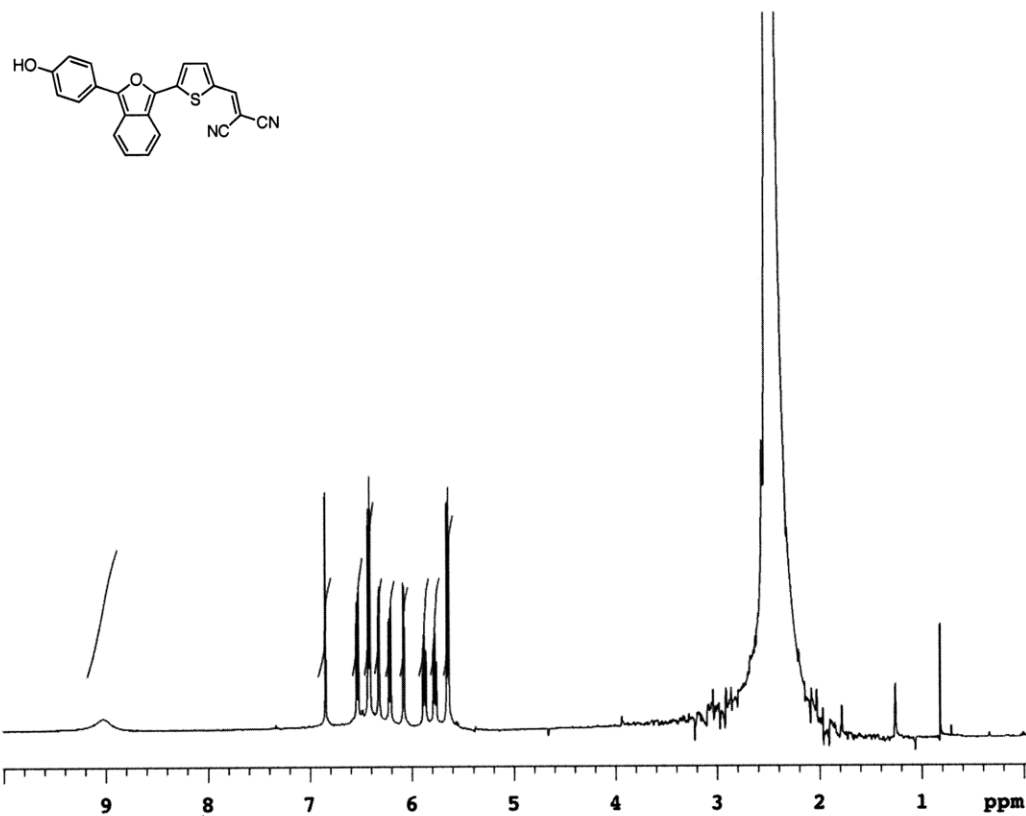
Figure 2.A.27 ^{1}H NMR (500 MHz, DMSO-d$_6$) of **11c**
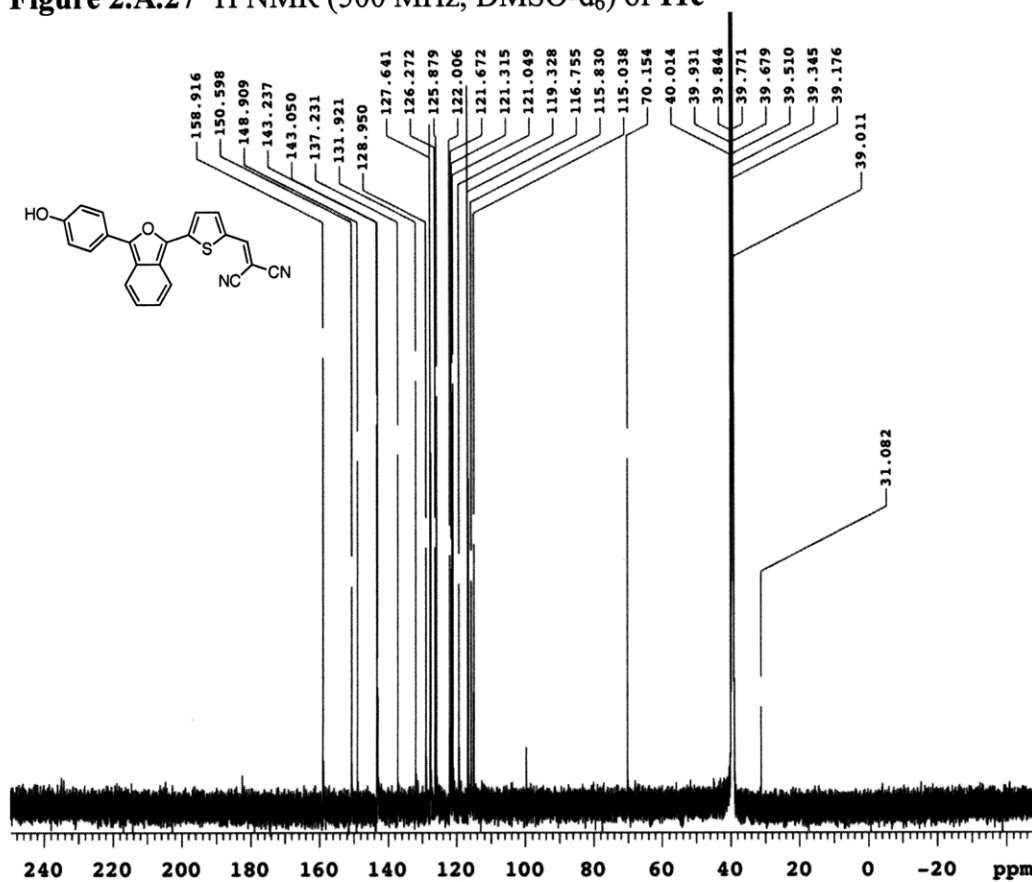
Figure 2.A.28 ^{13}C NMR (125 MHz, DMSO-d$_6$) of **IBF-NIAD 3**

89
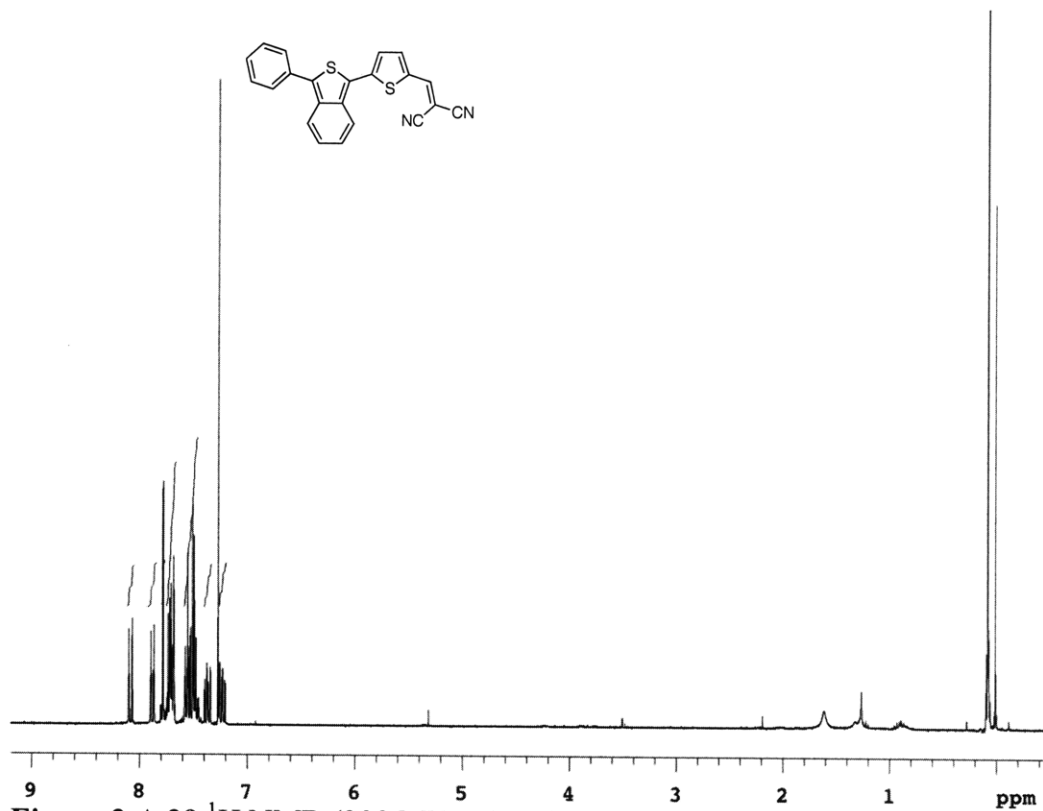
Figure 2.A.29 ^{1}H NMR (300 MHz, CDCl$_3$) of **ITN-NIAD 0**
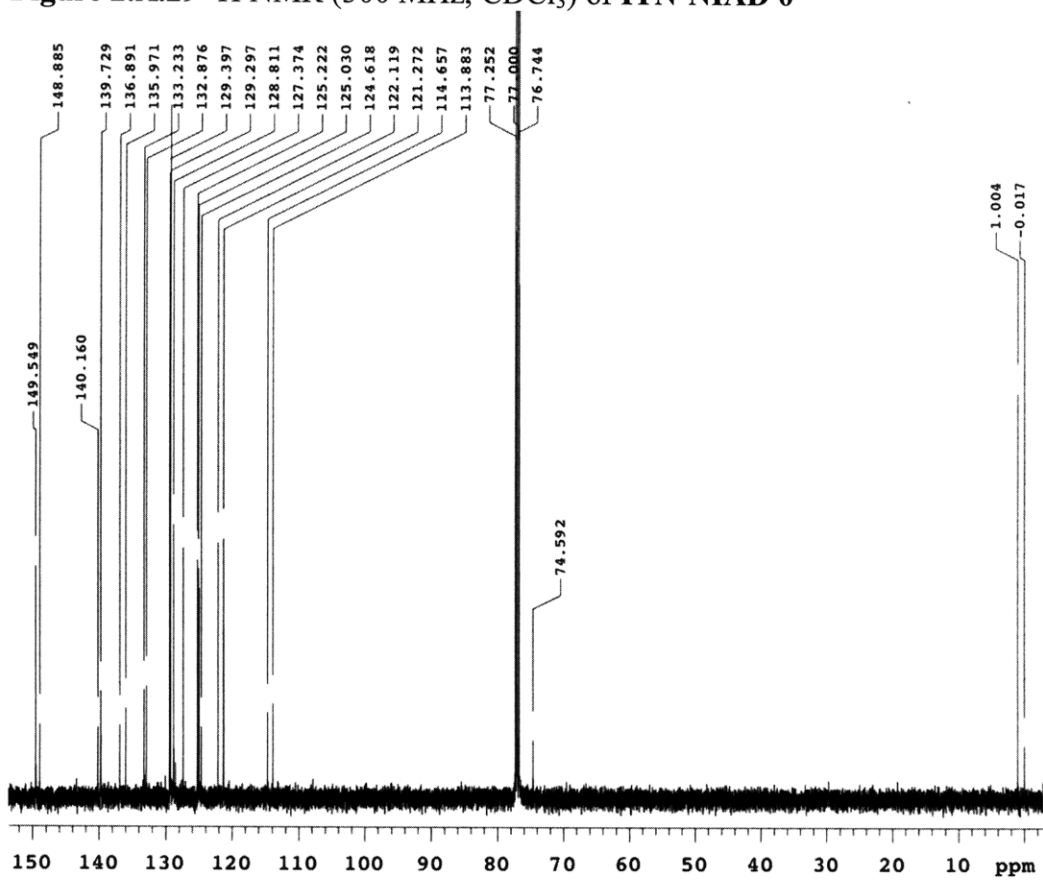
Figure 2.A.30 ^{13}C NMR (500 MHz, CDCl$_3$) of **ITN-NIAD 0**
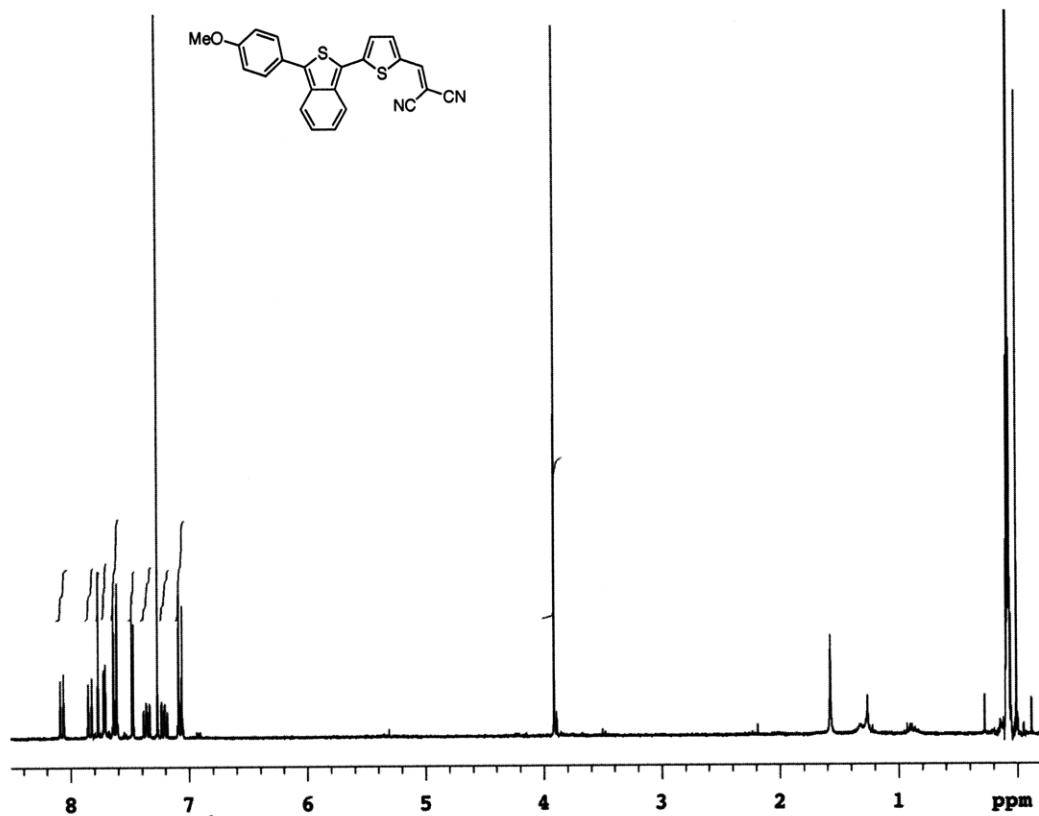
Figure 2.A.31 ^{1}H NMR (300 MHz, CDCl$_3$) of **ITN-NIAD 1**
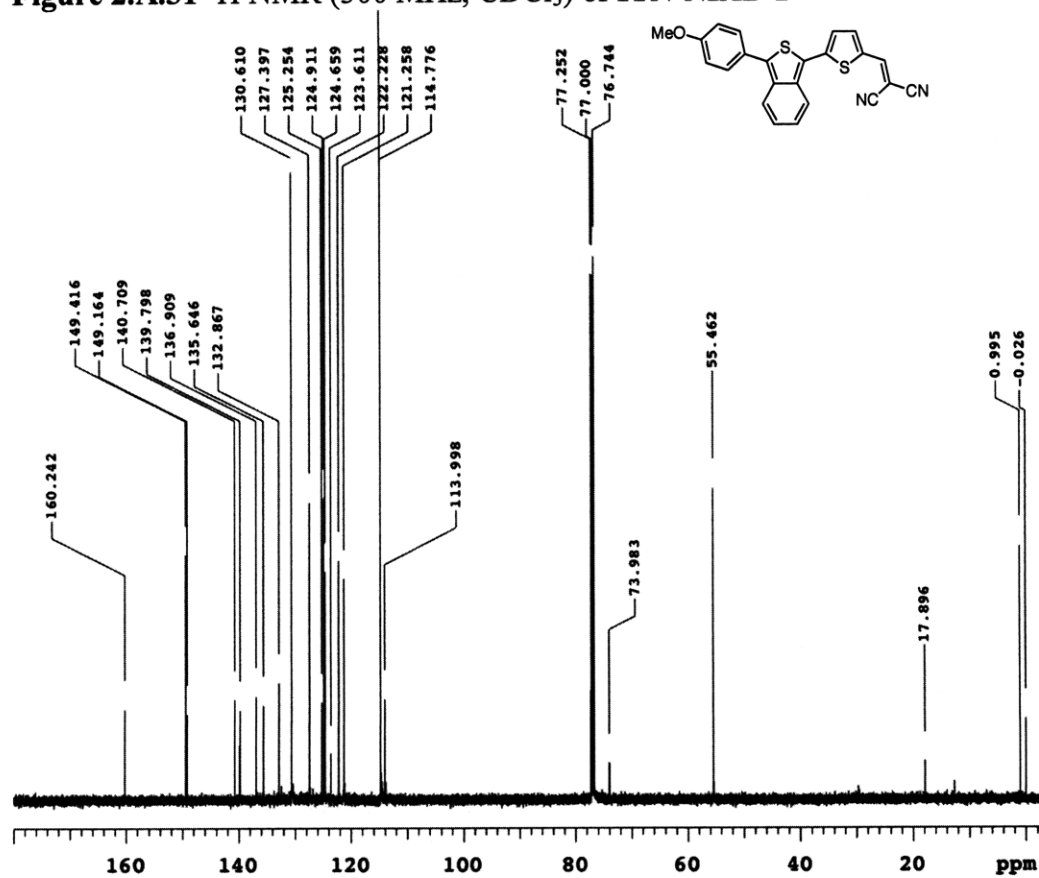
Figure 2.A.32 ^{13}C NMR (500 MHz, CDCl$_3$) of **ITN-NIAD 1**

Figure 2.A.33 ^{1}H NMR (300 MHz, CDCl$_3$) of **ITN-NIAD 2**

Figure 2.A.34 ^{13}C NMR (125 MHz, DMF-d$_7$) of **ITN-NIAD 2**
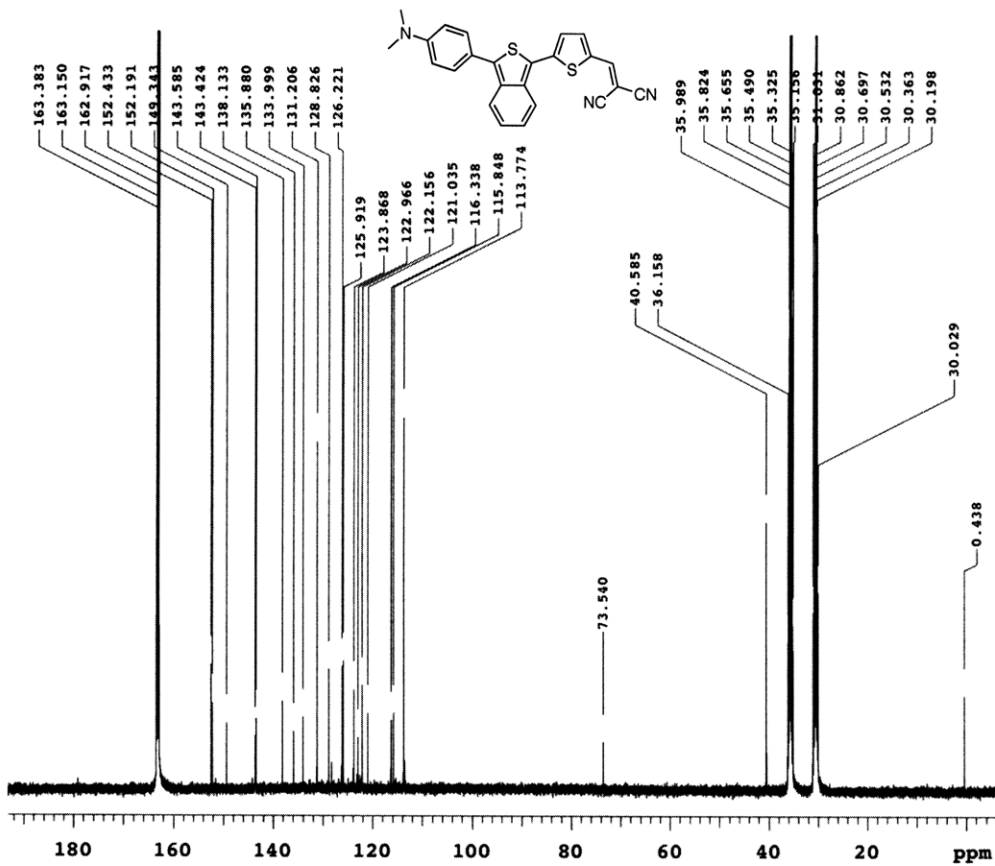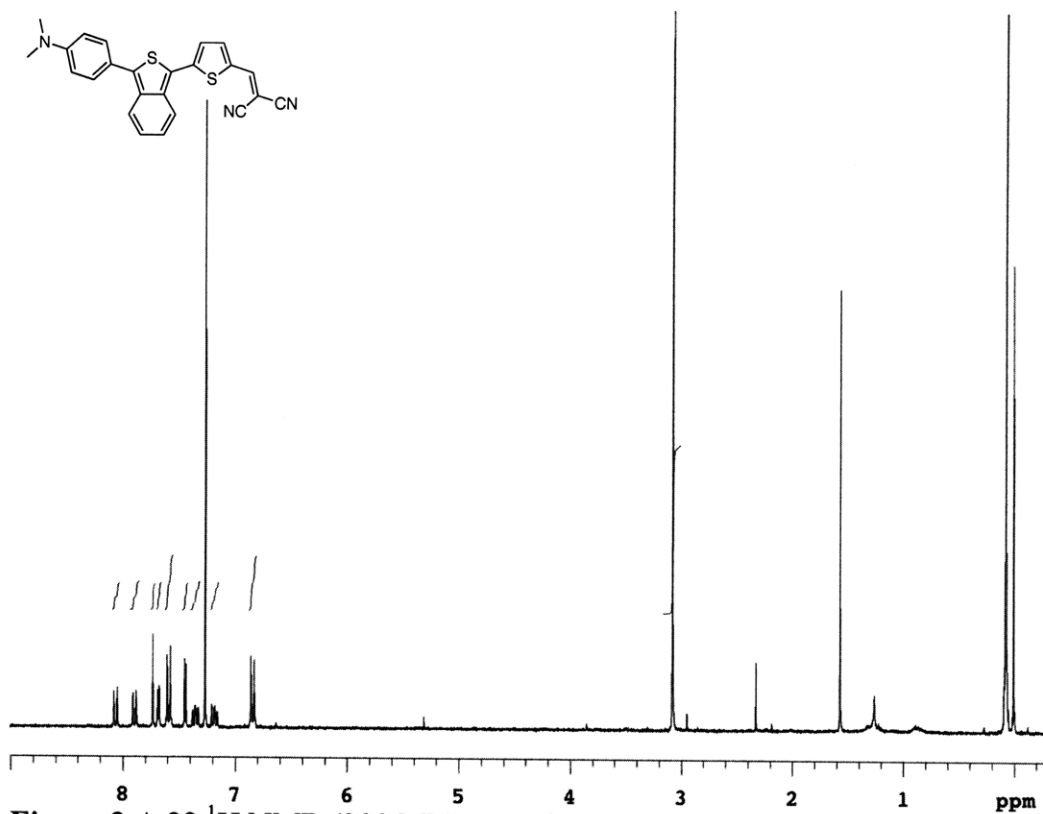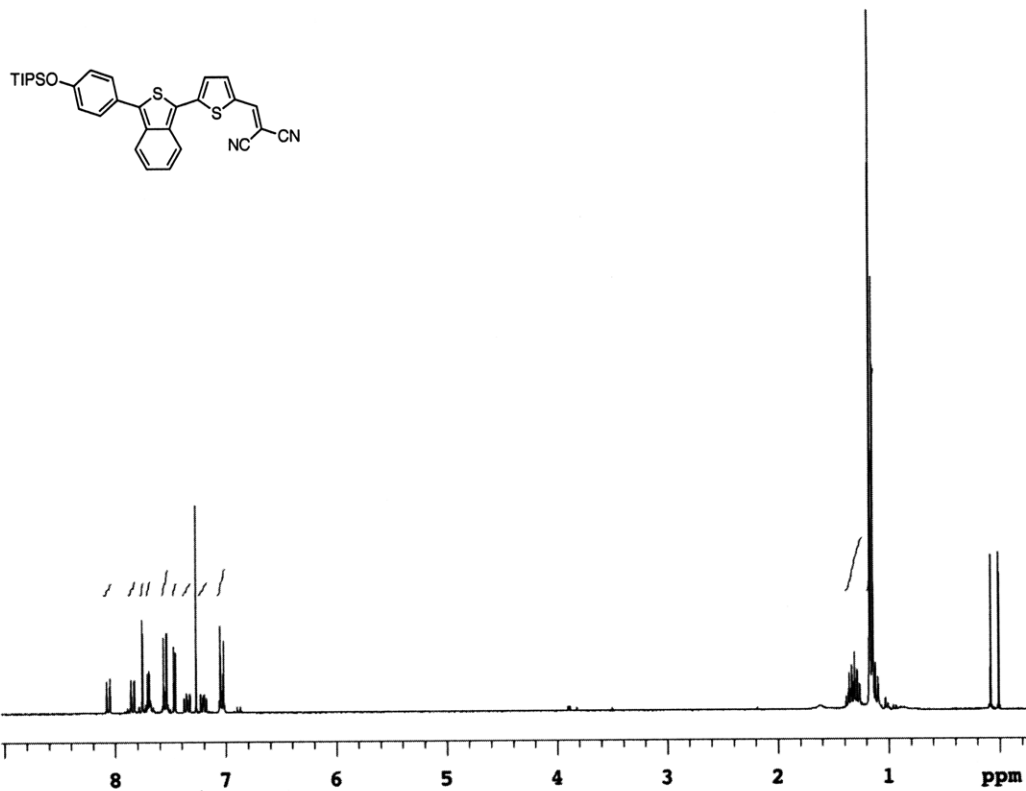
Figure 2.A.35 ^{1}H NMR (300 MHz, CDCl$_3$) of **TiPS-ITN-NIAD 3**
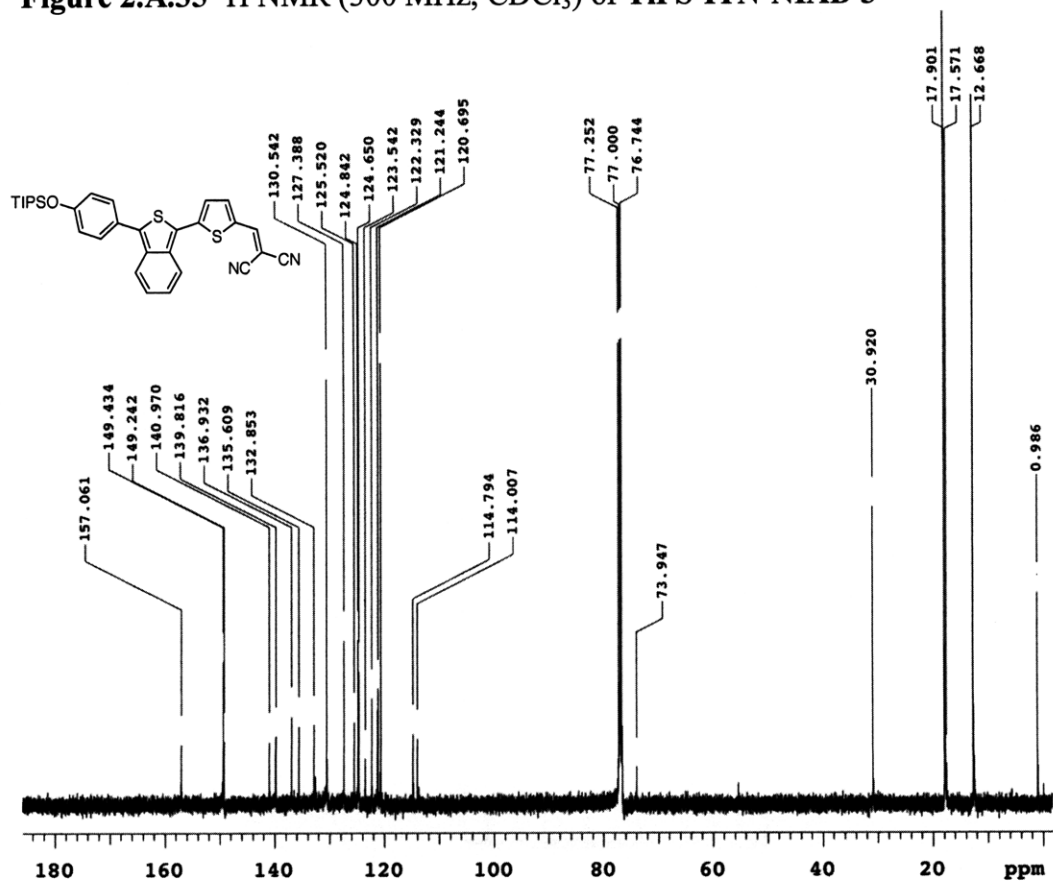
Figure 2.A.36 ^{13}C NMR (125 MHz, CDCl$_3$) of **TiPS-ITN-NIAD 3**
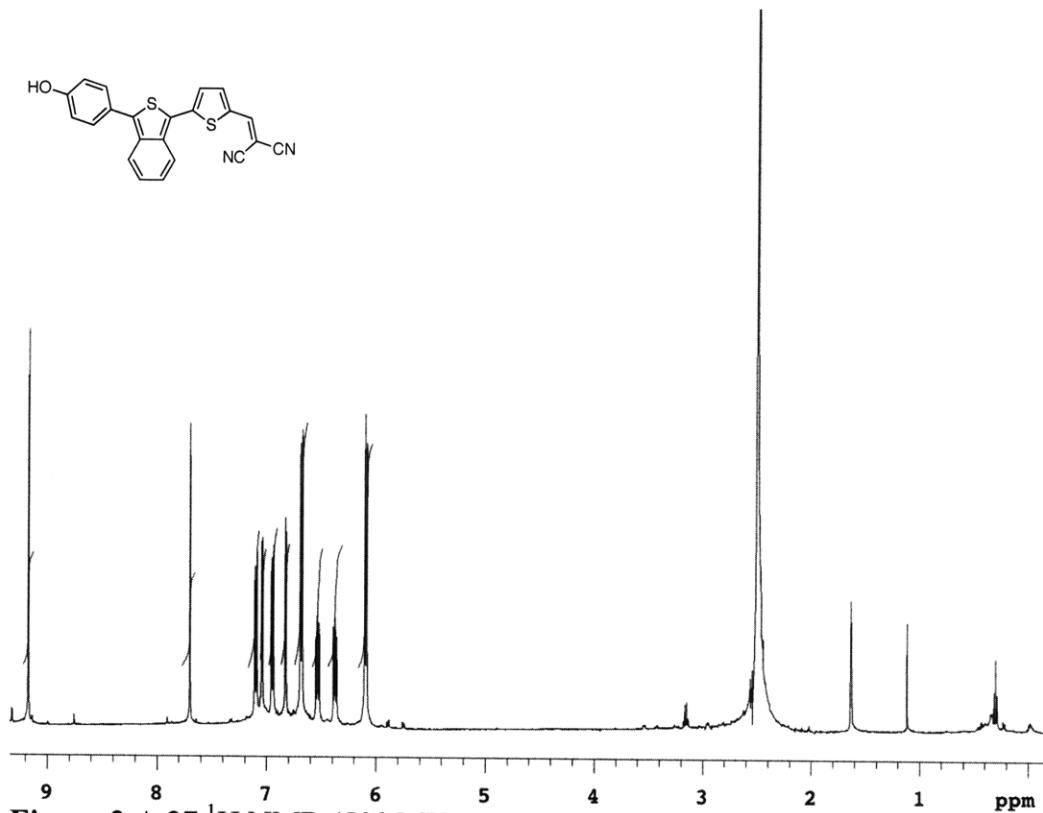
Figure 2.A.37 ^{1}H NMR (500 MHz, DMSO-d$_6$) of **ITN-NIAD 3**
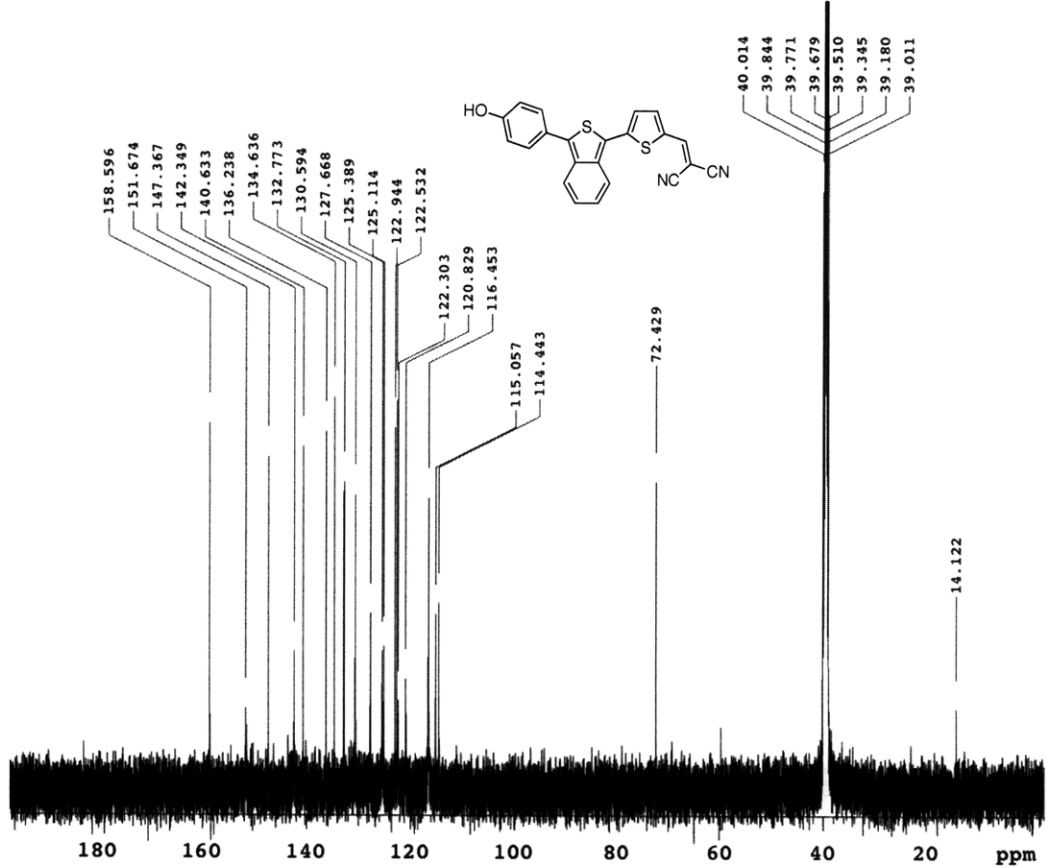
Figure 2.A.38 ^{13}C NMR (125 MHz, DMSO-d$_6$) of **ITN-NIAD 3**

Chapter 3

Isobenzofuran Near-Infrared Probes for β-Amyloid Imaging

3.1 Introduction: Imaging Alzheimer's

As discussed in previous chapters, near-infrared fluorescence (NIRF) imaging has the potential to provide non-invasive, relatively inexpensive diagnostic tools. One area in which this technique could prove particularly useful is Alzheimer's Disease (AD), a terminal, progressive, neurodegenerative condition which afflicts 5 million individuals in the United States.[1] Symptoms include memory loss, cognitive impairment, and dementia.[2] The disease is most prevalent in people over the age of 65, and as the population ages, the number is projected to increase to 106 million worldwide by 2050.[3] Currently AD has neither a cure nor a definitive methodology for diagnosis, with cases evaluated either symptomatically, or via autopsy.

a)   b)
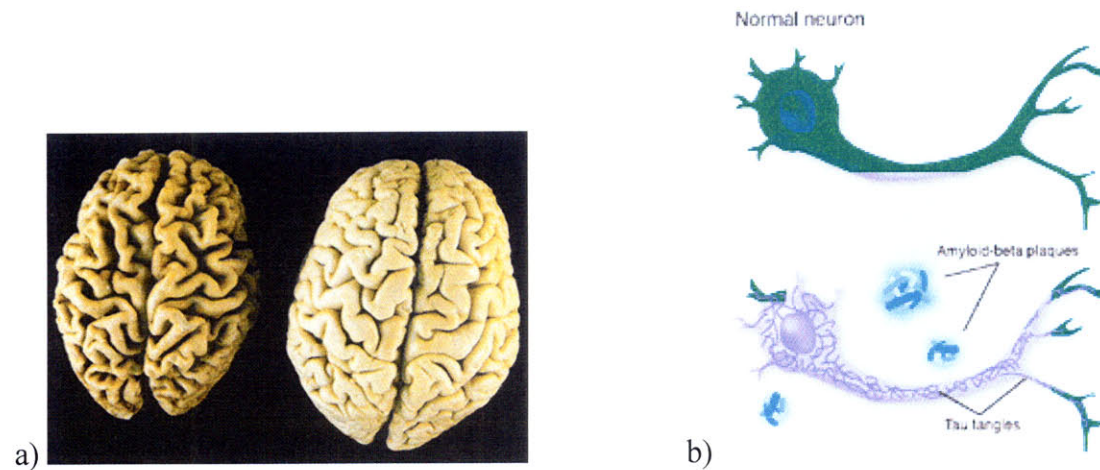
Figure 3.1 (a) Human brain afflicted with Alzheimer's Disease (left) and normal brain (right)[4], (b) graphic representing β-amyloid plaques and Tau tangles (Reprinted from reference 8).

Extensive research has been undertaken to elucidate the biological processes associated with AD[5], though a detailed discussion of this work lies beyond the scope of this thesis and, indeed, research in this field is continually evolving. The main indicators of AD pathology are neuronal loss and formation of senile plaques (SPs) and neurofibrilary tangles (NFTs). SPs are

composed of fibrillar aggregates of β-amyloid (Aβ) proteins. Amyloid proteins are critical for the function of a heathy brain, however the plaques form when amyloid precursor protein (APP) is fragmented into 39- 42 amino acid sections, called β-amyloids, which subsequently build up and aggregate into plaques. NFTs are aggregates of tau protein. Tau proteins aid the structural integrity of microtubules[6], which are integral to intracellular transport. In AD, neuronal tau proteins become hyperphosphorylated and form fibrils, disrupting the neurons transports systems.[7] The exact interplay between these two structures and how they contribute to the neuropathy associated with AD is not fully understood and is currently a source of debate.[8] It is known that SPs form in the brain before symptoms develop,[9] and many researchers believe their presence to be pivotal to the progression of AD.[10] Thus, in order to better diagnose AD, to better understand its biochemistry and progression, and to evaluate effective treatments in murine models and ultimately in humans, in vivo methods to visualize SPs and NFTs must be developed.[11]

Several techniques have been explored for imaging Aβ plaques, including magnetic resonance imaging (MRI), multiphoton microscopy, positron emission tomography (PET) and near-infrared fluorescence (NIRF) imaging. Of these, multiphoton microscopy was the first to allow in vivo detection of SPs, exploiting Thioflavin S (Figure 3.2) as a contrast agent.[12] Multiphoton microscopy has also been used to evaluate the SP labeling properties of PET lingand PIB.[13] Unfortunately, multiphoton microscopy necessitates removal of part of the skull, and thus the invasive nature of this technique renders it unsuitable for human subjects. Gd and monocrystalline iron oxide
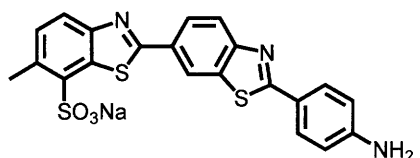
Figure 3.2: Thioflavin S

nanoparticles and have been used to image SPs in vivo in mice with MRI,[14] but the technique suffers from low resolution, allowing visualization of only the largest plaques.

Of the techniques explored thus far, PET is the most developed technology: numerous reports of PET imaging agents for Aβ plaques have been published in the last 10 years,[15] culminating in four compounds, ^{18}F-FDDNP,[16] ^{11}C-PIB,[17] ^{11}C-SB13,[18] and ^{11}C-BF-227[19] (Figure 3.3); these have been tested clinically with human AD patients.[20] The results from these studies are extremely promising, and clearly PET imaging will play a key role in Alzheimer's research. However, PET suffers certain limitations. It is hindered by the high cost of the associated instrumentation, its limited availability, and the short lifespan of the radiolabeled contrast agents. Unless these issues can be resolved or ameliorated, other imaging technologies will have to be developed to allow widespread diagnosis and early detection of AD.
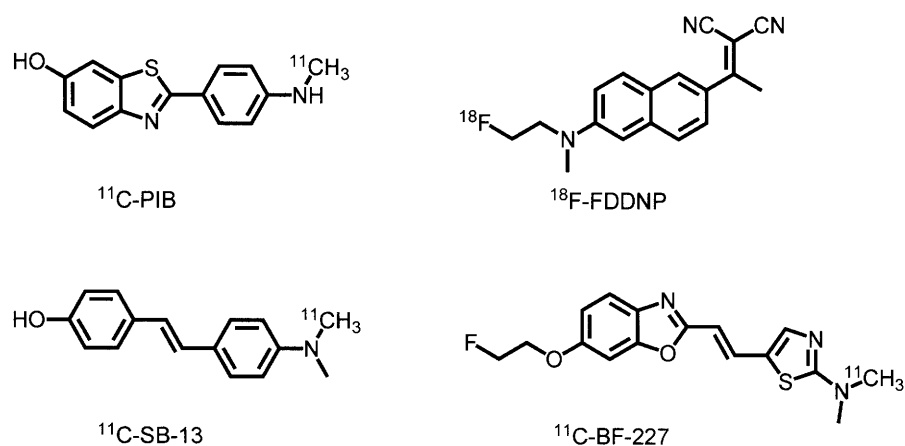
Figure 3.3 PET contrast agents. Refer to the text for a discussion.

NIRF imaging, in contrast, can provide high resolution with relatively inexpensive equipment.[21] NIR Fluorescent probes should have several design qualities. First, they must pass through the blood brain barrier (BBB), the tight junctions formed by cerebral endothelial cells

that mediate entry of compounds to the brain. The biological processes that mediate BBB permeability are extremely complex and our understanding of them is continually evolving, however, some basic guidelines exist. In general, compounds should have a molecular weight of less than 500 Da, a log octanol/water (Log P) coefficient[22] between -0.5 and 6.0, and should not have any formal charge.[23] Probes should bind to Aβ aggregates, and while the structure of these aggregates has not yet been solved by crystallography or multidimensional NMR, they are believed to have extensive β-sheet character with a thin hydrophobic groove along the long axis of the fibril.[24] Thus fluorophores should be relatively planar, allowing for intercalation into this hydrophobic cavity. In order to maintain contrast between bound and unbound dye, probes should exhibit a photophysical change upon binding.[25] An increase in the quantum yield of the dye provides a "turn-on" response. A change in the wavelengths of absorption or fluorescence emission can be measured using liquid crystal tunable filters with 10 nm resolution.[26] Changes in the fluorescence lifetime of the dye can be measured with fluorescence lifetime imaging (FLIM)
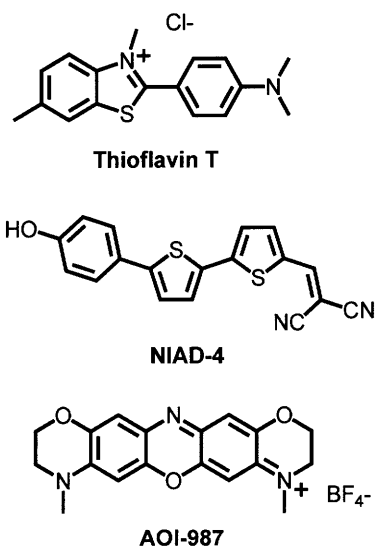
Figure 3.4: Thioflavin T, NIAD 4 and AOI-987

(see chapter 1 for discussion).[27] In order to maximize these effects, the dye should undergo a structural change on binding, such as planarization or rigidification, thus allowing for a decrease in the molecular vibrational-rotational processes that couple ground and excited states. This rigidification effect has been studied extensively with Thioflavin T (Figure 3.4), which undergoes significant spectral changes (93 nm red-shift in absorption maximum, 35 nm red-shift in emission maximum, 12.5 fold increase in fluorescence intensity)[28]

99

on binding to Aβ fibrils.[29] When these factors are all taken into account, we are looking for a small, neutral fluorophore with a flexible, planarizable backbone.

Two NIR fluorophores have been reported to detect SPs in vivo. The first, **AOI-987** (Figure 3.4) is an oxazine dye with absorption and emission maxima at 650 nm and 670 nm respectively and a quantum yield of 0.41.[30] **AOI-987** passes the blood brain barrier (a rare exception to the 'no formal charge' guideline) and binds to SPs, and, indeed, an increased fluorescence signal is observed for APP23 transgenic mice over similarly treated wild type mice. The photophysical properties of **AOI-987** do not improve on binding, with a slight decrease in fluorescence intensity, and thus the spatial resolution of its images are limited.[31] Our group has previously reported **NIAD-4**, a donor-acceptor dye (Figure 3.4) that also passes the BBB and binds to SPs.[32] Due to its flexible backbone, **NIAD-4** exhibits marked optical contrast on binding to Aβ fibrils, with a 70 nm red-shift in the absorption maxima and a 400 fold increase in fluorescence intensity (Figure 3.5). However, **NIAD-4**'s absorption is not far enough into the NIR to permit imaging without a cranial window. Thus, while **NIAD-4** illustrates the effectiveness of the "smart-probe" design paradigm, such invasive procedures limit its applicability in murine and human diagnostic techniques and necessitate the development of red-shifted derivatives.
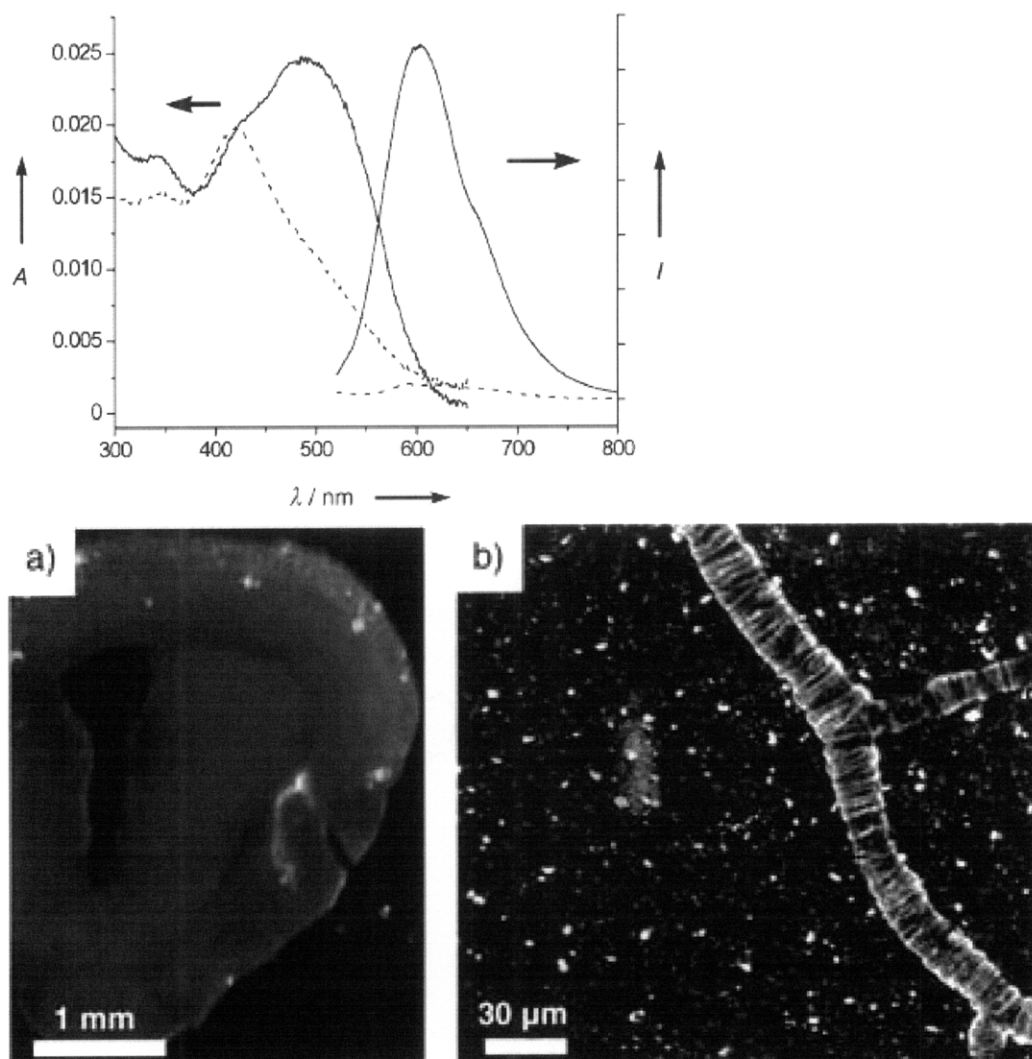
Figure 3.5: (top) Absorption and fluorescence spectra of NIAD-4 (4.1 μM) in aqueous PBS solution in the presence of aggregated amyloid-b protein (10 μM, solid line) and without the protein (dashed line). (bottom) (a) Image of a coronal section of brain from an aged APP transgenic mouse labeled with a solution of NIAD-4. White spots are fluorescent signals from labeled SPs (b) In vivo fluorescent detection of both senile plaques and amyloid angiopathy using multiphoton microscopy immediately following intravenous injection of 2 mg/kg of NIAD-4. Images reproduced from reference 32.

Chapter 2 demonstrated that isobenzofuran and isothianaphthene could be used as proquinoidal components of small molecule donor-acceptor near-infrared dyes, based a similar framework to **NIAD-4**. In this chapter, we expand this dye series and modify our basic design to improve physical and photophysical properties in order to maximize optical response upon Aβ

binding and ultimately blood-brain barrier permeability. We also install functional handles onto the dyes to enable integration into other NIR sensing applications. The modifications we explore include changing the electron-withdrawing group, changing the phenyl ring and the 5-membered heterocycle in the conjugated backbone, and changing the electron-donating group (Figure 3.6).
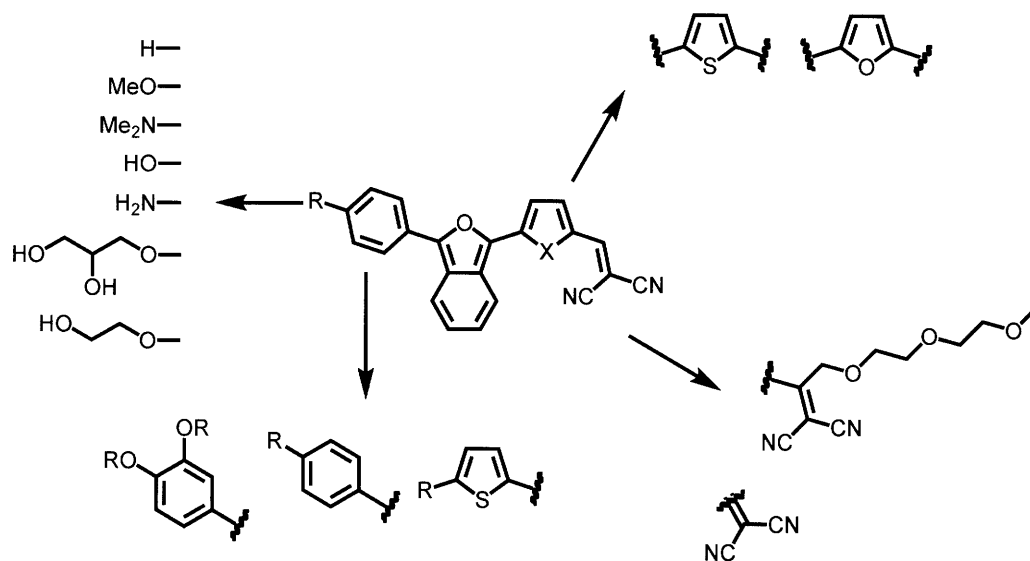
Figure 3.6 Potential modifications to IBF-NIAD series.

3.2 Results and Discussion

3.2.1 Aβ Binding interactions of IBF-NIAD 0-3

As a starting point in our dye design, we explored the interactions between **IBF-NIAD 0-3** and aggregated β-amyloid proteins. Aβ(1-40) protein (Figure 3.7) is the model system most commonly employed for this purpose in the literature, as it readily forms fibrils with lamellar β-sheet structures upon incubation in PBS buffer.[27] The results of these binding tests are displayed in Figures 3.8 – 3.11.

H-Asp-Ala-Glu-Phe-Arg-His-Asp-Ser-Gly-Tyr-Glu-Val-His-His-Gln-Lys-Leu-Val-Phe-Phe-Ala-Glu-Asp-Val-Gly-Ser-Asn-Lys-Gly-Ala-Ile-Ile-Gly-Leu-Met-Val-Gly-Gly-Val-Val-OH

Figure 3.7 Amino acid sequence of Aβ(1-40).
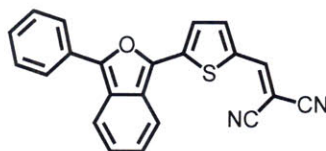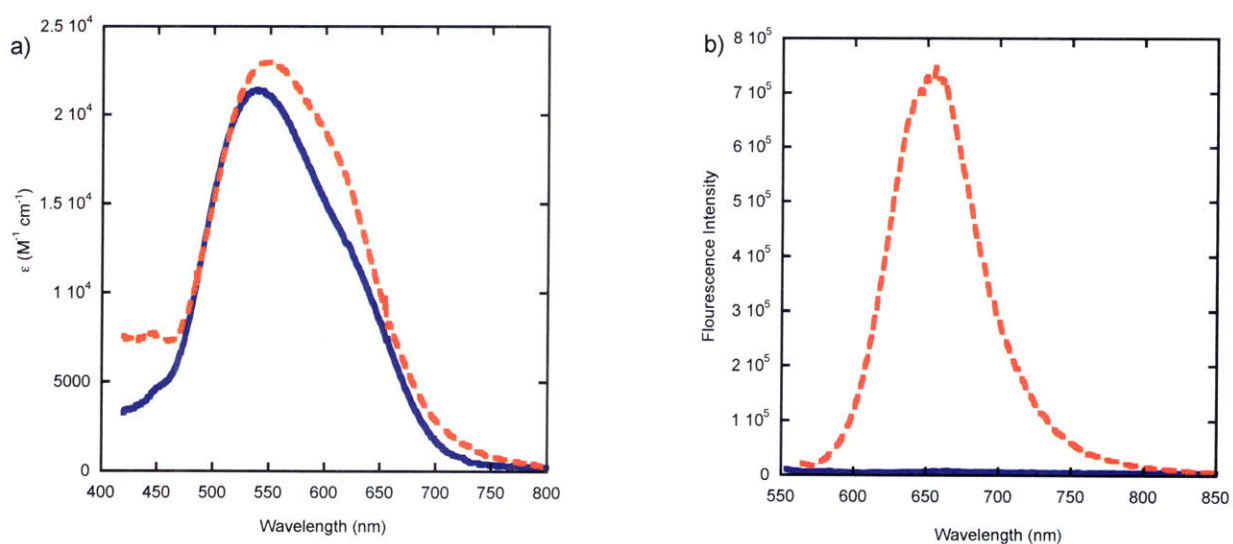
IBF-NIAD 0

Figure 3.8 Absorption (a) and fluorescence (b) spectra of **IBF-NIAD 0** (2.5 μM) in PBS buffer (blue solid line) and 10 μM aggregated Aβ(1-40) in PBS buffer (red dashed line).
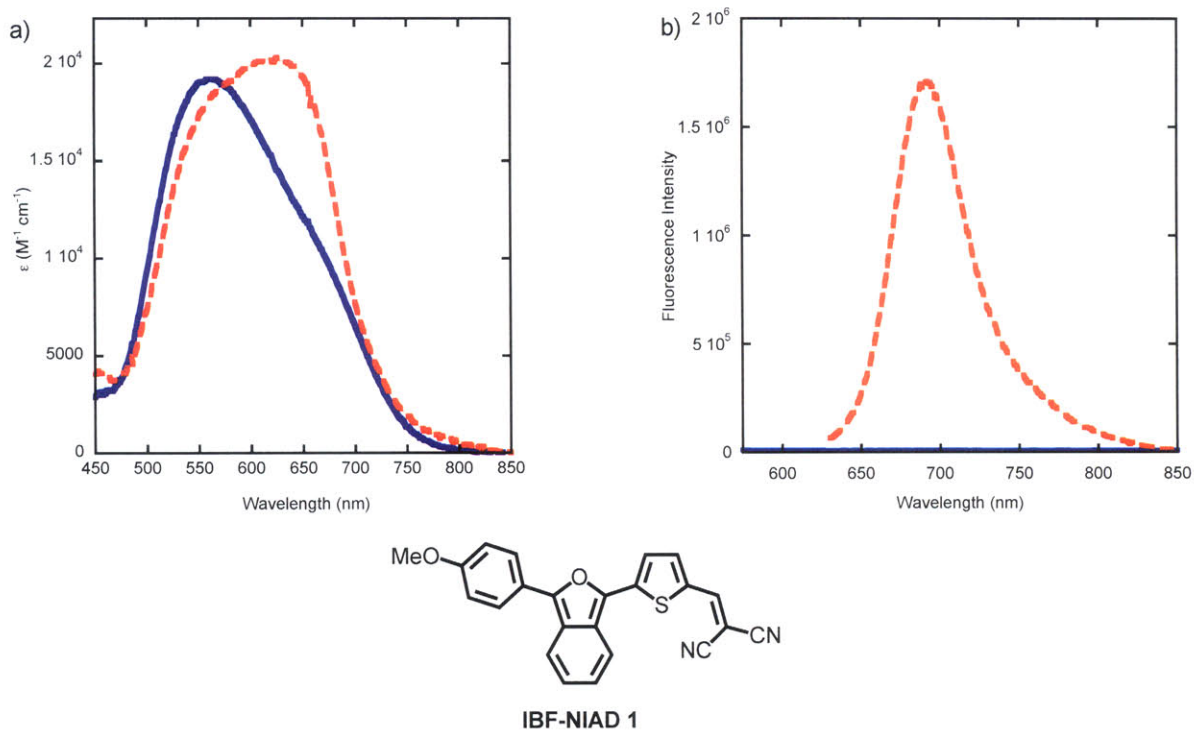
Figure 3.9 Absorption (a) and fluorescence (b) spectra of **IBF-NIAD 1** (2.50 μM) in PBS buffer (blue solid line) and 10 μM aggregated Aβ(1-40) in PBS buffer (red dashed line).
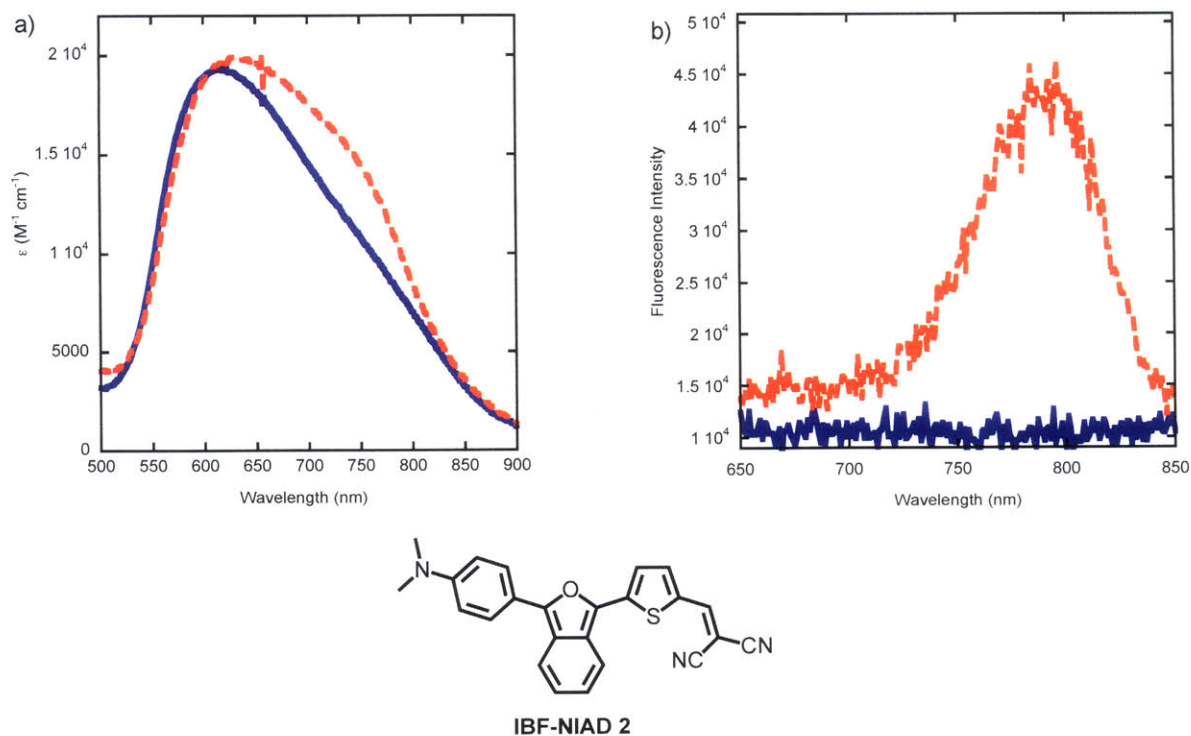
Figure 3.10 Absorption (a) and fluorescence (b) spectra of **IBF-NIAD 2** (2.50 μM) in PBS buffer (blue solid line) and 10 μM aggregated Aβ(1-40) in PBS buffer (red dashed line).
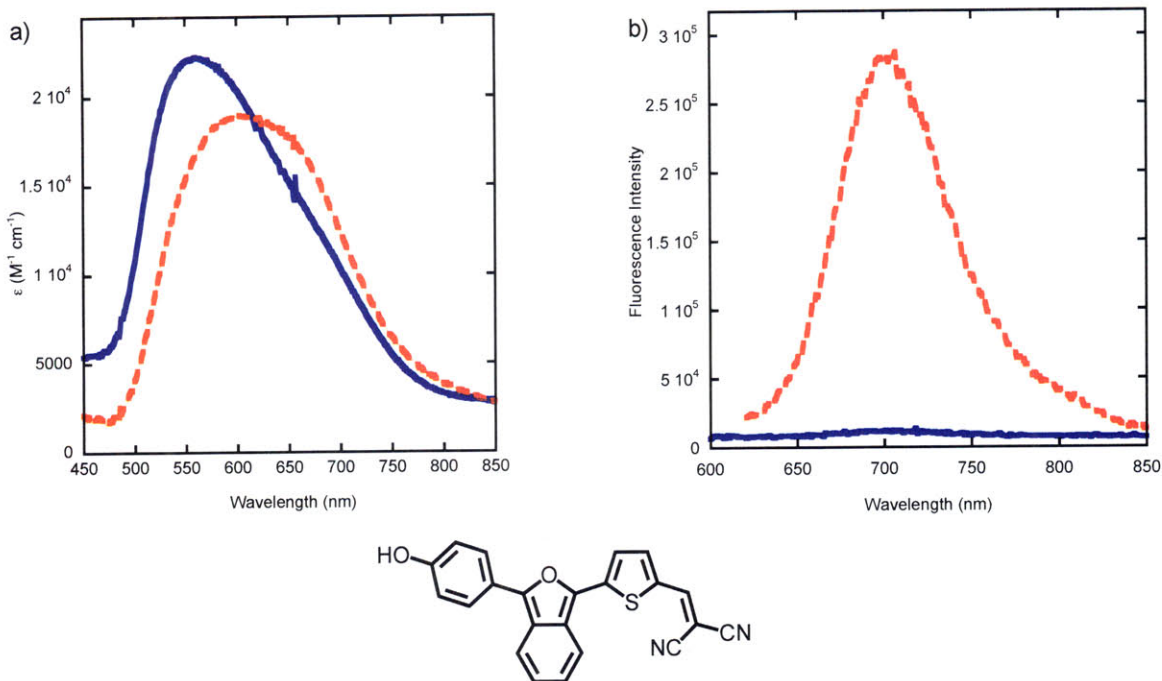
Figure 3.11 Absorption (a) and fluorescence (b) spectra of **IBF-NIAD 3** (2.74 µM) in PBS buffer (blue solid line) and 10 µM aggregated Aβ(1-40) in PBS buffer (red dashed line).

Table 3.1 Summary of Aβ(1-40) Assay Results for IBF-NIAD 0-3

Dye (R-)	λ_{max} Abs. (nm)		λ_{max} Em. (nm)		Red-shift (nm)		$\epsilon_{A\beta}/\epsilon_{PBS}$	$\Phi_{A\beta}/\Phi_{PBS}$
	PBS	Aβ[a]	PBS	Aβ[a]	Abs.	Em.		
IBF-NIAD 0 (H-)	539	550	665	656	11	-9	1.07	190
IBF-NIAD 1 (MeO-)	560	612	_[b]	690	52	_[b]	1.06	800[b]
IBF-NIAD 2 (Me₂N-)	621	627	_[b]	796	6	_[b]	1.03	20[b]
IBF-NIAD 3 (HO-)	560	603	701	704	43	3	0.85	62

[a] Aβ(1-40) concentration was 10 µM. [b] Fluorescence intensity in PBS was undetectable, thus values are not available or are estimates.

These results indicate interaction of **IBF-NIAD 0-3** with aggregated Aβ proteins. In all cases we observed a marked increase in the fluorescence intensity. The shapes of the absorption spectra of the dyes in PBS buffer suggest the formation of disordered H-type aggregates.[33] This

arrangement, in which chromophores stack directly on each other produces a blue shift in the absorption. However, as can be seen in all of the spectra, there is a shoulder on the red edge of the absorption that results from a second transition, which comes from a minority species in the aggregate. Changes to the absorption spectra were modest for **IBF-NIAD 0** and **2**, with red-shifts in absorption maxima of 6 nm and 11 nm respectively. This lack of significant red-shift suggests that the dyes are highly aggregated in PBS solution, and thus only very small amounts are able to interact with the Aβ fibrils, though those that do interact show a significant turn-on fluorescence response. The red-shifts for **IBF-NIAD 1** and **3** are more substantial, at 52 nm and 43 nm, and these dyes show significant absorption at 650 nm, with the extinction coefficients at that wavelength only decreasing by 5% and 7% respectively. Indeed, the absorption maximum of Aβ bound **IBF-NIAD 1** is red shifted 13 nm beyond its absorption maximum in CHCl₃. **IBF-NIAD 0-3** do not, however, stain SPs when incubated with cerebral tissue sections of an aged APP/PS1 mouse, and we attribute this negative result to aggregation of the dyes in PBS solution.

3.2.2 IBF-NIAD 4: Integration of Thiophene

The first modification we explored was the replacement of the phenyl ring with thiophene. We speculated that, due to thiophene's lesser aromaticity,[34] its integration would further red-shift the absorbance and emission of the dye. Thiophene is also more hydrophilic than benzene (Log P 1.90 vs 2.0),[35] thus we also hoped to reduce the hydrophobicity of the dye. The synthesis of this dye is described in Scheme 3.1. Phthalide **3** was produced by Friedel-Crafts acylation of 2-methoxythiophene with phthalic anhydride followed by reduction of resulting carboxylic acid **2** with NaBH₄ under basic conditions and cyclization with HCl. This phthalide was then submitted to the synthetic pathway used for **IBF-NIAD 0-3**, to afford **IBF-NIAD 4**.

Scheme 3.1 Synthesis of IBF-NIAD 4
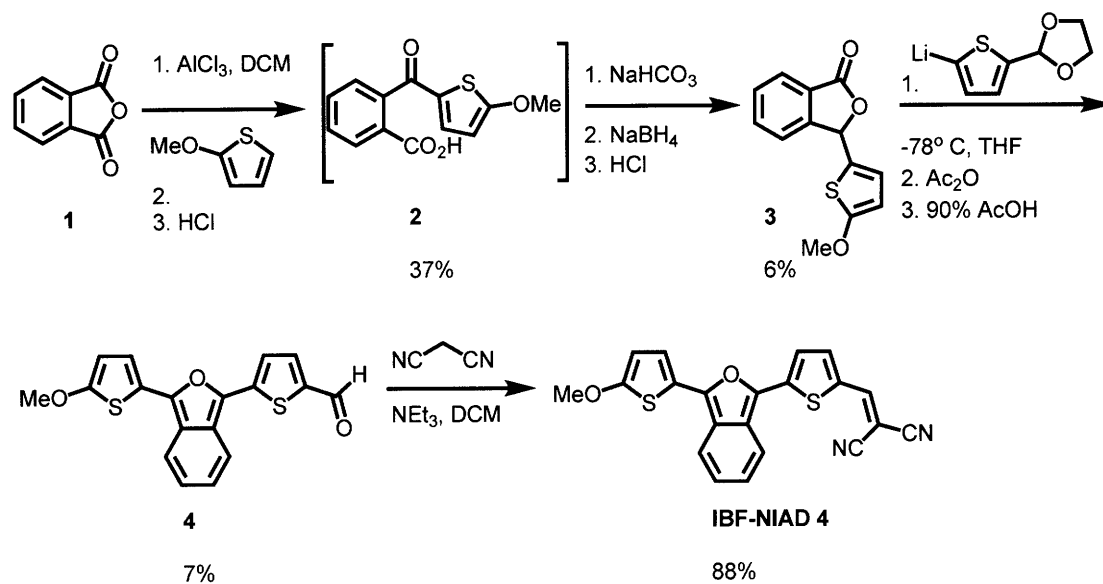
The absorbance and fluorescence emission spectra of **IBF-NIAD 4** are depicted in Figure 3.12. Compared to **IBF-NIAD 1**, **IBF-NIAD 4** displays a 29 nm red shift in absorption maximum and 48 nm red shift in fluorescence emission maximum in MeOH, with similar red shifts in CHCl$_3$. The quantum yields, however, are significantly decreased. This reduction can be attributed to the internal heavy atom effect, which will be discussed in detail in Section 3.2.3.

MeOH
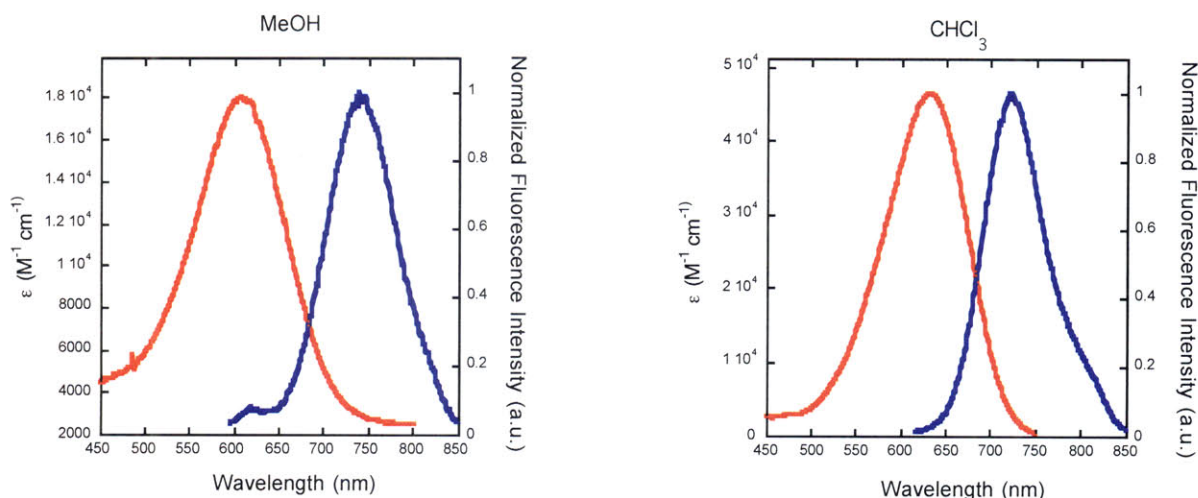
CHCl₃

Dye	λ_{max} Abs. (nm)		λ_{max} Emission (nm)		Φ		ε (M^{-1} cm^{-1})	
	MeOH	CHCl₃	MeOH	CHCl₃	MeOH	CHCl₃	MeOH	CHCl₃
IBF-NIAD 4	607	631	734	722	0.0078	0.023	46500	18100

Figure 3.12 Absorbance and Fluorescence Emission spectra of **IBF-NIAD 4** and a summary of its spectroscopic properties.
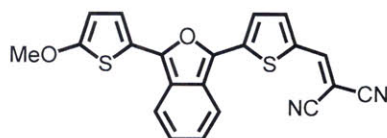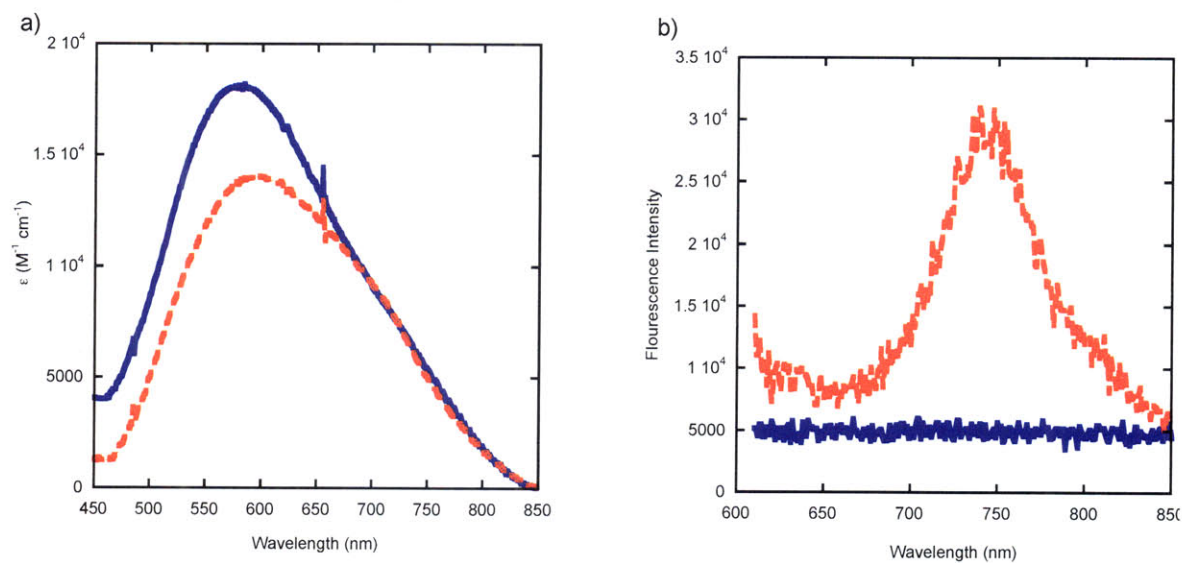
IBF-NIAD 4

Figure 3.13 Absorption (a) and fluorescence (b) spectra of **IBF-NIAD 4** (2.50 μM) in PBS buffer (blue solid line) and 10 μM aggregated Aβ(1-40) in PBS buffer (red dashed line).

Table 3.2: Summary of Aβ(1-40) Assay Results for IBF-NIAD 4

Dye	λ_{max} Abs. (nm)		λ_{max} Em. (nm)		Red-shift (nm)		$\varepsilon_{A\beta}/\varepsilon_{PBS}$	$\Phi_{A\beta}/\Phi_{PBS}$
(R-)	PBS	$A\beta^a$	PBS	$A\beta^a$	Abs.	Em.		
IBF-NIAD 4 (MeO-Th-)	586	601	$-^b$	739	15	$-^b$	0.77	30^b

[a] Aβ(1-40) concentration was 10 μM. [b] Fluorescence intensity in PBS was undetectable, thus values are not available or are estimates.

IBF-NIAD 4 also shows changes in its photophysical properties when bound to Aβ(1-40) with a red shift in absorption maximum of 15 nm and a substantial increase in fluorescence intensity. In in vitro tissue studies with coronal brain sections of an aged APP/PS1 mouse, **IBF-NIAD 4** stains SPs (figure 3.14). Unfortunately, the fluorophore does not cross the blood brain barrier, and thus cannot be utilized for in vivo imaging.
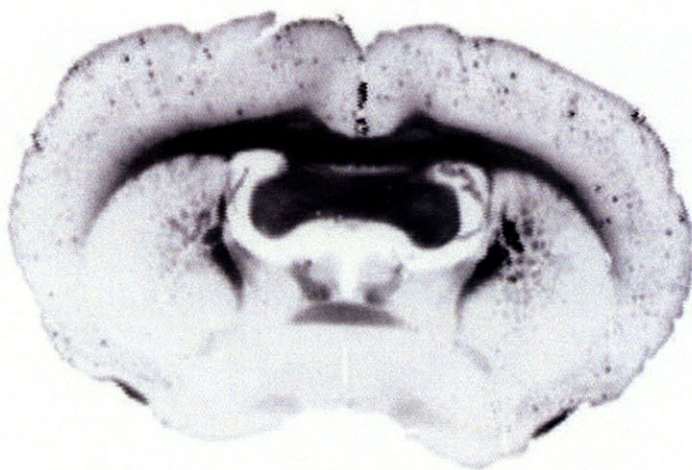
Figure 3.14 Image of a cross section of an aged APP/PS1 mouse brain stained with **IBF-NIAD 4**. Image taken with excitation at 685 nm and emission viewed through a 700 nm longpass filter. The black spots are fluorescent signals indicating staining of SPs by the dye. Image obtained by Brian Ferrara at Massachusetts General Hospital.

3.2.3 IBF-NIAD 11-14: Integration of a Furan Subunit

As a next step in our dye tuning process, we explored the effect of exchanging the thiophene subunit with furan. Furan is more hydrophilic than thiophene (Log P = 1.34 vs. Log P = 1.90),[36] and has lesser aromatic stabilization (RE = 27.2 kcal/mol vs. RE = 43.0 kcal/mol).[37] It has also been reported that exchanging thiophene with furan in certain fluorescent oligomeric systems leads to an increased quantum yield in those systems,[38] thus we hoped that the incorporation of furan would prove advantageous to our design. The synthesis of **IBF-NIAD 11-14**, the furan containing analogues of **IBF-NIAD 0-3**, is shown in Scheme 3.2. In general, the synthetic methods are very similar to the original dye set but with an acetal-protected bromofuran **6** used in place of a acetal-protected bromothiophene.

Scheme 3.2 Synthesis of IBF-NIAD 11-14

8a: R= H- : 38%
8b: R= MeO- : 25%
8c: R= Me$_2$N- : 25%
8d: TIPSO- : 24%

IBF-NIAD 14: R= H- : 82%
IBF-NIAD 11: R= MeO- : 81%
IBF-NIAD 13: R= Me$_2$N- : 77%
9d: TIPSO- : 87%

9d
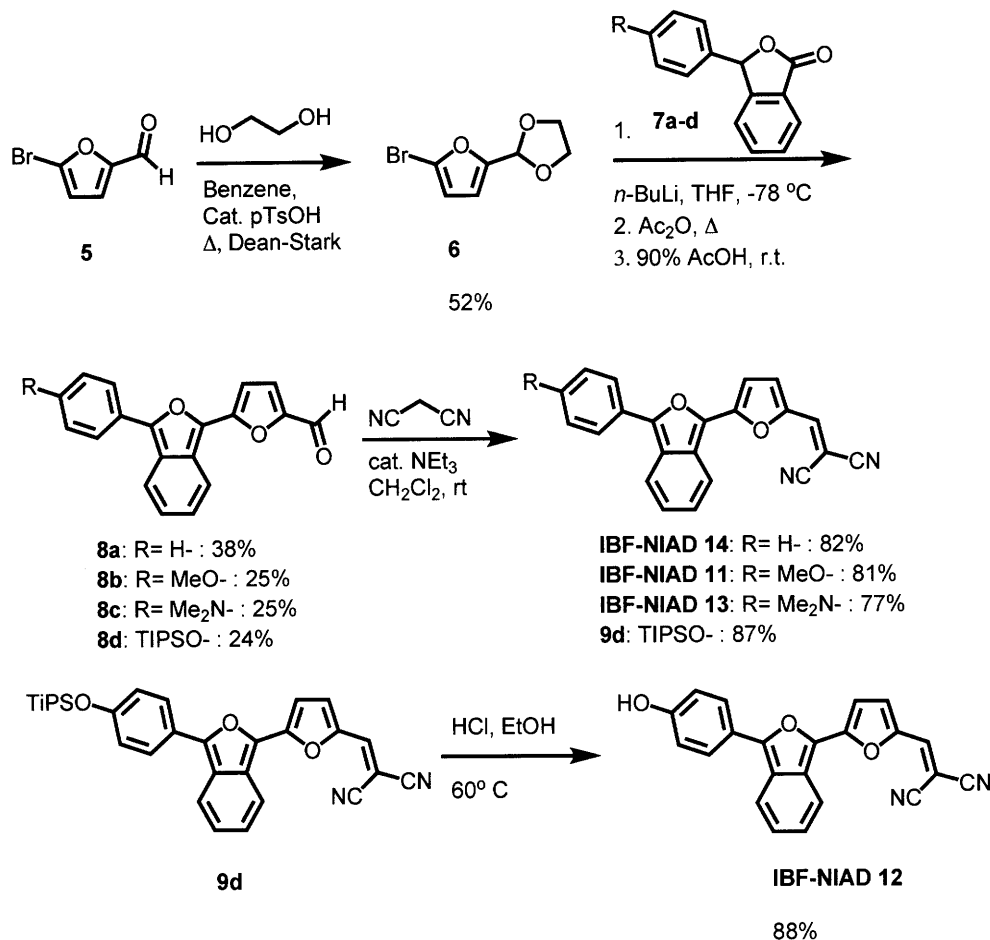
IBF-NIAD 12
88%

The absorbance and fluorescence emission spectra of **IBF-NIADs 11-14** are shown in Figure 3.15 and Figure 3.16, and their spectroscopic properties are summarized in Table 3.3. Compared to **IBF-NIADs 0-3**, **IBF-NIADs 11-14** exhibit a slight (4-12 nm) blue-shift in absorption maxima and a 6-24 nm blue shift in fluorescence emission maxima.
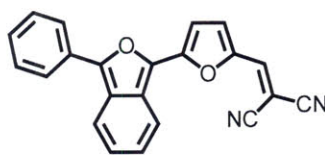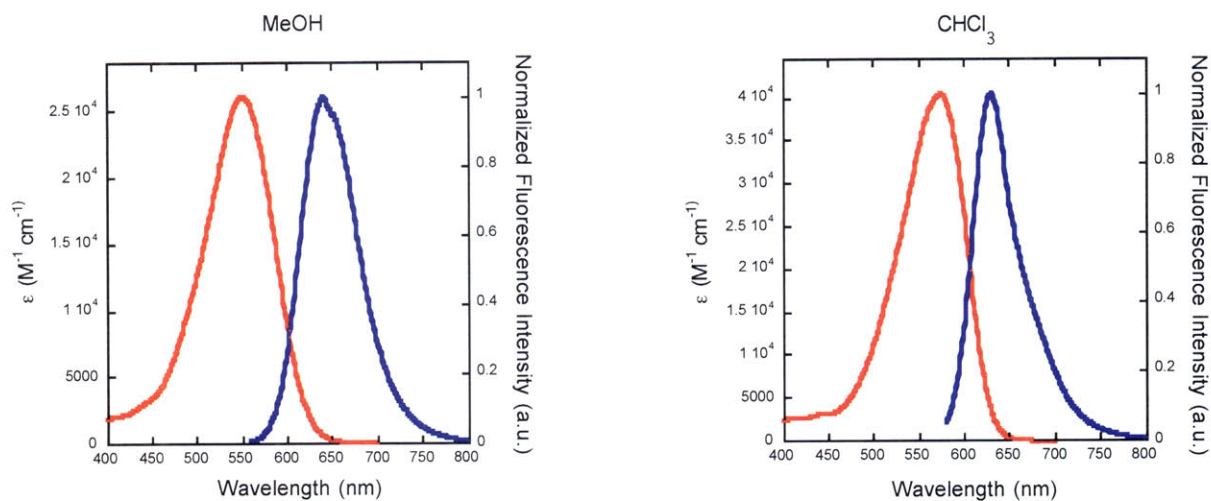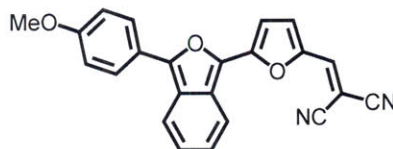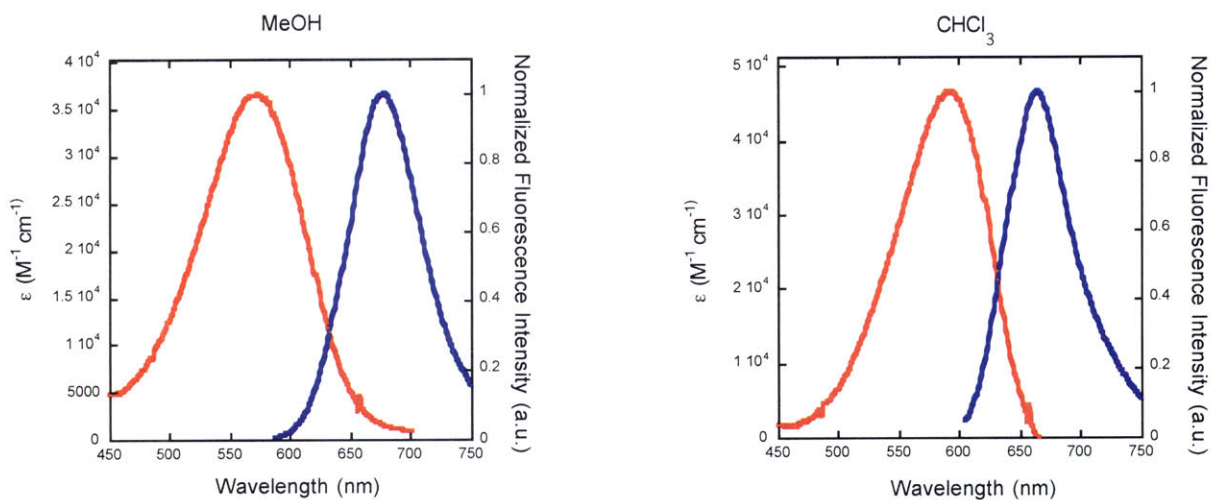
111

Figure 3.15 Absorbance (red) and normalized fluorescence intensity (blue) spectra of **IBF-NIAD 14 and 11** in MeOH (left) and CHCl₃ (right).

MeOH · **CHCl₃**

IBF-NIAD 12

MeOH · **CHCl₃**
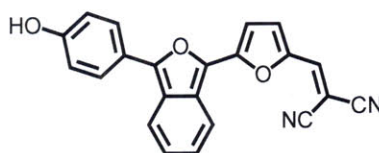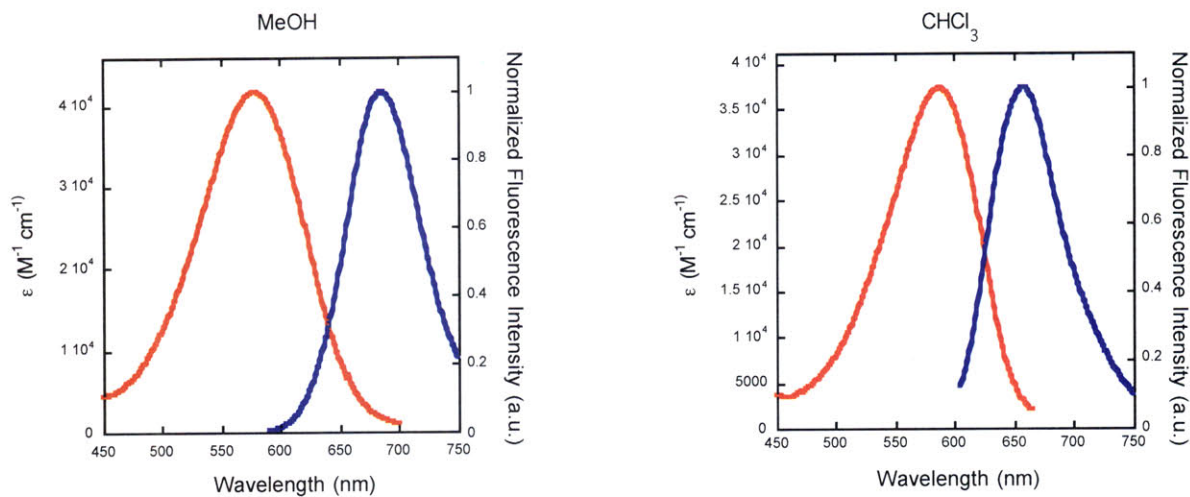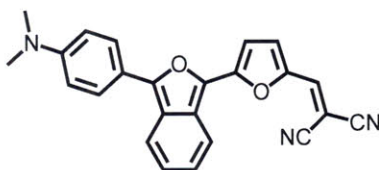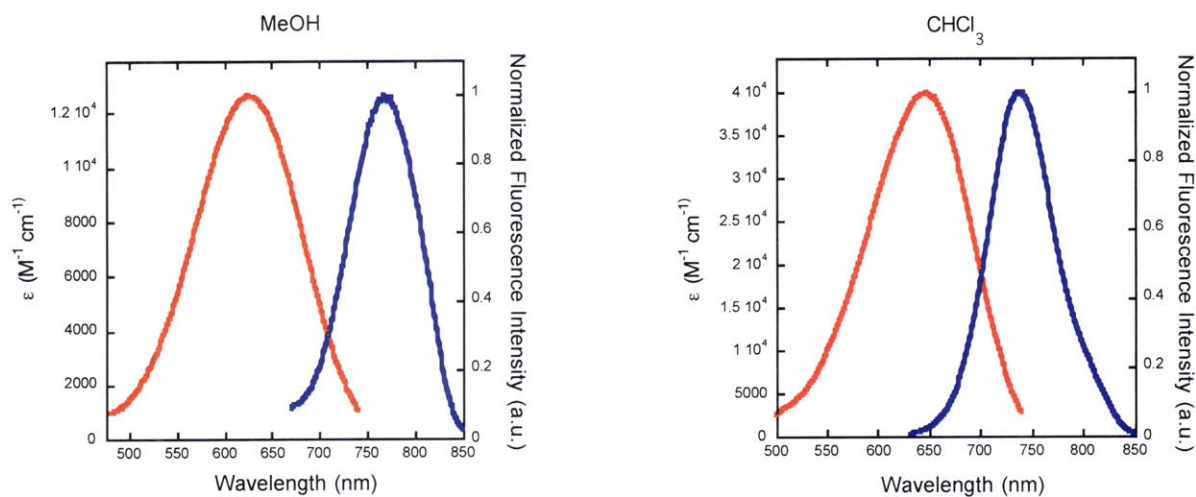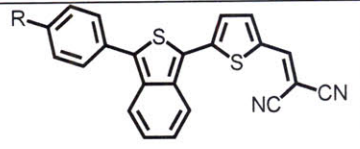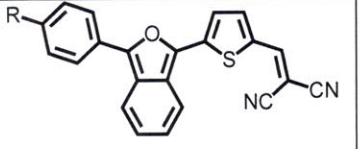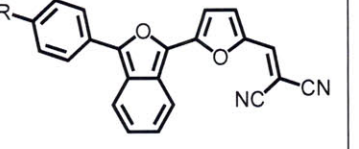
IBF-NIAD 13

Figure 3.16 Absorbance (red) and normalized fluorescence intensity (blue) spectra of **IBF-NIAD 12-13** in MeOH (left) and CHCl₃ (right).

113

Table 3.3 Spectroscopic Properties of IBF-NIAD 11-14

Dye	λ_{max} Abs. (nm)		λ_{max} Emission (nm)		Φ		ϵ (M^{-1} cm^{-1})	
	MeOH	CHCl$_3$	MeOH	CHCl$_3$	MeOH	CHCl$_3$	MeOH	CHCl$_3$
IBF-NIAD 14	551	571	640	629	0.11	0.12	26100	40500
IBF-NIAD 11	572	590	678	664	0.13	0.18	36700	46700
IBF-NIAD 12	579	588	686	658	0.10	0.16	37500	41800
INF-NIAD 13	625	646	769	738	0.014	0.076	12700	40100

As predicted, the quantum yield does increases with the transition from sulfur to oxygen, up to approximately 100% depending on the dye and solvent. As mentioned above, this effect has been reported previously in the literature and has been attributed to the internal heavy atom effect.[39] Due to its larger nucleus, the sulfur atom has greater spin-orbit coupling, enabling intersystem crossing, and thereby lowering the quantum yield.[40] This effect is also evident for the sulfur-oxygen substitution of isothianaphthene to isobenzofuran (Table 3.4). Thus, as the sulfur is replaced with oxygen in the conjugated backbone, the quantum yields of the dyes increase. It is also possible that solvation plays a role in this trend, as the ratios of quantum yields in MeOH and CHCl$_3$ are smaller as the number of oxygen molecules in the conjugated backbone increases, and the gains in quantum yield are more substantial in MeOH than in CHCl$_3$.

Table 3.4 Quantum Yield Comparison of S and O Containing Dyes

R-	Φ (MeOH)	Φ (CHCl₃)	Φ (MeOH)	Φ (CHCl₃)	Φ MeOH	Φ (CHCl₃)
H-	0.061	0.079	0.077	0.075	0.11	0.12
MeO-	0.046	0.099	0.078	0.16	0.13	0.18
HO-	0.023	0.071	0.049	0.12	0.10	0.16
Me₂N-	0.0015	0.021	0.0055	0.046	0.014	0.076
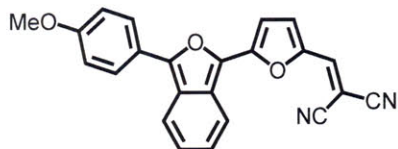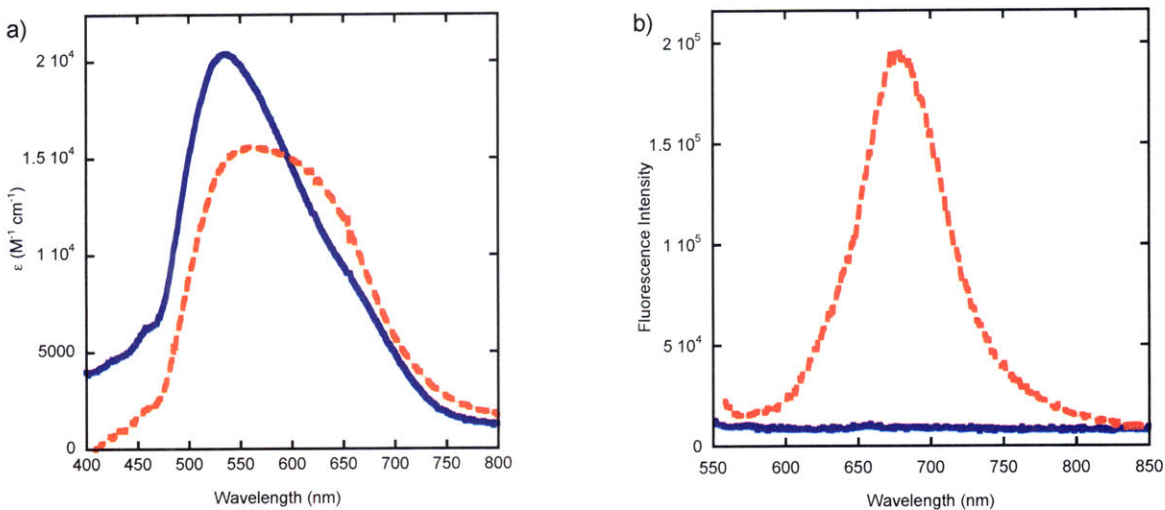
IBF-NIAD 11

Figure 3.17 Absorption (a) and fluorescence (b) spectra of **IBF-NIAD 11** (2.50 µM) in PBS buffer (blue solid line) and 10 µM aggregated Aβ(1-40) in PBS buffer (red dashed line).
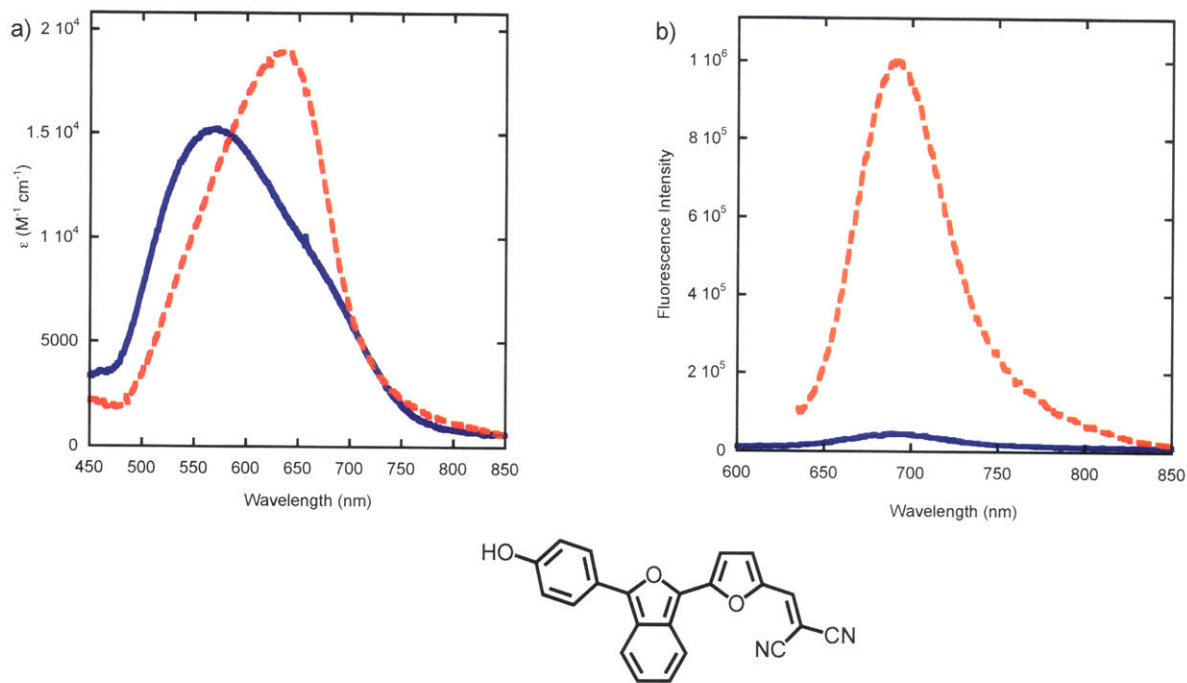
IBF-NIAD 12

Figure 3.18 Absorption (a) and fluorescence (b) spectra of **IBF-NIAD 12** (2.50 µM) in PBS buffer (blue solid line) and 10 µM aggregated Aβ(1-40) in PBS buffer (red dashed line).
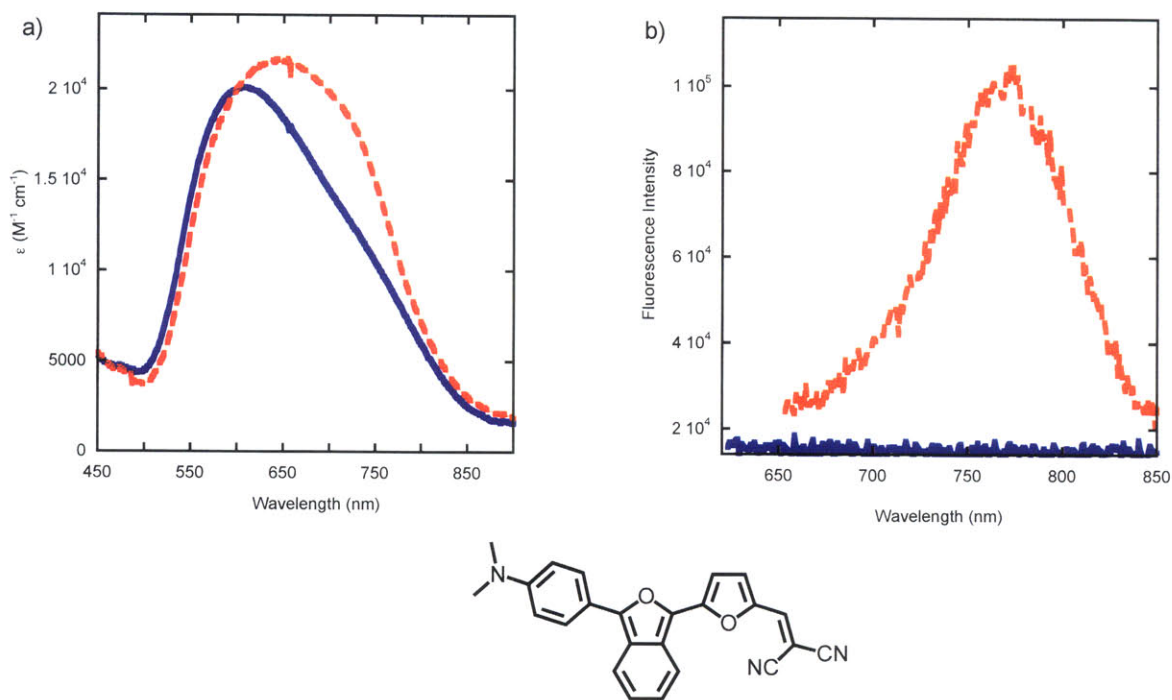
IBF-NIAD 13

Figure 3.19 Absorption (a) and fluorescence (b) spectra of **IBF-NIAD 13** (2.50 µM) in PBS buffer (blue solid line) and 10 µM aggregated Aβ(1-40) in PBS buffer (red dashed line).

116
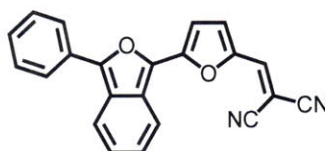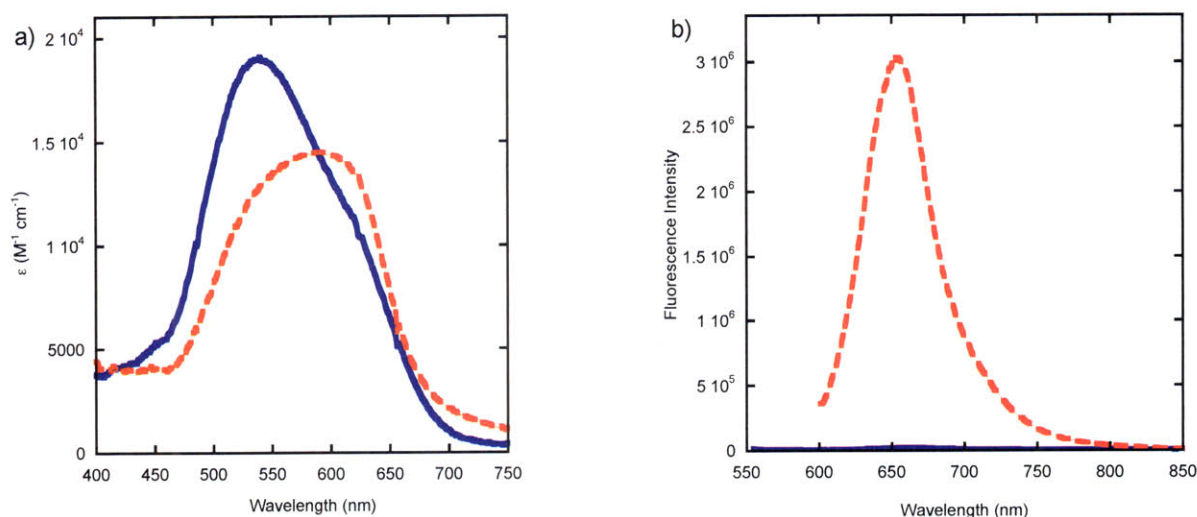
IBF-NIAD 14

Figure 3.20 Absorption (a) and fluorescence (b) spectra of **IBF-NIAD 14** (2.50 μM) in PBS buffer (blue solid line) and 10 μM aggregated Aβ(1-40) in PBS buffer (red dashed line).

Table 3.5 Summary of Aβ(1-40) Assay Results for IBF-NIAD 11-14

Dye (R-)	λ_{max} Abs. (nm)		λ_{max} Em. (nm)		Red-shift (nm)		$\varepsilon_{A\beta}/\varepsilon_{PBS}$	$\Phi_{A\beta}/\Phi_{PBS}$
	PBS	Aβ[a]	PBS	Aβ[a]	Abs.	Em.		
IBF-NIAD 11 (MeO-)	536	562	659	678	26	19	0.76	130
IBF-NIAD 12 (HO-)	572	634	700	691	62	-9	1.24	21
IBF-NIAD 13 (Me₂N-)	608	638	_[b]	772	30	_[b]	1.09	60[b]
IBF-NIAD 14 (H-)	540	591	661	653	51	-8	0.76	290

[a] Aβ(1-40) concentration was 10 μM. [b] Fluorescence intensity in PBS was undetectable, thus values are not available or are estimates.

The results of the Aβ(1-40) assay for **IBF-NIAD 11-14** (Figure 3.17-3.20) are generally improved over those for **IBF-NIAD 0-3**, with larger red shifts in absorption maxima (Table 3.5). **IBF-NIAD 12** exhibits the strongest response, with a 62 nm red shift in absorption maximum,

117

and also a 24% increase in extinction coefficient when bound to Aβ(1-40). The Aβ bound absorption maximum for this dye is red shifted 46 nm over its value in CHCl₃ solution, and absorption spectrum of the bound dye extends well into the NIR with extinction coefficient reduced only by 4% at 650 nm. The peak width for **IBF-NIAD 12** is also substantially narrower than that of **IBF-NIAD 3** (143 nm versus 200 nm at half maximum).

IBF-NIAD 12 stains SPs when incubated with brain tissue sections of an APP/PS1 mouse, as can be seen in Figure 3.21. **IBF-NIAD 11, 13,** and **14** do not bind to SPs in tissue staining studies, presumably due to aggregation of dyes in PBS buffer solution. **IBF-NIAD 13** does, however, stain white matter (Figure 3.22),[41] and may be useful in NIRF imaging of myelin pathologies, such multiple sclerosis.[42]
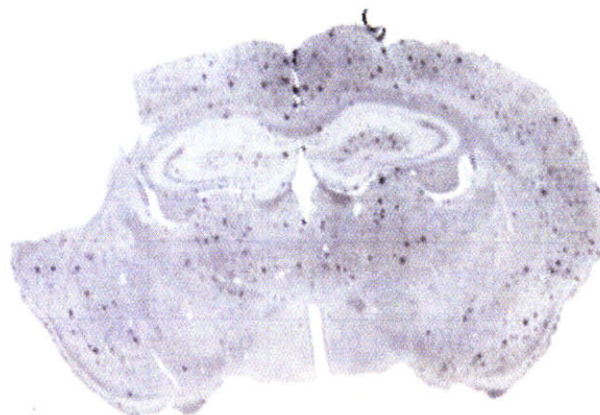
Figure 3.21 Image of a cross section of an aged APP/PS1 mouse brain stained with **IBF-NIAD 12**. Image taken with excitation at 685 nm and emission viewed through a 700 nm longpass filter. The black spots are fluorescent signals indicating staining of SPs by the dye. Image obtained by Brian Ferrara at Massachusetts General Hospital
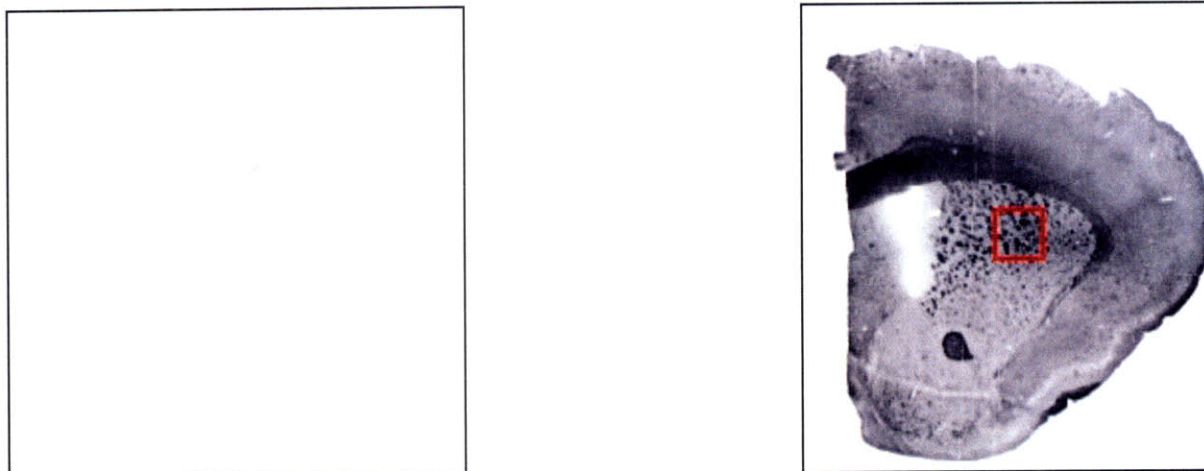
Figure 3.22 Image of (left) a cross section of an aged APP/PS1 mouse brain incubated with PBS buffer (unstained) and (right) with **IBF-NIAD 13**. Image taken with excitation at 633 nm. The red box is added to highlight staining of the white matter. Image obtained by Krista Neal at Massachusetts General Hospital.

3.2.4 IBF-NIAD 18-19: Controlling Amine Functionality

Our next step in the modifying this series was to attempt to control the functionality of the amine donor group. We hoped this would afford not only dyes with a free amine, which would help to decrease hydrophobicity and thus aggregation, but would also to allow the integration of this fluorophore technology into cleavable sensors, such as have be used to monitor enzyme activity[43] or detect thiols[44] and would provide a functional handle for conjugation to proteins or the addition of other chemical functionality. In order to accomplish this goal synthetically, we needed a protected amino phthalide, preferably one that could be cleaved at any step in the synthesis.

Our first attempt utilized the benzyl-protecting group, which would be able to survive the strongly acidic conditions of phthalide formation and the strongly basic conditions of the condensation used to form the isobenzofuran backbone. N,N-dibenzyl-aniline (**11**) was synthesized from aniline and benzylchloride and was then condensed with 2-

carboxybenzaldehyde to afford protected phthalide **13**, which proved amenable to the standard

dye synthesis procedure (Scheme 3.3).

Scheme 3.3: Synthesis of Benzyl-Protected Dye
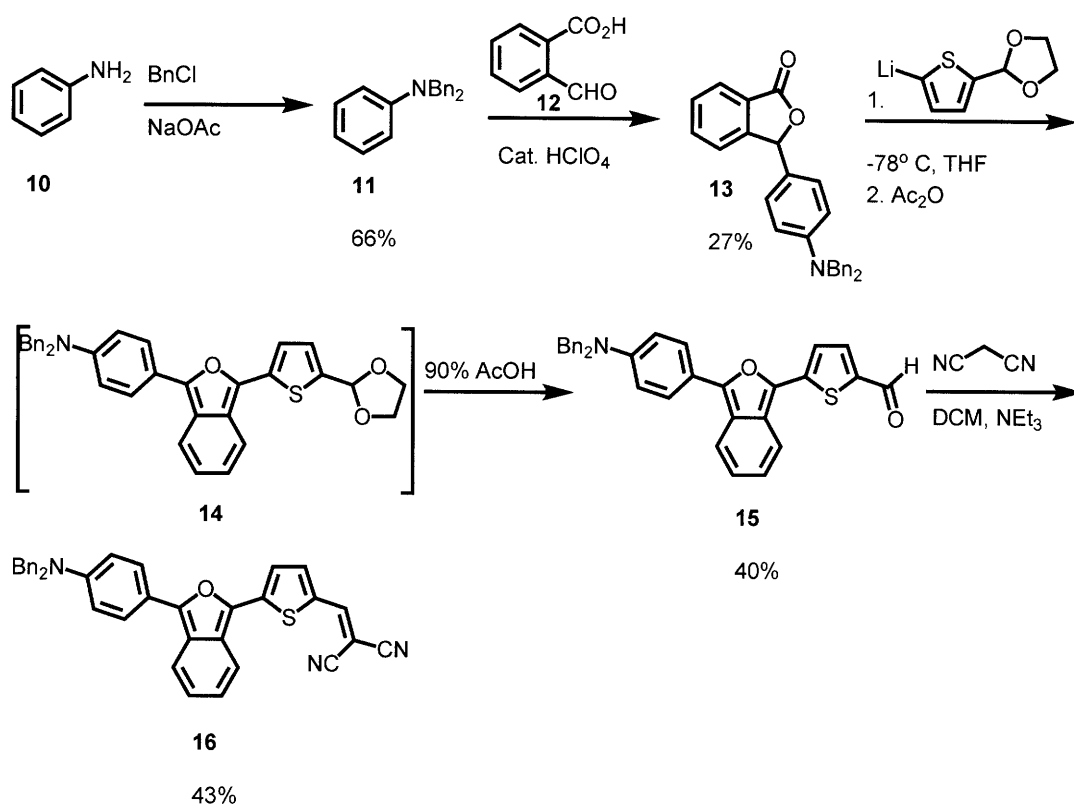
Cleavage of the benzyl protecting groups proved problematic. Hydrogenation with H_2 gas or

ammonium ammonium formate and palladium catalyst (Pd/C or Pearlman's catalyst) was

attempted on **13**, **14**, **15**, and **16**, and either did not remove the benzyl groups or resulted in

decomposition.

The complications involved with benzyl-deprotection lead us to explore alternate

protection schemes, and we finally settled on benzophenone imine, which is known to be stable

to aryl-lithium chemistry.[45] Amino-phthalide **18** was synthesized by the nitration of 3-

phenylphthalide with nitric acid and sulfuric acid,[46] followed by reduction with tin chloride. The

amine was then acidified, and the protecting group installed by transamination with benzophenonimine (Scheme 3.4).

Scheme 3.4 Synthesis of IBF-NIAD 18-19
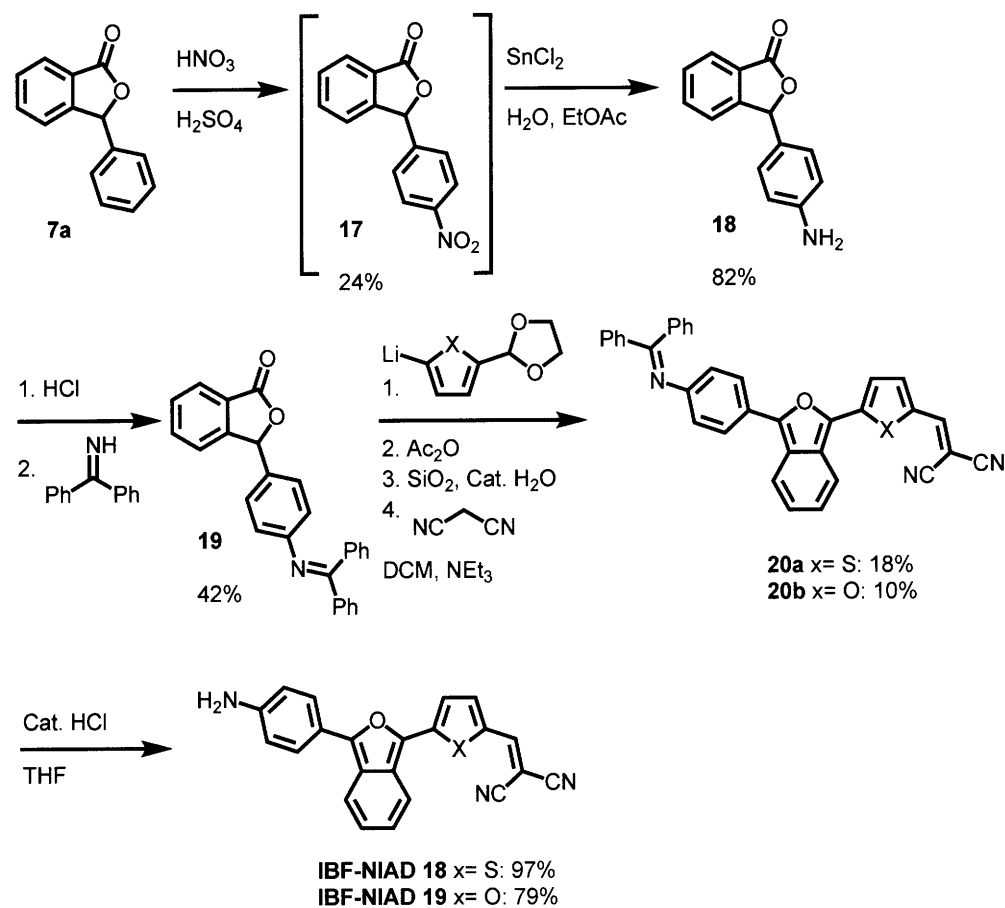
Synthesis of **IBF-NIAD 18** and **19** required selective deprotection of the acetal in the presence of the benzophenone imine, due to reaction of the free amine with the aldehyde under acid or basic conditions. This was accomplished by stirring the acetal in a DCM-silica gel slurry with catalytic H_2O.[47] It should also be noted that selective deprotection of the imine in the presence of the acetal can be achieved by transamination with hydroxylamine.[48] Final deprotection to afford **IBF-NIAD 18** and **19** was carried out with catalytic HCl in THF.
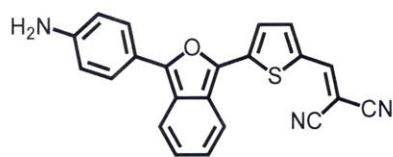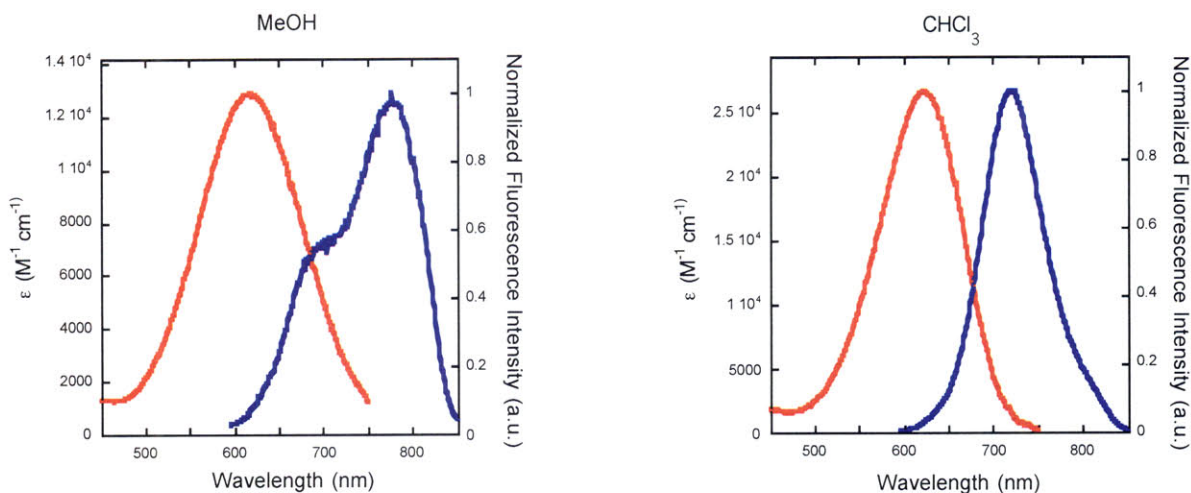
IBF-NIAD 18
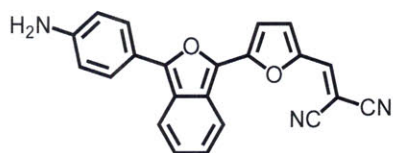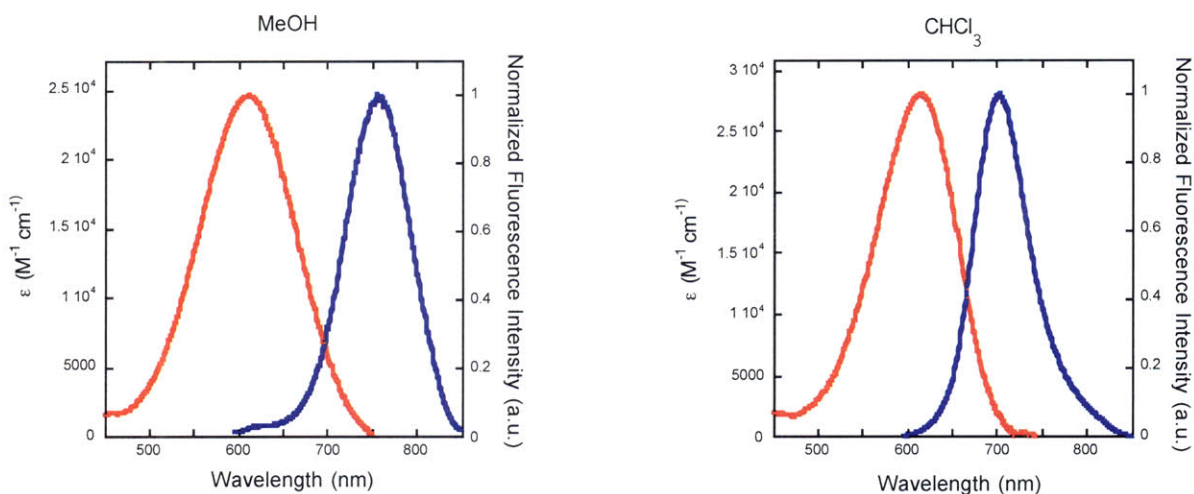
IBF-NIAD 19

Figure 3.23 Absorbance (red) and normalized fluorescence intensity (blue) spectra of **IBF-NIAD 12-13** in MeOH (left) and CHCl₃ (right).

Table 3.6 Spectroscopic Properties of IBF-NIAD 18-19

Dye	λ_{max} Abs. (nm)		λ_{max} Emission (nm)		Φ		ε (M^{-1} cm^{-1})	
	MeOH	CHCl$_3$	MeOH	CHCl$_3$	MeOH	CHCl$_3$	MeOH	CHCl$_3$
IBF-NIAD 18	618	620	776	718	0.0076	0.054	12900	26700
IBF-NIAD 19	611	615	755	702	0.014	0.094	24700	28100

The absorbance and fluorescence emission spectra are shown in Figure 3.23, and their spectroscopic properties are summarized in Table 3.6. Compared to **IBF-NIAD 2** and **IBF-NIAD 13**, the λ_{max} absorption of **IBF-NIAD 18** and **IBF-NIAD 19** are blue-shifted by 14-26 nm. This shift can probably be attributed to the lower electron density on the nitrogen in the absence of the electron donating methyl groups. The fluorescence emission maxima also experience a blue shift of 14-44 nm. We observe two emission bands for **IBF-NIAD 18** in MeOH, indicating two emitting species likely due to a partially aggregated state. In addition, the lower molar extinction coefficient for this molecule in MeOH, as compared to CHCl$_3$, suggests that the chromophore is aggregated. Quantum yields for **IBF-NIAD 18** and **IBF-NIAD 19** are slightly increased over their dimethylated counterparts.
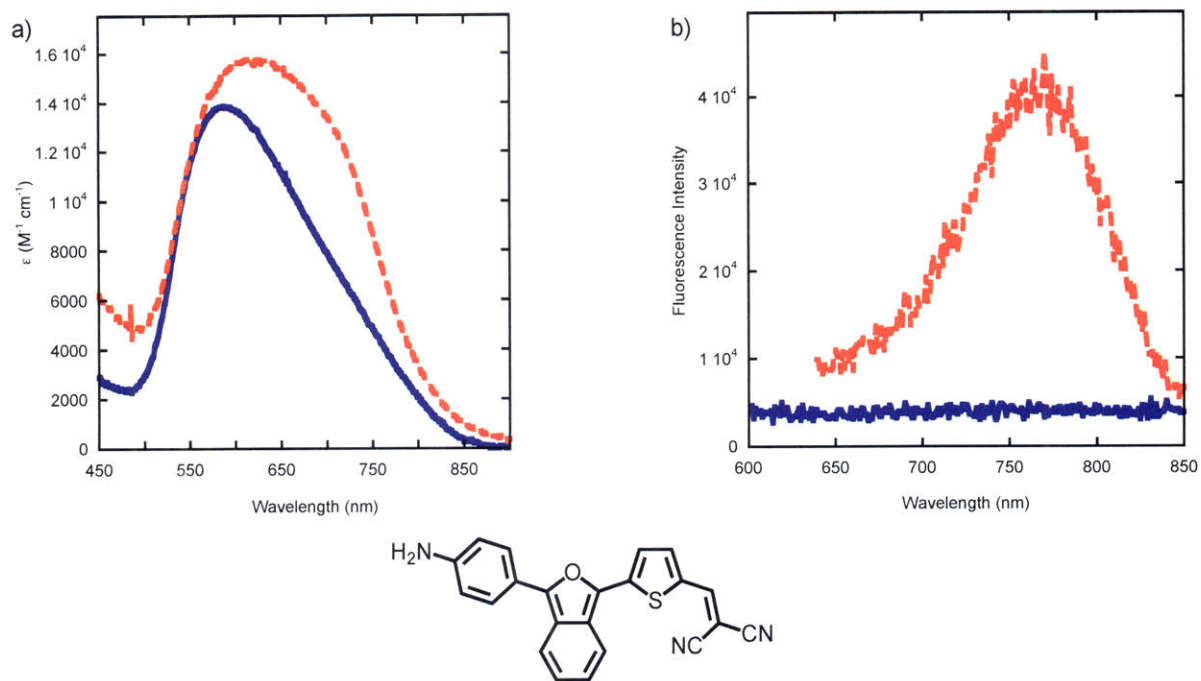
Figure 3.24 Absorption (a) and fluorescence (b) spectra of **IBF-NIAD 18** (2.50 μM) in PBS buffer (blue solid line) and 10 μM aggregated Aβ(1-40) in PBS buffer (red dashed line).
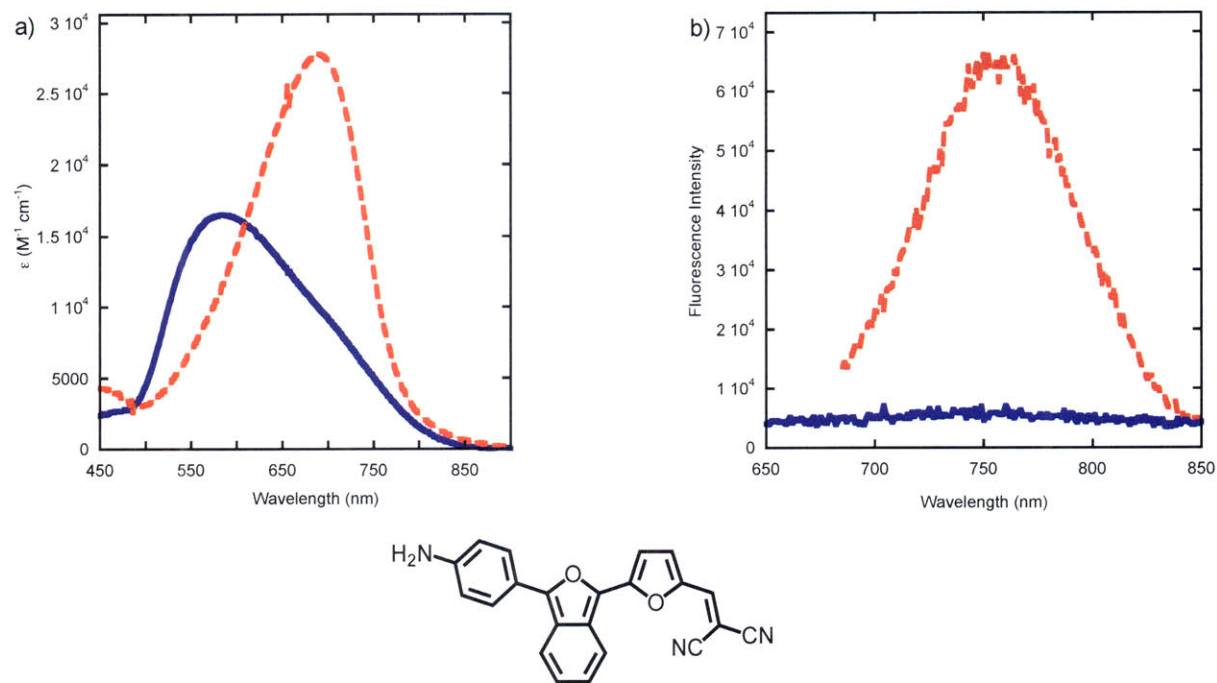
Figure 3.25 Absorption (a) and fluorescence (b) spectra of **IBF-NIAD 19** (3.68 μM) in PBS buffer (blue solid line) and 10 μM aggregated Aβ(1-40) in PBS buffer (red dashed line).

124

Table 3.7 Summary of Aβ(1-40) Assay Results for IBF-NIAD 18-19

Dye (R-)	λ_{max} Abs. (nm)		λ_{max} Em. (nm)		Red-shift (nm)		$\varepsilon_{A\beta}/\varepsilon_{PBS}$	$\Phi_{A\beta}/\Phi_{PBS}$
	PBS	Aβ[a]	PBS	Aβ[a]	Abs.	Em.		
IBF-NIAD 18 (H$_2$N-)	587	624	_[b]	770	37	_[b]	1.15	30[b]
IBF-NIAD 19 (H$_2$N-)	583	690	760	759	107	-1	1.68	14

[a] Aβ(1-40) concentration was 10 μM. [b] Fluorescence intensity in PBS was undetectable, thus values are not available or are estimates.

The results of the Aβ(1-40) assay for **IBF-NIAD 18** and **19** are shown in Figure 3.24 and Figure 3.25 and are summarized in Table 3.7. **IBF-NIAD 18** exhibits a modest 34 nm red shift in absorption maximum and 15% increase in extinction coefficient on binding. However, the spectroscopic changes experienced by **IBF-NIAD 19** on binding to Aβ are more pronounced. The absorption maximum is shifted to 690 nm, a 107 nm and 75 nm red shift from PBS and CHCl$_3$ solutions respectively; the extinction coefficient enjoys a 68% enhancement. Its peak width is comparable to that of Aβ bound **IBF-NIAD 12** (149 nm versus 143 nm at half maximum) While **IBF-NIAD 19** stains SPs in APP/PS1 tissue, **IBF-NIAD 18** does not.

Figure 3.26 Image of (left) a cross section of an aged APP/PS1 mouse brain incubated with PBS buffer (unstained) and (right) with 5 μM **IBF-NIAD 19**. Image taken with excitation at 633 nm. Black spots are fluorescent signals indicating staining of SPs by **IBF-NIAD 19**. Image obtained by Krista Neal at Massachusetts General Hospital.

3.2.5 IBF-NIAD 22-25: Exploration of Water Solublizing groups

In order to further decrease the hydrophobicity of our dyes, we explored several different strategies for the integration of water solublizing groups into our fluorophore design. Our first thought was to add additional hydroxyl groups to the phenyl ring, and we were able to synthesize TiPS protected catechol-phthalide **22** and TiPS protected glycol-catechol-phthalide **24** (Scheme 3.5). Unfortunately, the resulting IBF compounds, **23** and **25**, were unstable, possibly due to their ease of oxidation.

Scheme 3.5 Attempted Synthesis of Catechol IBF-NIADs
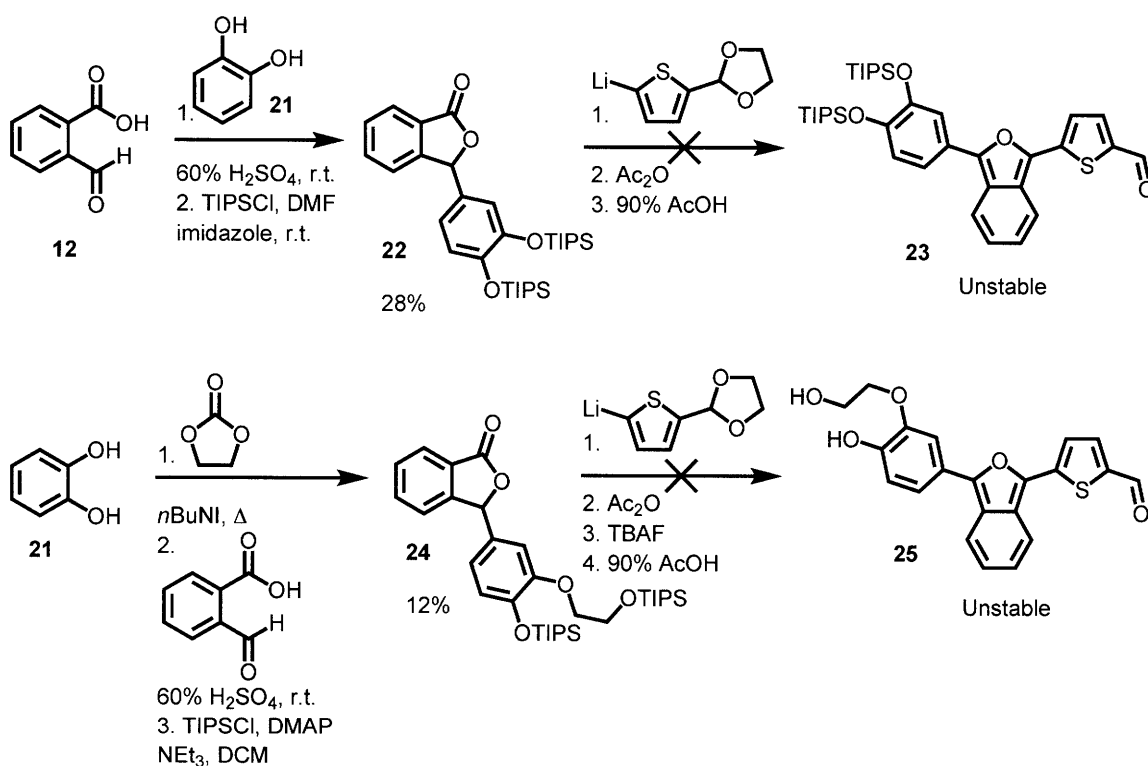
We also attempted to install a water solublizing chain, in this case a diethylene glycol methyl ether, onto the acceptor end of the dye (Scheme 3.6). Triethylene glycol monomethyl ether was oxidized with $KMnO_4$ under basic conditions to carboxylic acid **27**. Reaction of this

acid with oxalyl chloride followed by quenching with N,O-dimethylhydroxylamine hydrochloride afforded Weinreb amide **28**. Condensation of the amide with 2-bromo-5-lithiothiophene, followed by protection of the resulting ketone gave bromothiophene **29**. IBF dye precursor **30** proved unstable and difficult to isolate, and neither acid nor base catalyst nor the Lehnert conditions[49] were able to effect the Knoevenagel condensation with malonitrile, instead resulting in decomposition of the starting material.

Scheme 3.6 Attempted Installation of Diethylene Glycol Chain
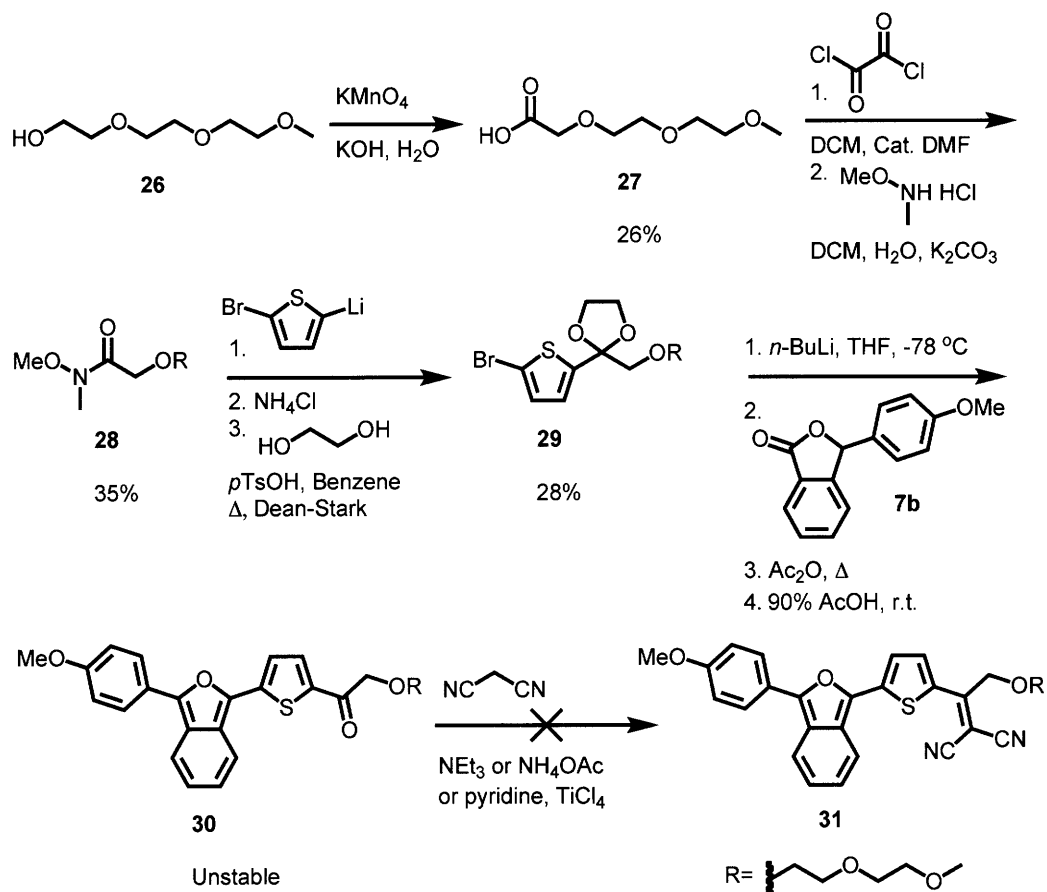
We next looked to the primary functional handle in this dye series, the electron donating group, as a location for water solubilizing groups. In particular, the addition of a glycol or propane-1,2-diol group to the oxygen electron donating group looked particularly attractive due

to their small size and the ease of integration into our fluorophore design and synthesis. Attempts were made to functionalize **IBF-NIAD 3** and **IBF-NIAD 12** directly, but with no success, thus, we had to design protected phthalides to integrate the glycol and propane-1,2-diol groups.

Scheme 3.7: Synthesis of IBF-NIAD 22 and IBF-NIAD 24
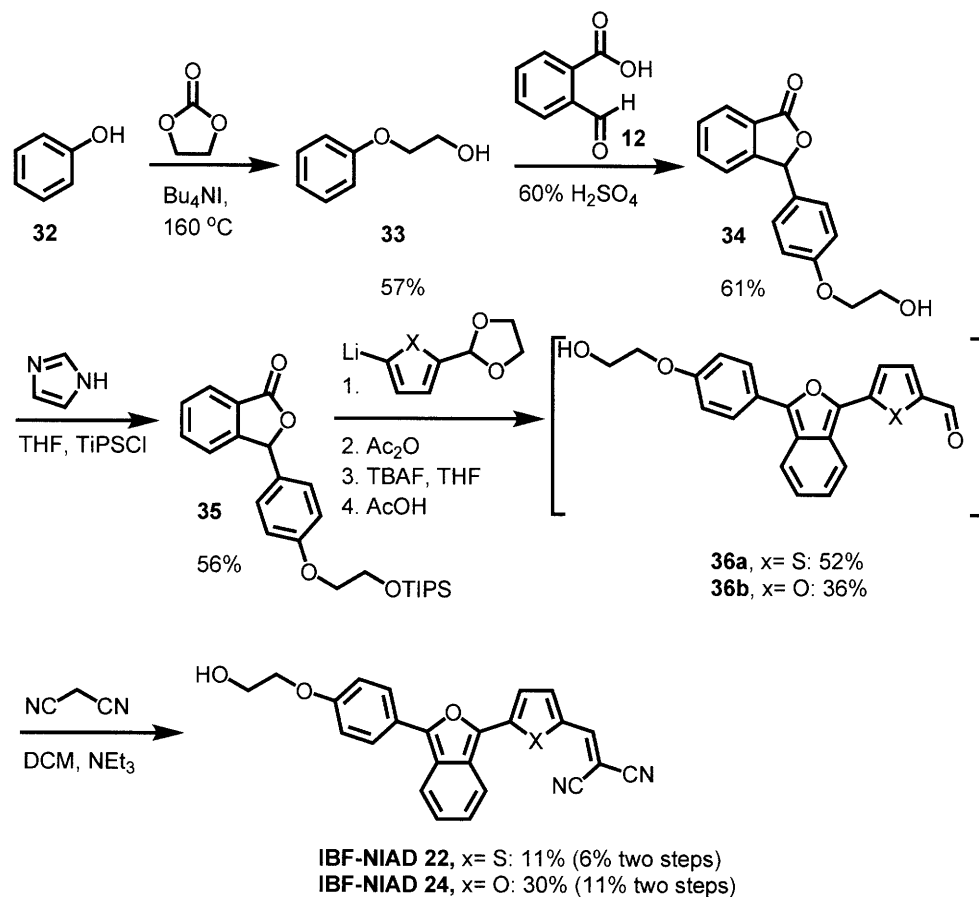
Protected glycol phthalide was synthesized in three steps (Scheme 3.7). Phenol was reacted with ethylene carbonate in the presence of catalytic tetrabutylammonium iodide to form ether **33**, which was in turn condensed with 2-carboxybenzaldehyde under acid conditions to yield phthalide **34**. Installation of a TIPS protecting group was accomplished with imidazole and TIPSCl. Phthalide **35** was submitted to the standard dye synthesis procedure, with cleavage of

the TiPS group with tetrabutylammonium fluoride before hydrolysis of the acetal, to afford **IBF-NIAD 22** and **24**.

Scheme 3.8: Synthesis of IBF-NIAD 23 and IBF-NIAD 25
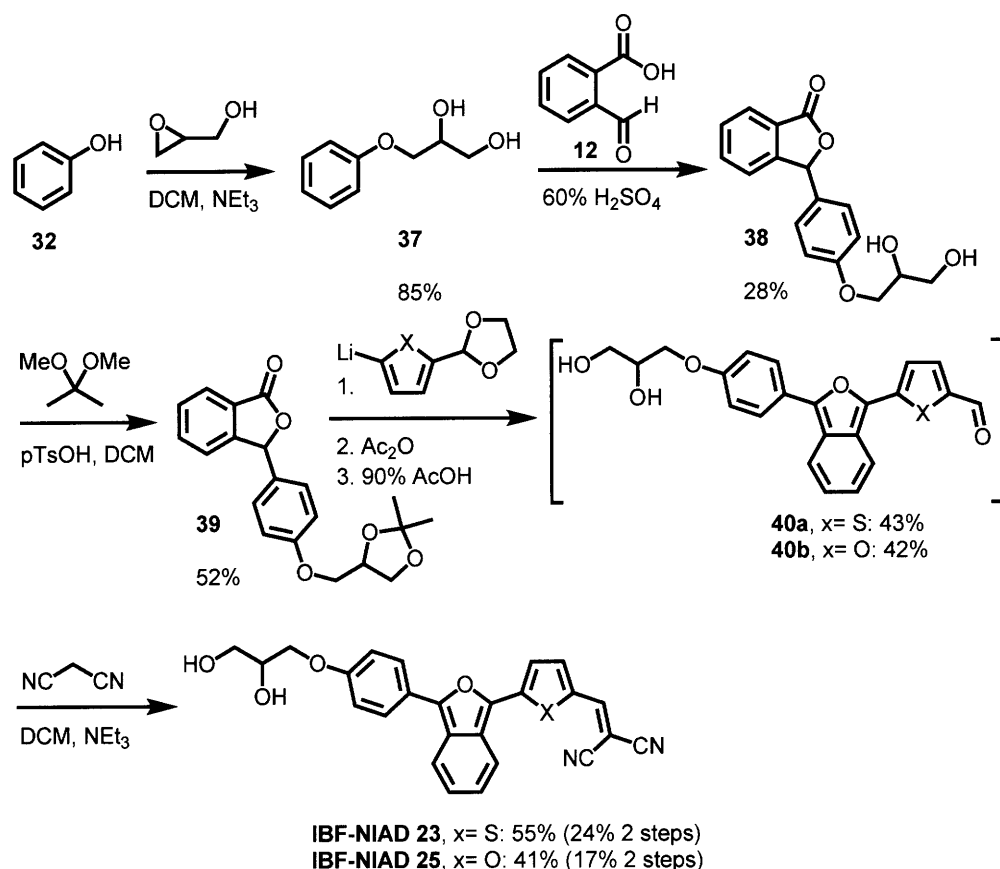
The synthesis of the phthalide with a protected propane-1,2-diol group was also achieved in three steps (Scheme 3.8). The epoxide of glycidol was opened with phenol in the presence of triethylamine to yield 1,2-diol **37**. Acid mediated condensation of **37** with 2-carboxybenzaldehyde afforded phthalide **38**, which was protected with 2,2-dimethoxy propane to give acetal protected phthalide **39**. Phthalide **39** could also be protected with TiPS, but the acetal provided superior yields, and better atom economy. Phthalide **39** was submitted to the standard dye synthesis conditions to afford **IBF-NIAD 23** and **IBF-NIAD 25**. The absorption and

fluorescence emission spectra of **IBF-NIAD 22-25** are presented in Figures 3.27 and 3.28, and

the spectroscopic properties of these fluorophores are summarized in Table 3.8.
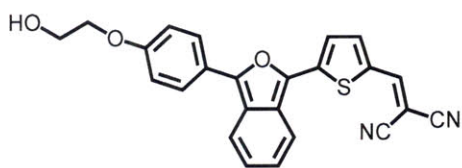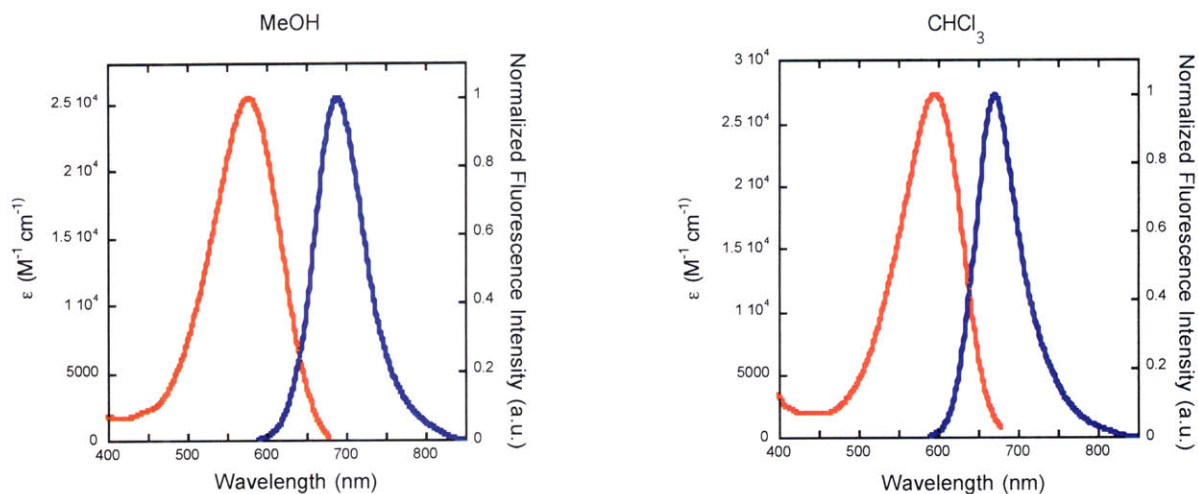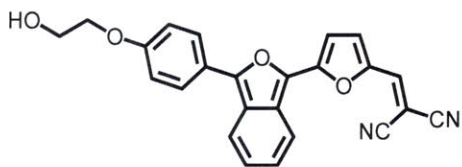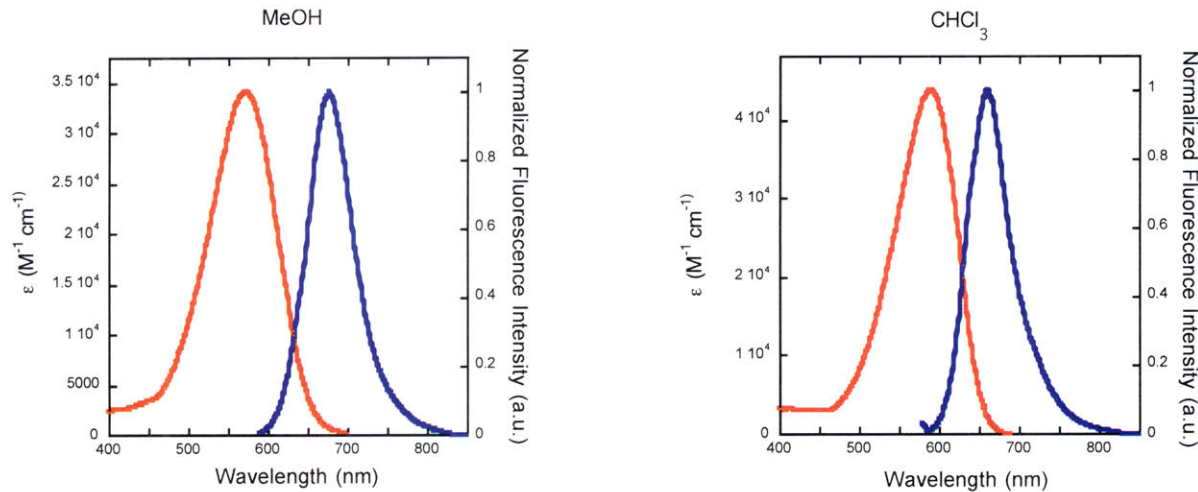
Figure 3.27 Absorption (red) and normalized fluorescence emission (blue) spectra of **IBF-NIAD 22** and **IBF-NIAD 24** in MeOH (left) and CHCl₃ (right).
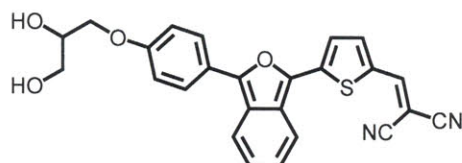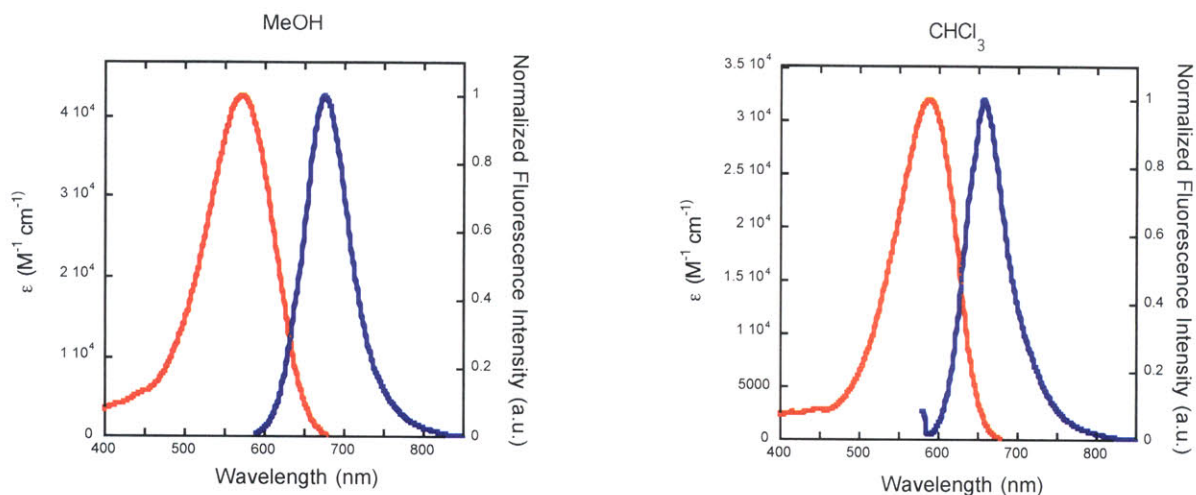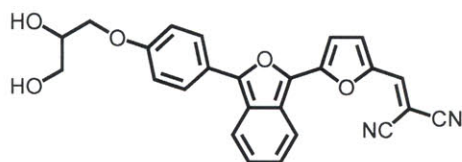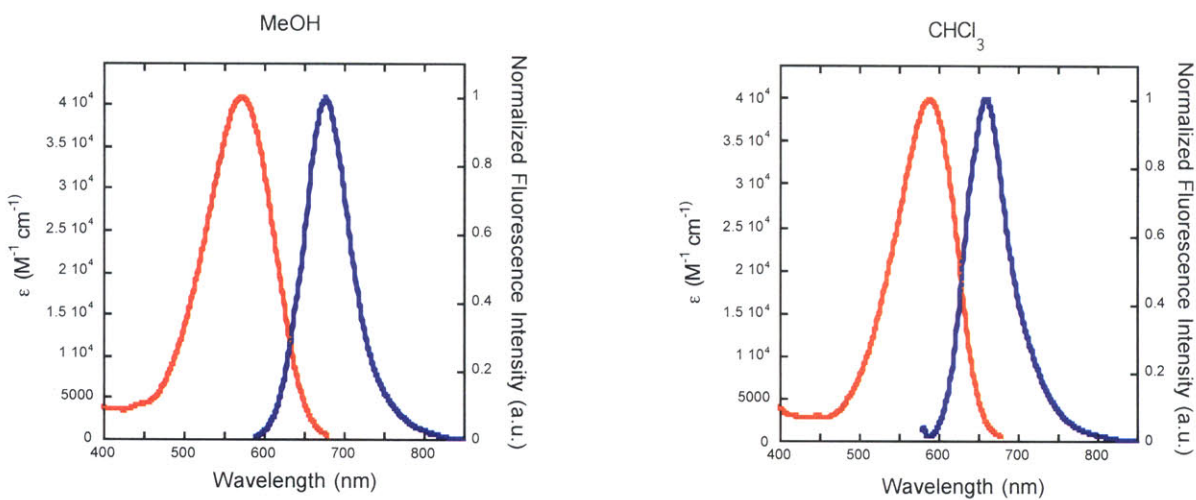
Figure 3.28 Absorption (red) and normalized fluorescence emission (blue) spectra of IBF-NIAD 23 and IBF-NIAD 25 in MeOH (left) and CHCl₃ (right).

132

Table 3.8 Spectroscopic Properties of IBF-NIAD 22-25

Dye	λ_{max} Abs. (nm)		λ_{max} Emission (nm)		Φ		ε (M^{-1} cm^{-1})	
	MeOH	CHCl$_3$	MeOH	CHCl$_3$	MeOH	CHCl$_3$	MeOH	CHCl$_3$
IBF-NIAD 22	577	597	688	671	0.071	0.14	25500	27400
IBF-NIAD 24	572	589	677	661	0.12	0.16	34200	43800
IBF-NIAD 23	571	589	676	659	0.11	0.15	42700	32000
INF-NIAD 25	572	587	676	660	0.11	0.15	40900	39900
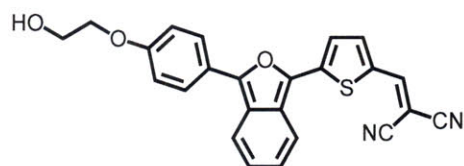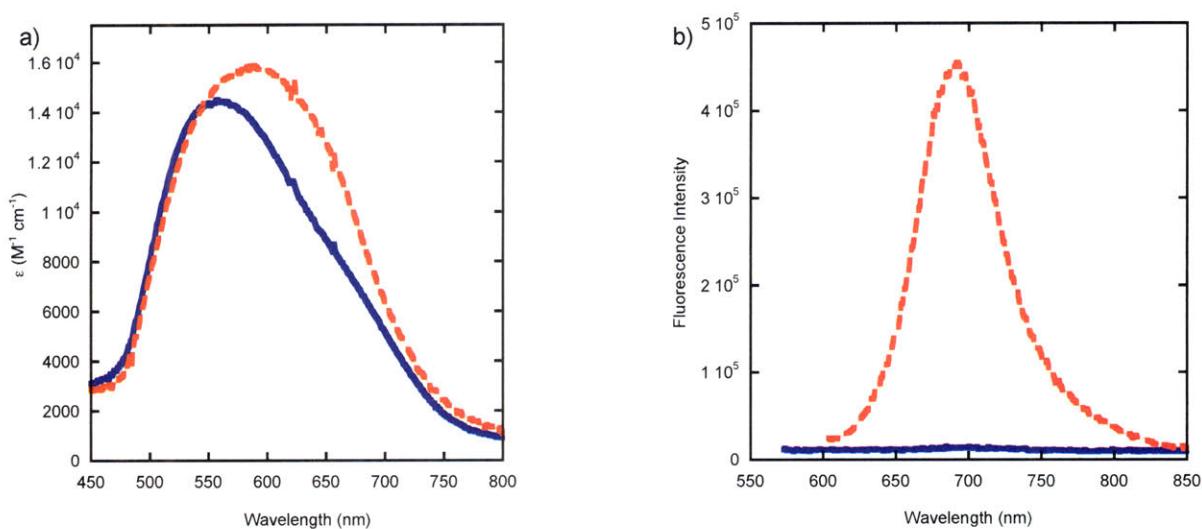
IBF-NIAD 22

Figure 3.29 Absorption (a) and fluorescence (b) spectra of **IBF-NIAD 22** (2.50 μM) in PBS buffer (blue solid line) and 10 μM aggregated Aβ(1-40) in PBS buffer (red dashed line).

133
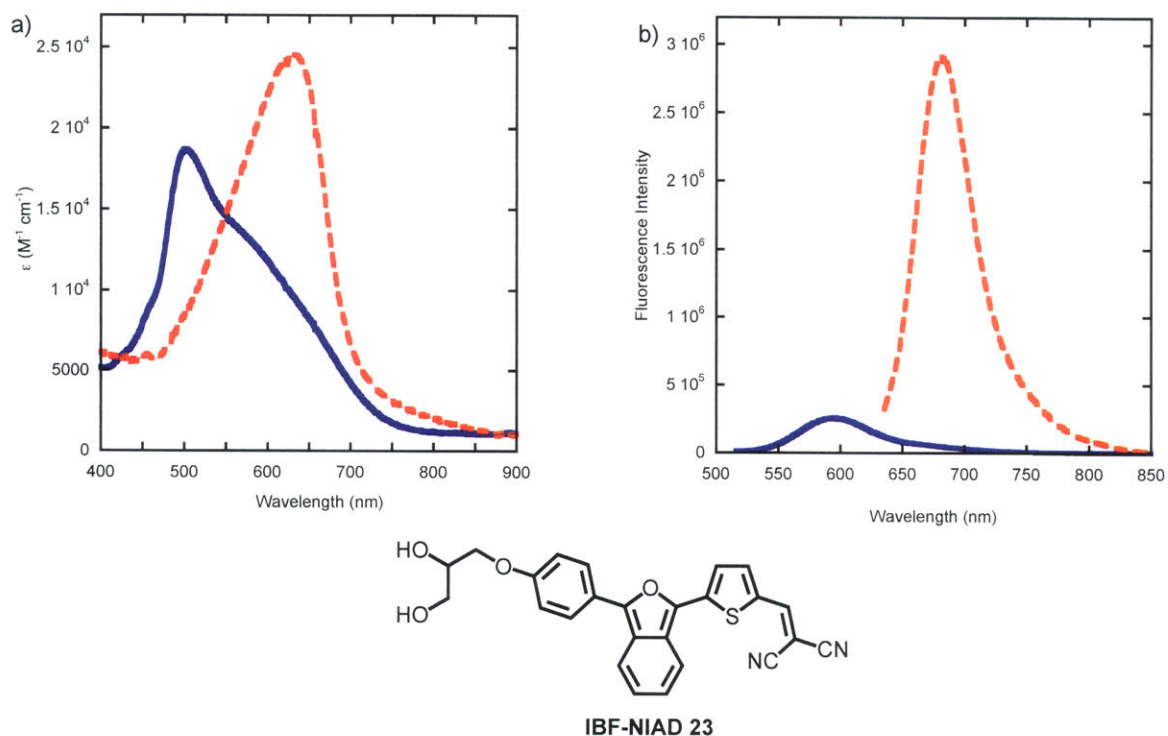
Figure 3.30 Absorption (a) and fluorescence (b) spectra of **IBF-NIAD 23** (2.50 µM) in PBS buffer (blue solid line) and 10 µM aggregated Aβ(1-40) in PBS buffer (red dashed line).
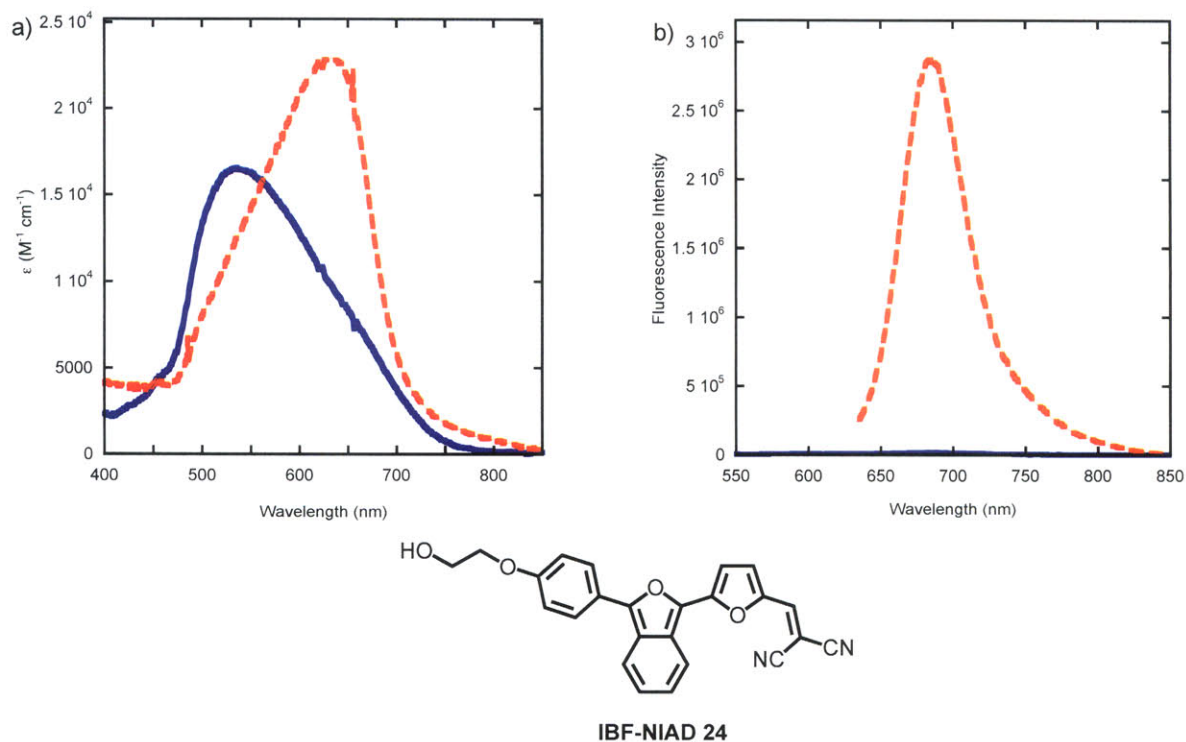
Figure 3.31 Absorption (a) and fluorescence (b) spectra of **IBF-NIAD 24** (2.50 µM) in PBS buffer (blue solid line) and 10 µM aggregated Aβ(1-40) in PBS buffer (red dashed line).
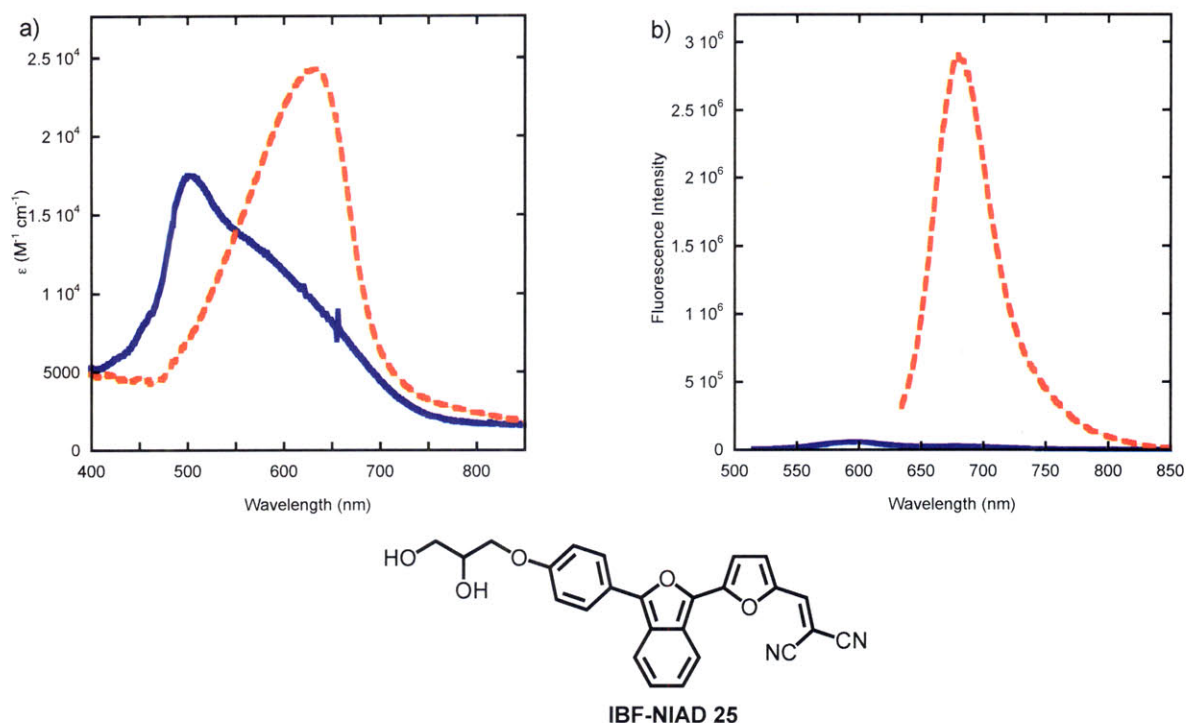
IBF-NIAD 25

Figure 3.32 Absorption (a) and fluorescence (b) spectra of **IBF-NIAD 25** (2.50 μM) in PBS buffer (blue solid line) and 10 μM aggregated Aβ(1-40) in PBS buffer (red dashed line).

Table 3.9: **Summary of Aβ(1-40) Assay Results for IBF-NIAD 22-25**

Dye (R-)	λ_{max} Abs. (nm)		λ_{max} Em. (nm)		Red-shift (nm)		$\varepsilon_{A\beta}/\varepsilon_{PBS}$	$\Phi_{A\beta}/\Phi_{PBS}$
	PBS	Aβ[a]	PBS	Aβ[a]	Abs.	Em.		
IBF-NIAD 22 (glycol-)	558	589	685	689	31	4	1.10	100
IBF-NIAD 23 (1,2-diol-)	501	630	594	683	129	89	1.31	6.9
IBF-NIAD 24 (glycol-)	535	633	683	686	98	3	1.39	68
IBF-NIAD 25 (1,2-diol-)	501	634	597	680	133	83	1.39	24

[a] Aβ(1-40) concentration was 10 μM. [b] Fluorescence intensity in PBS was undetectable, thus values are not available or are estimates.

IBF-NIAD 22-25 all experience enhanced optical properties when bound to Aβ(1-40). In PBS buffer these materials showed a more defined blue shifted band consistent with H-aggregate formation, and this aggregate is clearly disassembled by Aβ(1-40). Of this set, the weakest

response comes from **IBF-NIAD 22**, with a red shift in absorption maximum of 31 nm, and 10% increase in extinction coefficient. **IBF-NIAD 23, 24,** and **25** show similar optical response to **IBF-NIAD 12**, with absorption maxima around 630 nm in the bound state and increases in extinction coefficient of 31-39%. The absorption maxima for these dyes in PBS buffer are blue shifted compared to **IBF-NIAD 12**, which contribute to their larger red shifts on binding. **IBF-NIAD 23** and **25** form weakly emissive species, presumably aggregates, with emission maximum of 594 nm and 597 nm respectively. When the dyes are bound to Aβ(1-40), they experience about an 85 nm red shift in fluorescence emission maximum, as well as increased fluorescence intensity. **IBF-NIAD 22, 23,** and **25** stain SPs in aged APP/PS1 mouse brain tissue (Figure 3.33-3.35). The fluorescence lifetimes of these dyes have also been evaluated (Figure 3.36), and found to increase on binding to Aβ (Table 3.10), thus opening up the possibility of using them as NIR FLIM contrast agents.
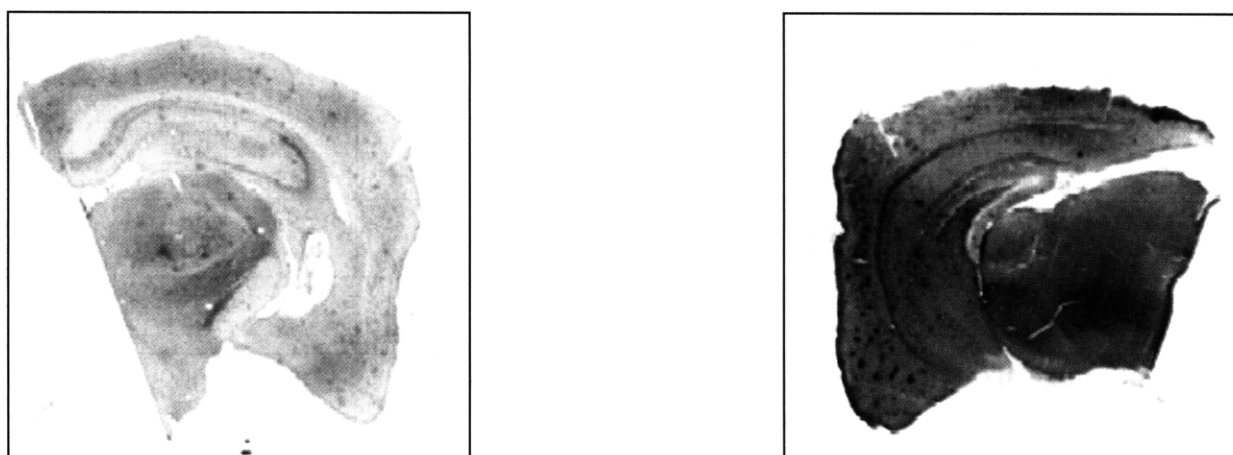
Figure 3.33: Image of (left) a cross section of an aged APP/PS1 mouse brain incubated with PBS buffer (unstained) and (right) with 5 µM **IBF-NIAD 22**. Image taken with excitation at 633 nm. Black spots are fluorescent signals indicating staining of SPs by **IBF-NIAD 22**. Image obtained by Krista Neal at Massachusetts General Hospital.
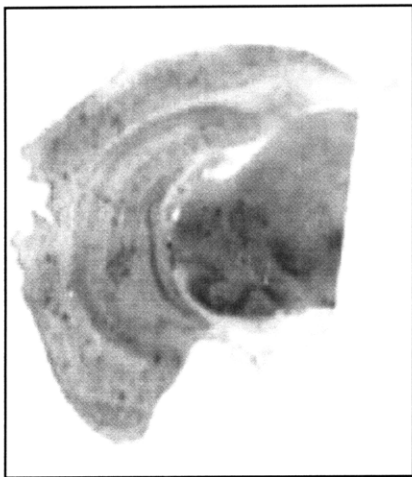
200 µm
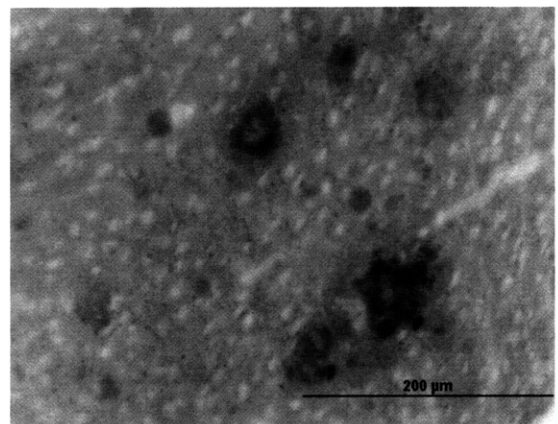
200 µm

Figure 3.34 Image of (top left) a cross section of an aged APP/PS1 mouse brain incubated with PBS buffer (unstained), (top right) with 5 µM **IBF-NIAD 23**, (bottom left) a cross section of an aged APP/PS1 mouse brain incubated with PBS buffer (unstained), (bottom right) with 5 µM **IBF-NIAD 23**. Top images were taken with excitation at 543 nm, bottom images with excitation at 620 nm. Black spots are fluorescent signals indicating staining of SPs by **IBF-NIAD 23**. Images obtained by Krista Neal at Massachusetts General Hospital
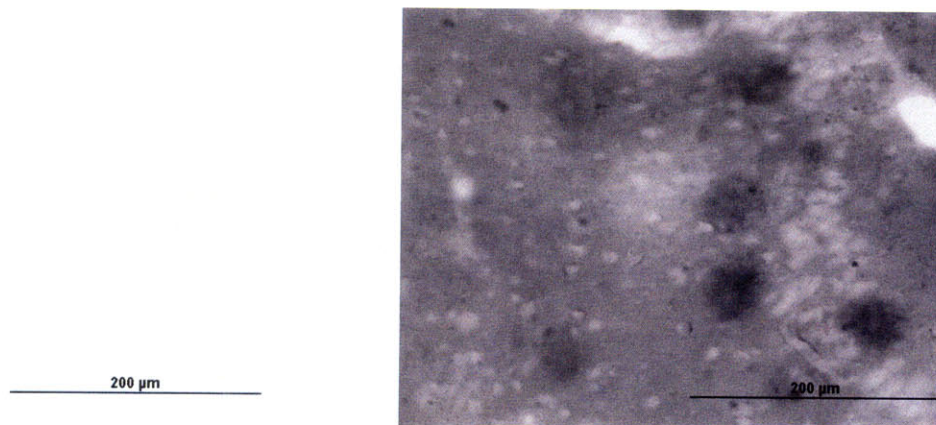
Figure 3.35 Image of (left) a cross section of an aged APP/PS1 mouse brain tissue incubated with PBS buffer (unstained) and (right) with 5 µM **IBF-NIAD 25**. Image taken with excitation at 620 nm. Black spots are fluorescent signals indicating staining of SPs by **IBF-NIAD 25**. Images obtained by Krista Neal at Massachusetts General Hospital
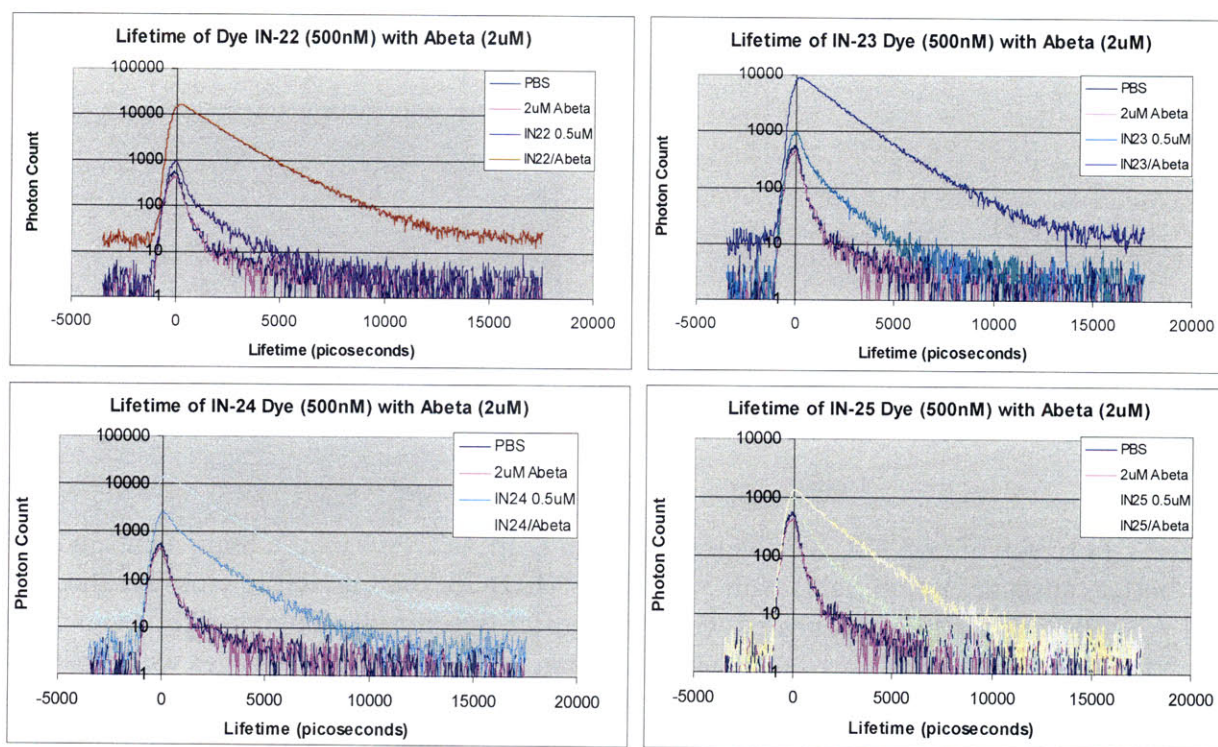
Figure 3.36 Fluorescence lifetime of (top left) **IBF-NIAD 22**, (top right) **IBF-NIAD 23**, (bottom left) **IBF-NIAD 24**, and (bottom right) **IBF-NIAD 25**. Data collected by Krista Neal at Massachusetts General Hospital.

Table 3.10 Fluorescence Lifetimes of IBF-NIAD 22-25

Dye	τ unbound (ps)	τ bound (ps)
IBF-NIAD 22	200, 1330 (biexponential)	1410 (monoexponential)
IBF-NIAD 23	190, 1240 (biexponential)	1660 (monoexponential)
IBF-NIAD 24	420, 1490 (biexponential)	1320 (monoexponential)
IBF-NIAD 25	990 (monoexponential)	1620 (monoexponential)

3.3 Conclusions

Table 3.11 Summary of Dye-Aβ Interactions

Dye (R-)	λ_{max} Aβ (nm)		Red-Shift (nm)		$\varepsilon_{A\beta}/\varepsilon_{PBS}$	$\Phi_{A\beta}/\Phi_{PBS}$	Tissue Staining	τ increase
	Abs.	Em.	Abs.	Em.				
IBF-NIAD 0 (H-)	550	656	11	-9	1.07	190	No	
IBF-NIAD 1 (MeO-)	612	690	52	_[a]	1.06	800[a]	No	
IBF-NIAD 2 (Me₂N-)	627	796	6	_[a]	1.03	20[a]	No	
IBF-NIAD 3 (HO-)	603	704	43	3	0.85	62	No	
IBF-NIAD 4 (MeO-Th-)	601	739	15	_[a]	0.77	30[a]	Yes	
IBF-NIAD 11 (MeO-)	562	678	26	19	0.76	130	No	
IBF-NIAD 12 (HO-)	634	691	62	-9	1.24	21	Yes	
IBF-NIAD 13 (Me₂N-)	638	772	30	_[a]	1.09	64[a]	No[b]	
IBF-NIAD 14 (H-)	591	653	51	-8	0.76	290	No	
IBF-NIAD 18 (H₂N-)	624	770	37	_[a]	1.15	30[a]	No	
IBF-NIAD 19 (H₂N-)	690	759	107	-1	1.68	14	Yes	
IBF-NIAD 22 (glycol-)	589	689	31	4	1.10	100	Yes	Yes
IBF-NIAD 23 (1,2-diol-)	607	683	106	89	1.31	6.9	Yes	Yes
IBF-NIAD 24 (glycol-)	633	686	98	3	1.39	68	No	Yes
IBF-NIAD 25 (1,2-diol-)	634	680	133	83	1.39	24	Yes	Yes

[a]Fluorescence signal in PBS solution is too weak to quantify, thus values are not available or are estimates. [b] White matter staining observed.

In summary, we have synthesized a library of small, neutral donor-acceptor near-infrared fluorophores based on the **IBF-NIAD** design, and have been able to tune the photophysical

140

properties by modifying the conjugated backbone and the electron donating group. We have also been able to install water solublizing groups, and a free amine functional handle for integration into other sensory applications and bioconjugation. The dyes all experience changes in their optical properties on binding to aggregated Aβ(1-40) (Table 3.11), with red shifted absorption and increases in fluorescence quantum yield as is consistent with rigidification of the dye's conjugated backbone. The strongest optical contrast was, in general observed for the less hydrophobic dyes, indicating that a significant barrier to dye-protein interaction may be dye aggregation in aqueous media. Changes in fluorescence lifetime were also observed for **IBF-NIAD 22-25**. Six of our fluorophores, **IBF-NIAD 4, 12, 19, 22, 23,** and **25,** stain senile plaques in APP/PS1 mouse tissue, and, in general, these are the dyes that exhibit the largest optical contrast in the aggregated Aβ(1-40) assay. Currently, the blood brain barrier permeability of these compounds is being studied by the Bacskai Group at Massachusetts General Hospital, in hope of developing new diagnostic methods for Alzheimer's disease.

3.4 Experimental Section

Materials. Commercial reagents were purchased from Sigma Aldrich, Alfa Aesar, or GFS Chemicals, and used as received. Dry solvents were obtained using a solvent purification system (Innovative Technologies, Inc.), and handled under an argon atmosphere, unless otherwise noted. Flash chromatography was performed using SiliaFlash F60 (230-400 mesh) from Silicycle.

Instrumentation. Melting points were determined in open capillaries using a Mel-Temp II apparatus and are uncorrected. Proton nuclear magnetic resonance (1H NMR) spectra and carbon nuclear magnetic resonance (^{13}C NMR) spectra were recorded on a Varian Mercury-300 (300 MHz) or an Inova-500 (500 MHz) NMR spectrometer. Chemical shifts for protons are reported in parts per million downfield from tetramethylsilane and are referenced to residual protium in the NMR solvent ($CHCl_3$: δ 7.27, DMSO-d_6: δ 2.50). Chemical shifts for carbon are reported in parts per million downfield from tetramethylsilane and are referenced to the carbon resonances of the solvent ($CDCl_3$: δ 77.0, DMSO-d_6 δ 39.23). Data are represented as follows: chemical shift, integration, multiplicity (br = broad, s = singlet, d = doublet, t = triplet, q = quartet, quin = quintet, sex = sextet, sp = septet, m = multiplet), and coupling constants in Hertz (Hz). High-resolution mass spectra (HRMS) were obtained at the MIT Department of Chemistry Instrumentation Facility using a peak-matching protocol to determine the mass and error range of the molecular ion, employing either electron impact or electrospray as the ionization technique. Fluorescence spectra were measured on a SPEX Fluorolog-τ3 fluorimeter (model FL-321, 450 W Xenon lamp) using right-angle detection. Ultraviolet-visible absorption spectra were measured with an Agilent 8453 diode array spectrophotometer and corrected for background signal with a solvent-filled cuvette. Fluorescence quantum yields were determined by the optically dilute

method using cresyl violet perchlorate in methanol (Φ=0.54) or zinc phthalocyanine in 1% pyridine in toluene (Φ=0.30) as standards and were corrected for solvent refractive index and absorption differences at the excitation wavelength.

Procedure for Aggregation of Aβ(1-40)

Aβ(1-40) (1 mg) was purchased from BaChem as a trifluoroacetic acid salt. 2 mM NaOH (500 µl) were added directly to the vial, which was then vortexed for 10 seconds. The solution was then transferred to a 7 ml screw top glass vial equipped with a stirbar. The original vial was then washed with 2 mM NaOH (5x100 µl) and the washings were added to the glass vial. 100 mM NaOH (10 µl) was then added to the glass vial, and the mixture was sonicated for 1 minute. Water (140 µl) was then added, followed by 2x PBS buffer solution (1.15 ml), and the solution was stirred at 1100 rpm for 3 days. After approximately 6 hours, the solution became noticeably cloudy. The solution was vortexed twice a day to break up fibrils forming at the meniscus. The solution (100 µM) was either used immediately, or aliquoted into sample vials and stored at -35 °C. Aggregation was confirmed by Thioflavin T assay.

Procedure for in vitro Aβ(1-40) tests

A solution of aggregated Aβ(1-40) (1.5 ml, 10 µM) was pipetted into a 0.5 cm cuvette. A solution of dye in DMSO (~0.7 mg in 5 ml) was added to make the final dye concentration 2.50 µM. The cuvette was vortexed for 10 seconds, and then allowed to equilibrate for 10 minutes at room temperature before acquisition of UV-vis or fluorescence spectra.

Synthetic Procedures
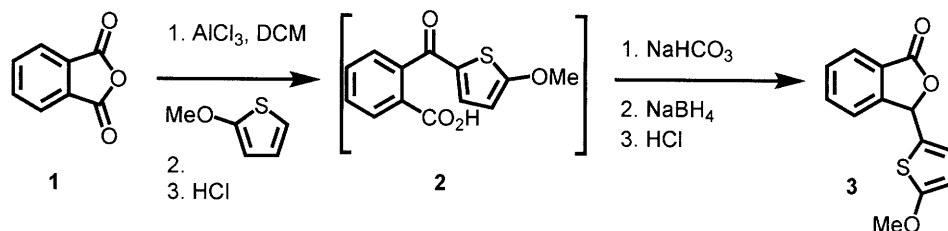
To an ice cooled, stirred suspension of phthalic anhydride **1** (3.52 g, 0.0238 mol) in dry

DCM (30 ml) was added aluminum trichloride (5.22 g, 0.0391 mol) in portions. To the resulting

mixture was added a solution of 2-methoxythiophene (2.27 g, 0.0198 mol) in dry DCM (8 ml)

dropwise. The reaction mixture was then allowed to warm to room temperature and was stirred

overnight. The reaction mixture was then poured into ice and concentrated HCl and stirred until

the mixture reached room temperature, at which point the precipitate was removed by filtration.

The precipitate was taken up in 5% NaOH and washed with DCM. The basic solution was then

acidified and extracted with EtOAc. The organic layer was dried with $MgSO_4$ and concentrated.

The resulting solid was triturated with 1:1 hexane:DCM and collected by suction filtration to

yield **2** (2.3 g, 8.8 mmol, 44% yield) as a crude product. Acid **2** was then dissolved in water (200

ml) with $NaHCO_3$ (1.37 g, 16.3 mmol), and the solution was heated to 60 °C. Sodium

Borohydride (4.8 g, 0.13 mol) was then added in portions over 2 hours, and the solution was then

stirred for 24h at 60 °C, and 100 °C for 1h. The solution was cooled to r.t. and acidified to pH 2

and stirred overnight. The solution was extracted with EtOAc, and the organic layer was washed

with brine, dried over $MgSO_4$, and concentrated. Flash chromatography (silica gel, DCM)

yielded **3** (0.25 g, 10 mmol,12% yield) as an off-white solid.

^{1}H NMR (500 MHz, $CDCl_3$): 7.94 (1H, d, 7.8 Hz), 7.71 (1H, t, 7.5 Hz), 7.59 (1H, t, 7.6 Hz), 7.47

(1H, d, 7.6 Hz), 6.82 (1H, d, 4.0 Hz), 6.51 (1H, s), 6.09 (1H, d, 4.0 Hz), 3.85 (3H, s) ^{13}C NMR

(125 MHz, CDCl$_3$): 169.7, 168.4, 148.2, 134.2, 129.7, 126.9, 126.1, 125.5, 124.2, 123.2, 103.3, 79.0, 60.2 HRMS (ESI): 247.0430 [calc'd for M+H$^+$: 247.0423]
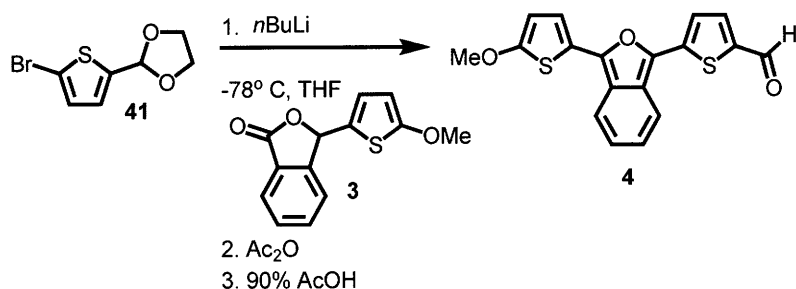
Bromo-thiophene **41** (0.13 g, 0.55 mmol) was dissolved in dry THF (2 ml) and cooled to -78 °C. To this solution was added *n*-BuLi (0.35 ml 1.6 M solution, 0.56 mmol) dropwise and the solution was stirred at -78 °C for 1.5h. A solution of phthalide **3** (0.12 g, 0.49 mmol) in dry THF (2 ml) was then added dropwise, and the solution was stirred for an additional 45 min at -78 °C, after which Ac$_2$O (0.06 ml, 0.63 mmol) was added. The reaction mixture was allowed to warm to room temperature, and was then refluxed for 10 min. The solution was then poured into saturated aqueous NaHCO$_3$, and extracted with EtOAc. The organic layer was washed with brine, dried over MgSO$_4$, and concentrated. The resulting orange viscous product was stirred with AcOH (5 ml of 90% solution in water) for 4 hours at room temperature under argon atmosphere. A small portion of saturated aqueous NaHCO$_3$ was added, and the resulting solution was extracted with EtOAc. The combined organic layers were washed with water and saturated aqueous NaHCO$_3$ and concentrated in vacuo. The residue was purified by column chromatography (silica gel, DCM) and recrystalization from MeOH to afford aldehyde **4** (0.013 g, 0.038 mmol, 7% yield) as a red solid .

^{1}H NMR (500 MHz, CDCl$_3$): 9.87 (1H, s), 7.71-7.64 (3H, m), 7.43 (1H, d, 4.1 Hz), 7.22 (1H, d, 4.1 Hz), 7.15 (1H, dd, 8.5 Hz, 6.7 Hz), 7.04 (1H, dd, 8.9 Hz, 6.7 Hz), 6.29 (1H, d, 4.1 Hz), 3.99

(3H, s) ^{13}C NMR (125 MHz, CDCl$_3$): 182.1, 167.7, 143.0, 142.2, 139.7, 137.53, 137.50, 127.5, 125.2, 124.5, 122.5, 121.3, 120.8, 120.5, 119.2, 119.4, 105.1, 60.5 HRMS (ESI): 389.0424 [calc'd for M+H$^+$: 389.0413]
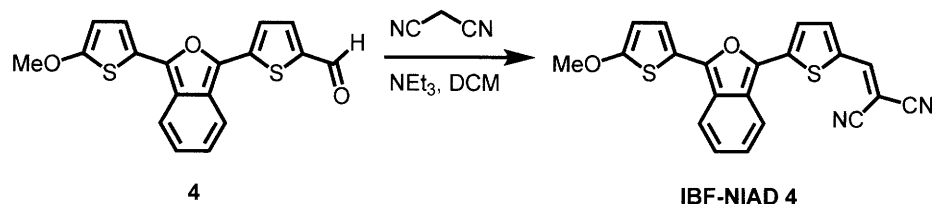
Aldehyde **4** (0.013 g, 0.038 mmol) was dissolved in DCM (1.5 ml) with malonitrile (0.003 g, 0.045 mmol). Triethylamine (1 drop) was then added, and the solution was stirred for 30 min at r.t. The solution was then purified by flash chromatography (silica gel, DCM) to afford **IBF-NIAD 4** (0.013 g, 0.037 mmol, 97%) as a blue solid.

^{1}H NMR (500 MHz, CDCl$_3$): 7.72 (1H, d, 8.9 Hz), 7.67 (1H, d, 8.9 Hz), 7.63 (1H, s), 7.56 (1H, d, 4.3 Hz), 7.38 (1H, d, 4.3 Hz), 7.32 (1H, d, 4.3 Hz), 7.25 (1H, dd, 8.7 Hz, 6.6 Hz), 7.12 (1H, dd, 8.9 Hz, 6.6 Hz), 6.33 (1H, d, 4.3 Hz) ^{13}C NMR (125 MHz, CDCl$_3$): 168.9, 148.6, 145.2, 143.9, 140.4, 137.3, 131.8, 128.9, 126.2, 125.8, 124.2, 121.5, 121.4, 120.9, 119.5, 118.5, 115.3, 114.5, 105.5, 71.8, 60.6 HRMS (ESI): 389.0424 [calc'd for M+H$^+$: 389.0413] UV-Vis λ_{max}: 607 nm (MeOH, ε= 18100), 631 nm (CHCl$_3$, ε= 46500)
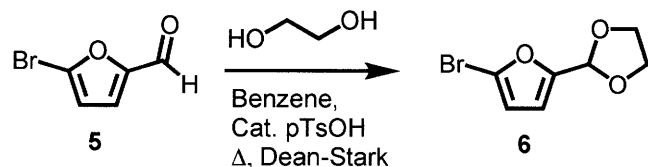
Bromo-furan **5** (3.0 g, 17 mol), *p*-toluenesulfonic acid (0.06 g, 0.3 mmol), and ethylene glycol (3.2 ml, 57 mmol) were mixed together in benzene (100 ml) and refluxed overnight with a Dean-

Stark trap. The reaction mixture was then cooled to room temperature, concentrated in vacuo, taken up in ethyl acetate and washed with saturated sodium bicarbonate and brine. The organic layer was dried over magnesium sulfate and concentrated in vacuo. The residue was purified with vacuum distillation (40-45 °C, 100 mtorr) to afford **6** as a clear liquid (1.9 g, 8.8 mmol, 52% yield), which was stored at -35 °C in a nitrogen atmosphere glovebox.

^{1}H NMR (500 MHz, CDCl$_3$): 6.42 (1H, d, 3.3 Hz), 6.28 (1H, d, 3.3 Hz), 5.87 (1H, s), 4.18-3.96 (4H, m) ^{13}C NMR (125 MHz, CDCl$_3$): 152.9, 122.9, 111.8, 111.3, 97.2, 65.1 HRMS (ESI): 218.9660 [calc'd for M+H$^+$: 218.9651]
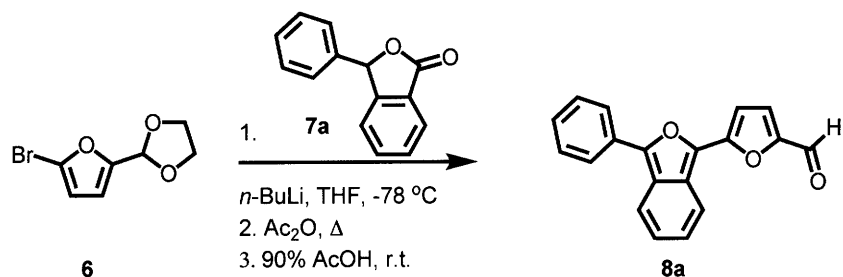
Bromo-furan **6** (0.40 g, 1.8 mmol) was dissolved in dry THF (8ml) and cooled to -78 °C. To this solution was added *n*-BuLi (1.20 ml 1.6 M solution, 1.9 mmol) dropwise and the solution was stirred at -78 °C for 1.5h. A solution of phthalide **7a** (0.35 g, 1.7 mmol) in dry THF (8 ml) was then added dropwise, and the solution was stirred for an additional 45 min at -78 °C, after which Ac$_2$O (0.20 ml, 2.1 mmol) was added. The reaction mixture was allowed to warm to room temperature, and was then refluxed for 10 min. The solution was then poured into saturated aqueous NaHCO$_3$, and extracted with EtOAc. The organic layer was washed with brine, dried over MgSO$_4$, and concentrated. The resulting orange viscous product was stirred with AcOH (15 ml of 90% solution in water) for 4 hours at room temperature under argon atmosphere. The resulting red solution was poured into water and stirred. A small portion of saturated aqueous

NaHCO$_3$ was added, and the resulting solution was extracted with EtOAc. The combined organic layers were washed with water and saturated aqueous NaHCO$_3$ and concentrated in vacuo. The residue was purified by column chromatography (silica gel, 2:1 hexane:EtOAc) to afford aldehyde **8a** as red solid (0.20 g, 0.69 mmol, 38% yield)

^{1}H NMR (500 MHz, CDCl$_3$): 8.02 (1H, d, 8.7 Hz), 7.93 (1H, d, 7.3 Hz), 7.84 (1H, d, 8.9 Hz), 7.50 (2H, t, 7.8 Hz), 7.38-7.33 (2H, m), 7.16 (1H, dd, 8.7 Hz, 6.4 Hz), 7.10 (1H, dd, 9.6 Hz, 7.2 Hz), 6.89 (1H, d, 4.0 Hz) ^{13}C NMR (125 MHz, CDCl$_3$): 176.1, 152.5, 151.5, 146.9, 135.3, 130.7, 129.0, 128.4, 128.0, 127.1, 126.3, 125.3, 125.1, 121.8, 120.3, 120.0, 107.2 HRMS (ESI): 289.0871 [calc'd for M+H$^+$: 289.0859]
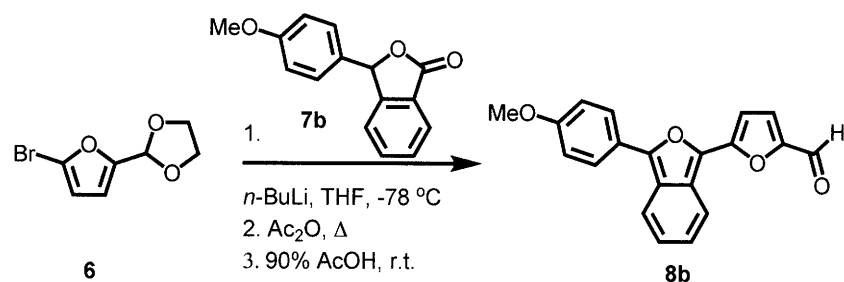
Bromo-furan **6** (0.30 g, 1.4 mmol) was dissolved in dry THF (5 ml) and cooled to -78 °C. To this solution was added *n*-BuLi (0.89 ml 1.6 M solution, 1.4 mmol) dropwise and the solution was stirred at -78 °C for 1.5h. A solution of phthalide **7b** (0.30 g, 1.3 mmol) in dry THF (5 ml) was then added dropwise, and the solution was stirred for an additional 45 min at -78 °C, after which Ac$_2$O (0.18 ml, 1.9 mmol) was added. The reaction mixture was allowed to warm to room temperature, and was then refluxed for 10 min. The solution was then poured into saturated aqueous NaHCO$_3$, and extracted with EtOAc. The organic layer was washed with brine, dried over MgSO$_4$, and concentrated. The resulting orange viscous product was stirred with AcOH (15 ml of 90% solution in water) for 4 hours at room temperature under argon atmosphere. The

resulting red solution was poured into water and stirred. A small portion of saturated aqueous NaHCO$_3$ was added, and the resulting red precipitate was filtered, washed with water and saturated aqueous NaHCO$_3$. Recrystalization from MeOH afforded aldehyde **8b** (0.13 g, 0.324 mmol, 25% yield) as a red powder.

^{1}H NMR (500 MHz, CDCl$_3$): 9.62 (1H, s), 7.96 (1H, d, 8.7 Hz), 7.85 (2H, dm, 8.7 Hz), 7.76 (1H, d, 8.8 Hz), 7.34 (1H, d, 3.9 Hz), 7.13 (1H, dd, 8.9 Hz, 6.4 Hz), 7.06-7.00 (3H, m), 6.82 (1H, d, 3.8 Hz), 3.88 (3H, s) ^{13}C NMR (125 MHz, CDCl$_3$): 175.9, 159.6, 152.7, 151.4, 147.3, 134.5, 127.1, 126.9, 125.7, 125.2, 124.2, 123.6, 120.8, 120.4, 120.1, 114.6, 106.6, 55.4 HRMS (ESI): 319.0974 [calc'd for M+H$^+$: 319.0965]
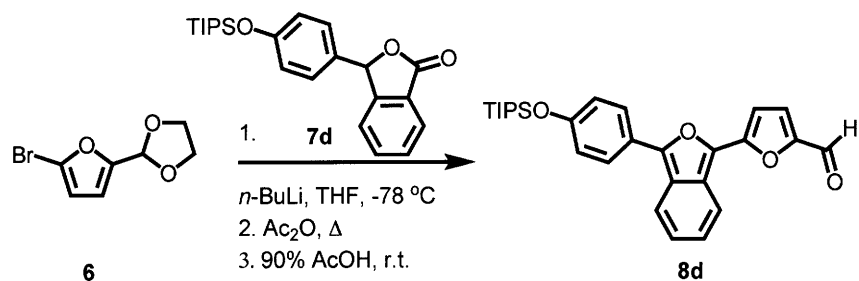
Bromo-furan **6** (0.18 g, 0.81 mmol) was dissolved in dry THF (3ml) and cooled to -78 °C. To this solution was added *n*-BuLi (0.53 ml 1.6 M THF solution, 0.84 mmol) dropwise and the solution was stirred at -78 °C for 1.5h. A solution of phthalide **7d** (0.30 g, 0.79 mmol) in dry THF (3 ml) was then added dropwise, and the solution was stirred for an additional 45 min at -78 °C, after which Ac$_2$O (0.11 ml, 1.2 mmol) was added. The reaction mixture was allowed to warm to room temperature, and was then refluxed for 10 min. The solution was then poured into saturated aqueous NaHCO$_3$, and extracted with EtOAc. The organic layer was washed with brine, dried over MgSO$_4$, and concentrated. The resulting orange viscous product was dissolved in THF (6 ml) and cooled in an ice bath. HClO$_4$ (2.4 ml, 3N aqueous solution) was added

dropwise, and the solution was warmed to r.t. and stirred for 3 hours. The resulting red solution was poured into water and extracted with EtOAc. The combined organic layers were washed with water and saturated aqueous NaHCO₃ and concentrated in vacuo. The residue was purified by column chromatography (silica gel: DCM) to afford aldehyde **8d** as red amorphous solid (0.091 g, 0.20 mmol, 24% yield)

^{1}H NMR (500 MHz, CDCl₃): 9.62 (1H, s), 7.97 (1H, d,), 7.84-7.76 (3H, m), 7.35 (1H, d,), 7.13 (1H, dd,,), 7.07-7.00 (3H, m), 6.82 (1H, d,), 1.32 (3H, sept,), 1.15 (18H, d,) ^{13}C NMR (125 MHz, CDCl₃): 175.9, 156.4, 152.7, 151.3, 147.4, 134.4, 127.1, 126.8, 125.7, 125.2, 123.9, 120.8, 120.6, 120.2, 120.1, 106.6, 17.8, 12.6 (1 missing) HRMS (ESI): 461.2158 [calc'd for M+H⁺: 461.2143]
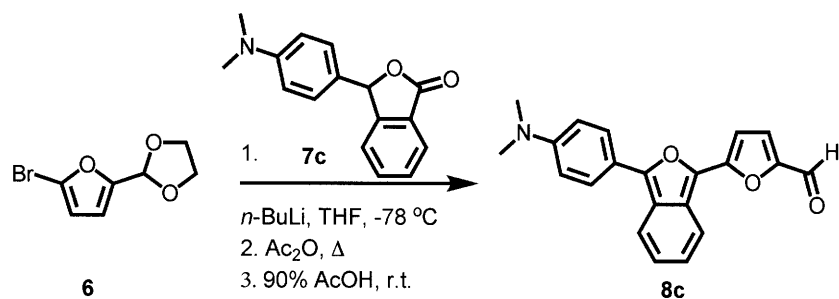
Bromo-furan **6** (0.30 g, 1.4 mmol) was dissolved in dry THF (8ml) and cooled to -78 °C. To this solution was added *n*-BuLi (1.14 ml 1.6 M solution, 1.82 mmol) dropwise and the solution was stirred at -78 °C for 1.5h. This solution was then added dropwise to a stirred solution of phthalide **7c** (0.32 g, 1.3 mmol) in dry THF (25 ml) cooled to -78 °C, and the resulting mixture was stirred for an additional 45 min at -78 °C, after which Ac₂O (0.15 ml, 1.6 mmol) was added. The reaction mixture was allowed to warm to room temperature, and was then refluxed for 10 min. The solution was then poured into saturated aqueous NaHCO₃, and extracted with EtOAc. The organic layer was washed with brine, dried over MgSO₄, and concentrated. The resulting orange

viscous product was stirred with AcOH (15 ml of 90% solution in water) for 4 hours at room temperature under argon atmosphere. The resulting red solution was poured into water and stirred. A small portion of saturated aqueous NaHCO$_3$ was added, and the resulting solution was extracted with EtOAc. The combined organic layers were washed with water and saturated aqueous NaHCO$_3$ and concentrated in vacuo. The residue was purified by column chromatography (silica gel, DCM) to afford aldehyde **8c** as dark purple solid (0.11 g, 0.33 mmol, 25% yield)

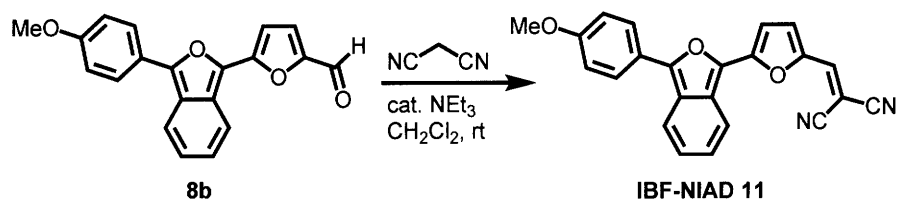^{1}H NMR (500 MHz, CDCl$_3$): 9.6 (1H, s), 7.98 (1H, d, 8.9 Hz), 7.84-7.80 (3H, m), 7.36 (1H, d, 4.0 Hz), 7.14 (1H, dd, 8.7 Hz, 6.3 Hz), 7.03 (1H, dd, 8.9 Hz, 6.4 Hz), 6.82-6.79 (3H, m), 3.06 (6H, s) ^{13}C NMR (125 MHz, CDCl$_3$): 175.7, 153.2, 151.0, 150.1, 148.8, 133.6, 127.2, 126.7, 125.6, 124.9, 123.4, 120.7, 120.1, 120.0, 118.9, 112.3, 106.0, 40.2 HRMS (ESI): 332.1291 [calc'd for M+H$^+$: 332.1281]

8b   **IBF-NIAD 11**

Aldehyde **8b** (0.050 g, 0.16 mmol) was dissolved in DCM (7 ml) with malonitrile (0.011 g, 0.17 mmol). Triethylamine (1 drops) was then added, and the solution was stirred for 1h at r.t. Hexane (5 ml) was added, and the solution was filtered to yield **IBF-NIAD 11** (0.047 g, 0.13 mmol, 81% yield) as a fluffy blue solid.

^{1}H NMR (500 MHz, CDCl$_3$): 8.37 (1H, bs), 7.93 (2H, d, 8.9 Hz), 7.85 (1H, d, 8.9 Hz), 7.34-7.20 (3H, m), 7.15 (1H, dd, 8.9 Hz, 6.6 Hz), 7.07 (2H, d, 8.9 Hz), 6.99 (1H, d, 4.0 Hz), 3.91 (3H, s) ^{13}C NMR (125 MHz, CDCl$_3$): 160.2, 151.9, 149.7, 148.7, 147.3, 138.5, 134.3, 128.5, 127.3,

127.2, 126.4, 123.2, 121.6, 120.8, 120.5, 115.6, 114.8, 114.6, 109.4, 70.9, 55.5 HRMS (ESI): 367.1086 [calc'd for M+H$^+$: 367.1077]. UV-Vis λ_{max}: 572 nm (MeOH, ε= 36700), 590 nm (CHCl$_3$, ε= 46700)

8d   9d
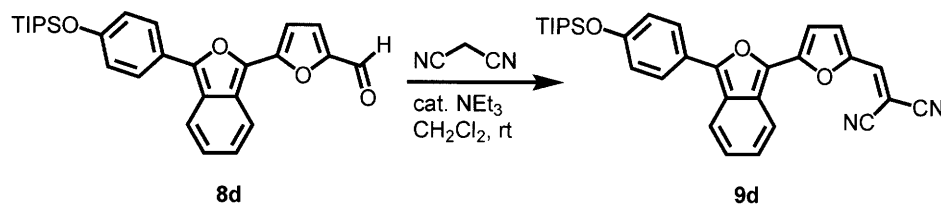
Aldehyde **8d** (0.090 g, 0.20 mmol) was dissolved in DCM (10 ml) with malonitrile (0.014 g, 0.22 mmol). Triethylamine (3 drops) was then added, and the solution was stirred for 1h at r.t. The solution was concentrated to 5 ml and was purified via flash chromatography (silica gel, DCM) to afford **9d** (0.089 g, 0.18 mmol, 87% yield) as a fluffy blue solid.

^{1}H NMR (500 MHz, CDCl$_3$): 8.32 (1H, bs), 7.88-7.80 (3H, m), 7.26-7.08 (4H, m), 7.02 (2H, d, 9.0 Hz), 6.92 (1H, 4.0 Hz), 1.32 (3H, sept, 7.3 Hz), 1.15 (18H, d, 7.3 Hz) ^{13}C NMR (125 MHz, CDCl$_3$): 157.1, 154.4 (bs), 149.8, 138.2 (bs), 134.2, 128.4, 127.2, 127.1, 126.3, 123.4, 121.5, 120.7, 120.5, 115.6, 114.6, 109.3, 70.6, 17.9, 12.7 (2 missing) HRMS (ESI): 509.2243 [calc'd for M+H$^+$: 509.2255]

9d   IBF-NIAD 12
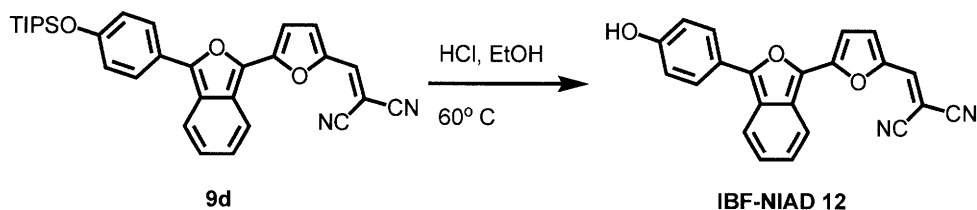
Protected fluorophore **9d** (0.048 g, 0.094 mmol) was dissolved in 56 ml of EtOH and the solution was heated to 60 °C. Concentrated HCl (4.6 ml, 36%) was added dropwise and the solution was stirred at 60 °C for 24h under argon atmosphere. The resulting mixture was poured

into water and extracted with EtOAc. The combined organic layers were washed with saturated aqueous NaHCO$_3$ and brine, dried over MgSO$_4$, and concentrated in vacuo. The resulting residue was purified via flash chromatography (silica gel, 5% MeOH in DCM) and recrystalization from CHCl$_3$ to afford **IBF-NIAD 12** (6.5 mg, 0.018 mmol, 19% yield).

^{1}H NMR (500 MHz, DMSO-d$_6$): 10.13 (1H, s), 8.25 (1H, d, 8.9 Hz), 8.15-8.00 (2H, m), 7.95 (2H, d, 8.7 Hz), 7.57 (1H, d, 4.0 Hz), 7.32 (1H, d, 4.1 Hz), 7.22 (1H, dd, 8.7 Hz, 6.4 Hz), 7.16 (1H, dd, 8.7 Hz, 6.6 Hz), 6.95 (2H, d, 8.0 Hz) ^{13}C NMR (125 MHz, DMSO-d$_6$): 160.7, 158.7, 157.1, 149.5, 147.5, 137.7, 133.3, 128.3, 127.4, 126.3, 126.2, 121.1, 120.9, 120.4, 120.1, 119.9, 116.4, 115.153, 110.2, 68.6 HRMS (ESI): 351.0779 [calc'd for M-H$^-$: 351.0775]. UV-Vis λ_{max}: 579 nm (MeOH, ε= 37500), 588 nm (CHCl$_3$, ε= 41800)

8c   IBF-NIAD 13
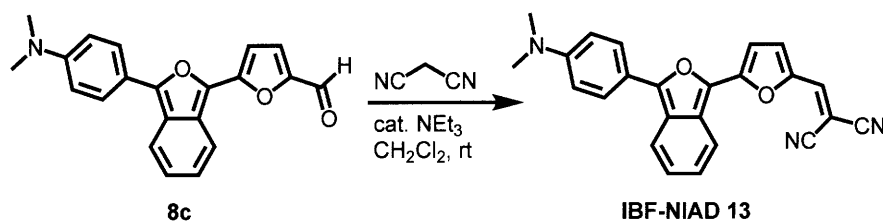
Aldehyde **8c** (0.016 g, 0.048 mmol) was dissolved in DCM (3 ml) with malonitrile (4.6 mg, 0.072 mmol). Triethylamine (1 drops) was then added, and the solution was stirred for 1h at r.t. The mixture was then purified via flash chromatography (silica gel, DCM) to afford **IBF-NIAD 13** (0.014 g, 0.037 mmol, 77% yield) as a green solid.
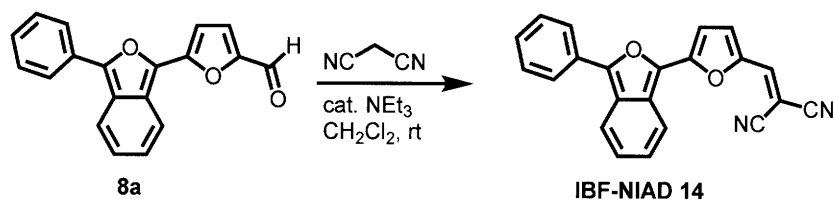
^{1}H NMR (500 MHz, DMF-d$_7$): 8.43 (1H, d, 8.5 Hz), 8.16 (1H, d, 8.5 Hz), 8.07 (2H, d, 9.0 Hz), 7.70 (1H, d, 3.8 Hz), 7.41 (1H, d, 4.0 Hz), 7.32 (1H, dd, 8.9 Hz, 6.4 Hz), 7.23 (1H, dd, 9.0 Hz, 6.3 Hz), 6.95 (2H, d, 9.0 Hz) ^{13}C NMR (125 MHz, CDCl$_3$): 150.6, 147.1, 144.0, 134.3, 133.2, 130.0, 128.7, 128.4, 127.2, 125.7, 124.3, 121.1, 120.7, 118.2, 115.0, 112.3, 107.3, 104.6, 99.8

40.2 (1 missing) HRMS (ESI): 380.1391 [calc'd for M-H⁻: 380.1394]. UV-Vis λ_{max}: 618 nm (MeOH, ε= 12700), 620 nm (CHCl₃, ε= 40100)

8a → **IBF-NIAD 14**

Aldehyde **8a** (0.050 g, 0.17 mmol) was dissolved in DCM (10 ml) with malonitrile (0.012 g, 0.19 mmol). Triethylamine (3 drops) was then added, and the solution was stirred for 1h at r.t. The mixture was then concentrated to 5 ml in vacuo and purified via flash chromatography (silica gel, DCM) to afford **IBF-NIAD 14** (0.047 g, 0.14 mmol, 82% yield) as a purple solid.

¹H NMR (500 MHz, CDCl₃): 8.38 (1H, bs), 7.97 (2H, d, 7.2 Hz), 7.89 (1H, d, 8.9 Hz), 7.53 (2H, t, 7.3 Hz), 7.41 (2H, t, 7.3 Hz), 7.32-7.22 (2H, m), 7.17 (1H, dd, 8.9 Hz, 6.4 Hz), 7.02 (1H, d, 4.0 Hz) ¹³C NMR (125 MHz, CDCl₃): 147.5, 137.9, 135.0, 133.5, 131.4, 130.3, 130.1, 129.2, 128.8, 128.6, 128.3, 126.9, 125.6, 122.4, 120.9, 120.3, 115.3, 114.3, 109.8, 71.8 HRMS (ESI): 337.0984 [calc'd for M+H⁺: 337.0972]. UV-Vis λ_{max}: 551 nm (MeOH, ε= 26100), 571 nm (CHCl₃, ε= 40500)

10 → **11**
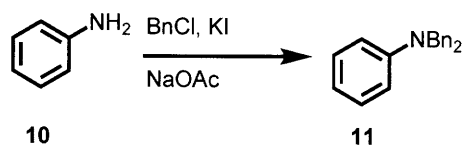
Aniline **10** (10 ml, 0.11 mol), benzylchloride (25 ml, 0.22 mol), sodium acetate (17.5 g, 0.21 mol) and potassium iodide (0.10 g, 0.60 mmol) were mixed together and the reaction mixture was heated at 100 °C with stirring overnight. The reaction mixture was allowed to cool to room temperature then poured into ice water (100 ml) and concentrated ammonium hydroxide (20 ml).

154

An oily product came out of solution that solidified upon sitting. The solid was collected by suction filtration and washed with water. The solid was crushed and slurried in MeOH. A small amount of ammonium hydroxide was added and then the solution was filtered. The resulting solid was washed with methanol, water, and again with methanol. The solid was again slurried in MeOH with a few drops of ammonium hydroxide. After filtration and washing with MeOH and water, the solid was allowed to dry on the filter overnight to afford aniline **11** (20.5 g, .073 mol, 66%). (Adopted from literature procedure)[50]

^{1}H NMR (500 MHz, CDCl$_3$): 7.32-7.20 (9H, m), 7.15 (2H, t, 7.3 Hz), 6.78-6.67 (3H, m), 4.63 (4H, s) ^{13}C NMR (125 MHz, CDCl$_3$): 149.1, 138.5, 129.2, 128.6, 126.8, 126.6, 116.7, 112.4, 54.1 HRMS (ESI): 274.1592 [calc'd for M+H$^+$: 274.1590]
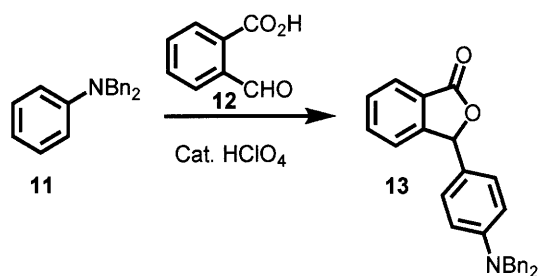
Aniline **11** (2.0 g, 7.1 mmol) and 2-carboxybenzaldehyde **12** (1.1 g, 7.3 mmol) were melted together at 100 °C. HClO$_4$ (10 drops, 70%) was added, and the reaction mixture was stirred for 12h at 100 °C. The mixture was then cooled to r.t. The resulting blue solid was purified by flash chromatography (silica gel, DCM) to afford phthalide **13** (0.78 g, 1.9 mmol, 27% yield) as an off white foam.

^{1}H NMR (500 MHz, CDCl$_3$): 7.95 (1H, d, 7.6 Hz), 7.65 (1H, t, 7.5 Hz), 7.54 (1H, t, 7.5 Hz), 7.34 (4H, t, 7.3 Hz), 7.29-7.22 (6H, m), 7.03 (2H, d, 8.9 Hz), 6.70 (2H, d, 8.9 Hz), 6.34 (1H, s), 4.67

(4H, s) ^{13}C NMR (125 MHz, CDCl$_3$): 137.9, 134.0, 129.1, 128.9, 128.7, 127.0, 126.5, 126.3, 125.4, 123.5, 123.1, 112.3, 83.3, 54.2 HRMS (ESI): 428.1628 [calc'd for M+Na$^+$: 428.1621]
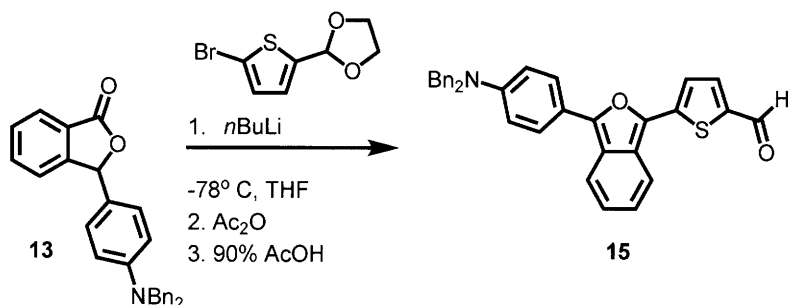
Bromo-thiophene **41** (0.40 g, 1.7 mmol) was dissolved in dry THF (8 ml) and cooled to -78 °C. To this solution was added *n*-BuLi (0.35 ml 1.6 M solution, 0.56 mmol) dropwise and the solution was stirred at -78 °C for 1.5h. A solution of phthalide **13** (0.74 g, 1.8 mmol) in dry THF (8 ml) was then added dropwise, and the solution was stirred for an additional 45 min at -78 °C, after which Ac$_2$O (0.20 ml, 2.1 mmol) was added. The reaction mixture was allowed to warm to room temperature, and was then refluxed for 10 min. The solution was then poured into saturated aqueous NaHCO$_3$, and extracted with EtOAc. The organic layer was washed with brine, dried over MgSO$_4$, and concentrated. The resulting orange viscous product was stirred with AcOH (20 ml of 90% solution in water) for 4 hours at room temperature under argon atmosphere. A small portion of saturated aqueous NaHCO$_3$ was added, and the resulting precipitate was collected with suction filtration and washed with water. The residue was purified by flash chromatography (silica gel, DCM) to afford aldehyde **4** (0.34 g, 0.68 mmol, 40% yield) as a purple solid.

^{1}H NMR (500 MHz, CDCl$_3$): 9.85 (1H, s), 7.80-7.74 (3H, m), 7.72-7.66 (2H, m), 7.42-7.20 (11H, m), 7.13 (1H, dd, 8.9 Hz, 6.6 Hz), 6.99 (1H, dd, 8.9 Hz, 6.6 Hz), 6.86 (2H, d, 8.7 Hz) ^{13}C NMR (125 MHz, CDCl$_3$): 182.0, 148.9, 147.9, 142.9, 139.2, 137.8, 137.6, 137.3, 128.8, 127.20,

127.15, 126.9, 126.5, 124.9, 124.7, 121.1, 120.8, 120.7, 119.33, 119.32, 112.7, 54.2 HRMS

(ESI): 500.1695 [calc'd for M+Na$^+$: 500.1679]

15   **16**
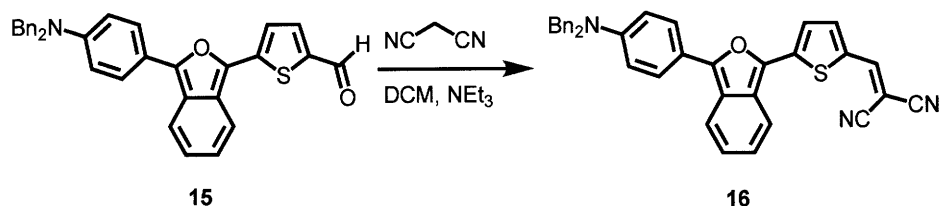
Aldehyde **15** (0.060 g, 0.12 mmol) was dissolved in DCM (2 ml) with malonitrile (8.0 mg, 0.13

mmol). Triethylamine (1 drops) was then added, and the solution was stirred for 1h at r.t. The

mixture was then purified via flash chromatography (silica gel, DCM) to afford **16** (0.028 g,

0.051 mmol, 43% yield) as a green solid.

^{1}H NMR (500 MHz, CDCl$_3$): 7.85-7.78 (3H, m), 7.67 (1H, d, 8.7 Hz), 5.57 (1H, s), 7.51 (1H, d,

4.1 Hz), 7.41-7.28 (11H, m), 7.22 (1H, dd, 8.7 Hz, 6.6 Hz), 7.07 (1H, dd 8.9 Hz, 6.6 Hz), 6.87

(2H, d, 9.0 Hz), 4.78 (4H, s) ^{13}C NMR (125 MHz, CDCl$_3$): 150.4, 149.6 148.4, 144.6, 137.6,

137.1, 131.3, 128.9, 128.6, 127.4, 127.3, 126.8, 126.5, 125.4, 121.7, 121.5, 120.9, 119.5, 118.6,

115.6, 114.7, 112.8, 70.9, 54.3 HRMS (ESI): 548.1795 [calc'd for M+H$^+$: 548.1791]

7a   **17**   **18**
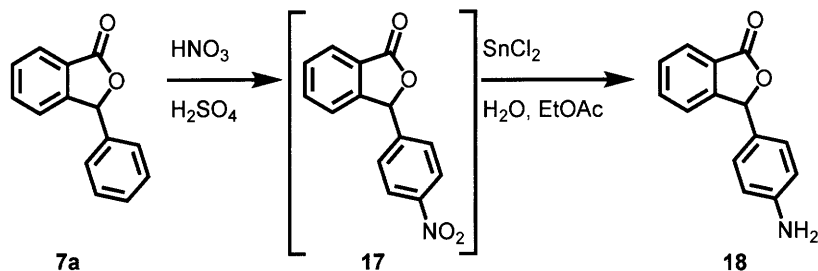
Phalide **7a** (6.4 g, 0.030 mol) was dissolved in concentrated H$_2$SO$_4$ (4.3 ml) and the solution was

cooled in an ice bath. Concentrated HNO$_3$ (3.1 ml) was added carefully, drop by drop, and the

reaction mixture was stirred at 70 °C for 1h. The reaction mixture was then poured into ice and

the resulting solid was collected by filtration. This solid was then stirred in saturated aqueous NaHCO₃, filtered, washed with water, and dried. Fractional recrystallization from benzene afforded nitro-phthalide **17** (1.8 g, 0.0071 mol, 24% yield) as a crude product. This product was dissolved in EtOAc (30 ml) and SnCl₂ (6.39 g, 0.034 mol) and water (9 ml) were added and the reaction mixture was stirred at r.t. overnight. The solution was then filtered, and the filtrate was washed with water and brine, dried over MgSO₄, and concentrated in vacuo to afford phthalide **18** (1.3 g, 0.0058 mol, 82% yield, 34% over 2 steps).

^{1}H NMR (500 MHz, CDCl₃): 7.94 (1H, d, 7.8 Hz), 7.65 (1H, t, 7.5 Hz), 7.54 (1H, t, 7.5 Hz), 7.31 (1H, d, 7.6 Hz), 7.00 (2H, d, 8.5 Hz), 6.64 (2H, d, 8.4 Hz), 6.32 (1H, s), 3.83 (2H, bs) ^{13}C NMR (125 MHz, CDCl₃): 170.7, 149.8, 147.6, 134.1, 129.1, 128.8, 126.0, 125.4, 125.3, 123.0, 115.0, 83.2 HRMS (ESI): 226.0868 [calc'd for M+H$^+$: 226.0863]
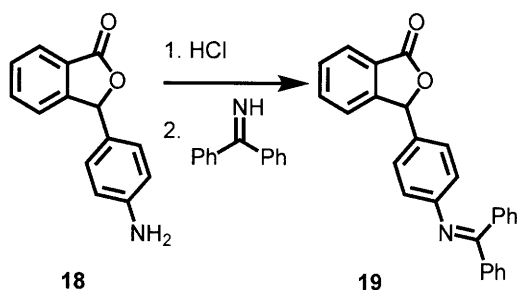
Phthalide **18** (0.90 g, 4.0 mmol) was dissolved in DCM (5 ml), and a solution of HCl (4.5 ml, 1.0 M solution in Et₂O) was added dropwise with stirring. Hexane was then added, and the resulting precipitate was collected by suction filtration and washed with hexane. The filtrate was allowed to dry for 30 minutes on the filter, and was then suspended in DCM (9 ml). Benzophenone imine (0.72 ml, 4.3 mmol) was added dropwise, and the reaction mixture was stirred for 4 hours at r.t. The reaction mixture was then poured into water, and extracted with EtOAc. The combined organic layers were washed with saturated aqueous NaHCO₃ and brine, dried over MgSO₄, and

concentrated in vacuo. The residue was purified by recrystalization from MeOH to afford

phthalide **19** as an off-white powder (0.61 g, 1.7 mmol, 43 % yield)

^{1}H NMR (500 MHz, CDCl$_3$): 7.90 (1H, d, 7.6 Hz), 7.72-7.68 (2H, m), 7.61 (1H, t, 7.5 Hz), 7.51

(1H, t, 7.6 Hz), 7.45 (1H, t, 7.3 Hz), 7.37 (2H, t, 7.6 Hz), 7.30-7.20 (4H, m), 7.08-7.04 (2H, m),

7.00 (2H, d, 8.2 Hz), 6.69 (2H, d, 8.5 Hz), 6.27 (1H, s) ^{13}C NMR (125 MHz, CDCl$_3$): 170.5,

168.8, 152.3, 149.7, 139.3, 135.7, 134.2, 130.9, 130.6, 129.4, 129.3, 129.2, 128.8, 128.2, 128.0,

127.7, 125.7, 125.5, 122.9, 121.3, 82.7 HRMS (ESI): 390.1485 [calc'd for M+H$^+$: 390.1489]
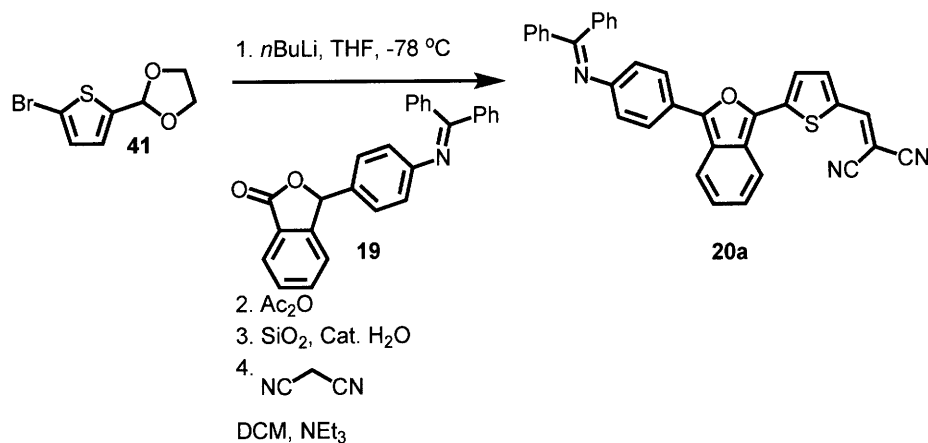
Bromo-thiophene **41** (0.29 g, 1.2 mmol) was dissolved in dry THF (5 ml) and cooled to -78 °C.

To this solution was added n-BuLi (0.80 ml 1.6 M solution, 1.3 mmol) dropwise and the solution

was stirred at -78 °C for 1.5h. A solution of phthalide **19** (0.50 g, 1.4 mmol) in dry THF (8 ml)

was then added dropwise, and the solution was stirred for an additional 45 min at -78 °C, after

which Ac$_2$O (0.16 ml, 1.7 mmol) was added. The reaction mixture was allowed to warm to room

temperature, and was then refluxed for 10 min. The solution was then poured into saturated

aqueous NaHCO$_3$, and extracted with EtOAc. The organic layer was washed with brine, dried

over MgSO$_4$, and concentrated. The resulting orange viscous product was passed through a silica

gel column (DCM), and the resulting orange product was dissolved in DCM, to which was added

silica gel (10 g) and water (0.5 ml), and this suspension was stirred, under argon, overnight. The suspension was then filtered, and the silica gel was washed with DCM. The combined filtrates were dried over MgSO$_4$ and concentrated in vacuo. The red product was taken up in DCM (6 ml) with malonitrile (0.020 g, 0.32 mmol). Triethylamine (2 drops) were added, and the reaction mixture was stirred for 1h at r.t. The reaction mixture was then purified by flash chromatography (silica gel, DCM) to afford **20a** (0.12 g, 0.23 mmol, 19% yield) as a blue solid.

^{1}H NMR (500 MHz, CDCl$_3$): 7.89 (1H, d, 8.9 Hz), 7.84-7.76 (4H, m), 7.74 (1H, s), 7.56-7.41 (4H, m), 7.34-7.11 (8H, m), 6.90 (2H, d, 8.7 Hz) ^{13}C NMR (125 MHz, CDCl$_3$): 168.9, 152.0, 149.1, 148.9, 144.3, 139.2, 138.0, 135.9, 132.4, 132.2, 131.1, 130.1, 129.5, 129.0, 128.5, 128.31, 128.27, 128.2, 126.3, 126.1, 125.2, 122.4, 122.0, 121.9, 121.4, 119.3, 115.1, 114.3, 72.7 HRMS (ESI): 532.1479 [calc'd for M+H$^+$: 532.1478]
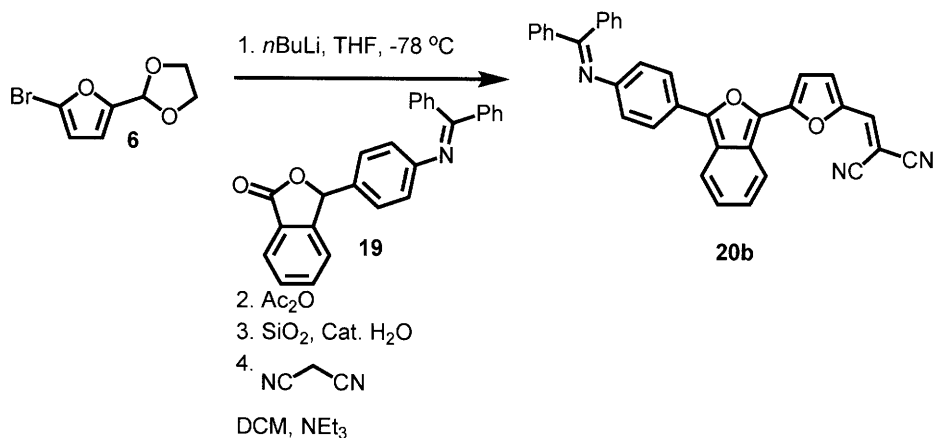
Bromo-furan **6** (0.27 g, 1.2 mmol) was dissolved in dry THF (5 ml) and cooled to -78 °C. To this solution was added *n*-BuLi (0.80 ml 1.6 M solution, 1.3 mmol) dropwise and the solution was stirred at -78 °C for 1.5h. A solution of phthalide **19** (0.50 g, 1.4 mmol) in dry THF (8 ml) was then added dropwise, and the solution was stirred for an additional 45 min at -78 °C, after which Ac$_2$O (0.16 ml, 1.7 mmol) was added. The reaction mixture was allowed to warm to room

temperature, and was then refluxed for 10 min. The solution was then poured into saturated aqueous NaHCO₃, and extracted with EtOAc. The organic layer was washed with brine, dried over MgSO₄, and concentrated. The resulting orange viscous product was passed through a silica gel column (DCM), and the resulting orange product was dissolved in DCM, to which was added silica gel (10 g) and water (0.5 ml), and this suspension was stirred, under argon, overnight. The suspension was then filtered, and the silica gel was washed with DCM. The combined filtrates were dried over MgSO₄ and concentrated in vacuo. The red product was passed through a silica gel column (1:1 hexane:EtOAc), and the resulting product was concentrated in vacuo, and taken up in DCM (5 ml) with malonitrile (0.022 g, 0.35 mmol). Triethylamine (2 drops) were added, and the reaction mixture was stirred for 1h at r.t. The reaction mixture was then purified by flash chromatography (silica gel, DCM) to afford **20b** (0.059 g, 0.12 mmol, 10% yield) as a blue solid.

^{1}H NMR (500 MHz, CDCl₃): 7.85-7.77 (5H, m), 7.52 (1H, t, 7.5 Hz), 7.45 (1H, t, 7.9 Hz), 7.34-7.22 (6H, m), 7.20-7.17 (2H, m), 7.13 (1H, dd, 8.9 Hz, 6.4 Hz), 6.98 (1H, d, 4.1 Hz), 6.89 (2H, d, 8.9 Hz) ^{13}C NMR (125 MHz, CDCl₃): 169.6, 152.7, 150.3, 148.1, 139.9, 136.7, 135.2, 131.8, 130.8, 130.22, 130.18, 129.7, 129.2, 129.0, 128.9, 128.8, 127.9, 127.9, 127.2, 126.7, 126.0, 122.7, 121.6, 121.3, 116.3, 115.2, 110.2, 71.8 (2 missing) HRMS (ESI): 516.1711 [calc'd for M+H^{+}: 516.1707]

20a   **IBF-NIAD 18**
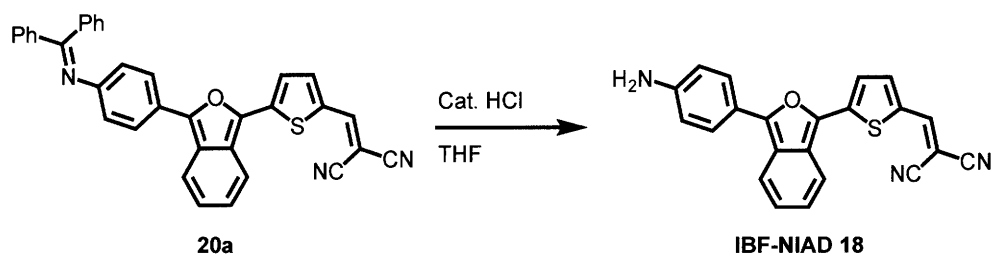
Compound **20a** (0.034 g, 0.065 mmol) was taken up in THF (1 ml). HCl (1 drop, 2 M) was added, and the reaction mixture was stirred for 30 min at r.t. The reaction mixture was then

partitioned between 2:1 hexane:EtOAc and HCl (0.5 M). The aqueous layer was separated, made alkaline, and extracted with DCM. The organic layer was dried over $MgSO_4$ and concentrated in vacuo. Flash chromatography (silica gel, 2:1 EtOAc: hexane) afforded **IBF-NIAD 18** as a purple solid (0.023 g, 0.063 mmol, 97% yield).

^{1}H NMR (500 MHz, DMSO-d_6): 8.42 (1H, s), 8.05 (1H, d, 8.4 Hz), 7.86 (1H, d, 4.4 Hz), 7.84-7.75 (3H, m), 7.70 (1H, d, 4.4 Hz), 7.35 (1H, dd, 8.9 Hz, 6.6 Hz), 7.16 (1H, dd, 8.9 Hz, 6.6 Hz) 6.75 (2H, d, 8.4 Hz), 5.99 (2H, bs) ^{13}C NMR (125 MHz, DMSO-d_6): 150.8, 150.7, 150.3, 143.3, 136.2, 131.0, 129.3, 128.6, 127.4, 126.4, 125.6, 122.2, 121.4, 120.5, 119.1, 116.7, 115.8, 115.2, 114.3, 68.8 HRMS (ESI): 366.0714 [calc'd for M-H: 366.0707] UV-Vis λ_{max}: 618 nm (MeOH, ε= 12900), 620 nm (CHCl$_3$, ε= 26700)

20b   Cat. HCl / THF   IBF-NIAD 19
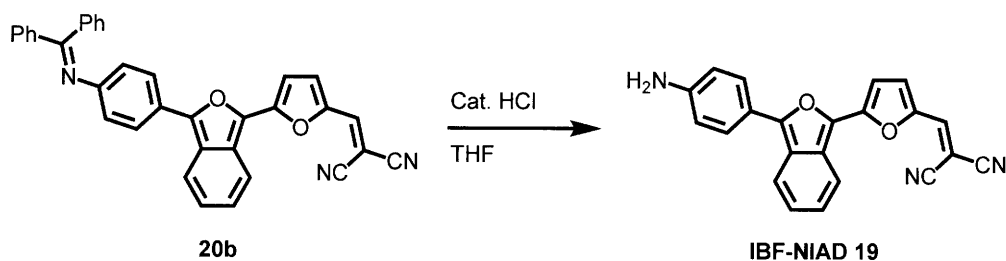
Compound **20b** (0.050 g, 0.097 mmol) was taken up in THF (5 ml). HCl (8 drops, 2 M) was added, and the reaction mixture was stirred for 30 min at r.t. The reaction mixture was then partitioned between 2:1 hexane:EtOAc and HCl (0.5 M). The aqueous layer was separated, made alkaline, and extracted with DCM. The organic layer was dried over $MgSO_4$ and concentrated in vacuo. Flash chromatography (silica gel, 2:1 EtOAc: hexane) afforded **IBF-NIAD 19** as a purple solid (0.027 g, 0.077 mmol, 79% yield).

^{1}H NMR (500 MHz, DMSO-d_6): 8.26 (1H, d, 8.9 Hz), 8.05 (1H, d, 9.0 Hz), 7.93 (1H, s), 7.85 (2H, d, 8.7 Hz), 7.56 (1H, d, 4.1 Hz), 7.29 (1H, d, 4.1 Hz), 7.24 (1H, dd, 8.9 Hz, 6.1 Hz), 7.14 (1H, 6.73 (2H, d, 8.7 Hz) ^{13}C NMR (125 MHz, DMSO-d_6): 153.5, 151.4, 150.6, 147.3, 139.2

(bs), 132.2, 130.7 (bs), 128.6, 127.4, 126.9, 125.6, 121.8, 119.8, 116.9, 116.3, 115.5, 114.2,

109.7, 66.8 (1 missing) HRMS (ESI): 352.1084 [calc'd for M+H$^+$: 352.1081] UV-Vis λ_{max}: 611

nm (MeOH, ε= 24700), 615 nm (CHCl$_3$, ε= 28100)
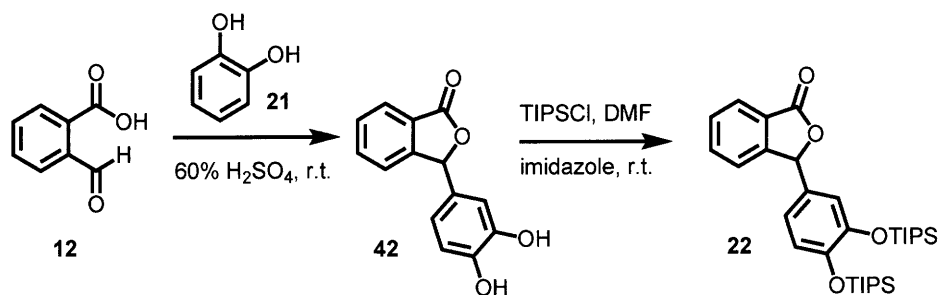
2-Carboxybenzaldehyde **12** (1.0 g, 6.7 mmol) was dissolved in H$_2$SO$_4$ (6 ml, 60% aqueous

solution) and stirred at r.t. for 10 min. Catechol **21** (0.73 g, 6.6 mmol) was added, and the

reaction mixture was stirred for 3h at r.t. The reaction mixture was then poured into ice water,

and the resulting mixture was stirred until it reached r.t. The mixture was extracted with EtOAc,

and the combined organic layers were washed with saturated aqueous NaHCO$_3$ and brine, dried

over MgSO$_4$, and concentrated in vacuo. Flash chromatography (silica gel, EtOAc) afforded **x** as

a white solid (1.25 g, 5.2 mmol, 79% yield). Phthalide **42** (1.25 g, 5.2 mmol) and imidazole (2.8

g, 41 mmol) were then dissolved in DMF (40 ml). Triisopropylsilyl chloride (1.2 ml, 19 mmol)

was added drop wise and the reaction mixture was stirred at r.t. overnight. The mixture was then

poured into water and extracted with DCM. The combined organic layers were dried over

MgSO$_4$ and concentrated in vacuo. The resulting product was purified by flash chromatography

(silica gel, DCM) to afford **22** (1.0 g, 1.8 mmol, 35% yield, 28% over two steps).

^{1}H NMR (500 MHz, CDCl$_3$): 7.95 (1H, d, 7.6 Hz), 7.65 (1H, t, 7.5 Hz), 7.56 (1H, t, 7.3 Hz), 7.31

(1H, d, 7.6 Hz), 6.81 (1H, d, 8.2 Hz), 6.73 (1H, dd, 8.2 Hz, 2.1 Hz), 6.57 (1H, d, 2.1 Hz), 6.30

(1H, s), 1.29 (3H, sept, 7.5 Hz), 1.16 (3H, sept, 7.5 Hz), 1.10 (18H, dd, 7.5 Hz, 3.1 Hz), 1.02

(18H, 8.1 Hz) ^{13}C NMR (125 MHz, CDCl$_3$): 170.5, 149.8, 148.0, 147.3, 134.0, 129.2, 128.4, 125.9, 125.4, 123.0, 120.4, 119.9, 118.9, 82.8, 17.9, 17.8, 13.1, 12.9 HRMS (ESI): 577.3160 [calc'd for M+Na$^+$: 577.3140]
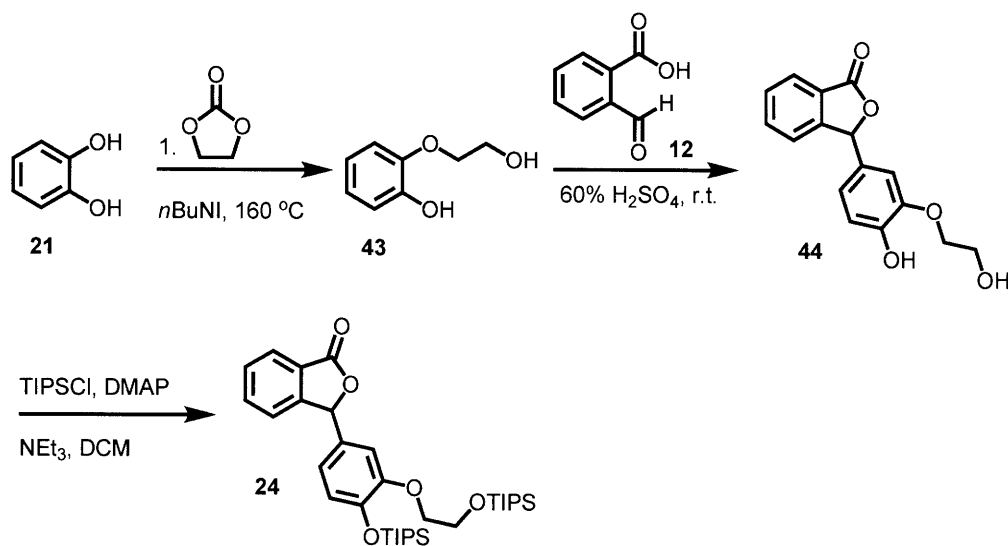
Catechol **21** (11 g, 0.10 mol) and ethylene carbonate (8.8 g, 0.10 mol) were stirred together at 160 °C, and then nBu$_4$NI (1.2 g, 0.0033 mol) was added and the mixture was stirred at 160 °C for 5h at which point the evolution of CO$_2$ had ceased. The mixture was taken up in EtOAc, and washed with water. The combined organic layers were dried over MgSO$_4$ and concentrated to afford **43** as an gray solid (8.9 g, 0.058 mol, 58% yield). 2-Carboxybenzaldehyde **12** (2.91 g, 0.019 mol) was dissolved in H$_2$SO$_4$ (14 ml, 60% aqueous solution) and stirred at r.t. for 10 min. Compound **43** (3.0 g, 0.019 mol) was added, and the reaction mixture was stirred for 3h at r.t. The reaction mixture was then poured into ice water, and the resulting mixture was stirred until it reached r.t. The mixture was extracted with EtOAc, and the combined organic layers were washed with saturated aqueous NaHCO$_3$ and brine, dried over MgSO$_4$, and concentrated in vacuo to afford **44** as a viscous liquid (2.9 g, 0.01 mol, 53% yield). Phthalide **44** (2.62 g, 9.2 mmol) and DMAP (0.034 g, 0.28 mmol) were then dissolved in DCM (15 ml) and cooled in an

ice bath. Triisopropylsilyl chloride (3.34 ml, 53 mmol) was added drop wise followed by triethylamine (2.8 ml, 20 mmol) and the reaction mixture was stirred at r.t. overnight. The mixture was then poured into water and extracted with DCM. The combined organic layers were dried over $MgSO_4$ and concentrated in vacuo. The resulting product was purified by flash chromatography (silica gel, DCM) to afford **24** (2.2 g, 3.7 mmol, 40% yield, 12% yield over 3 steps) as a viscous oil that solidified on standing.

^1H NMR (500 MHz, $CDCl_3$): 7.95 (1H, d, 7.6 Hz), 7.65 (1H, t, 7.6 Hz), 7.55 (1H, t, 7.5 Hz), 7.32 (1H, d, 7.6 Hz), 6.84 (1H, d, 8.1 Hz), 6.73-6.70 (2H, m), 6.33 (1H, s), 4.08-3.95 (4H, m), 1.26 (3H, sept, 7.8 Hz), 1.15-0.80 (39H, m) ^{13}C NMR (125 MHz, $CDCl_3$): 170.6, 150.5, 149.7, 146.7, 134.1, 129.2, 128.9, 125.8, 125.5, 122.9, 120.5, 120.1, 112.6, 83.0, 70.0, 61.9, 17.9, 17.6, 12.7, 11.8) HRMS (ESI): 621.3400 [calc'd for $M+Na^+$: 621.3402]
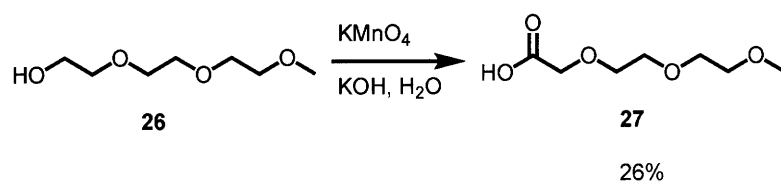
Triethyleneglycol monomethylether **26** (2.5 ml, 0.016 mol), potassium hydroxide (4.5 g, 0.080 mol), and potassium permanganate (9.50 g, 0.060 mol) were mixed together in water (200 ml) and stirred at r.t. overnight. The solution was then filtered to remove the brown precipitate and the filtrate was acidified with HCl to ~pH 2.0. The solution was then extracted with DCM, and the combined organic layers were dried over $MgSO_4$ and concentrated in vacuo to afford **27** (0.77 g, 27% yield) as a clear oil.

^1H NMR (300 MHz, $CDCl_3$): 8.25 (1H, bs), 4.12 (2H, s), 3.71-3.50 (8H, m), 3.33 (3H, s) ^{13}C NMR (75 MHz, $CDCl_3$): 173.3, 71.5, 70.7, 70.5, 70.1, 68.1, 58.7 HRMS (ESI): 177.0761 [calc'd for $M-H^-$: 177.0678]
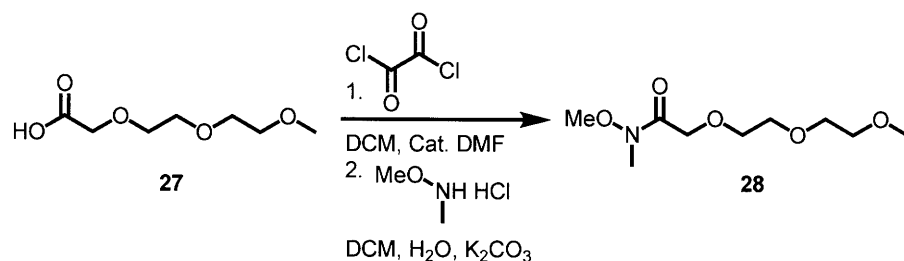
Acid **27** (2.16 g, 0.012 mol) was dissolved in dry DCM (60 ml) with DMF (0.2 ml) and the solution was cooled in an ice bath. Oxalyl chloride (1.4 ml, 0.017 mol) was added dropwise and then the solution was allowed to warm to r.t. and was stirred under argon atmosphere at r.t. overnight. The solution was then concentrated in vacuo. The resulting residue was taken up in DCM (10 ml) and this solution was added to a solution of N,O-dimethylhydroxylamine (0.98 g, 0.010 mol) in water (10 ml). The biphasic solution was cooled in an ice bath, and potassium carbonate (1.66 g, 0.012 mol) was added and the reaction mixture was allowed to warm to r.t. and was stirred at r.t. overnight. The layers were then separated, and the aqueous layer was extracted with DCM. The combined organic layers were washed with saturated $NaHCO_3$ and brine, dried over $MgSO_4$, and concentrated in vacuo to afford Weinreb amide **28** (1.5 g, 0.0072 mol, 60% yield) as a clear oil.

^{1}H NMR (300 MHz, CDCl$_3$): 4.24 (2H, s), 3.70-3.42 (11H, m), 3.27 (3H, s), 3.08 (3H, s) ^{13}C NMR (75 MHz, CDCl$_3$): 170.8, 71.7, 71.5, 70.5, 70.4, 68.3, 61.1, 58.7 HRMS (ESI): 244.1161 [calc'd for M+Na$^+$: 244.1155]
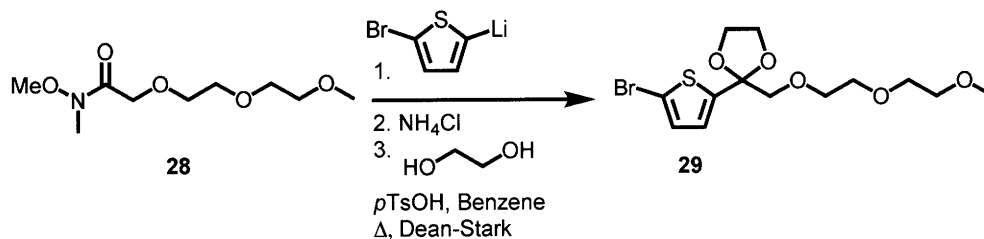
2,5-Dibromothiophene (0.75 ml, 6.8 mmol) was dissolved in dry THF (25 ml) and this solution was cooled to -78 °C. To this solution was added nBuLi (4.5 ml, 1.6M solution, 7.2 mmol) dropwise and the solution was then stirred for 1.5h at -78 °C. A solution of Weinreb amide **28** (1.5 g, 7.2 mmol) in dry THF (25 ml) was then added dropwise, and the solution was stirred at -78 °C for 4h and was then allowed to warm to r.t. Saturated ammonium chloride was added, and the reaction mixture was stirred at r.t. overnight. The solution was then extracted with EtOAc, and the combined organic layers were washed with brine and concentrated. The residue was dissolved in toluene (20 ml) with ethylene glycol (0.60 ml, 11 mmol) and p-TsOH (0.010 g, 0.053 mmol). The solution was then refluxed overnight with a Dean-Stark trap. The reaction mixture was cooled to r.t., poured into water, and extracted with EtOAc. The combined organic layers were dried over $MgSO_4$ and concentrated in vacuo. Flash chromatography afforded **29** (0.70 g, 1.9 mmol) as a brown oil.

^{1}H NMR (300 MHz, $CDCl_3$): 6.90 (1H, d, 3.8 Hz), 6.83 (1H, d, 3.8 Hz), 4.03 (4H, m), 3.76-3.71 (4H, m), 3.64-3.56 (4H, m), 3.53-3.47 (2H, m), 3.35 (3H, s) ^{13}C NMR (75 MHz, $CDCl_3$): 145.2, 129.6, 125.4, 112.3, 107.0, 75.1, 74.8, 71.8, 71.5, 70.5, 70.4, 65.4, 58.9 HRMS (ESI): 389.0043 [calc'd for M+H$^+$: 389.0029]
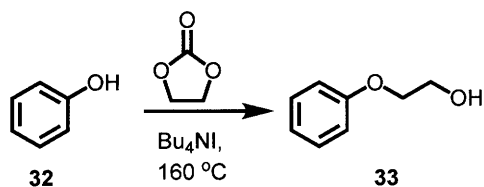
Phenol **32** (9.4 g, 0.10 mol) and ethylene carbonate (8.8 g, 0.10 mol) were stirred together at 160 °C, and then *n*Bu₄NI (1.2 g, 0.0033 mol) was added and the mixture was stirred at 160 °C for 5h at which point the evolution of CO_2 had ceased. The mixture was then purified by vacuum distillation (60-65 °C, 100 mtorr) to afford **33** as a clear liquid (7.9 g, 0.057 mol, 57% yield).

¹H NMR (300 MHz, CDCl₃): 7.31 (2H, dd, 8.7 Hz, 7.3Hz), 7.02-6.91 (3H, m), 4.09 (2H, t, 4.2 Hz), 3.97 (2H, q, 4.1 Hz), 2.46 (1H, t, 5.7 Hz) ¹³C NMR (75 MHz, CDCl₃): 158.5, 129.5, 121.0, 114.4, 69.0, 61.4 HRMS (ESI): 161.0575 [calc'd for M+Na⁺: 161.0573] (Data comparable to literature values)[51]
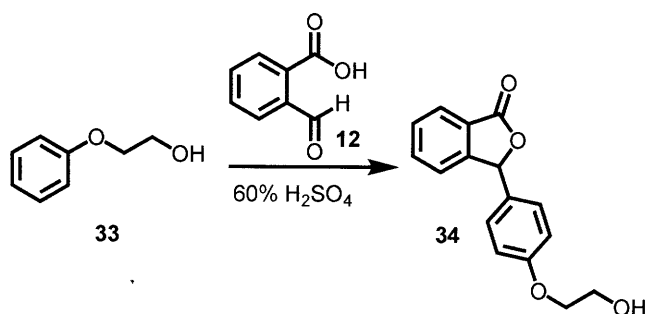
Compound **33** (3.0 g, 0.020 mol) was dissolved in H_2SO_4 (15 ml, 60% aqueous solution) and stirred at r.t. for 10 min. Compound **12** (2.76 g, 0.020 mol) was added, and the reaction mixture was stirred for 3h at r.t. The reaction mixture was then poured into ice water, and the resulting mixture was stirred until it reached r.t. The mixture was extracted with EtOAc, and the combined organic layers were washed with saturated aqueous NaHCO₃ and brine, dried over MgSO₄, and concentrated in vacuo. Flash chromatography (silica gel, EtOAc) afforded **34** as a white solid (3.3 g, 0.012 mol, 61% yield)

¹H NMR (500 MHz, CDCl₃): 7.95 (1H, d, 7.6 Hz), 7.66 (1H, t, 7.5 Hz), 7.56 (1H, t, 7.6 Hz), 7.31 (1H, d, 7.8 Hz), 7.17 (2H, d, 8.9 Hz), 6.90 (2H, d, 8.9 Hz), 6.37 (1H, s), 4.08 (2H, t, 4.3 Hz), 3.96 (2H, q, 4.3 Hz), 2.23 (1H, t, 6.3 Hz) ¹³C NMR (125 MHz, CDCl₃): 170.5, 159.4, 149.6,

134.3, 129.3, 128.8, 128.6, 125.8, 125.5, 122.9, 114.9, 82.6, 69.2, 61.3 HRMS (ESI): 293.0786 [calc'd for M+Na$^+$: 293.0784]
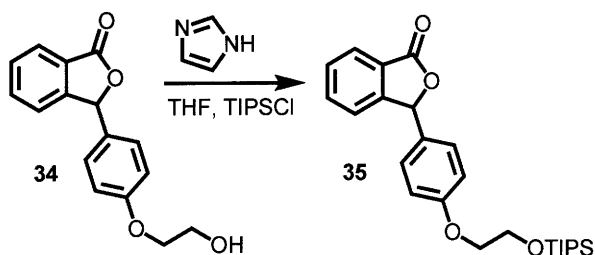
Phthalide **34** (1.0 g, 3.6 mmol) and imidazole (0.88 g, 13 mmol) were dissolved in THF (6 ml). Triisopropylsilyl chloride (1.2 ml, 5.7 mmol) was added drop wise and the reaction mixture was stirred at r.t. overnight. The reaction was then quenched by the addition of 5 ml saturated aqueous NaHCO$_3$. The mixture was then poured into water and extracted with DCM. The combined organic layers were dried over MgSO$_4$ and concentrated in vacuo. The resulting product was purified by recrystallization from MeOH to afford **35** (0.82 g, 2.0 mmol, 56% yield) ^{1}H NMR (500 MHz, CDCl$_3$): 7.96 (1H, d, 7.6 Hz), 7.65 (1H, t, 7.5 Hz), 7.56 (1H, t, 7.9 Hz), 7.31 (1H, d, 7.6 Hz), 7.16 (2H, d, 8.9 Hz), 6.91 (2H, d, 8.7 Hz), 6.37 (1H, s), 4.10-4.00 (4H, m), 1.12-1.01 (21H, m) ^{13}C NMR (125 MHz, CDCl$_3$): 170.5, 159.8, 149.7, 129.2, 128.7, 128.2, 125.9, 125.5, 122.9, 114.9, 82.7, 69.4, 62.1, 17.9, 11.9 HRMS (ESI): 449.2113 [calc'd for M+Na$^+$: 449.2119]
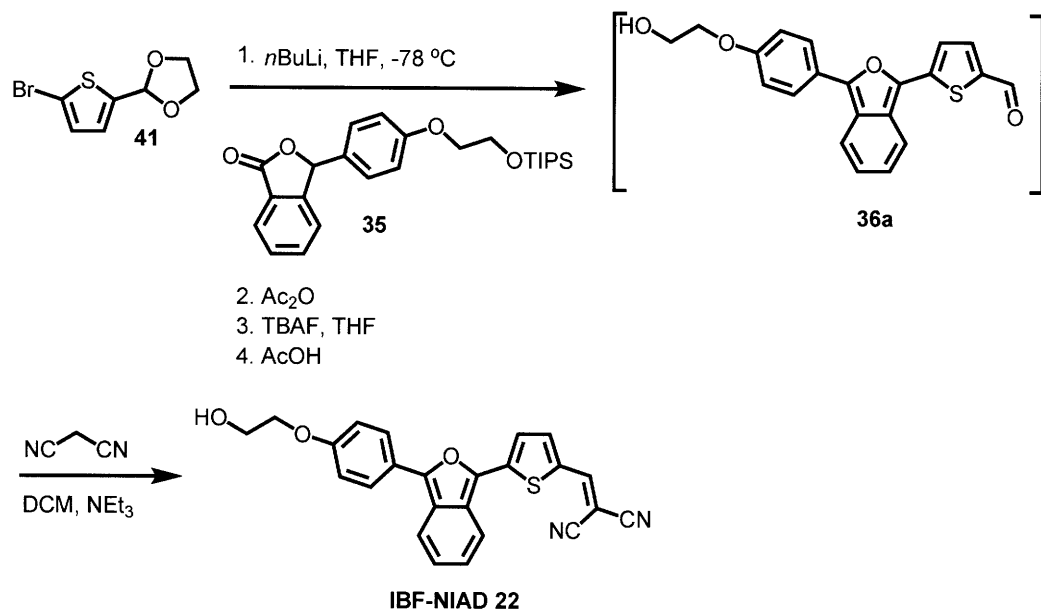
Bromo-thiophene **41** (0.40 g, 1.7 mmol) was dissolved in dry THF (8 ml) and cooled to -78 °C. To this solution was added *n*-BuLi (1.1 ml 1.6 M solution, 1.7 mmol) dropwise and the solution was stirred at -78 °C for 1.5h. A solution of phthalide **35** (0.71 g, 1.7 mmol) in dry THF (8 ml) was then added dropwise, and the solution was stirred for an additional 45 min at -78 °C, after which Ac$_2$O (0.18 ml, 1.9 mmol) was added. The reaction mixture was allowed to warm to room temperature, and was then refluxed for 10 min. The solution was then poured into saturated aqueous NaHCO$_3$, and extracted with EtOAc. The organic layer was washed with brine, dried over MgSO$_4$, and concentrated. The resulting orange viscous product was dissolved in THF (12 ml) and TBAF (2.0 ml, 1.0 m solution, 2.0 mmol) was added dropwise and the solution was stirred for 2 hours 52 room temperature under argon atmosphere. The resulting red solution was poured into water and extracted with EtOAc. The combined organic layers were washed with brine, dried over MgSO$_4$, and concentrated. The resulting orange viscous product was stirred with AcOH (20 ml of 90% solution in water) for 4 hours at room temperature under argon atmosphere. The resulting red solution was poured into water and stirred. A small portion of saturated aqueous NaHCO$_3$ was added, and the solution was extracted with EtOAc. The

combined organic layers were washed with saturated $NaHCO_3$, dried over $MgSO_4$, and concentrated. The red residue was taken up in DCM and precipitated in hexane to afford **36a** as a red solid (0.32 g, 0.88 mmol, 52% yield). Aldehyde **36a** (0.15 g, 0.41 mmol) was dissolved in DCM (12 ml) with malonitrile (0.030 g, 0.46 mmol). Triethylamine (3 drops) was added and the reaction mixture was stirred for 1h. Hexane (7 ml) was added and the blue precipitate was collected by suction filtration. Flash chromatography (silica gel, 10 % MeOH in DCM) afforded **IBF-NIAD 22** (0.019 g, 0.046 mmol, 11% yield, 5.7% yield for two steps) as a blue solid.

^{1}H NMR (500 MHz, $CDCl_3$): 8.39 (1H, s), 7.93 (1H, d, 8.9 Hz), 7.85 (2H, d, 8.7 Hz), 7.78 (1H, d, 4.3 Hz), 7.69 (1H, d, 8.7 Hz), 7.62 (1H, d, 4.4 Hz), 7.25 (1H, dd, 8.7 Hz, 6.6 Hz), 7.13 (1H, dd, 8.9 Hz, 6.6 Hz), 7.08 (2H, d, 8.9 Hz), 4.97 (1H, t, 5.5 Hz), 4.07 (2H, t, 4.7 Hz), 3.76 (2H, q, 5.0 Hz) ^{13}C NMR (125 MHz, $CDCl_3$): 159.4, 150.8, 147.9, 142.8, 137.3, 132.0, 128.7, 127.0, 126.2, 125.4, 122.3, 122.0, 121.30, 121.27, 119.2, 115.5, 115.4, 114.7, 70.6, 69.8, 59.5 (1 missing) HRMS (ESI): 413.0948 [calc'd for M+H$^+$: 413.0954] UV-Vis λ_{max}: 577 nm (MeOH, ε= 25500), 597 (CHCl$_3$, ε= 27400)
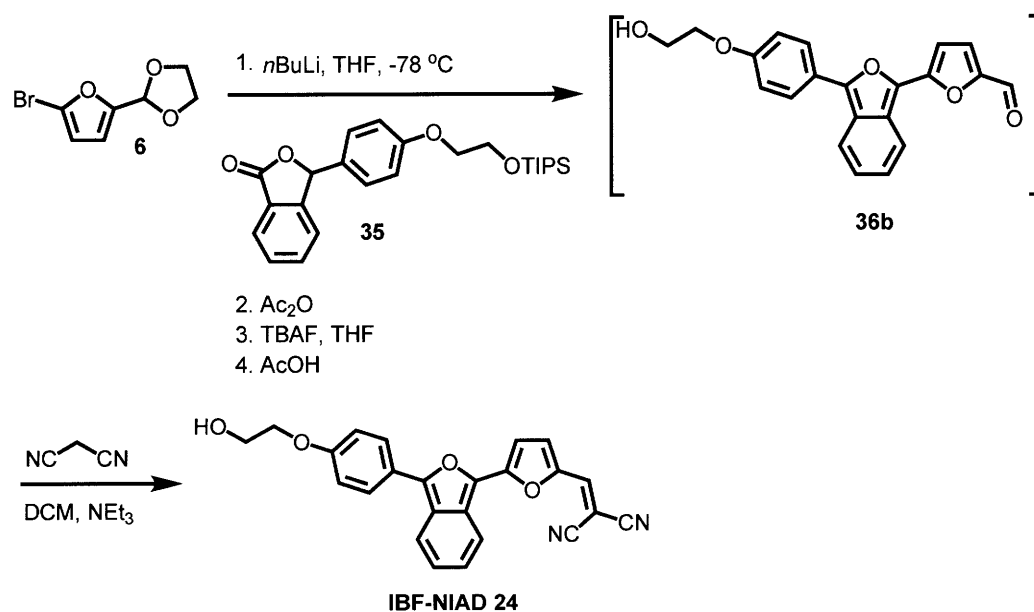
Bromo-furan **6** (0.40 g, 1.8 mmol) was dissolved in dry THF (8 ml) and cooled to -78 °C. To this solution was added *n*-BuLi (1.25 ml 1.6 M solution, 1.9 mmol) dropwise and the solution was stirred at -78 °C for 1.5h. A solution of phthalide **35** (0.75 g, 1.8 mmol) in dry THF (8 ml) was then added dropwise, and the solution was stirred for an additional 45 min at -78 °C, after which Ac_2O (0.25 ml, 2.7 mmol) was added. The reaction mixture was allowed to warm to room temperature, and was then refluxed for 10 min. The solution was then poured into saturated aqueous $NaHCO_3$, and extracted with EtOAc. The organic layer was washed with brine, dried over $MgSO_4$, and concentrated. The resulting orange viscous product was dissolved in THF (13 ml) and TBAF (2.0 ml, 1.0 m solution, 2.0 mmol) was added dropwise and the solution was stirred for 2 hours 52 room temperature under argon atmosphere. The resulting red solution was poured into water and extracted with EtOAc. The combined organic layers were washed with brine, dried over $MgSO_4$, and concentrated. The resulting orange viscous product was stirred with AcOH (20 ml of 90% solution in water) for 4 hours at room temperature under argon atmosphere. The resulting red solution was poured into water and stirred. A small portion of saturated aqueous $NaHCO_3$ was added, and the solution was extracted with EtOAc. The combined organic layers were washed with saturated $NaHCO_3$, dried over $MgSO_4$, and concentrated. The red residue was taken up in DCM and precipitated in hexane to afford **36b** as a red solid (0.224 g, 0.64 mmol, 36% yield). Aldehyde **36b** (0.10 g, 0.29 mmol) was dissolved in DCM (10 ml) with malonitrile (0.020 g, 0.30 mmol). Triethylamine (1 drop) was added and the reaction mixture was stirred for 1h. Hexane (5 ml) was added and the blue precipitate was collected by suction filtration to afford **IBF-NIAD 24** (0.035 g, 0. 088 mmol, 30% yield, 11% yield for two steps) as a blue solid.

^{1}H NMR (500 MHz, DMSO-d$_6$): 8.23 (1H, d, 8.7 Hz), 8.04-7.99 (4H, m), 7.56 (1H, d, 4.1 Hz),

7.33 (1H, d, 4.1 Hz), 7.21 (1H, dd, 8.4 Hz, 6.6 Hz), 7.17 (1H, dd, 8.9 Hz, 6.6 Hz), 7.10 (2H, d,

9.0 Hz), 4.96 (1H, t, 6.3 Hz), 4.09 (2H, t, 4.7 Hz), 3.76 (2H, q, 4.7 Hz) ^{13}C NMR (125 MHz,

DMSO-d$_6$): 159.4, 148.7, 147.6, 146.1, 143.5, 143.4, 133.6, 127.1, 127.0, 126.5, 126.0, 124.0,

122.6, 122.3, 120.8, 115.4, 115.0, 114.7, 109.9, 69.8, 68.8, 59.5 HRMS (ESI): 397.1171 [calc'd

for M+H$^+$: 397.1183] UV-Vis λ_{max}: 572 nm (MeOH, ϵ= 34200), 589 nm (CHCl$_3$, ϵ= 43800)
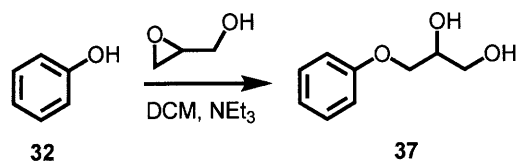
Phenol **32** (3.81 g, 0.041 mol) and glycidol (3.0 g, 0.041 mol) were mixed together in dry EtOH

(8 ml) with triethylamine (0.51 ml, 3.7 mmol) and the solution was refluxed for 3h. The solution

was then cooled to r.t. and concentrated in vacuo. The resulting residue was purified by flash

chromatography (silica gel, EtOAC) to afford **37** (4.6 g, 0.027 mol, 66% yield) as a clear viscous

liquid that solidified into a white solid on standing. (Adopted from a literature procedure)[52]

^{1}H NMR (500 MHz, CDCl$_3$): 7.30 (2H, dd, 8.7 Hz, 7.3 Hz), 6.99 (1H, t, 7.3 Hz), 6.92 (2H, dm,

7.8 Hz), 4.12 (1H, sex, 5.5 Hz), 4.06-4.02 (2H, m), 3.87-3.72 (2H, m), 3.07 (1H, 6.0 Hz), 2.59

(1H, t, 6.0 Hz) ^{13}C NMR (125 MHz, CDCl$_3$): 158.3, 129.5, 121.3, 114.5, 70.4, 67.0, 63.6 HRMS

(ESI): 191.0681 [calc'd for M+Na$^+$: 191.0679] (Adopted from literature procedure)[52]
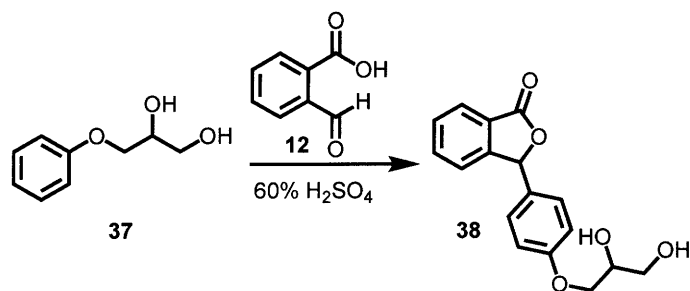
2-Carboxylbenzaldehyde **12** (3.6 g, 0.024 mol) was dissolved in H_2SO_4 (16 ml, 60% aqueous solution) and stirred at r.t. for 10 min. Compound **37** (3.2 g, 0.019 mol) was added, and the reaction mixture was stirred for 3h at r.t. The reaction mixture was then poured into ice water, and the resulting mixture was stirred until it reached r.t. The mixture was extracted with EtOAc, and the combined organic layers were washed with saturated aqueous $NaHCO_3$ and brine, dried over $MgSO_4$, and concentrated in vacuo. Flash chromatography (silica gel, EtOAc) afforded **38** as a white solid (1.5 g, 0.0050 mol, 26% yield)

^{1}H NMR (500 MHz, $CDCl_3$): 7.91 (1H, d, 7.6 Hz), 7.62 (1H, t, 7.5 Hz), 7.52 (1H, t, 7.6 Hz), 7.26 (1H, d, 7.8 Hz), 7.08 (2H, d, 8.7 Hz), 6.82 (2H, d, 8.9 Hz), 4.06 (1H, sex, 3.8 Hz), 3.97-3.93 (2H, m), 3.76 (1H, dd, 11.4 Hz, 3.7 Hz), 3.72-3.44 (3H, m) ^{13}C NMR (125 MHz, $CDCl_3$): 170.8, 159.2, 149.6, 134.4, 129.3, 128.7, 128.4, 125.5, 125.4, 122.9, 114.8, 82.7, 70.3, 68.9, 63.4 HRMS (ESI): 323.0891 [calc'd for M+Na$^+$: 323.0890]
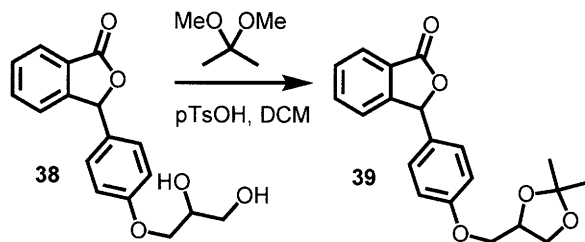
Phthalide **38** (1.5 g, 5.0 mmol) was dissolved in DCM (10 ml) with 2,2-dimethoxypropane (1.25 ml, 10 mmol). *p*-Toluenesulfonic acid monohydrate (0.015 g, 0.079 mmol) was added, and the solution was stirred at r.t. overnight. The reaction mixture was then concentrated in vacuo and purified by flash chromatography (silica gel, EtOAc) to afford **39** (1.35 g, 3.96 mmol, 79% yield) as a white solid.

^{1}H NMR (500 MHz, $CDCl_3$): 7.95 (1H, d, 7.6 Hz), 7.65 (1H, t, 7.5 Hz), 7.56 (1H, t, 7.5 Hz), 7.31 (1H, d, 7.8 Hz), 7.17 (2H, d, 8.7 Hz), 6.91 (2H, d, 8.9 Hz), 6.37 (1H, s), 4.47 (1H, quin, 6.0 Hz),

4.16 (1H, dd, 8.5 Hz, 6.6 Hz), 4.05 (1H, ddd, 9.5 Hz, 5.5 Hz, 2.4 Hz), 3.94 (1H, ddd, 9.5 Hz, 5.8 Hz, 1.7 Hz), 3.89 (1H, dd, 8.2 Hz, 5.8 Hz), 1.45 (3H, s), 1.40 (3H, s) ^{13}C NMR (125 MHz, CDCl$_3$): 170.4, 159.3, 149.6, 134.2, 129.3, 128.7, 125.8, 125.5, 122.9, 114.8, 109.8, 82.6, 73.8, 68.8, 66.7, 26.7, 25.3 HRMS (ESI): 341.1387 [calc'd for M+H$^+$: 341.1384]
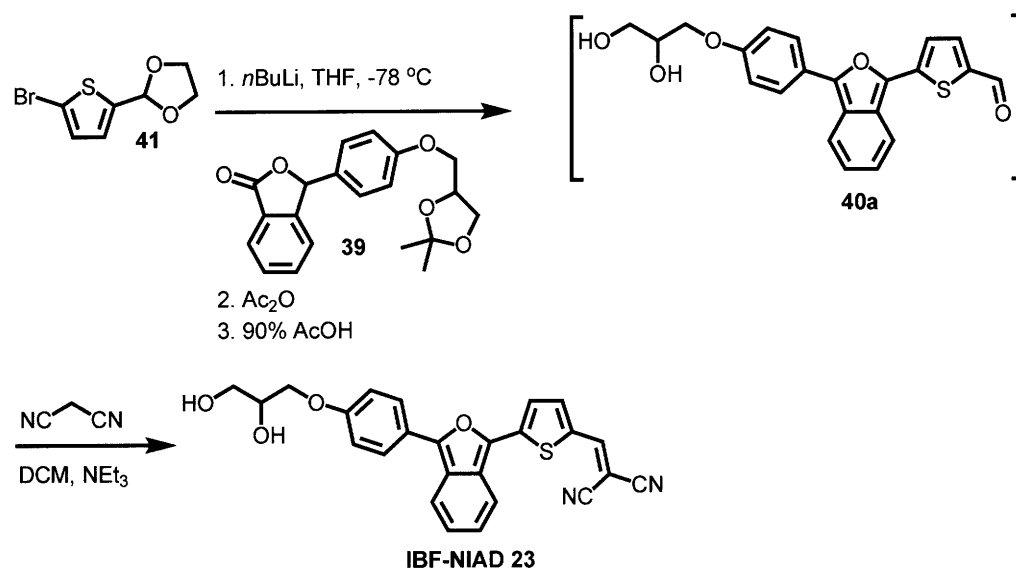
Bromo-thiophene **41** (0.20 g, 0.85 mmol) was dissolved in dry THF (3 ml) and cooled to -78 °C. To this solution was added *n*-BuLi (0.55 ml 1.6 M solution, 0.88 mmol) dropwise and the solution was stirred at -78 °C for 1.5h. A solution of phthalide **39** (0.30 g, 0.88 mmol) in dry THF (3 ml) was then added dropwise, and the solution was stirred for an additional 45 min at -78 °C, after which Ac$_2$O (0.12 ml, 1.3 mmol) was added. The reaction mixture was allowed to warm to room temperature, and was then refluxed for 10 min. The solution was then poured into saturated aqueous NaHCO$_3$, and extracted with EtOAc. The organic layer was washed with brine, dried over MgSO$_4$, and concentrated. The resulting orange viscous product was stirred with AcOH (15 ml of 90% solution in water) for 4 hours at room temperature under argon atmosphere. The resulting red solution was poured into water and stirred. A small portion of saturated aqueous NaHCO$_3$ was added, and the solution was extracted with EtOAc. The

combined organic layers were washed with saturated NaHCO$_3$, dried over MgSO$_4$, and concentrated. The red residue was subjected to flash chromatography (silica gel, 10% MeOH in DCM) to afford **40a** (0.15 g, 0.38 mmol, 43% yield) as a crude product. Aldehyde **40a** (0.15 g, 0.38 mmol) was dissolved in DCM (15 ml) with malonitrile (0.025 g, 0.38 mmol). Triethylamine (3 drops) was added and the reaction mixture was stirred for 1h. Hexane (5 ml) was added and the blue precipitate was collected by suction filtration to afford **IBF-NIAD 23** (0.093 g, 0.21 mmol, 55% yield, 24% yield for two steps) as a blue solid.

^{1}H NMR (500 MHz, DMSO-d$_6$): 8.13 (1H, d, 8.1 Hz), 7.96-7.90 (4H, m), 7.49 (1H, d, 4.1 Hz), 7.20 (1H, d, 4.0 Hz), 7.16-7.09 (2H, m), 7.07 (2H, d, 8.9 Hz), 5.10 (1H, d, 5.2 Hz), 4.81 (1H, t, 5.6 Hz), 4.09 (1H, dd, 9.9 Hz, 4.0 Hz), 3.95 (1H, dd, 10.1 Hz, 6.4 Hz), 3.84 (1H, sex, 5.6 Hz)

^{13}C NMR (125 MHz, DMSO-d$_6$): 159.6, 153.1, 148.8, 147.7, 140.2, 133.7, 130.3, 128.3, 127.2, 126.6, 126.1, 122.4, 121.0, 120.8, 120.0, 116.1, 115.5, 115.2, 110.4, 70.1, 69.9, 68.9, 62.8

HRMS (ESI): 441.1084 [calc'd for M-H$^-$: 441.0915] UV-Vis λ_{max}: 571 nm (MeOH, ε= 42700), 589 nm (CHCl$_3$, ε= 32000)

IBF-NIAD 25
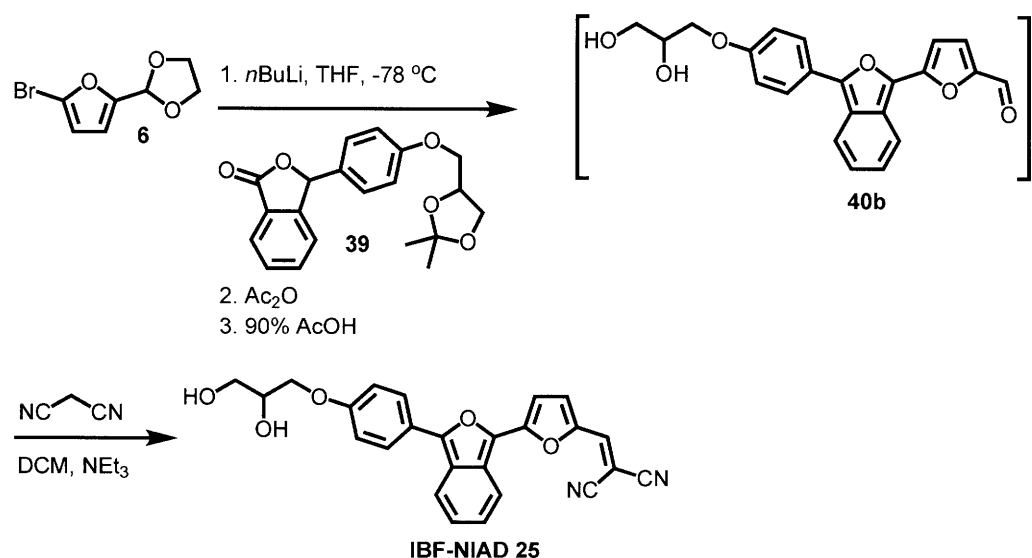
Bromo-furan **6** (0.22 g, 1.0 mmol) was dissolved in dry THF (3 ml) and cooled to -78 °C. To this solution was added *n*-BuLi (0.64 ml 1.6 M solution, 1.0 mmol) dropwise and the solution was stirred at -78 °C for 1.5h. A solution of phthalide **39** (0.30 g, 0.88 mmol) in dry THF (3 ml) was then added dropwise, and the solution was stirred for an additional 45 min at -78 °C, after which Ac_2O (0.13 ml, 1.4 mmol) was added. The reaction mixture was allowed to warm to room temperature, and was then refluxed for 10 min. The solution was then poured into saturated aqueous $NaHCO_3$, and extracted with EtOAc. The organic layer was washed with brine, dried over $MgSO_4$, and concentrated. The resulting orange viscous product was stirred with AcOH (15 ml of 90% solution in water) for 4 hours at room temperature under argon atmosphere. The resulting red solution was poured into water and stirred. A small portion of saturated aqueous $NaHCO_3$ was added, and the solution was extracted with EtOAc. The combined organic layers were washed with saturated $NaHCO_3$, dried over $MgSO_4$, and concentrated. The red residue was subjected to flash chromatography (silica gel, 10% MeOH in DCM) to afford **40b** (0.14 g, 0.37 mmol, 42% yield) as a crude product. Aldehyde **40b** (0.11 g, 0.29 mmol) was dissolved in DCM (12 ml) with malonitrile (0.021 g, 0.32 mmol). Triethylamine (3 drops) was added and the reaction mixture was stirred for 1h. Hexane (5 ml) was added and the blue precipitate was collected by suction filtration to afford **IBF-NIAD 25** (0.051 g, 0.12 mmol, 41% yield, 17% yield for two steps) as a blue solid.

^{1}H NMR (500 MHz, DMSO-d_6): 8.20 (1H, d, 8.2 Hz), 8.01-7.96 (4H, m), 7.53 (1H, d, 4.0 Hz), 7.28 (1H, d, 4.1 Hz), 7.20-7.12 (2H, m), 7.09 (2H, d, 9.0 Hz), 5.05 (1H, d, 5.1 Hz), 4.76 (1H, t, 5.6 Hz), 4.10 (1H, dd, 9.8 Hz, 4.0 Hz), 3.97 (1H, dd, 9.8 Hz, 6.3 Hz), 3.84 (1H, dd, 10.4 Hz, 6.1 Hz), 3.49 (2H, t, 5.6 Hz) ^{13}C NMR (125 MHz, DMSO-d_6): 159.5, 153.0, 148.7, 147.6, 140.2, 133.6, 130.2, 128.2, 127.1, 126.4, 126.0, 122.3, 120.9, 120.7, 119.9, 115.9, 115.4, 115.1, 110.3,

69.94, 69.87, 68.9, 62.7 HRMS (ESI): 449.1117 [calc'd for M+Na$^+$: 449.1108] UV-Vis λ_{max}:

572 nm (MeOH, ε= 40900), 587 nm (CHCl$_3$, ε= 39900)

3.5 References

(1)   http://www.alzinfo.org/alzheimers-disease-information.asp

(2)   Nowotny, P.; Kwon, J. M.; Goate, A. M.; Alzheimer's Disease in *Encyclopedia of Life Sciences*, Wiley-Blackwell, 2002.

(3)   Brookmeyer, R.; Johnson, E.; Ziegler-Graham, K.; Arrighi, H. M. *Alzheimers and Dementia*, **2007**, *3*, 186.

(4)   Picture from http://www.alzheimer.sk.ca/english/Just4Kids/alz_disease-brainpics.shtml

(5)   Nussbaum, R. L.; Ellis, C. E. *N. Engl. J. Med.* **2003**, *348*, 1356

(6)   Hanger, D. P.; Byers, H. L.; Wray, S.; Leung, K. Y.; Saxton, M. J.; Seereeram, A.; Reynolds, C. H.; Ward, M. A.; Anderson, B. H. *J. Biol. Chem.* **2007**, *282*, 23645.

(7)   Lee, V. M.; Balin, B. J.; Otvos, L., Jr.; Trojanowski, J. Q. *Science* **1991**, *251*, 675

(8)   Mandavilli, A. *Nature Med.* **2006**, *12*, 747

(9)   Golde, T. E. *J. Clin. Invest.* **2003**, *111*, 11.

(10)   Hardy, J.; Selkoe, D. J. *Science*, **2002**, *297*, 356-356

(11)   Zamrini, E.; De Santi, S.; Tolar, M. *Neurobiol. Aging* **2004**, *25*, 685

(12)   Bacskai, B. J.; Kajdasz, S. T., Christie, R. H.; Carter, C.; Games, D.; Seubert, P.; Schenk, D.; Hyman, B. T. *Nat. Med.* **2001**, *7*, 369.

(13)   Bacskai, B. J.; Hickey, G. A.; Skoch, J.; Kajdasz, S. T.; Wang, Y.; Huang, G.; Mathis, C. A.; Klunk, W. E.; Hyman, B. T. *Proc. Nat. Acad. Sci.* **2003**, *100*, 12462

(14)   Wadghiri, Y. Z.; Sigurdsson, E. M., Sadowski, M.; Elliott, J. I.; Li, Y.; Scholtzova, H.; Tang, C. Y.; Aguinaldo, G.; Pappolla, M.; Duff, K.; Wisniewski, T.; Turnbull, D. H. *Mag. Reson. Med.* **2003**, *50*, 293. (b) Poduslo, J. F.; Curran, G. L.; Peterson, J. A.; McCormick, D. J.; Fauq, A. H.; Khan, M. A.; Wengenack, T. M. *ACS Biochemistry* **2004**, *43*, 6064.

(15)   Henriksen, G.; Yousefi, B. H.; Drzezga, A.; Wester, H. *Eur. J. Nucl. Med. Mol. Imaging* **2008**, *35*, S75

(16)   (a) Agdeppa, E. D.; Kepe, V.; Liu, J.; Flores-Torres, S.; Satyamurthy, N.; Petric, A.; Cole, G. M.; Small, G. W.; Huang, S.-C.; Barrio, J. R.; *J. Neurosci.* **2001**, *21*, 189. (b)

Agdeppa, E. D.; Kepe, V.; Petric, A.; Satyamurthy, N.; Liu, J.; Small, G. W.; Cole, G. M.; Barrio, J. R.; *Neuroscience* **2003**, *117*, 723.

(17) (a) Mathis, C.A.; Wang, Y.M.; Holt, D. P.; Huang,G. F.; Debnath, M. F.; Klunk, W. E. *J. Med. Chem.* **2003**, *46*, 2740 –2754. (b) Klunk, W. E.; Engler, H.; Nordberg, A.; Wang, Y. M.; Blomqvist, G.; Holt, D. P.; Bergstrom, M.; Savitcheva, I. Huang, G. F.; Estrada, S.; Ausen, B.; Debnath, M. L.; Barletta, J.; Price, J. C.; Sandell, J.; Lopresti, B. J.; Wall, A.; Koivisto, P.; Antoni, G.; Mathis, C. A.; Langstrom, B.; *Ann. Neurol.* **2004**, *55*, 306 –319.

(18) Verhoeff, N. P.; Wilson, A. A.; Takeshita, S.; Trop, L.; Hussey, D.; Singh, K. et al. *Am. J. Geriatr. Psychiatry* **2004**, *12*, 584.

(19) Kudo, Y.; Okamura, N.; Furumoto, S. et. al. *J. Nucl. Med.* **2006**, *48*, 553.

(20) Nordberg, A. *Eur. J. Nucl. Med. Mol. Imaging* **2008**, *35*, S46.

(21) Skoch, J.; Dunn, A.; Hyman, B.T.; Bacskai, B.J. *J. Biomed. Opt.* **2005**, *10*, 011007.

(22) An octanol/water partition coefficient is defined as the ratio of the concentration of solute in octanol to the concentration of solute in water after the solute is added to an mixture of octanol and water and the phases are allowed to equilibrate.

(23) Begley, D. J. *Pharm. Thera.* **2004**, *104*, 29.

(24) Mathis, C. A.; Wang, Y.; Klunk, W.E.; *Curr. Pharm. Des.* **2004**, *10*, 1469.

(25) Raymond, S. B.; Skoch, J.; Hills, I. D.; Nesterov, E. E.; Swager, T. M.; Backskai, B. J. *Eur. J. Nucl. Med. Mol. Imaging* **2008**, *35*, S93.

(26) Kumar, A. T. N.; Raymond, S. B.; Boverman, G.; Boas, D. A.; Bacskai, B. J. *Opt. Express* **2006**, *14*, 12255.

(27) Godavarty, A.; Sevick-Muraca, E. M.; Eppstein, M. J. *Med. Phys.* **2005**, *32*, 992.

(28) Klunk, W. E.; Wang, Y.; Huang, G.; Debnath, M. L.; Holt, D. P.; Mathis, C. A. *Life Sci.* **2001**, *69*, 1471.

(29) E. S. Voropai, M. P. Samtsov, K. N. Kaplevskii, A. A. Maskevich, V. I. Stepuro, O. I. Povarova, I. M. Kuznetsova, K. K. Turoverov, A. L. Fink, V. N. Uverskii, *J. Appl. Spectrosc.* **2003**, *70*, 868.

(30) Hintersteiner, M.; Enz, A.;, Frey, P.; Jaton, A. L.; Kinzy, W.; Kneuer, R.; Neumann, U.; Rudin, M.; Staufenbiel, M.; Stoeckli, M.; Wiederhold, K-H.; Gremlich, H-U. *Nat. Biotechnol.* **2005**, *23*, 577.

(31) Golde, T. E.; Bacskai, B. J. *Nat. Biotechnol.* **2005**, *23*, 552.

(32) Nesterov, E. E.; Skoch, J.; Hyman, B. T.; Klunk, W. E., Bacskai, B. J.; Swager, T. M. *Angew. Chem. Int. Ed.* **2005**, *44*, 5452.

(33) Arik, M.; Meral, K.; Onganer, Y. *J. Lumin.* **2009**, *129*, 599.

(34) Bird, C. W. *Tetrahedron*, **1992**, *48*, 335.

(35) Na, K-S.; Kuroda, A.; Takiguchi, N.; Ikeda, T.; Ohtake, H.; Kato, J. *J. Biosci. Bioeng.* **2005**, *99*, 378.

(36) Yamagami, C.; Tachikawa, H. *Chem. Pharm. Bull.* **2003**, *51*, 1196.

(37) Bird, C. W. *Tetrahedron*, **1996**, *52*, 9945.

(38) Seixas de Melo, J.; Elisei, F.; Becker, R. S. *J. Chem. Phys.* **2002**, *117*, 4428.

(39) Mitschke, U.; Osteritz, E. M.; Debaerdemaeker, T.; Sokolowski, M.; Bauerle, P. *Chem. Eur. J.* **1998**, *4*, 2211.

(40) Valeur, Bernard *Molecular Fluorescence: Principles and Applications*; Wiley & Sons: New York, 2001.

(41) White mater is composed of myelinated axons and carries signals between grey matter portions of the brain, see Schmahmann, J. D.; Smith, E. E.; Eichler, F. S.; Filley, C. M. *Anal. N.Y. Acad. Sci.* **2008**, *1142*, 266.

(42) Compston, A.; Coles, A. *Lancet*, **2002**, *359*, 1221.

(43) Li, J.; Yao, S. Q. *Org. Lett.* **2009**, *11*, 405.

(44) Bouffard, J.; Kim, Y.; Swager, T. M.; Weissleder, R.; Hilderbrand, S. A. *Org. Lett.* **2008**, *10*, 37.

(45) Polt, R.; Peterson, M. A. *Tet. Lett.* **1990**, *31*, 4985.

(46) Bhatt, M. V.; Kamath, K. M. *J. Chem. Soc. (B)* **1968**, 1036.

(47) Huet, F.; Lechevallier, A.; Pallet, M.; Conia, J. M. *Synthesis* **1978**, 63.

(48) Wolfe, J. P.; Ahman, J.; Sadighi, J. P.; Singer, R. A.; Buchwald, S. L. *Tet. Lett.* **1997**, *38*, 6367.

(49) Bures, F.; Schweizer, W. B.; Boudon, C.; Gisselbrecht, J.-P.; Gross, M.; Diederich, F.

Eur. J. Org. Chem. **2008**, 994.

(50)   Pearson, J. C.; Weaver, M. A.; Fleischer, J. C.; King, G. A. U.S. Patent 2005040897, 2005.

(51)   Ram, R. N.; Singh, V. *J. Chem. Res.* **2006**, *12*, 800.

(52)   Bredikhina, Z. A.; Savel'ev, D. V.; Bredikhina, A. A. *Rus. J. Org. Chem.* **2002**, *38*, 233.

3.A Appendix

^{1}H NMR and ^{13}C NMR Spectra
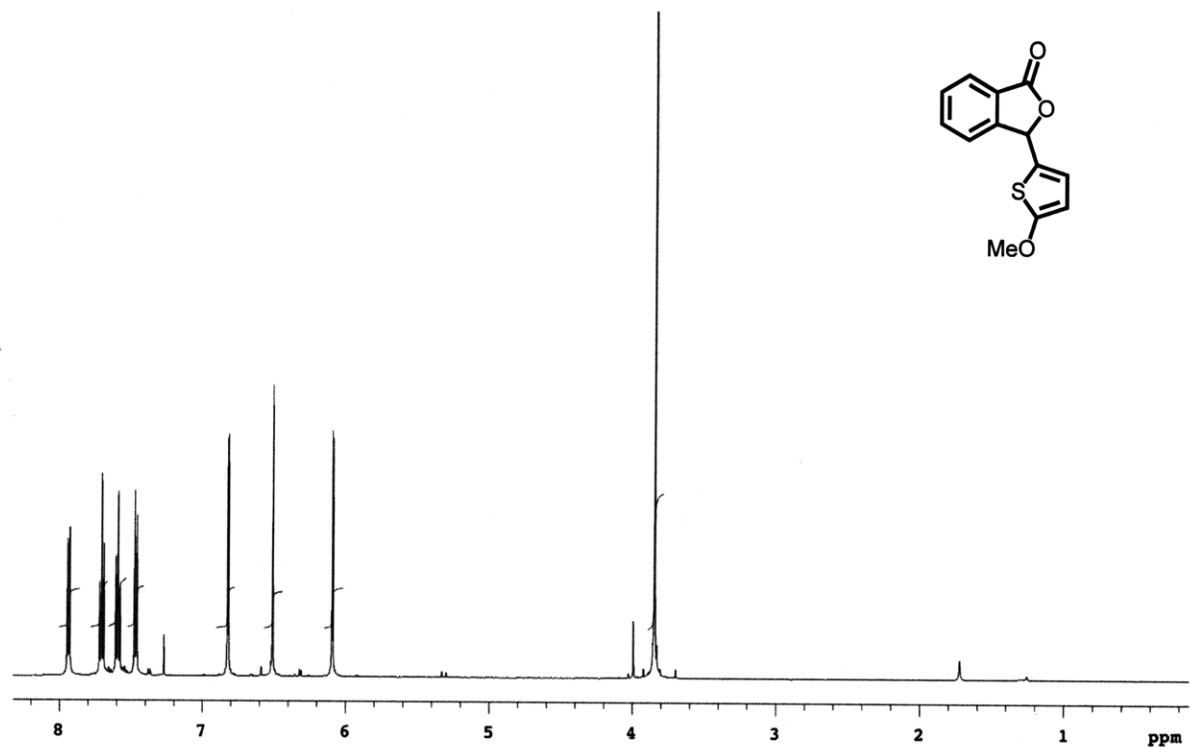
Figure 3.A.1 ^{1}H NMR (500 MHz, CDCl$_3$) of **3**
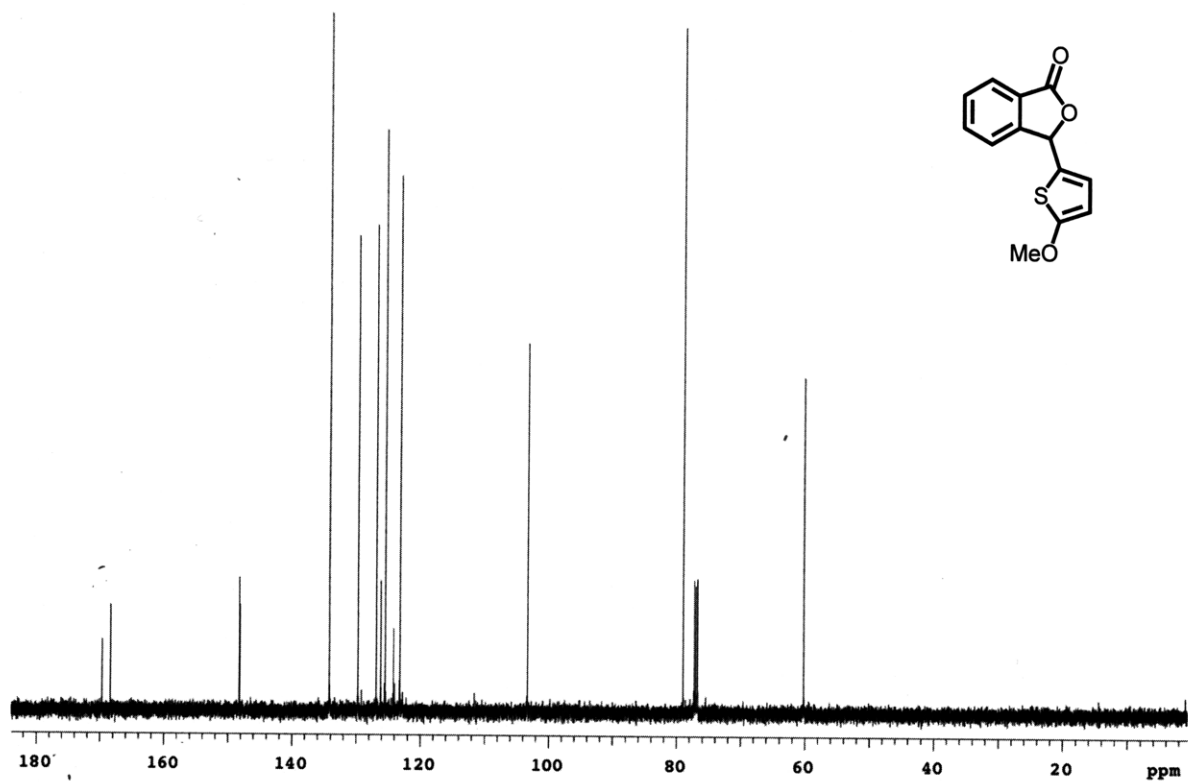
Figure 3.A.2 ^{13C} NMR (125 MHz, CDCl$_3$) of **3**
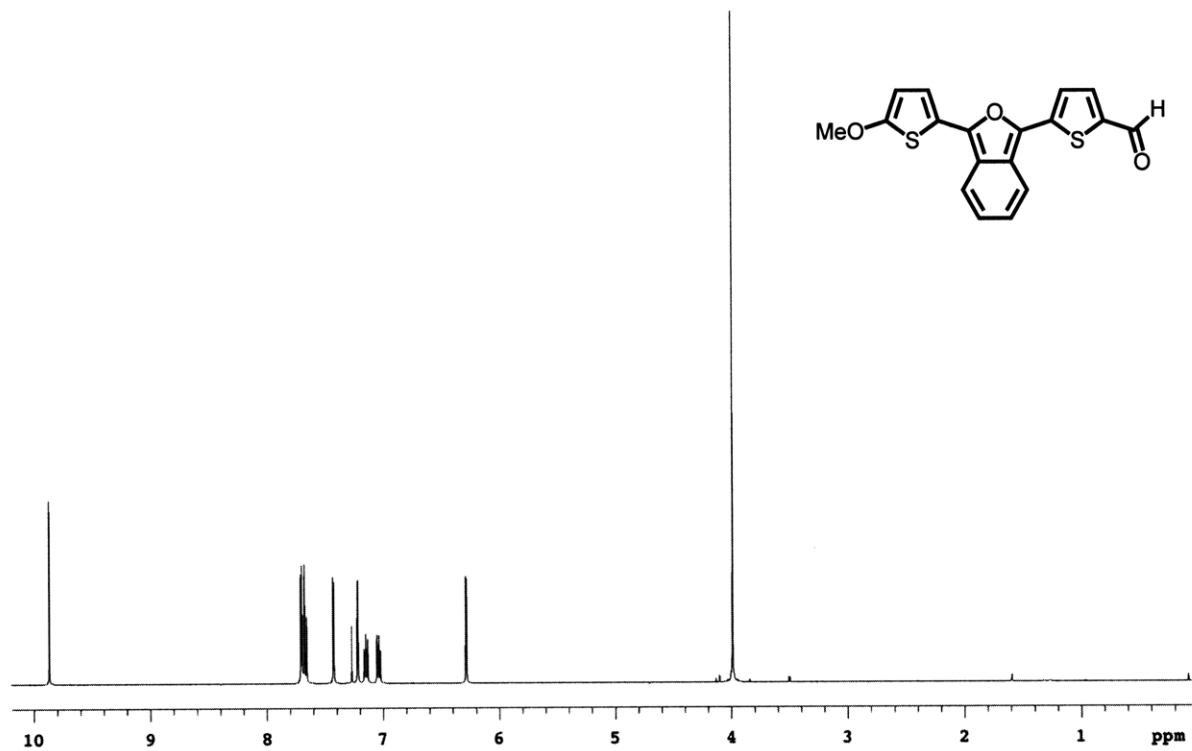
Figure 3.A.3 ^{1}H NMR (500 MHz, CDCl$_3$) of **4**
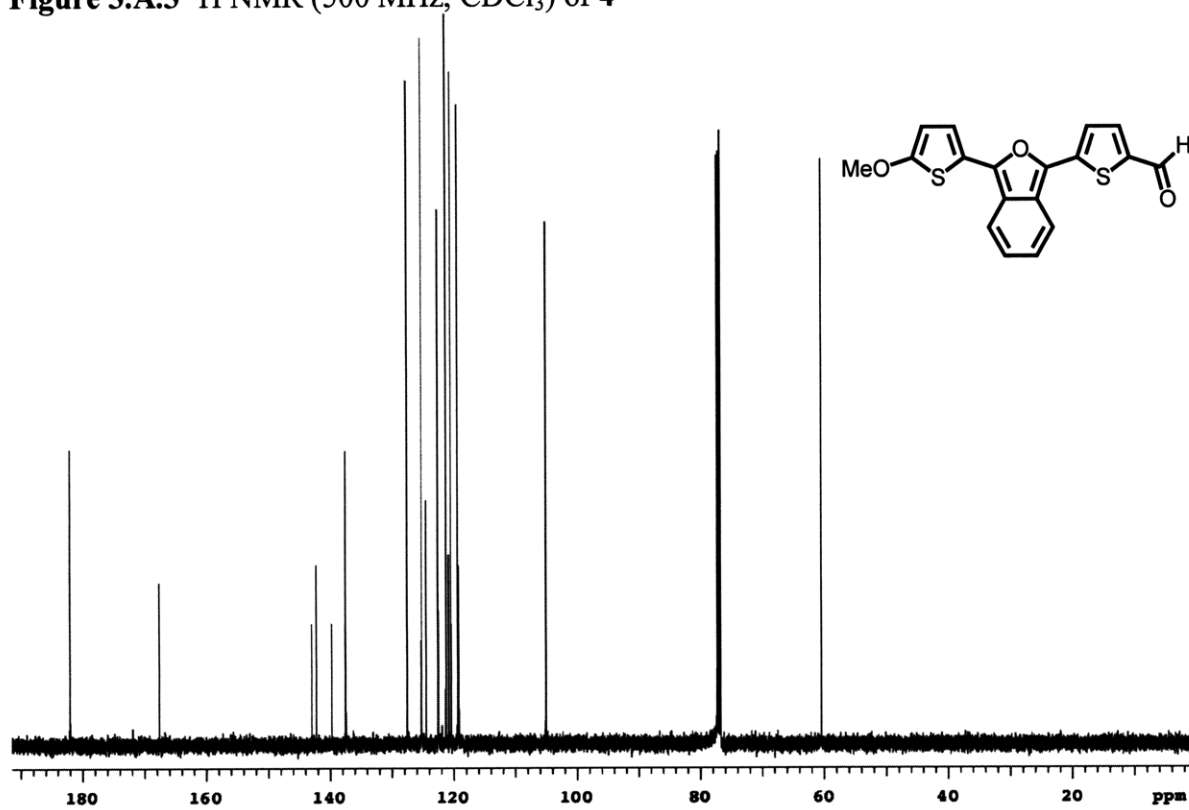
Figure 3.A.4 ^{13C} NMR (125 MHz, CDCl$_3$) of **4**
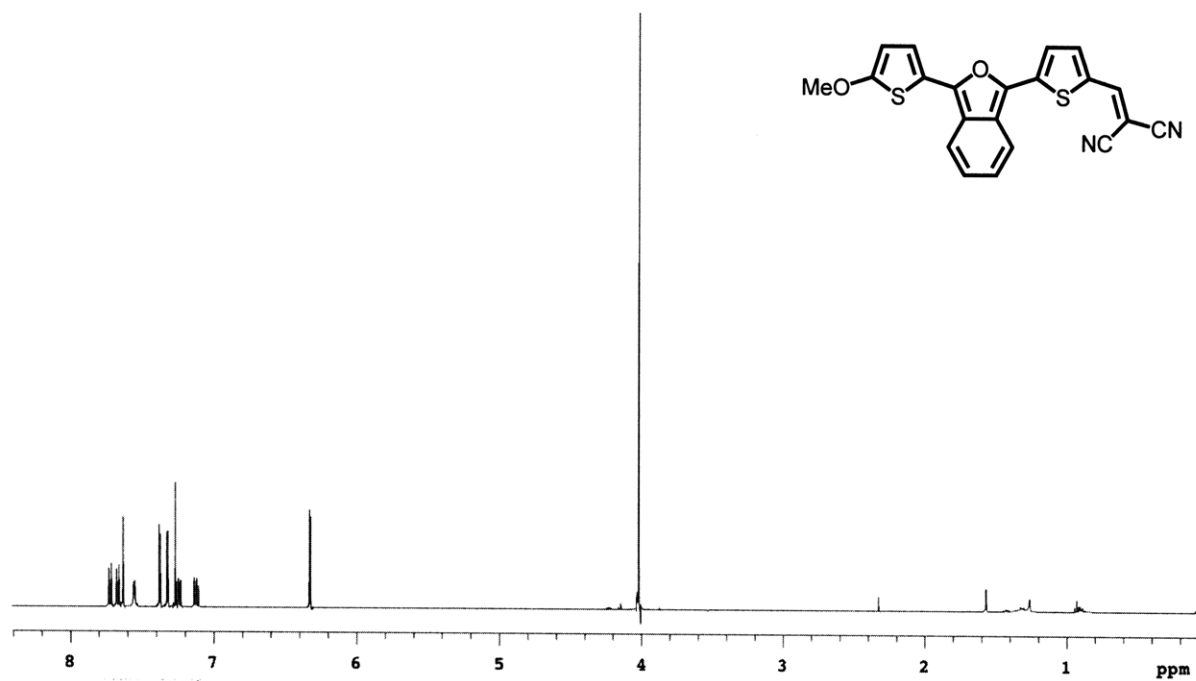
Figure 3.A.5 ^{1}H NMR (500 MHz, CDCl$_3$) of **IBF-NIAD 4**
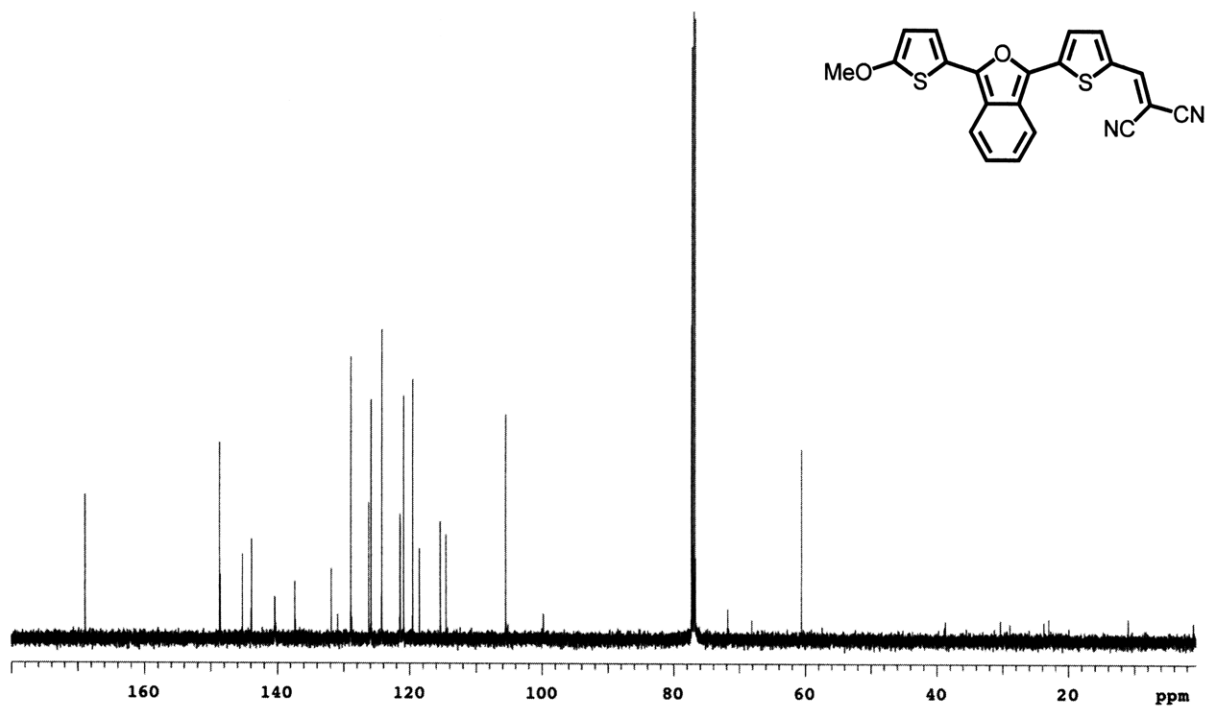
Figure 3.A.6 ^{13C} NMR (125 MHz, CDCl$_3$) of **IBF-NIAD 4**
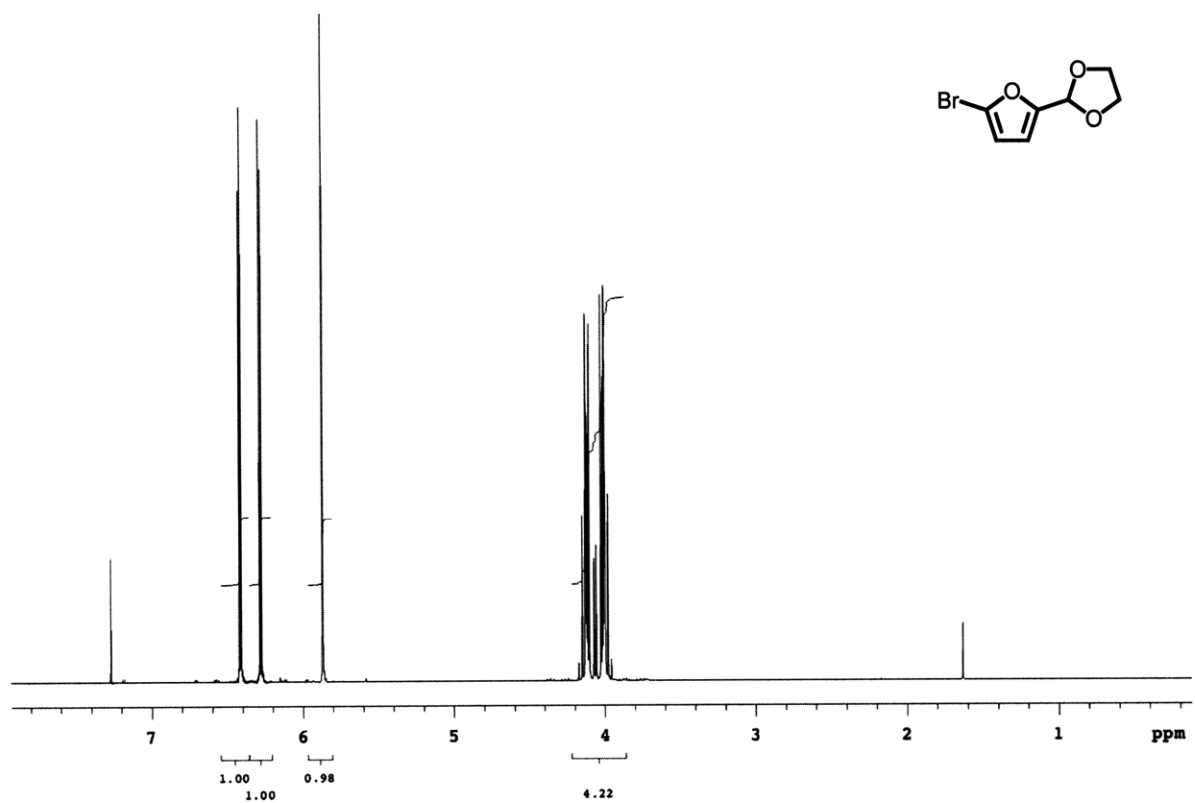
Figure 3.A.7 ^{1}H NMR (500 MHz, CDCl$_3$) of **6**
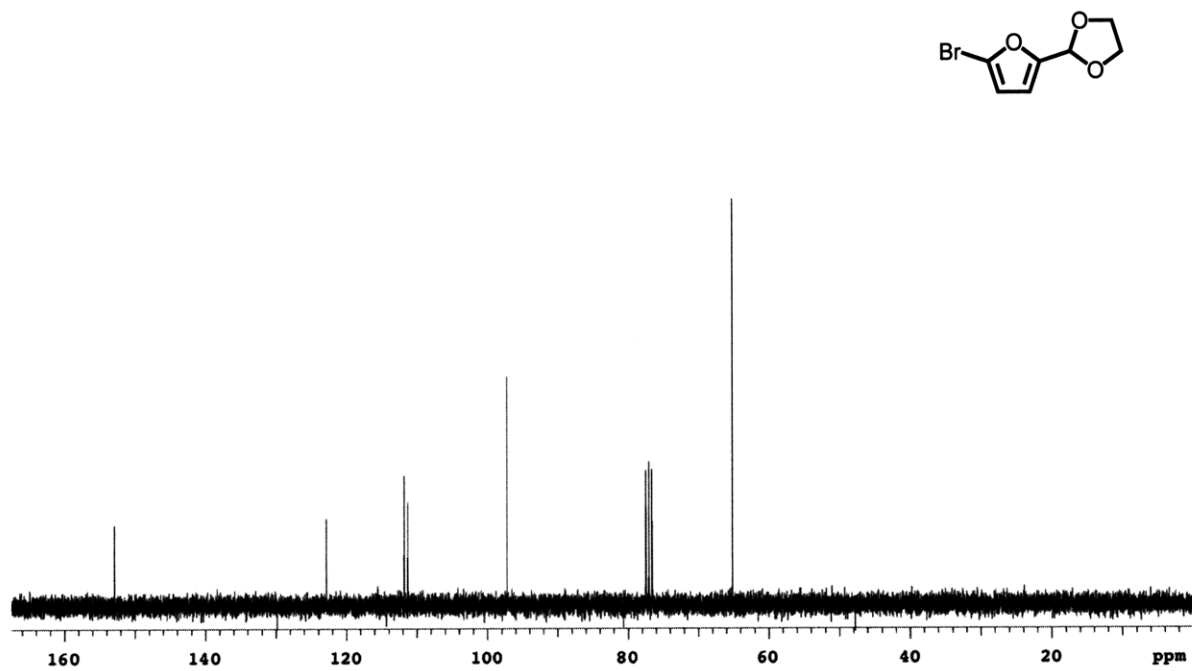
Figure 3.A.8 ^{13C} NMR (125 MHz, CDCl$_3$) of **6**
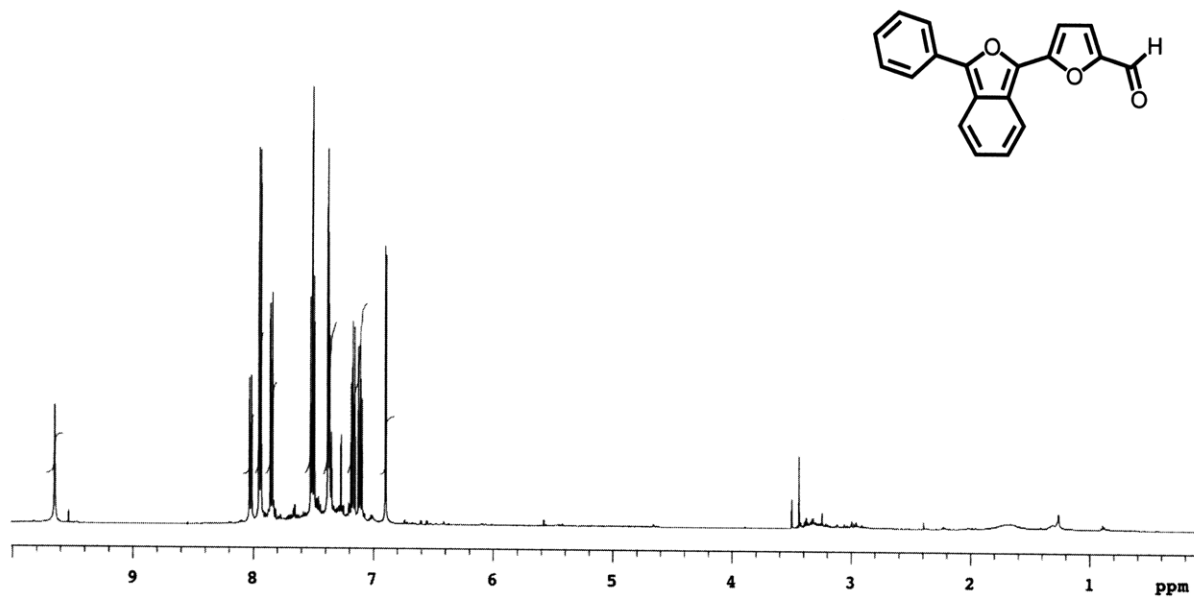
Figure 3.A.9 ^{1}H NMR (500 MHz, CDCl$_3$) of **8a**
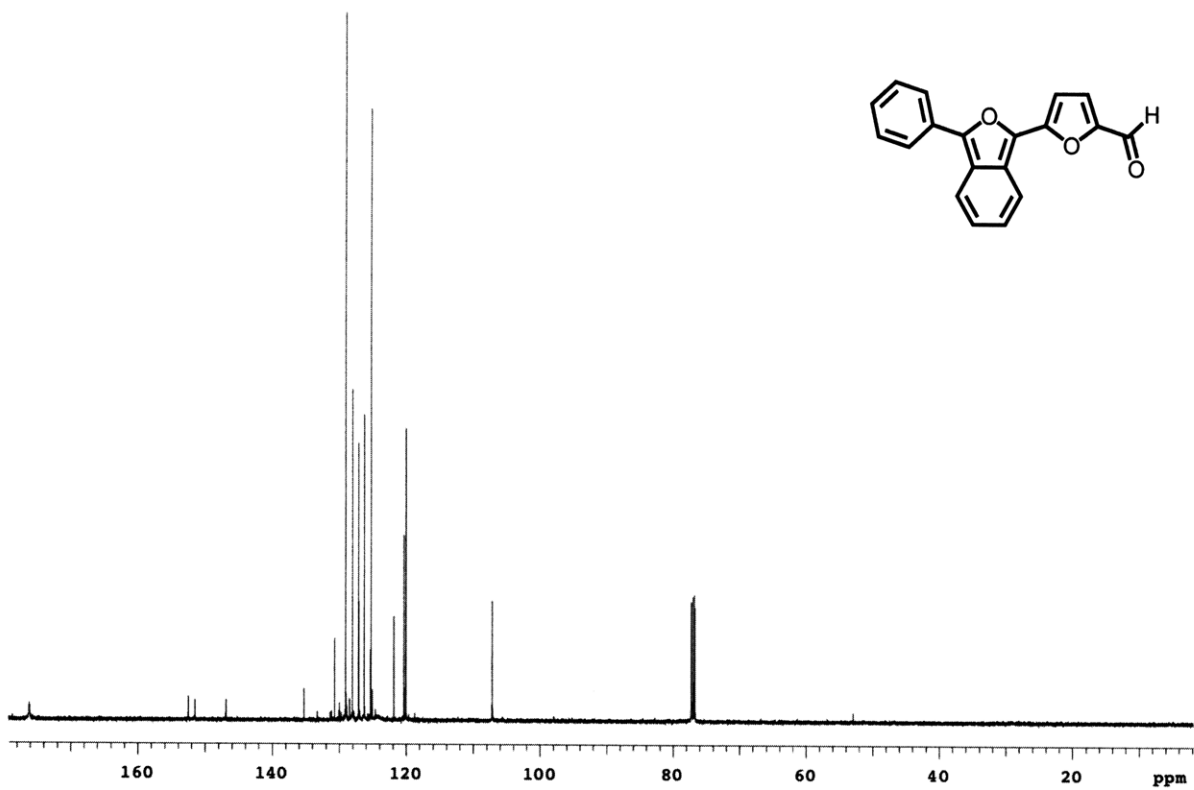
Figure 3.A.10 ^{13C} NMR (125 MHz, CDCl$_3$) of **8a**

188
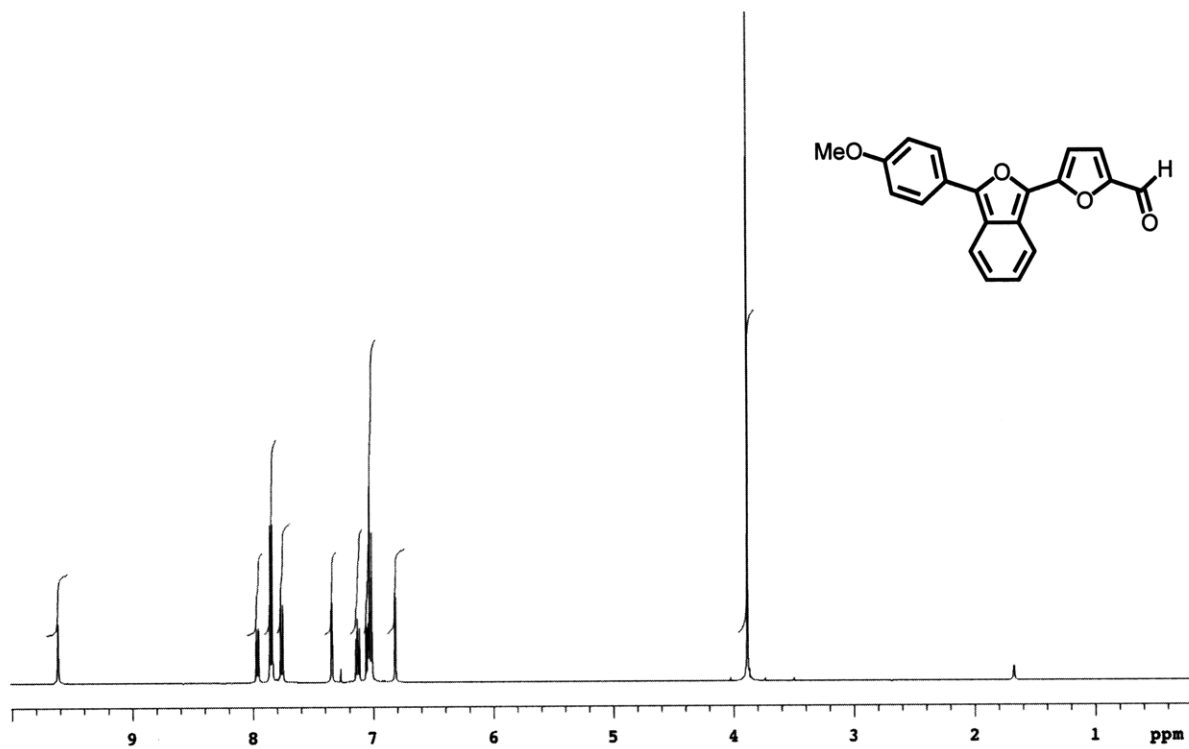
Figure 3.A.11 ^{1}H NMR (500 MHz, CDCl$_3$) of **8b**
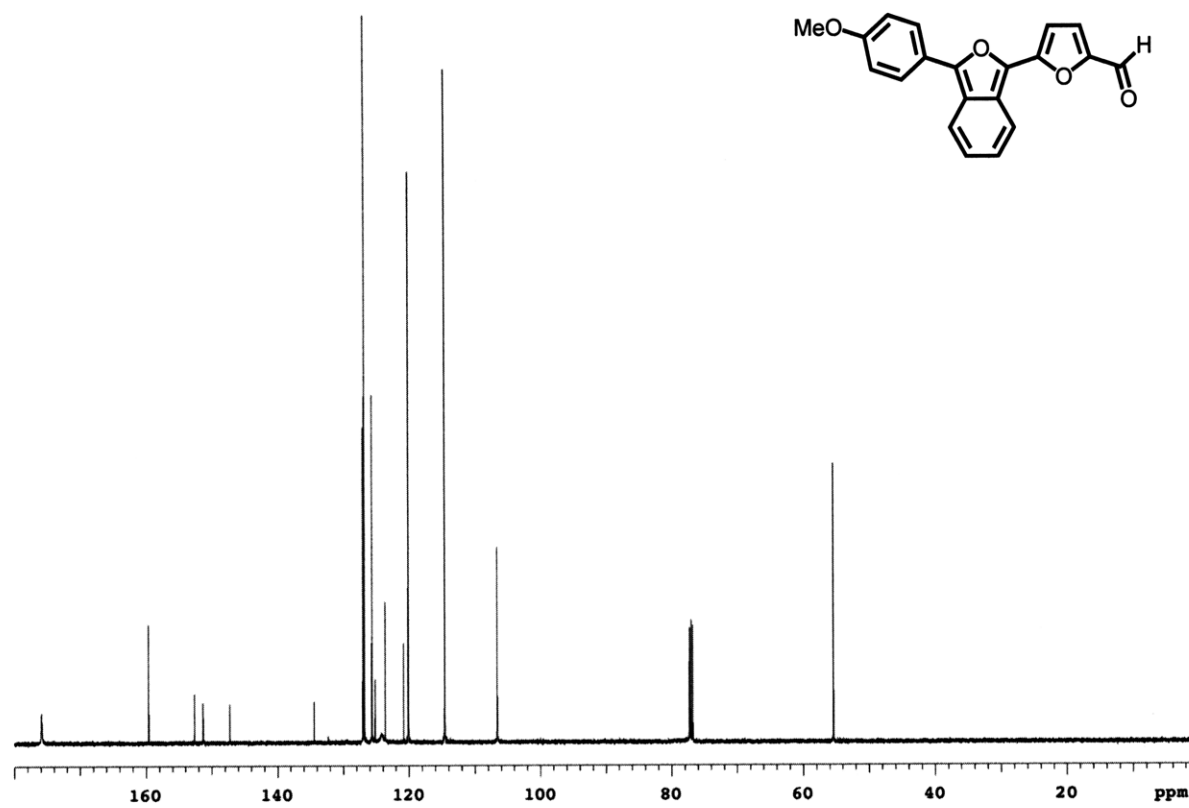
Figure 3.A.12 ^{13C} NMR (125 MHz, CDCl$_3$) of **8b**

189
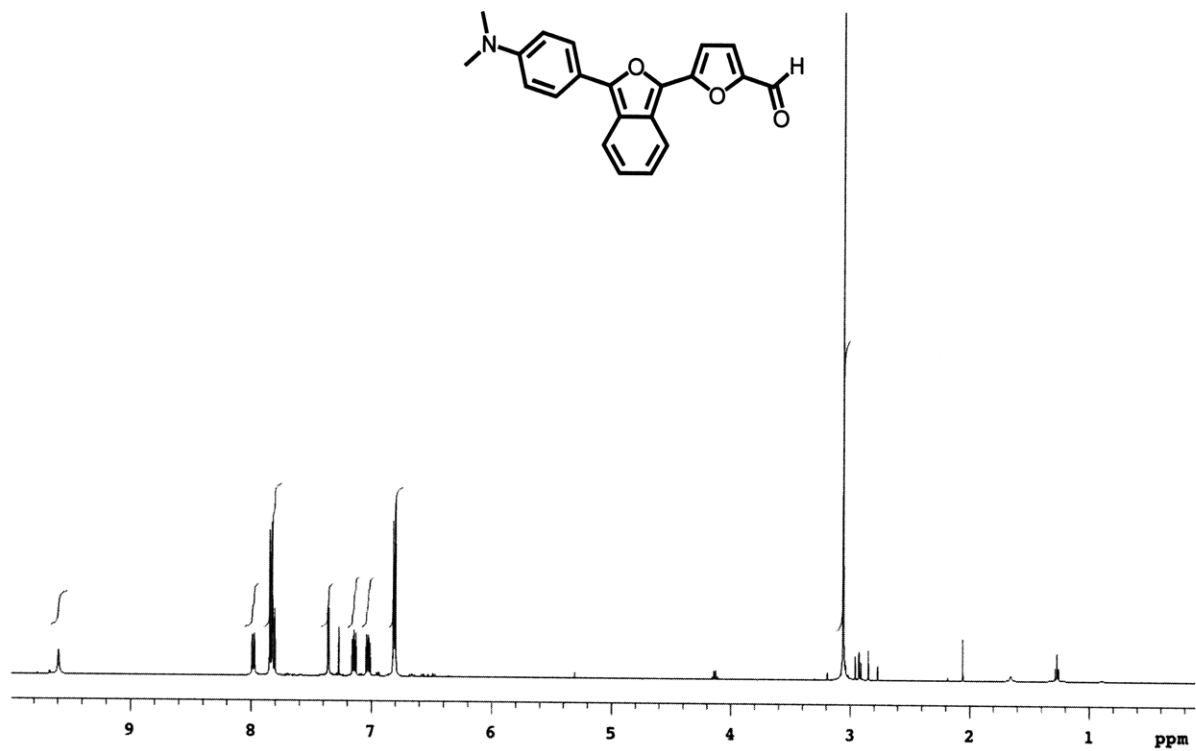
Figure 3.A.13 ^{1}H NMR (500 MHz, CDCl$_3$) of **8c**
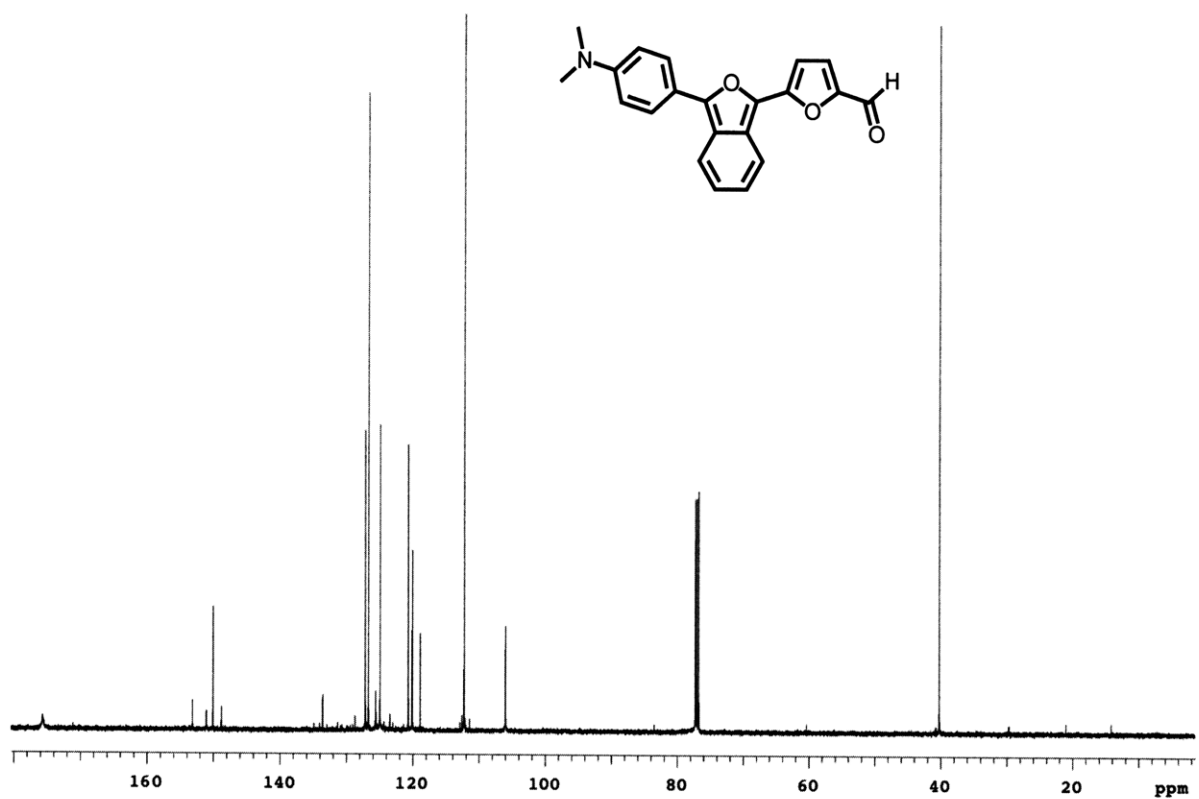
Figure 3.A.14 ^{13C}NMR (125 MHz, CDCl$_3$) of **8c**
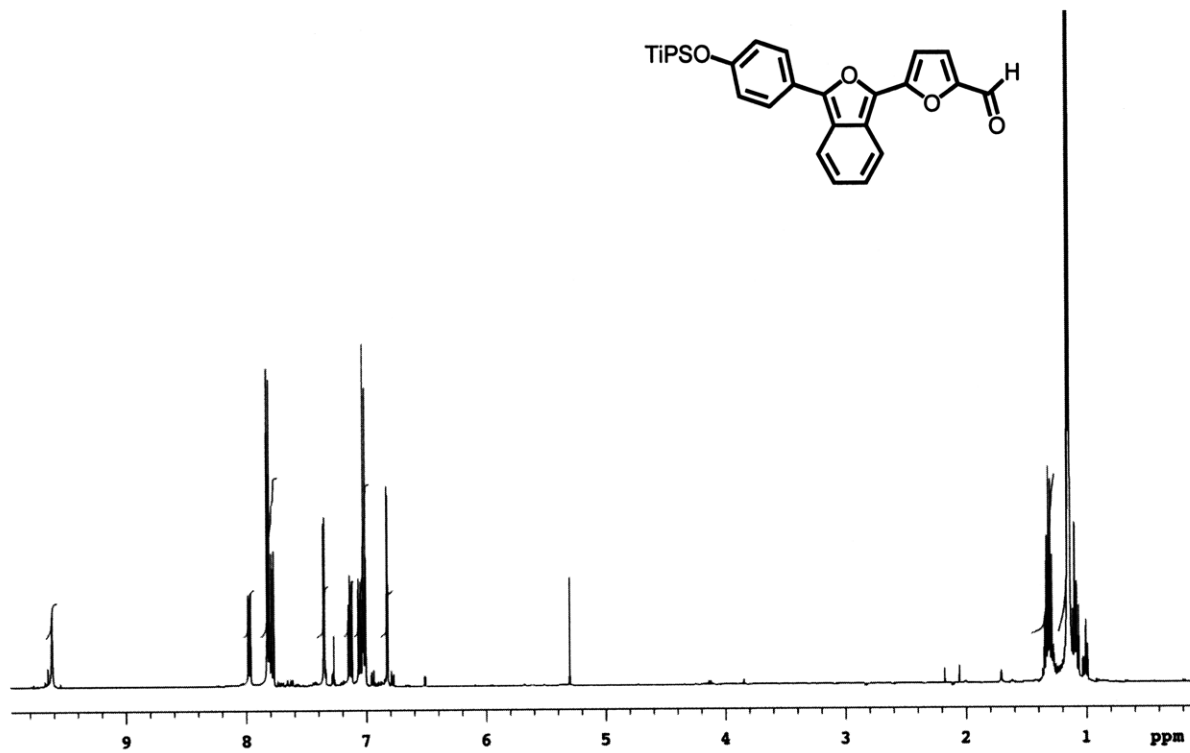
Figure 3.A.15 ^{1}H NMR (500 MHz, CDCl$_3$) of **8d**
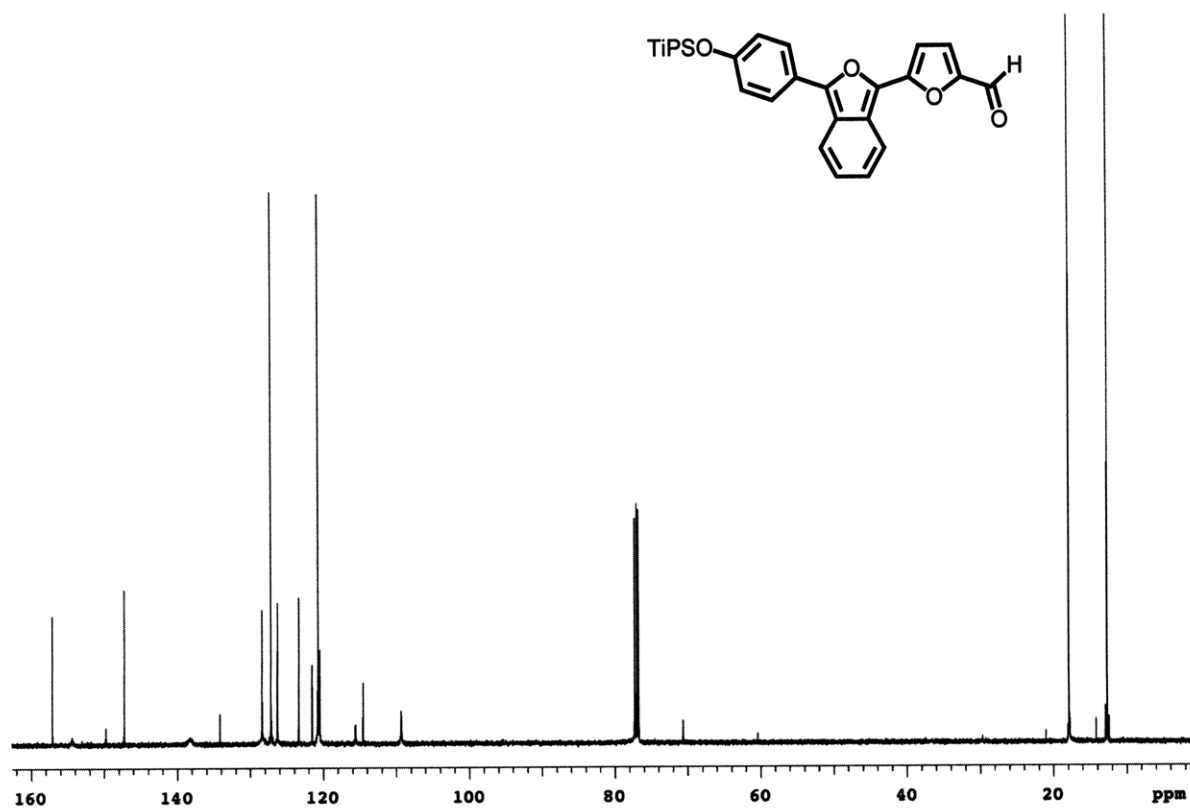
Figure 3.A.16 ^{13C} NMR (125 MHz, CDCl$_3$) of **8d**

191
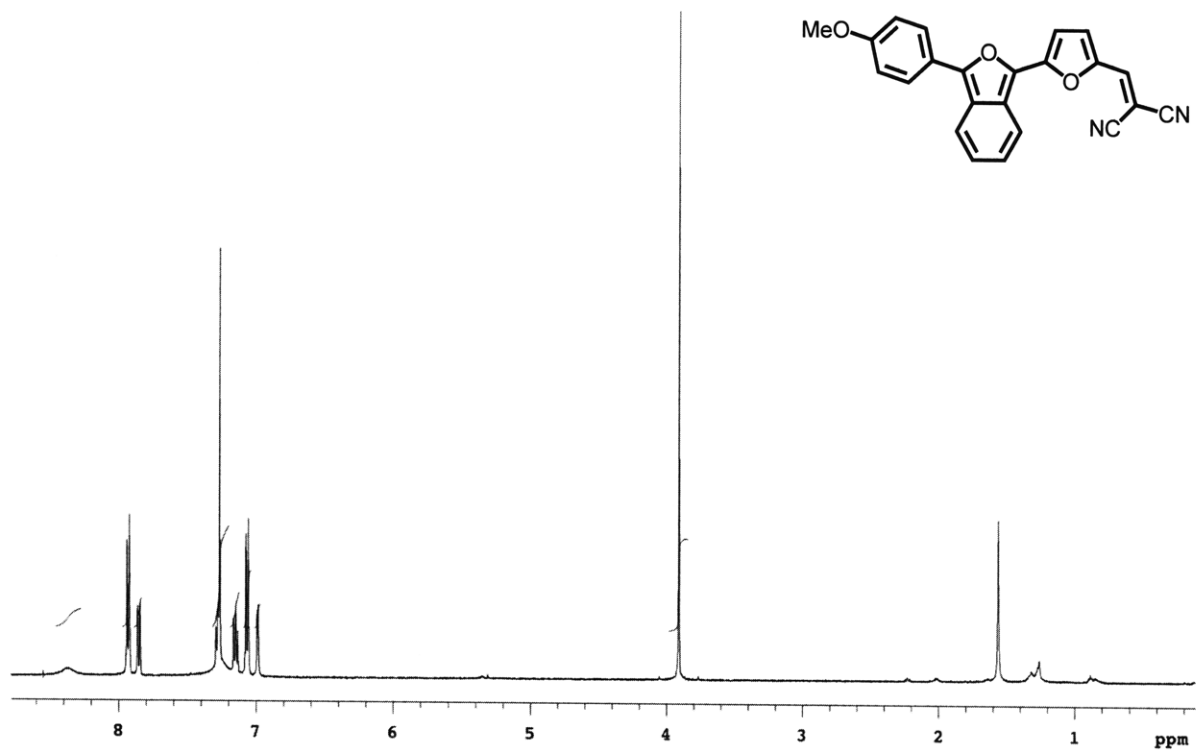
Figure 3.A.17 ^{1}H NMR (500 MHz, CDCl$_3$) of **IBF-NIAD 11**
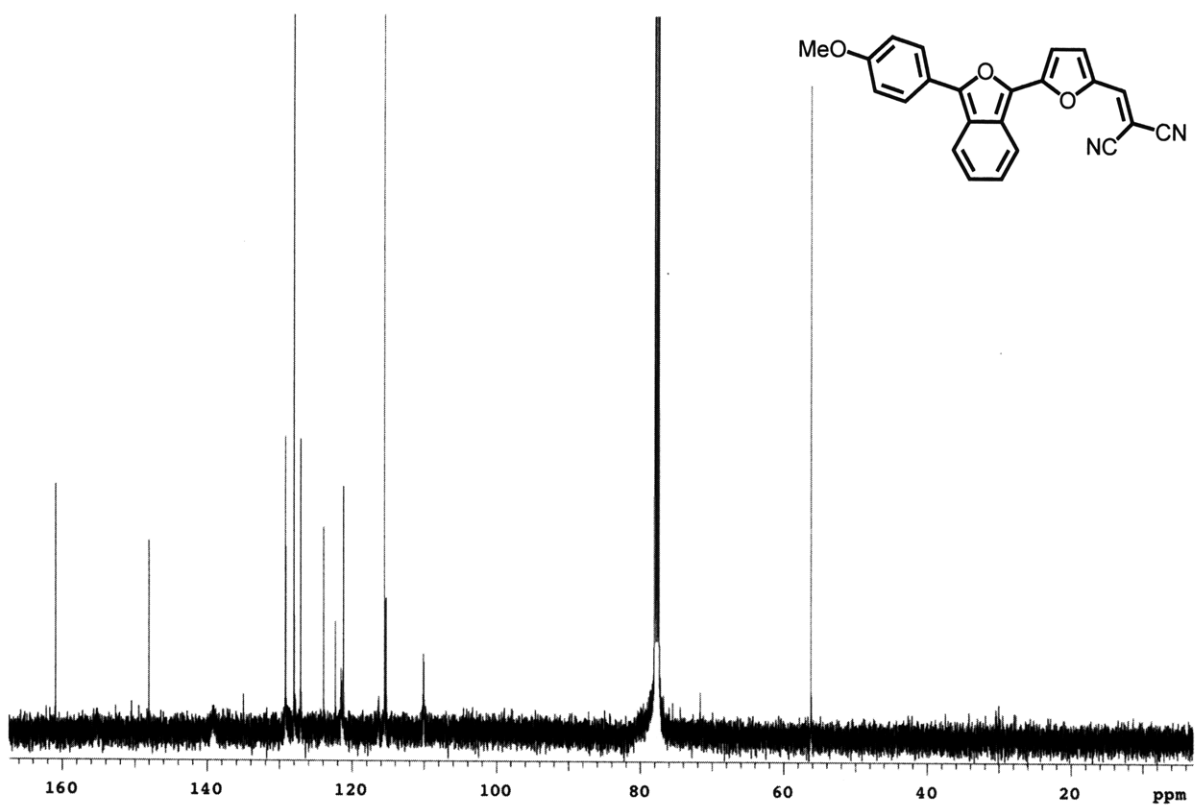
Figure 3.A.18 [13C] NMR (125 MHz, CDCl$_3$) of **IBD-NIAD 11**
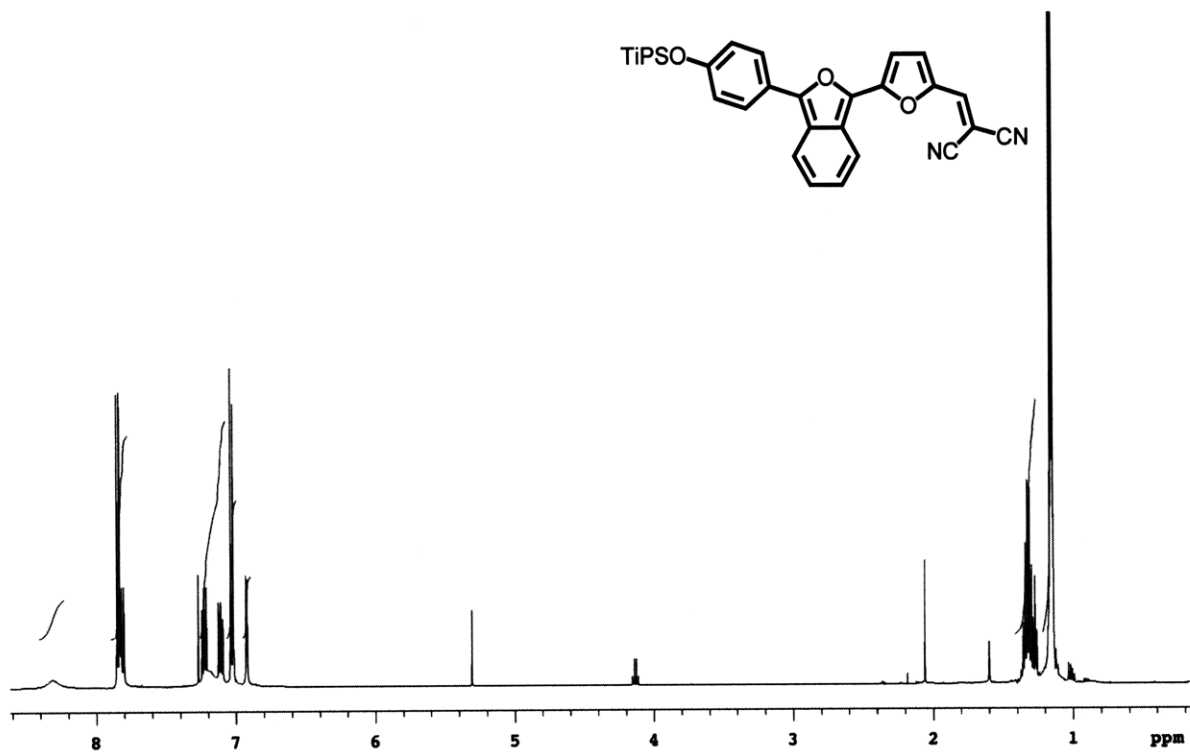
Figure 3.A.19 ^{1}H NMR (500 MHz, CDCl$_3$) of **IBF-NIAD 9d**
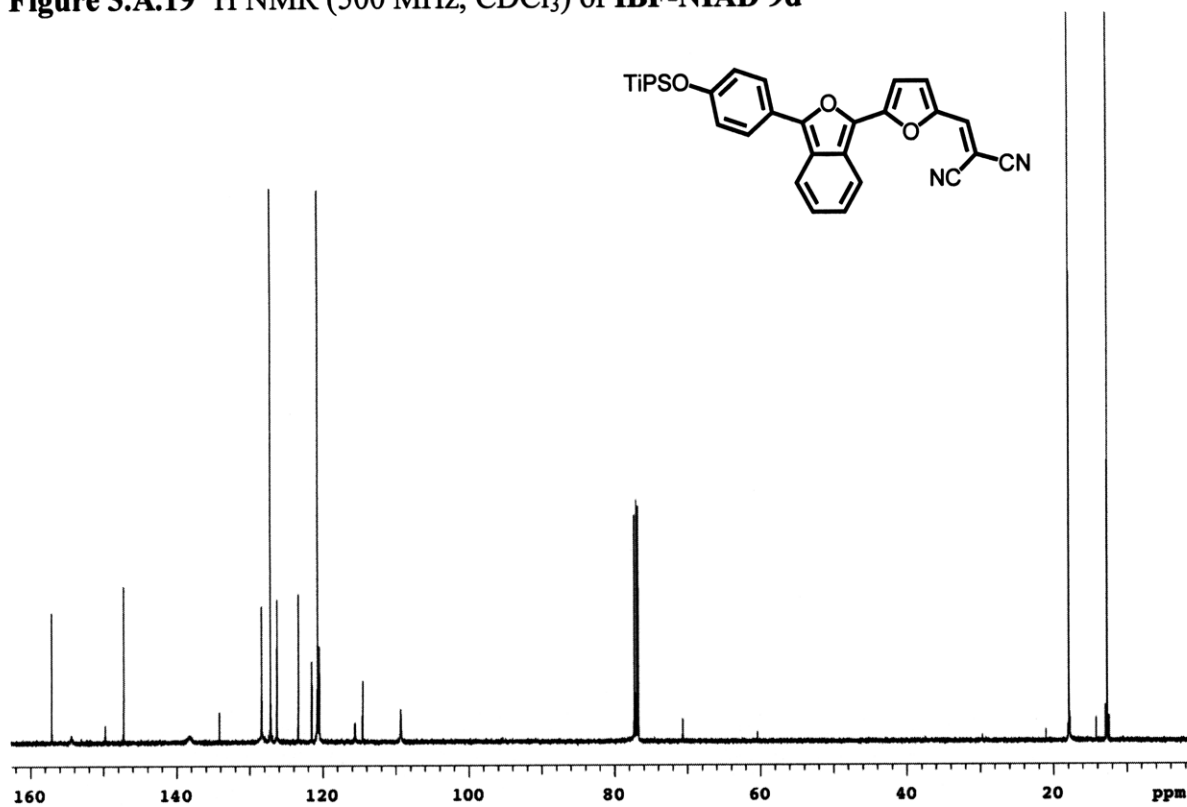
Figure 3.A.20 ^{13}C NMR (125 MHz, CDCl$_3$) of **IBD-NIAD 9d**
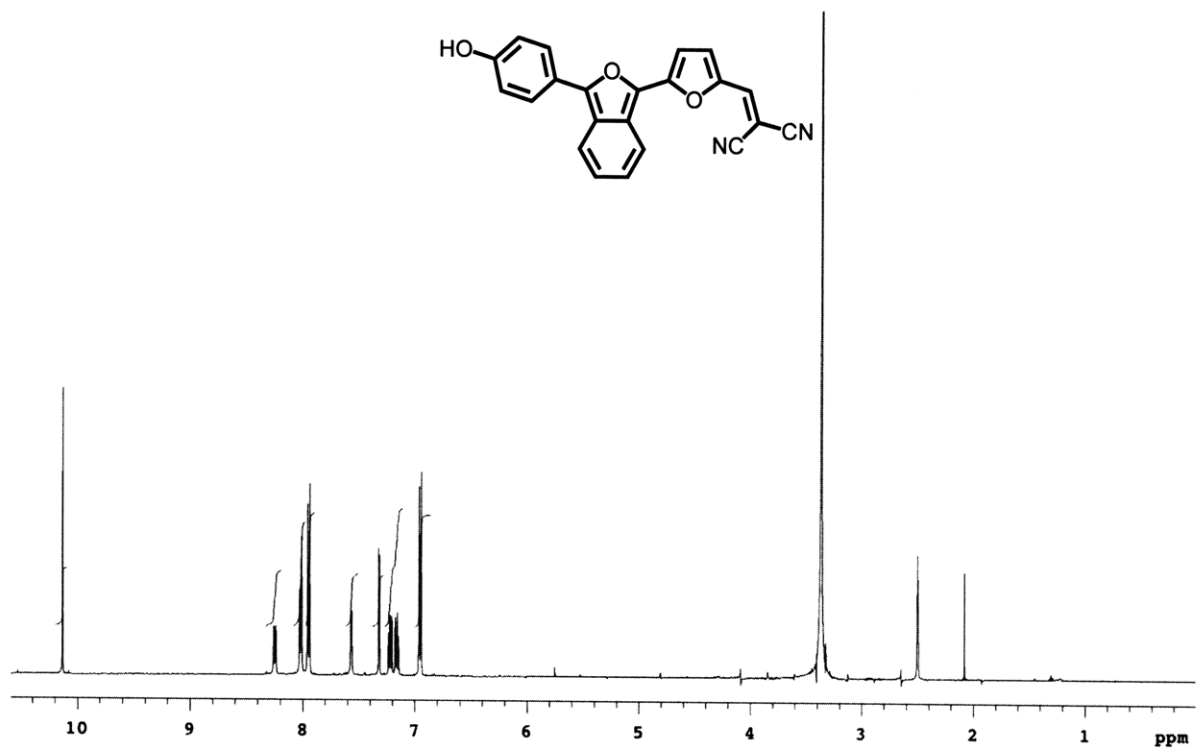
Figure 3.A.21 ^{1}H NMR (500 MHz, CDCl$_3$) of **IBF-NIAD 12**
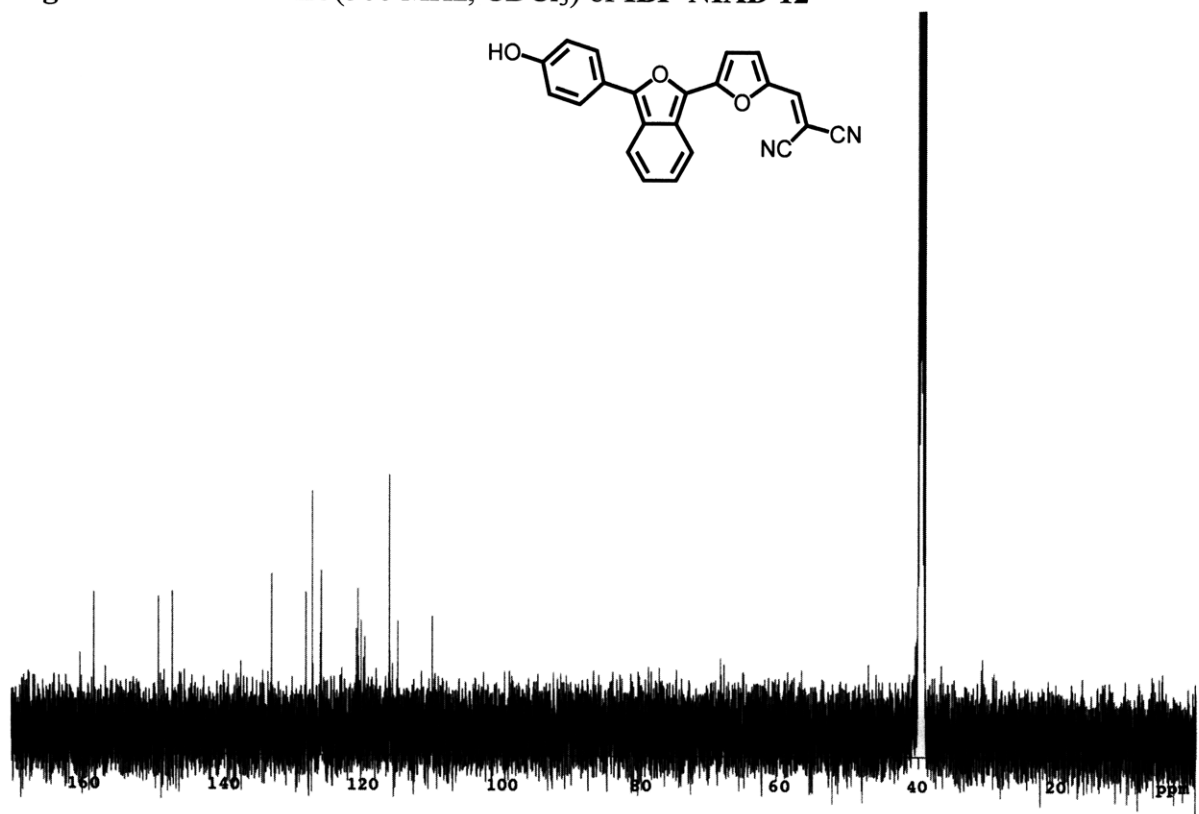
Figure 3.A.22 ^{13C} NMR (125 MHz, CDCl$_3$) of **IBD-NIAD 12**

194
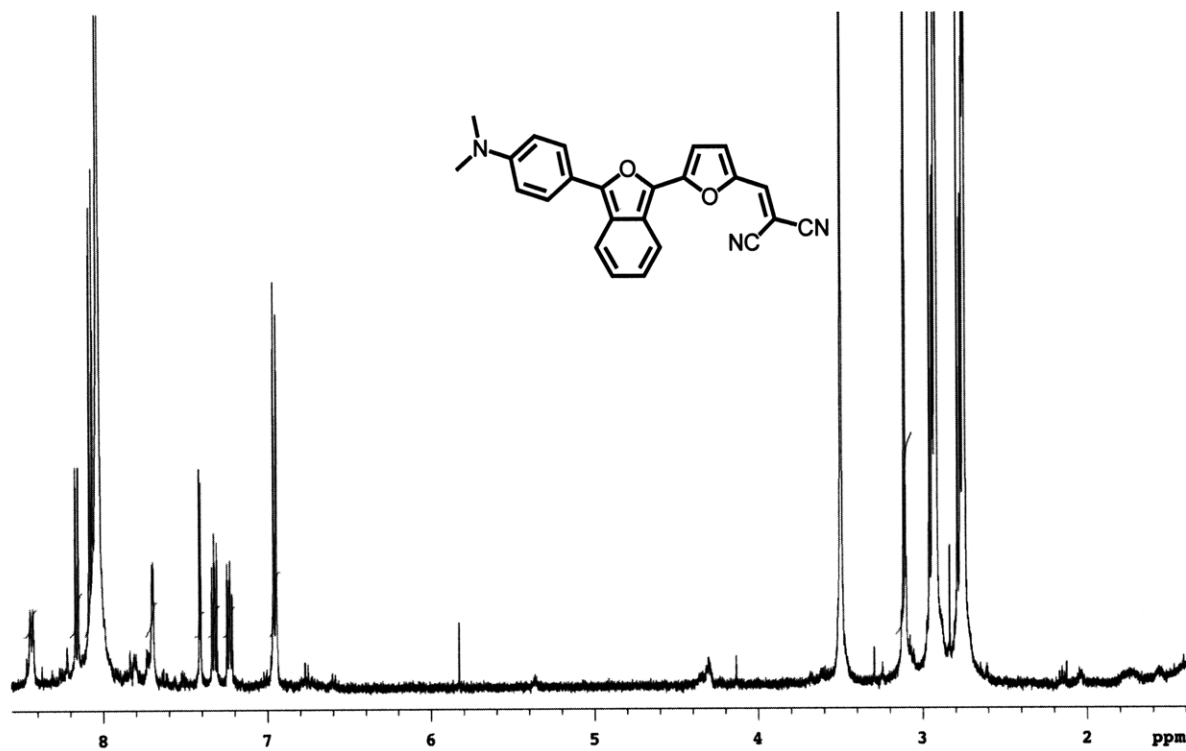
Figure 3.A.23 ^{1}H NMR (500 MHz, DMF-d$_{7}$) of **IBF-NIAD 13**
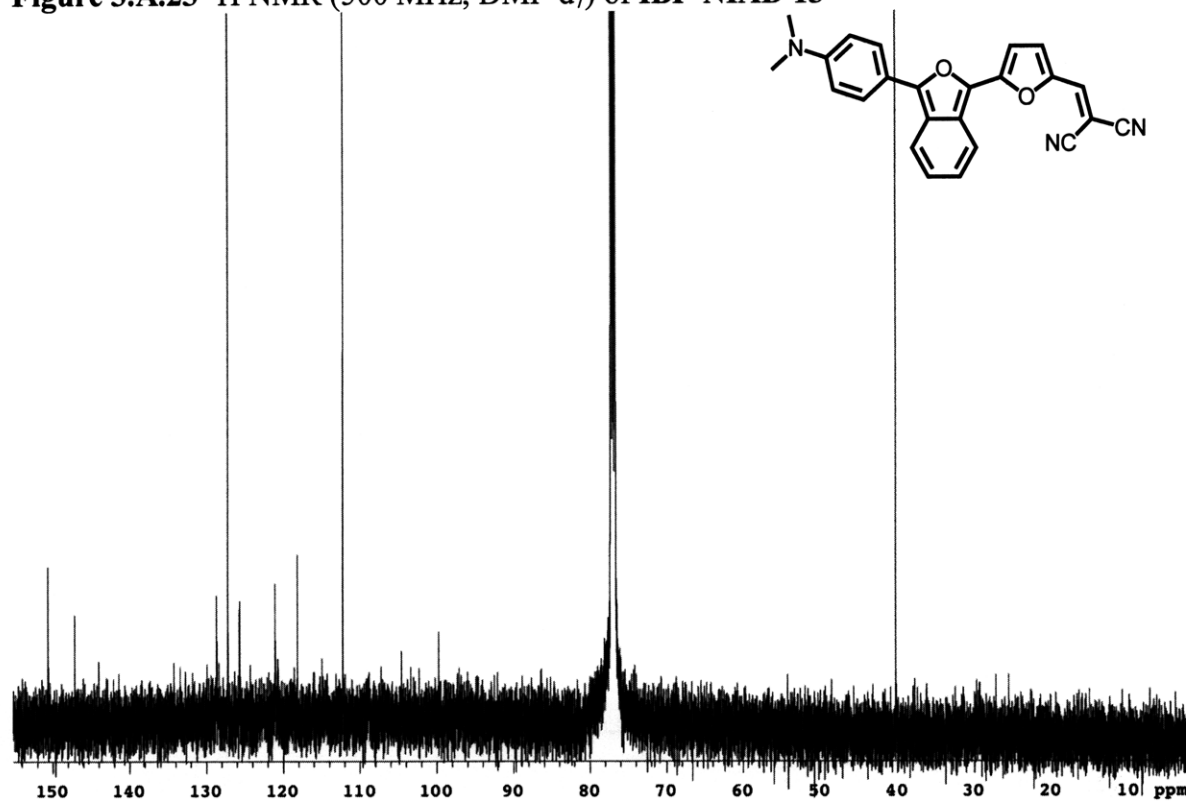
Figure 3.A.24 ^{13}C NMR (125 MHz, CDCl$_{3}$) of **IBD-NIAD 13**
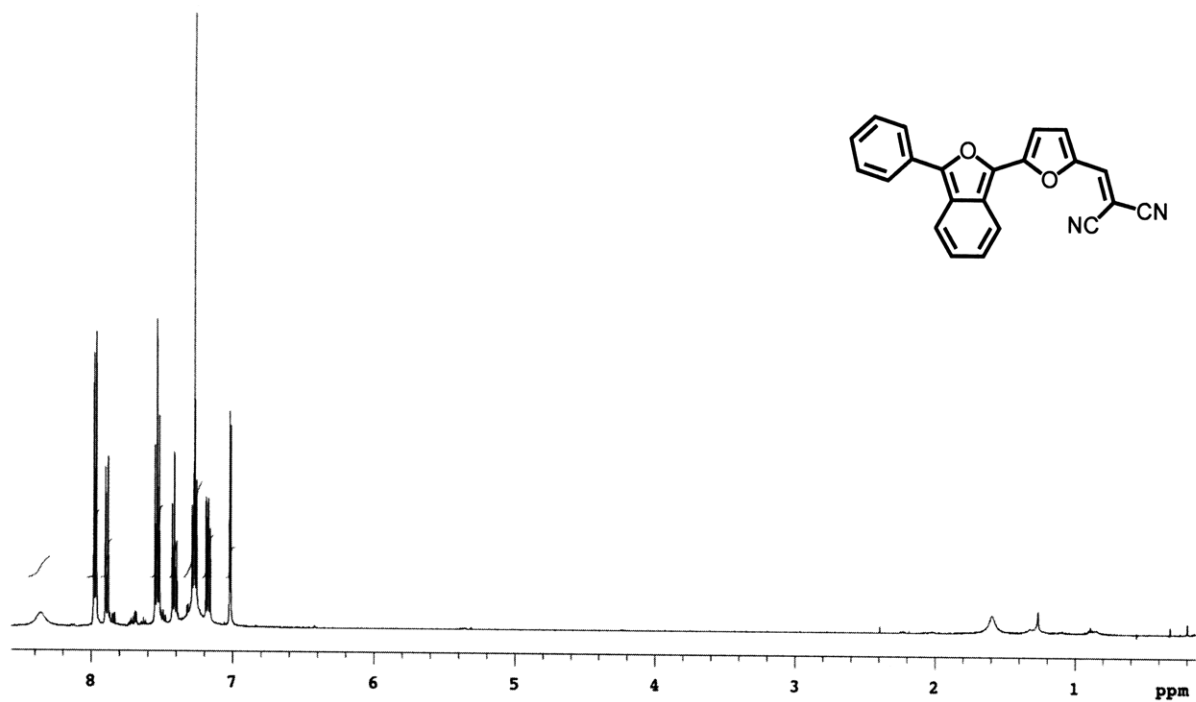
Figure 3.A.25 ^{1}H NMR (500 MHz, CDCl$_3$) of **IBF-NIAD 14**
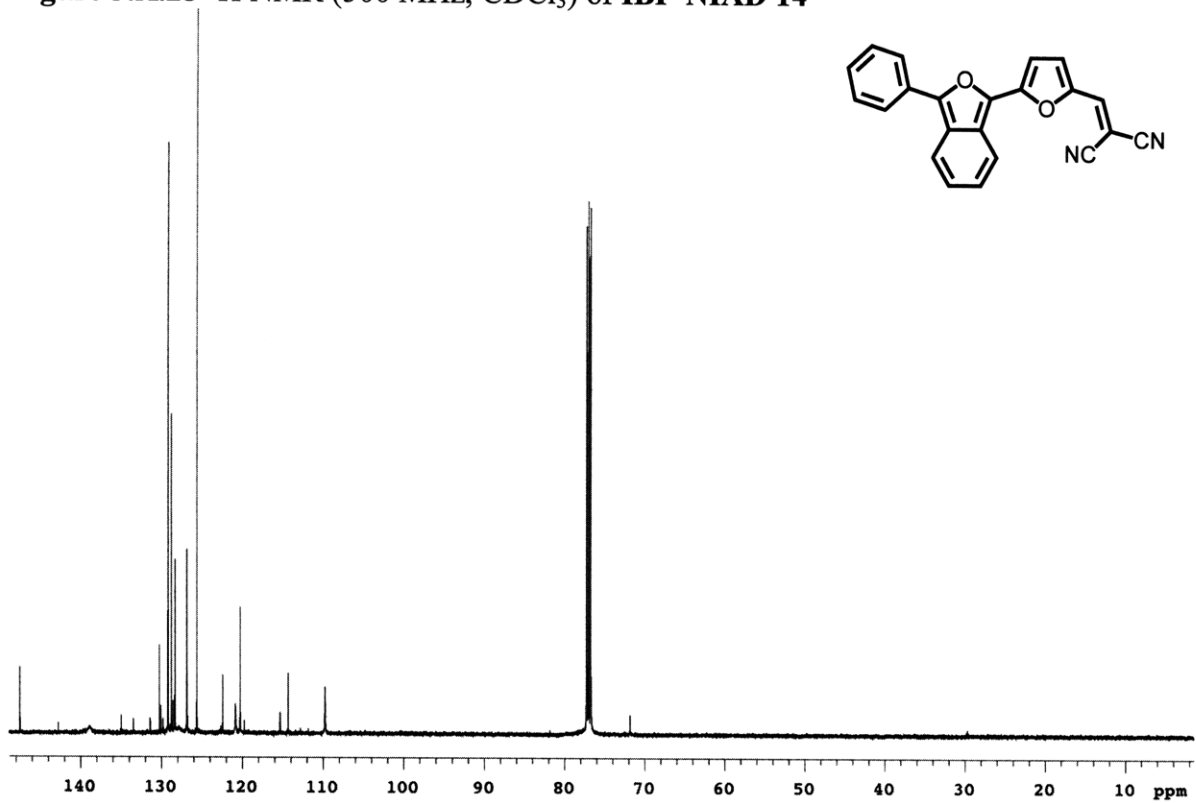
Figure 3.A.26 ^{13C}NMR (125 MHz, CDCl$_3$) of **IBD-NIAD 14**
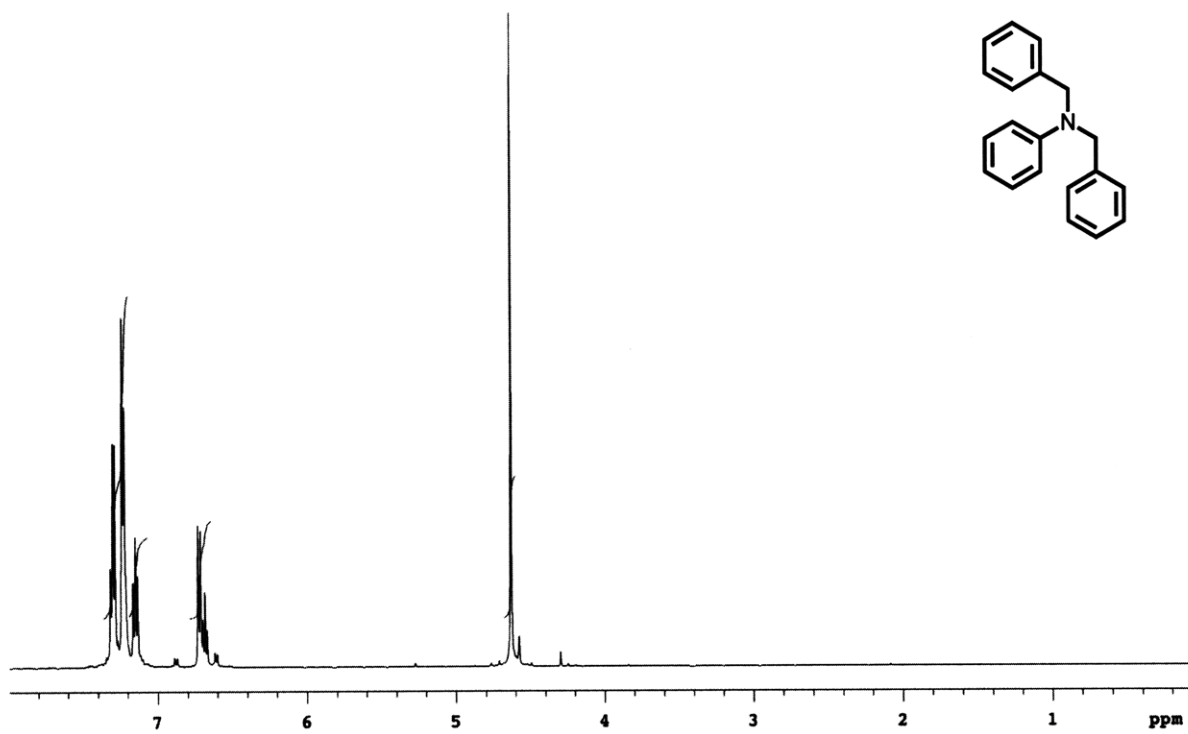
Figure 3.A.27 ^{1}H NMR (500 MHz, CDCl$_3$) of **11**
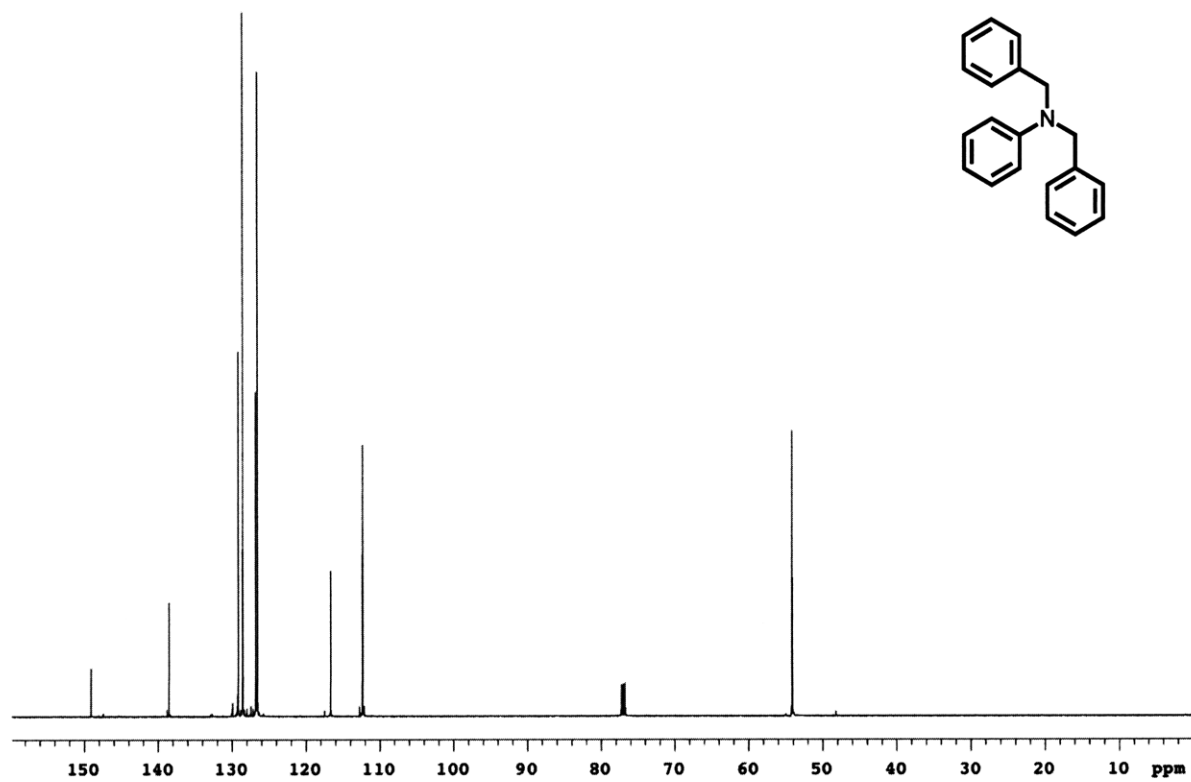
Figure 3.A.28 ^{13}C NMR (125 MHz, CDCl$_3$) of **11**
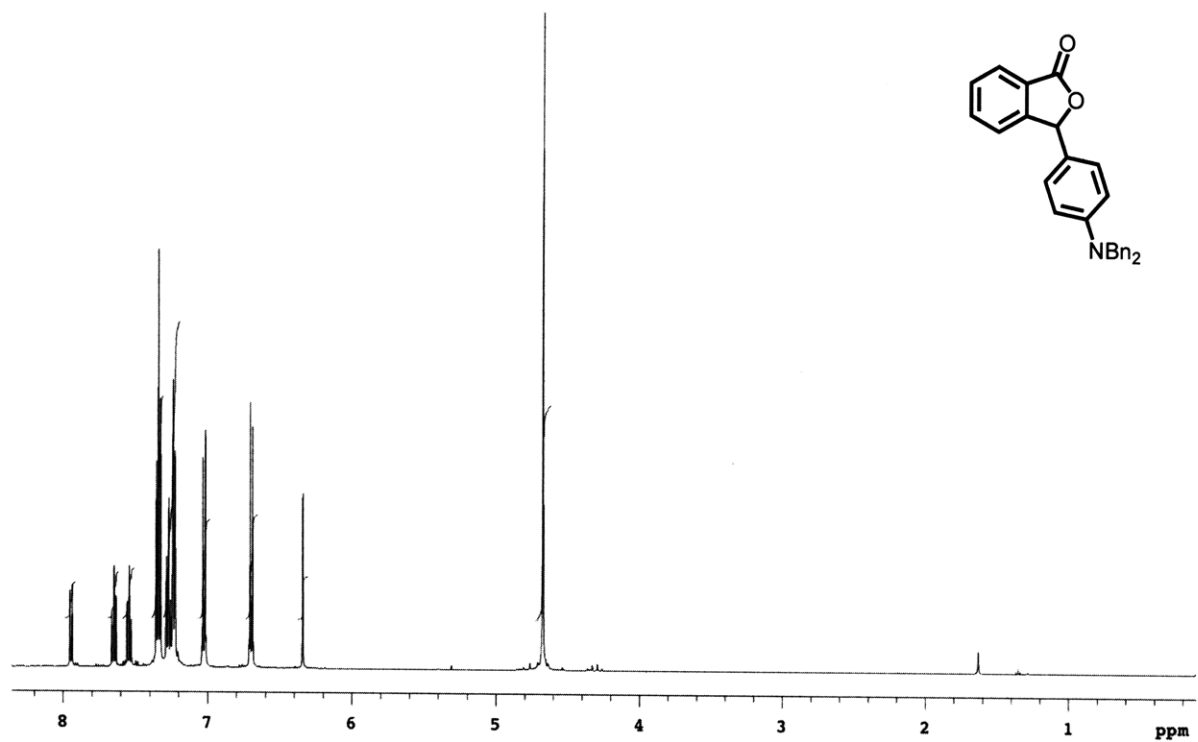
Figure 3.A.29 ^{1}H NMR (500 MHz, CDCl$_3$) of **13**
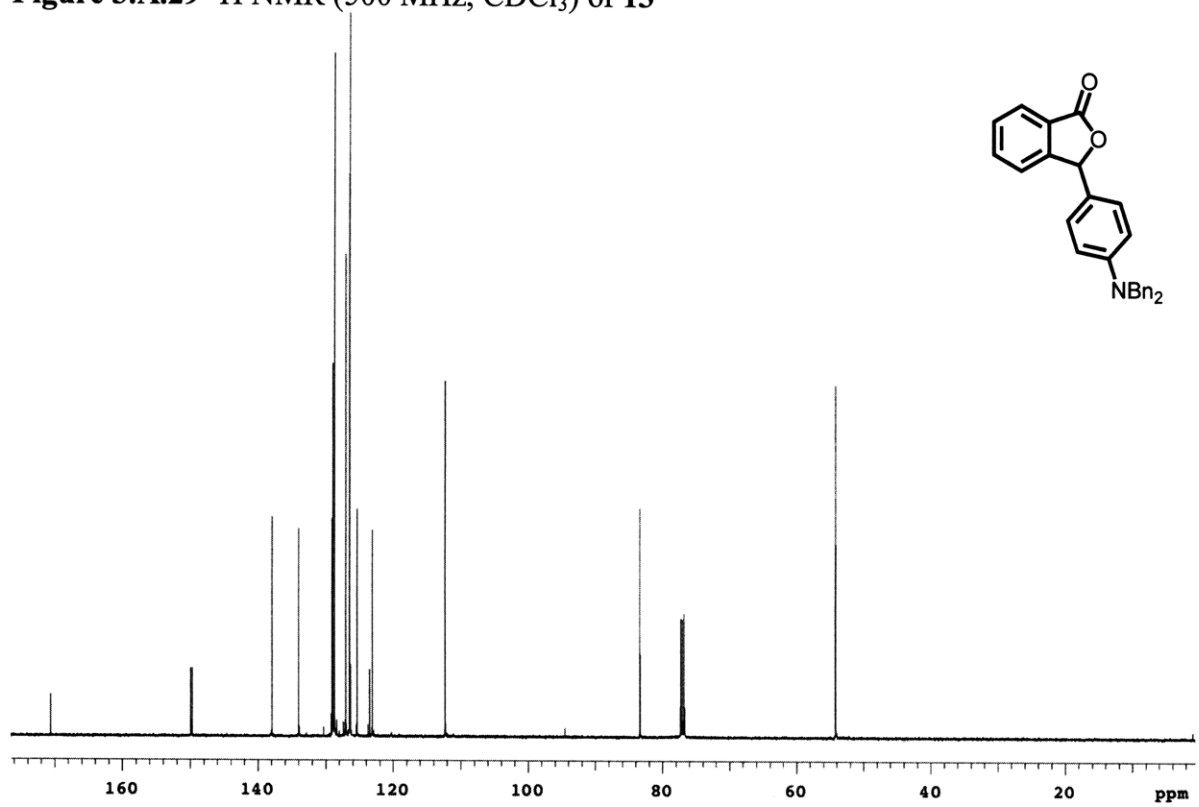
Figure 3.A.30 ^{13}C NMR (125 MHz, CDCl$_3$) of **13**

198
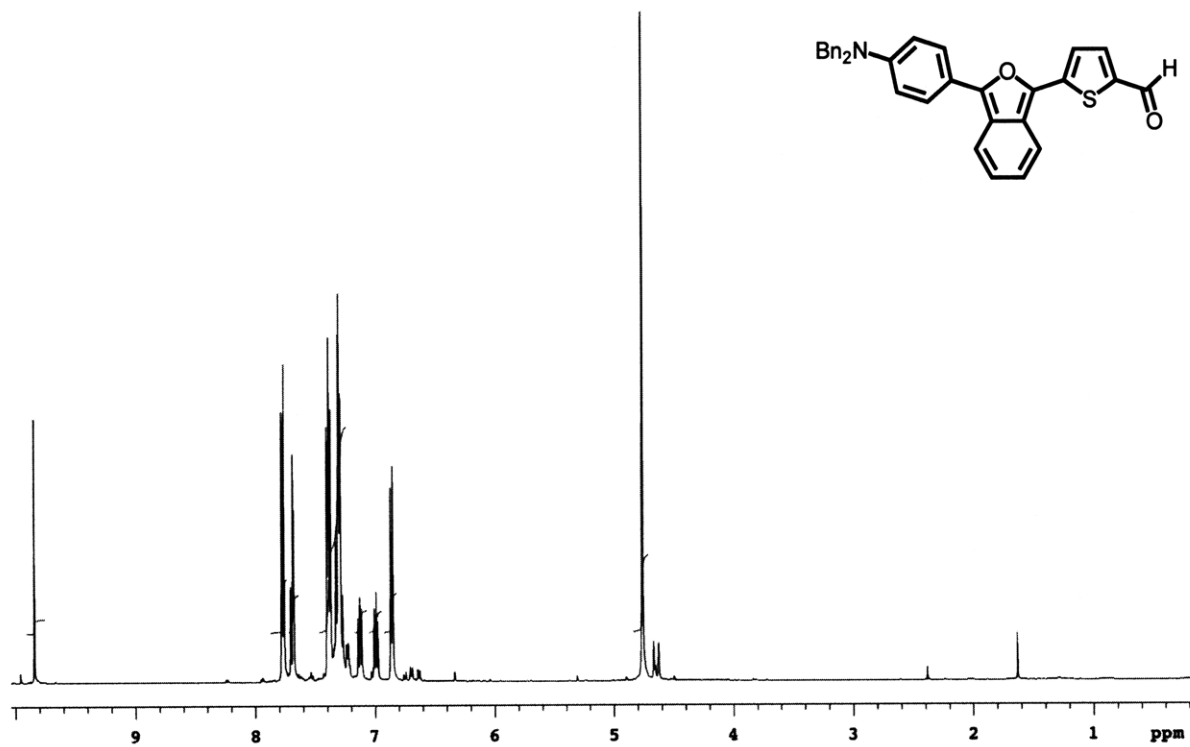
Figure 3.A.31 ^{1}H NMR (500 MHz, CDCl$_3$) of **15**
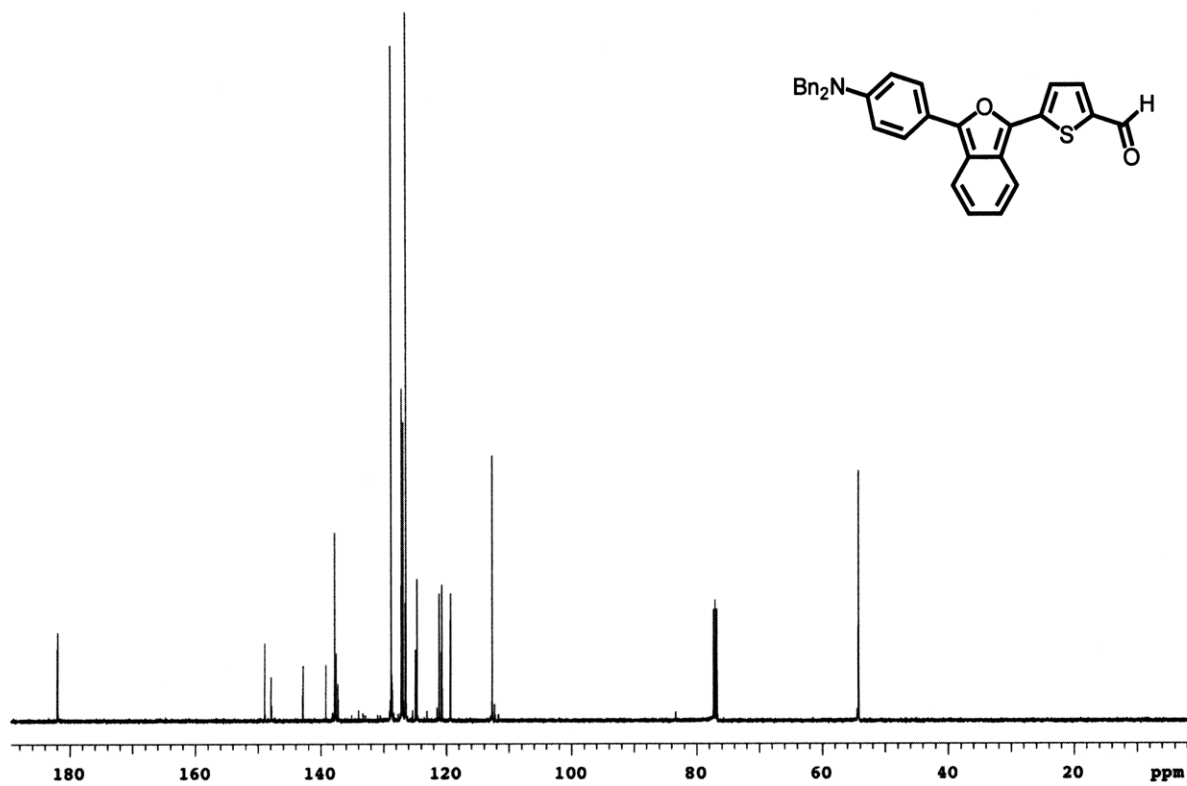
Figure 3.A.32 ^{13}C NMR (125 MHz, CDCl$_3$) of **15**
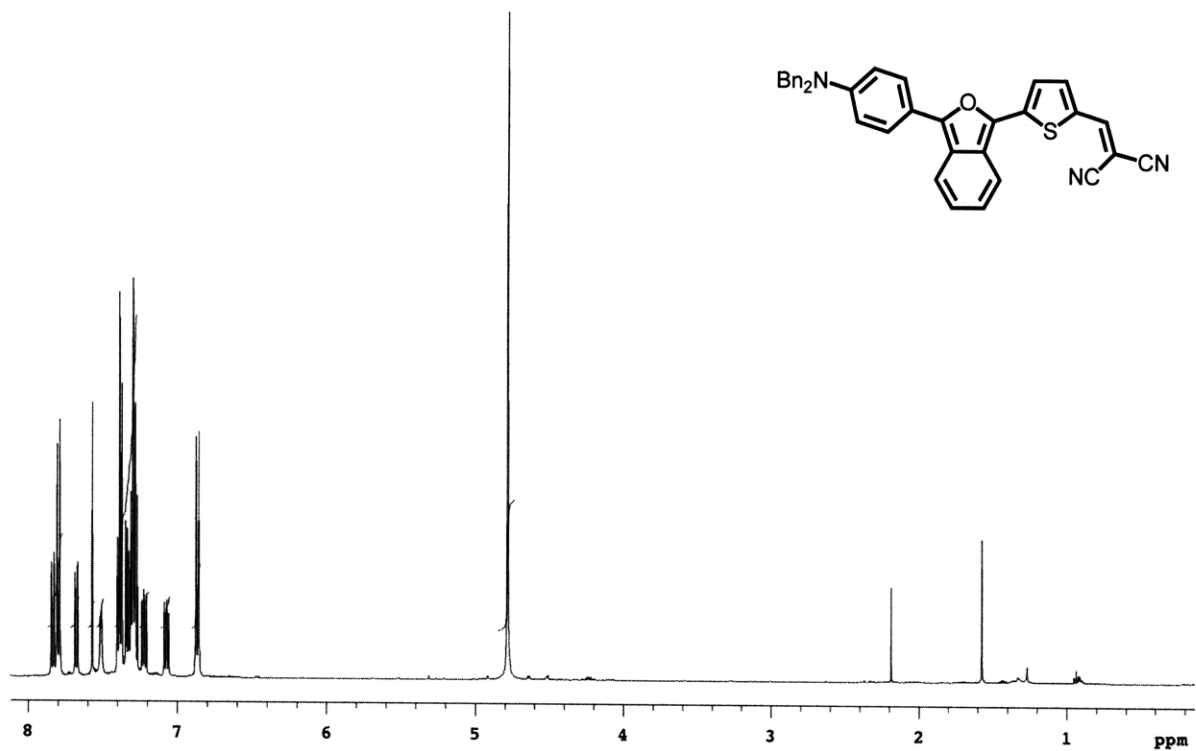
Figure 3.A.33 ^{1}H NMR (500 MHz, CDCl$_3$) of **16**
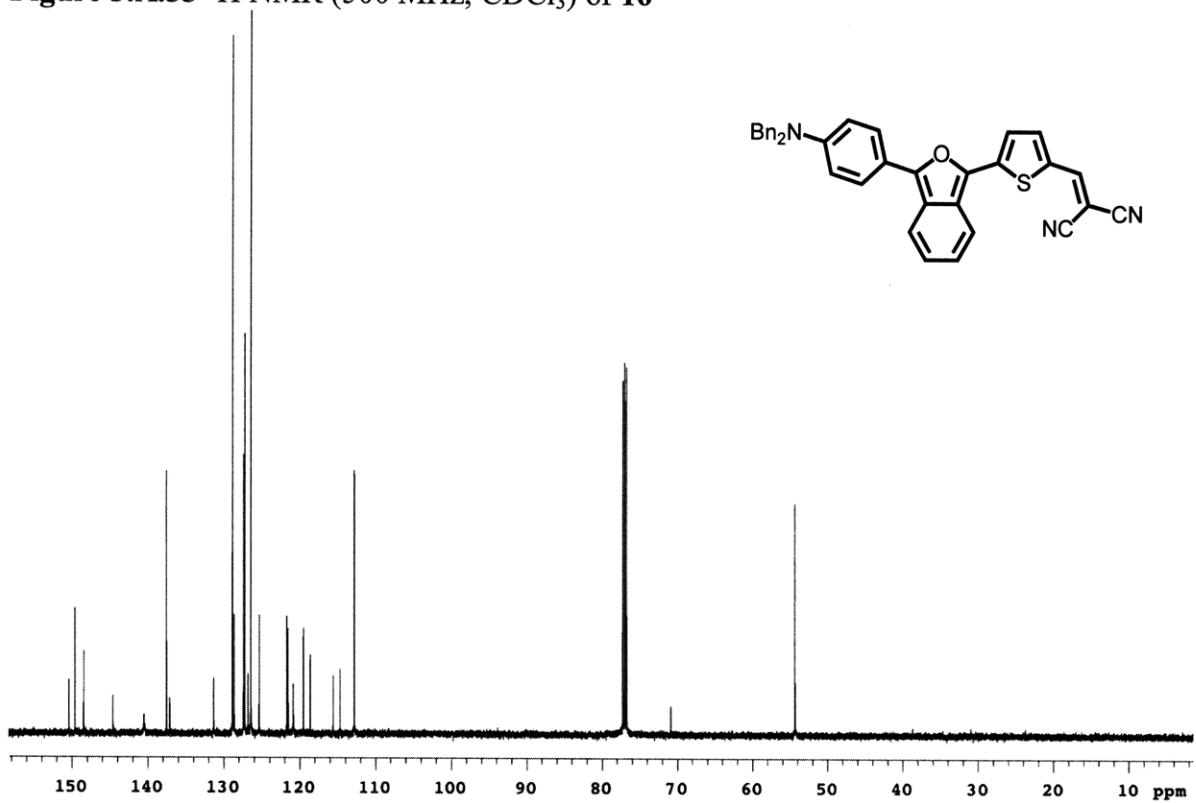
Figure 3.A.34 ^{13}C NMR (125 MHz, CDCl$_3$) of **16**
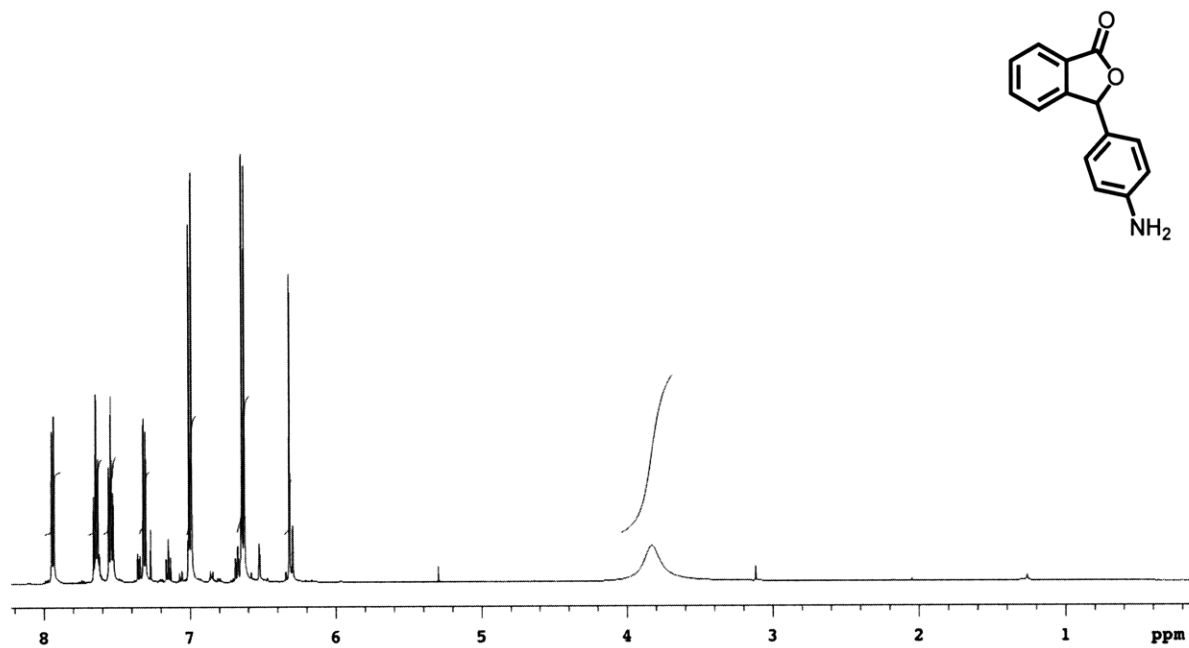
Figure 3.A.35 ^{1}H NMR (500 MHz, CDCl$_3$) of **18**
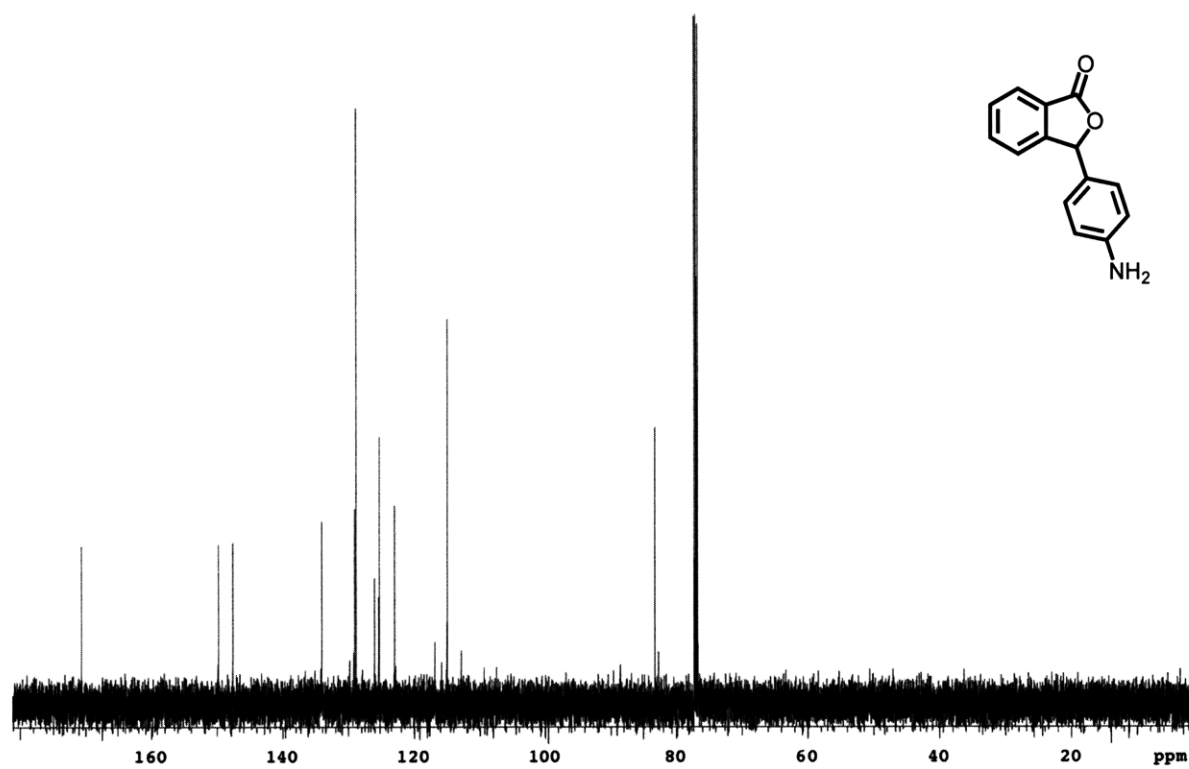
Figure 3.A.36 ^{13}C NMR (125 MHz, CDCl$_3$) of **18**
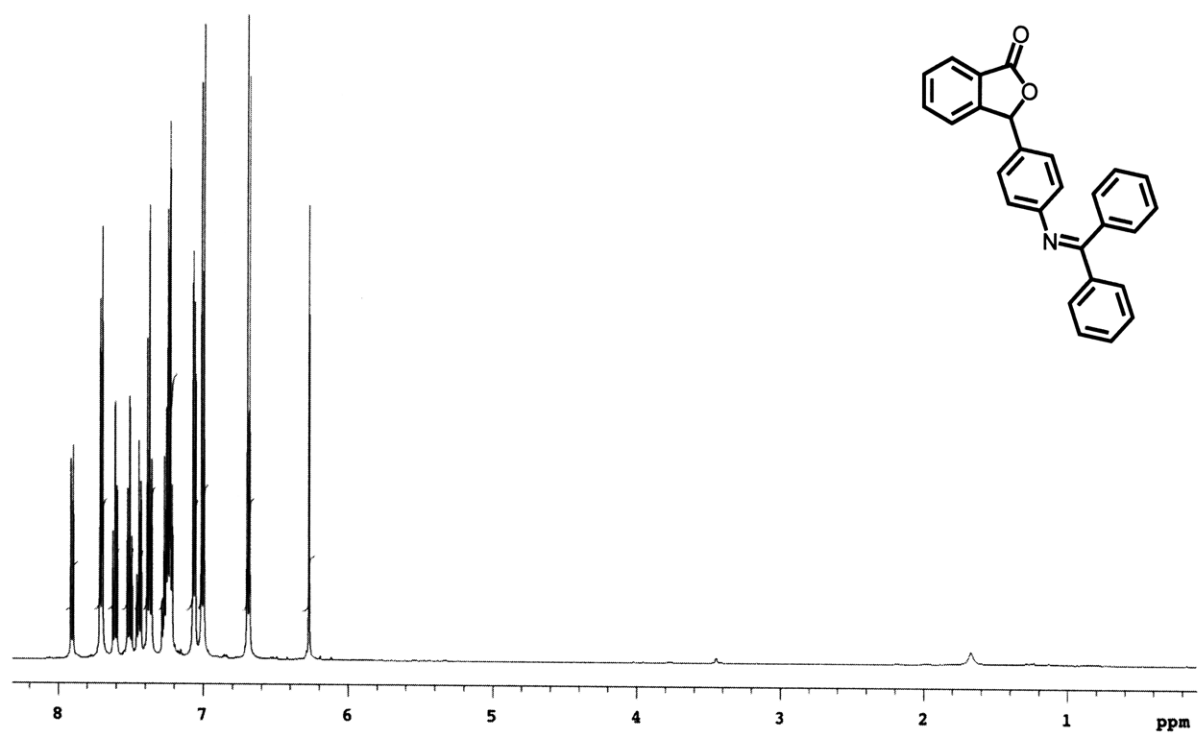
Figure 3.A.37 ^{1}H NMR (500 MHz, CDCl$_3$) of **19**
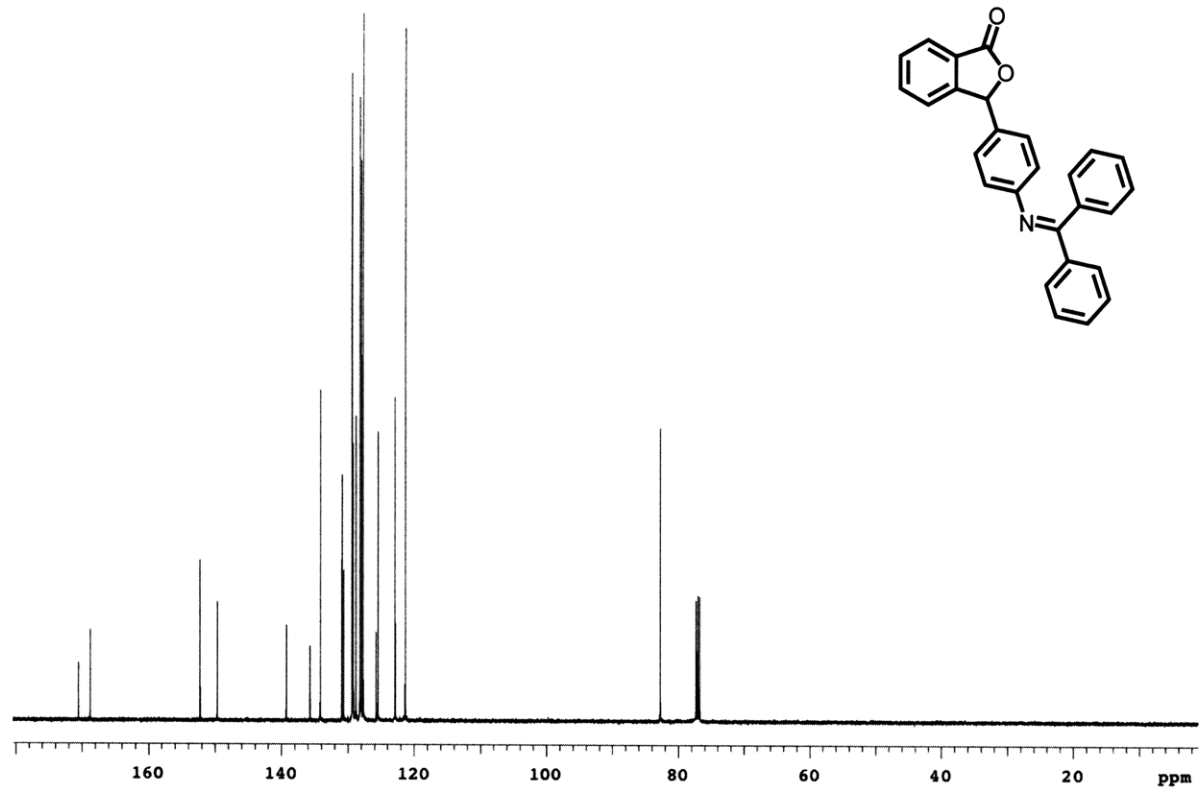
Figure 3.A.38 ^{13}C NMR (125 MHz, CDCl$_3$) of **19**
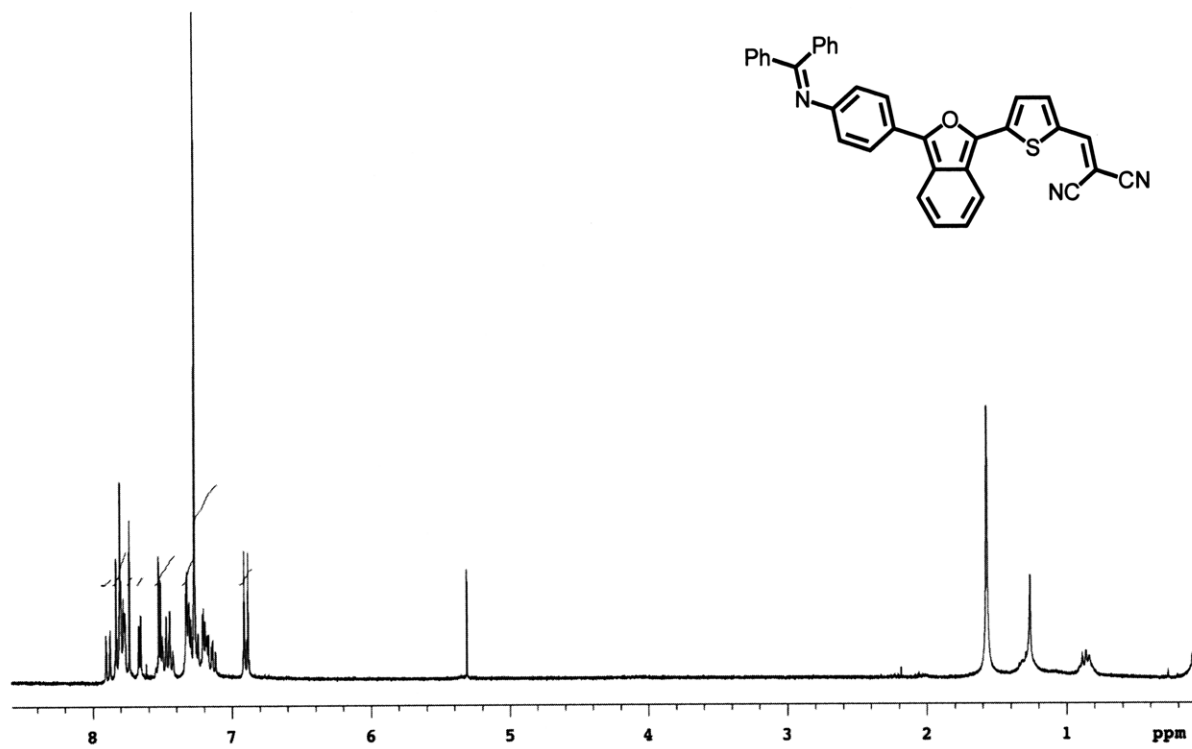
Figure 3.A.39 ^{1}H NMR (300 MHz, CDCl$_3$) of **20a**
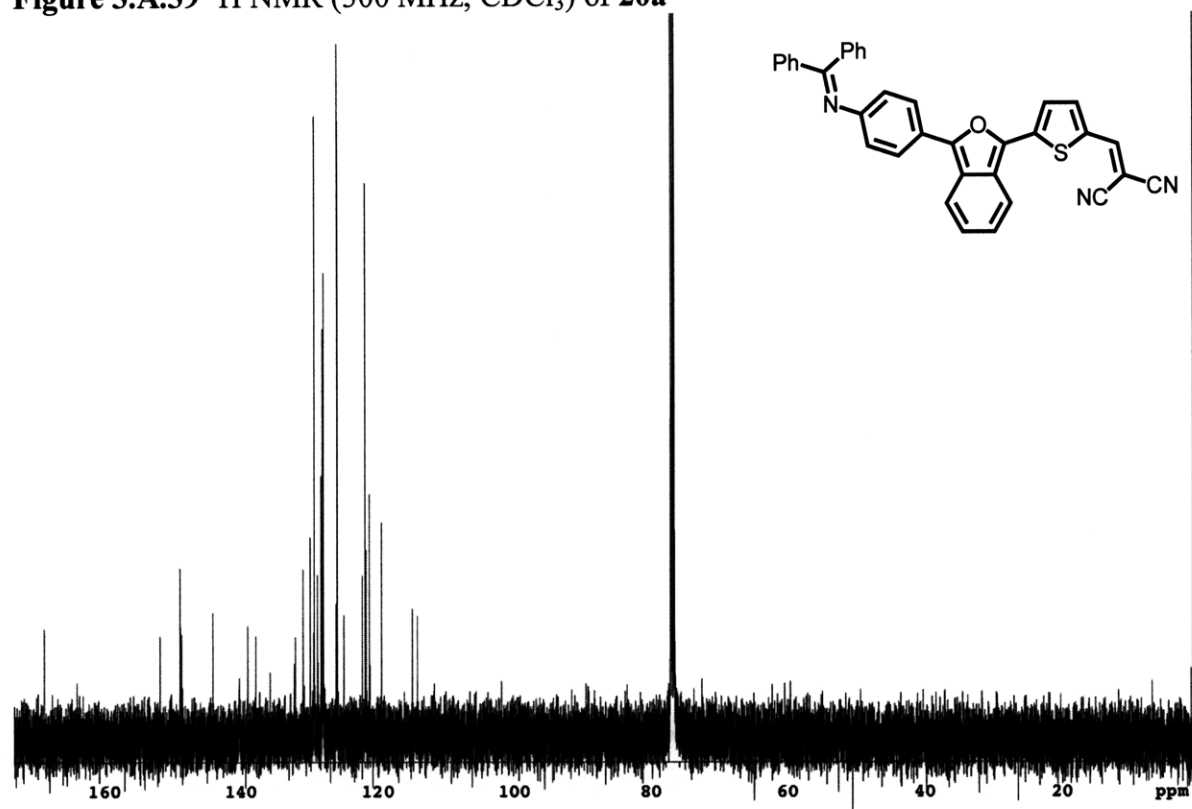
Figure 3.A.40 ^{13}C NMR (125 MHz, CDCl$_3$) of **20a**
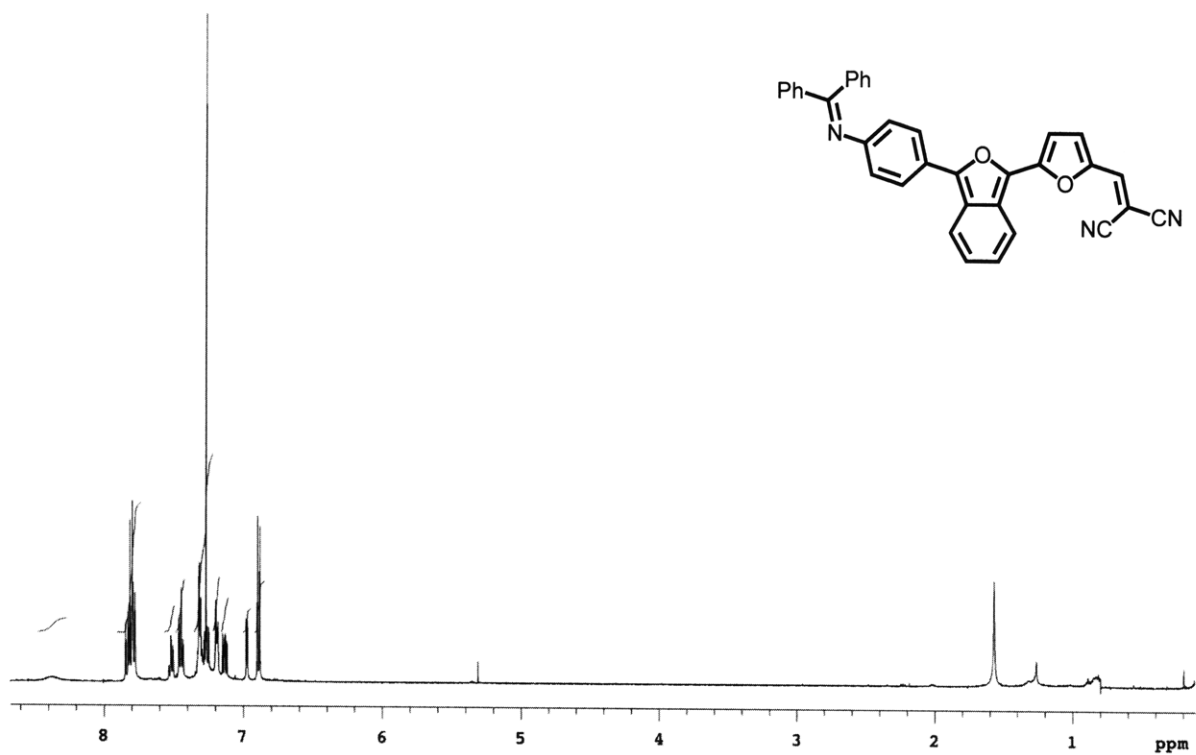
Figure 3.A.41 ^{1}H NMR (500 MHz, CDCl$_3$) of **20b**
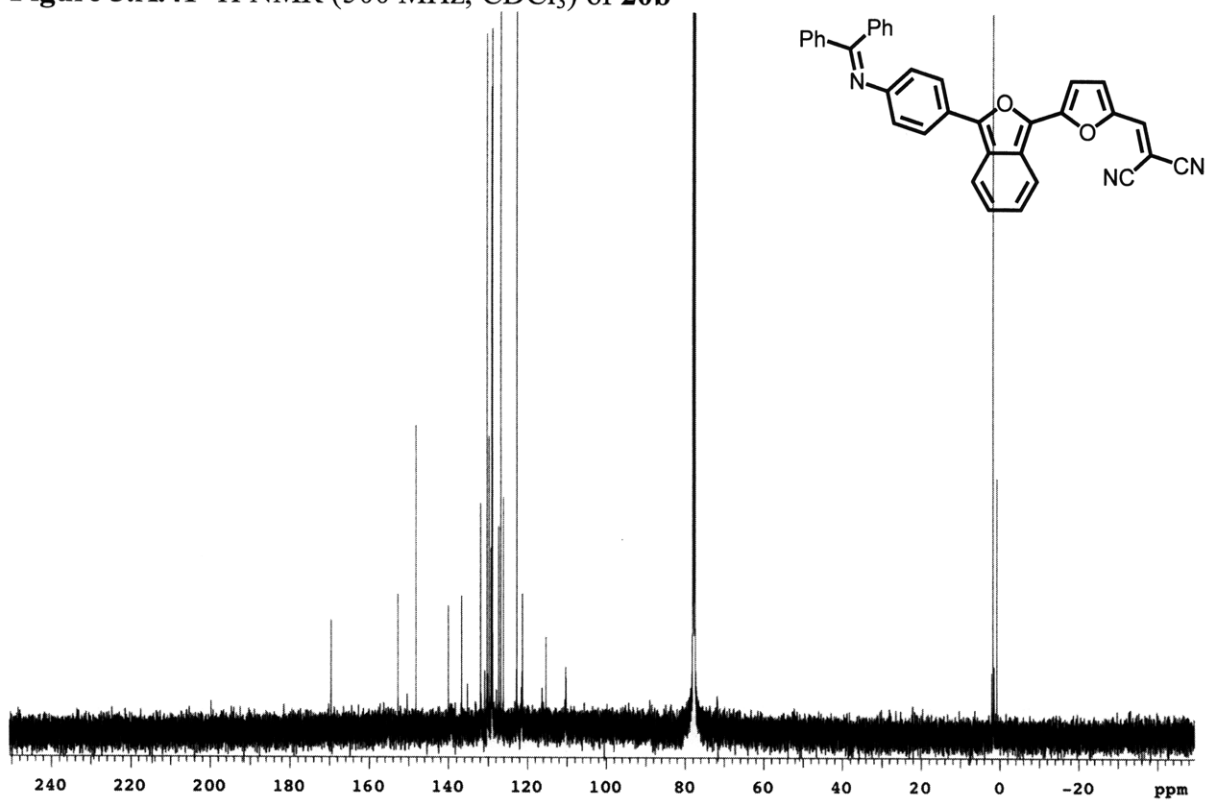
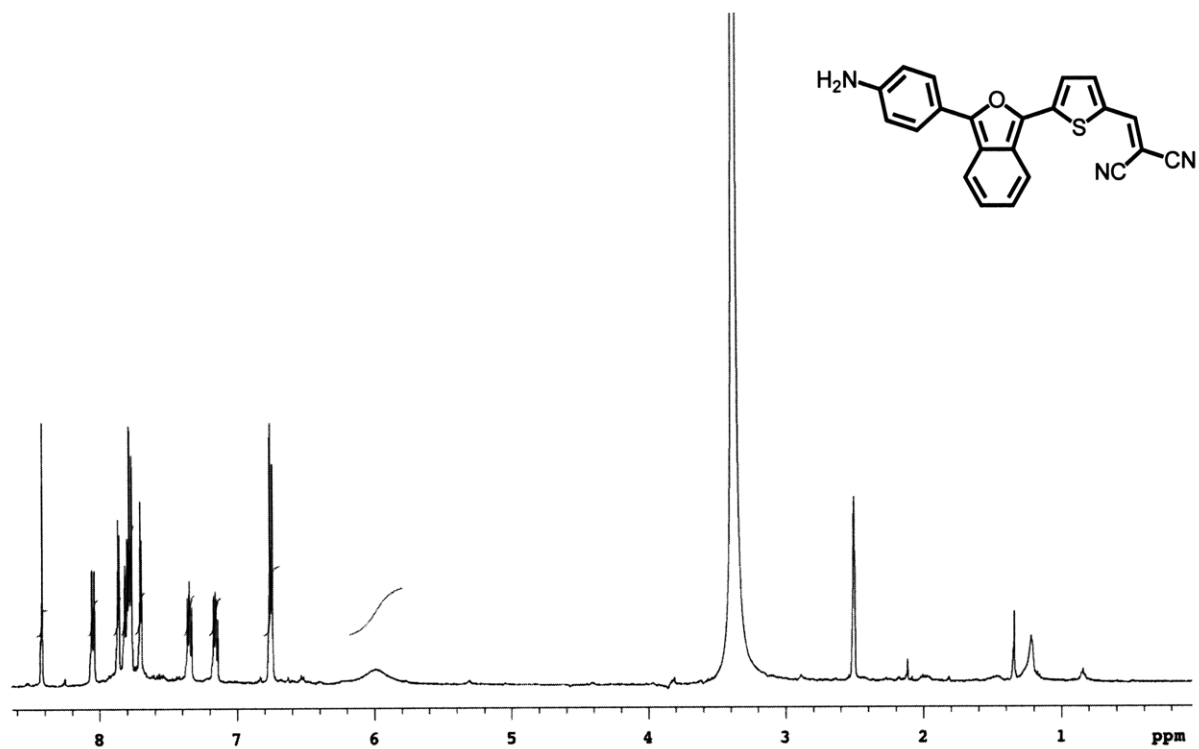**Figure 3.A.42** ^{13}C NMR (125 MHz, CDCl$_3$) of **20b**

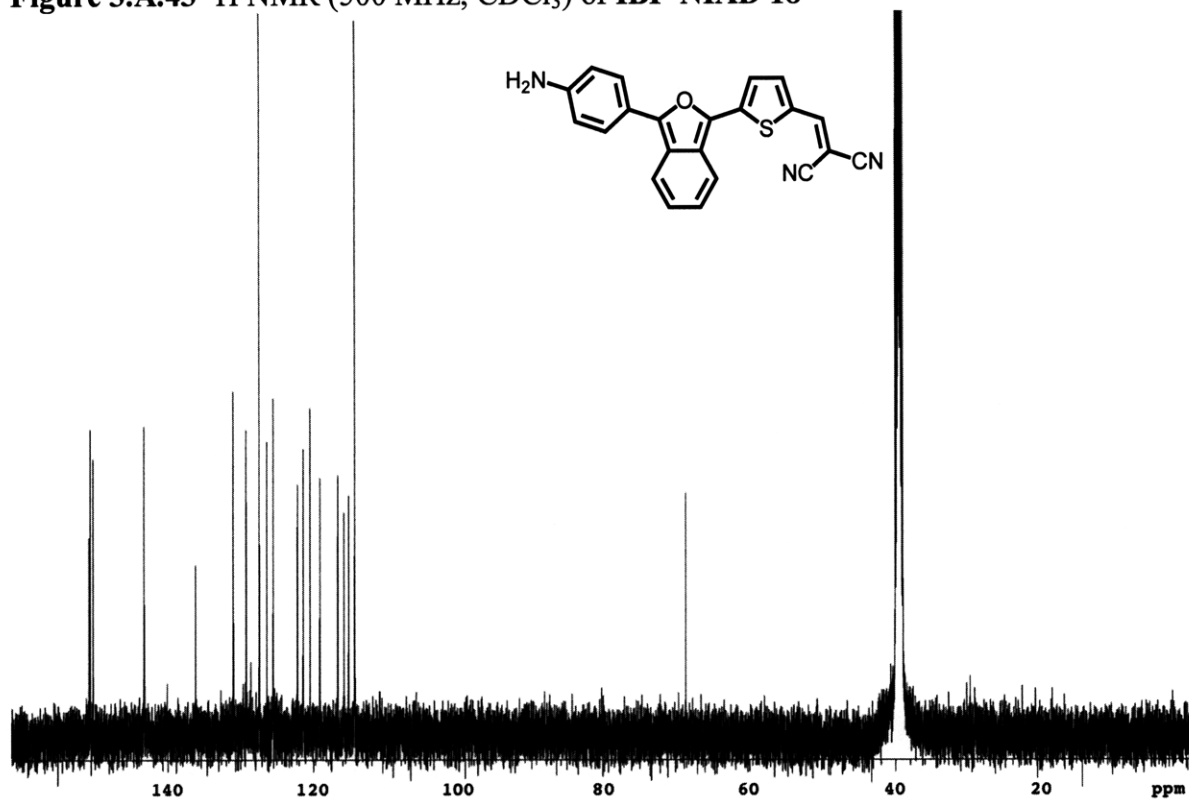**Figure 3.A.43** ^{1}H NMR (500 MHz, CDCl$_3$) of **IBF-NIAD 18**

Figure 3.A.44 ^{13}C NMR (125 MHz, CDCl$_3$) of **IBF-NIAD 18**
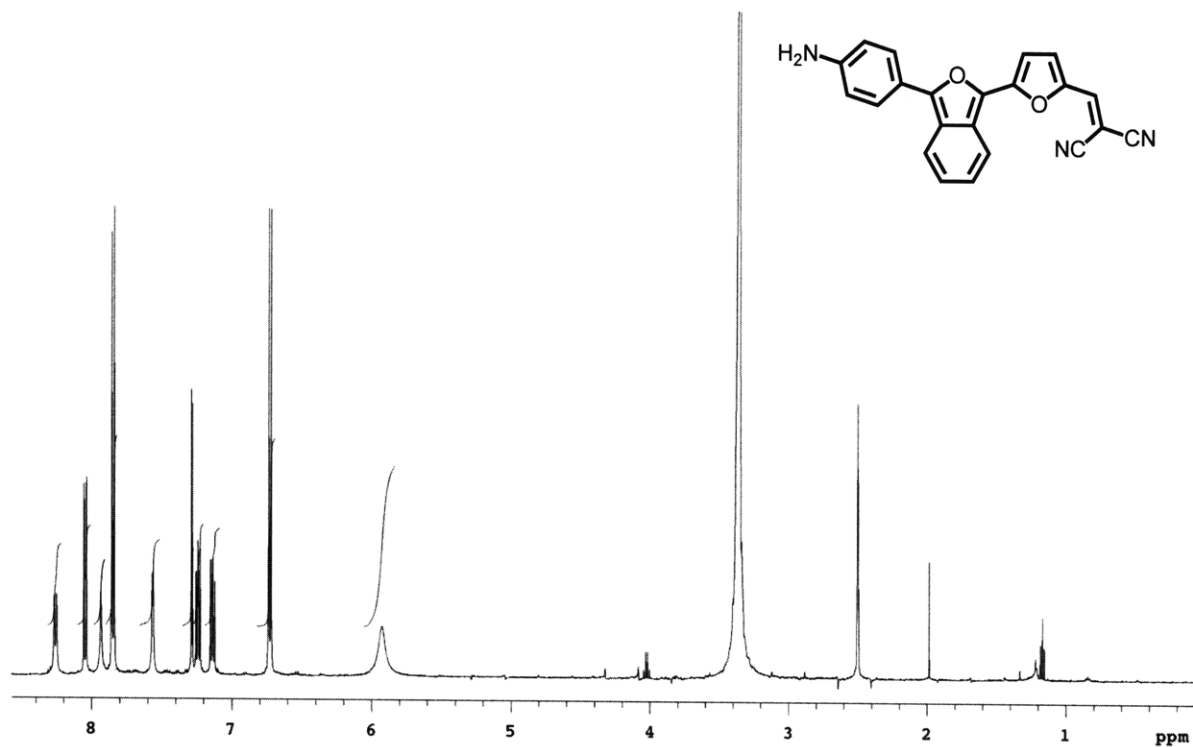
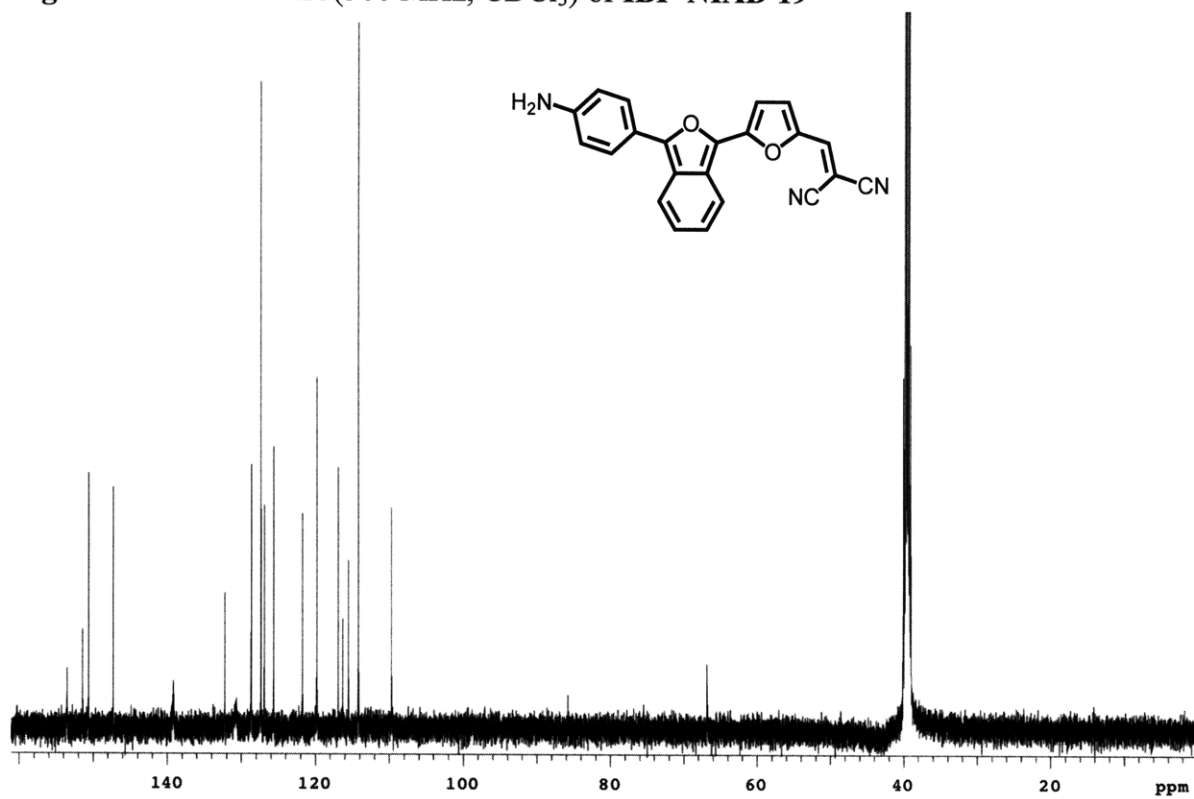**Figure 3.A.45** ^{1}H NMR (500 MHz, CDCl$_3$) of **IBF-NIAD 19**

Figure 3.A.46 ^{13}C NMR (125 MHz, CDCl$_3$) of **IBF-NIAD 19**
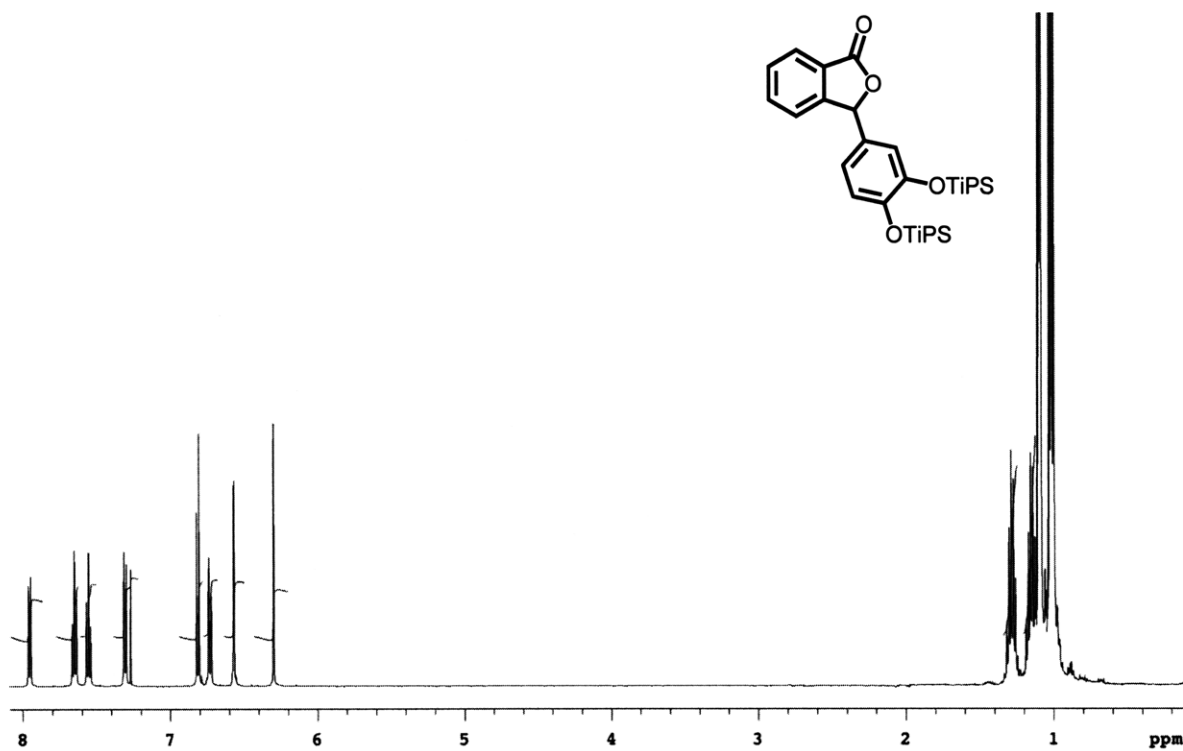
Figure 3.A.47 ^{1}H NMR (500 MHz, CDCl$_3$) of **22**
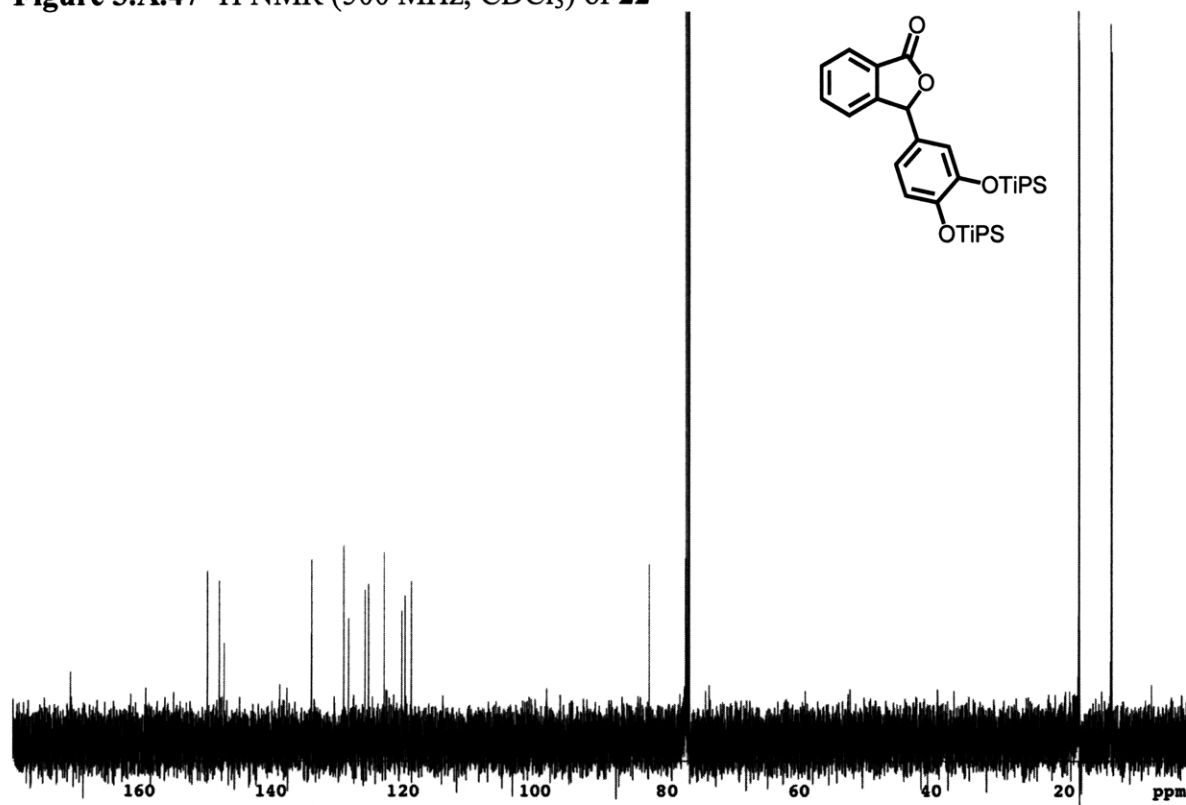
Figure 3.A.48 ^{13}C NMR (125 MHz, CDCl$_3$) of **22**
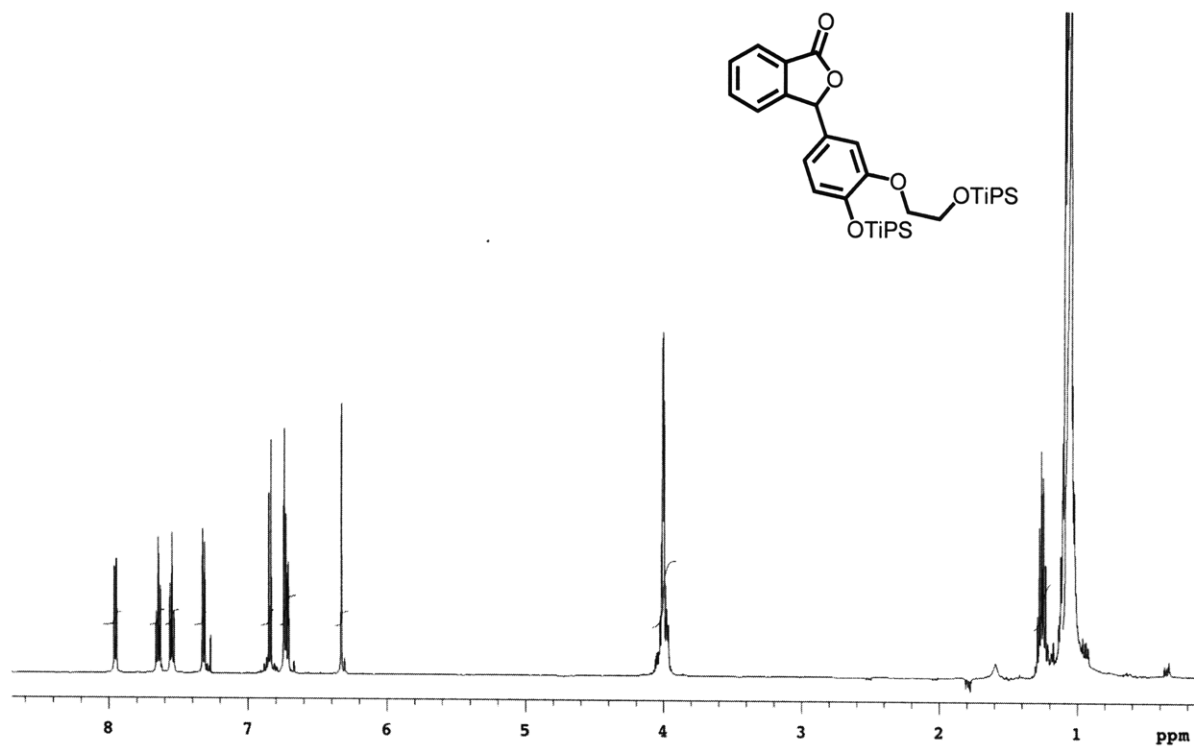
Figure 3.A.49 ^{1}H NMR (500 MHz, CDCl$_3$) of **24**
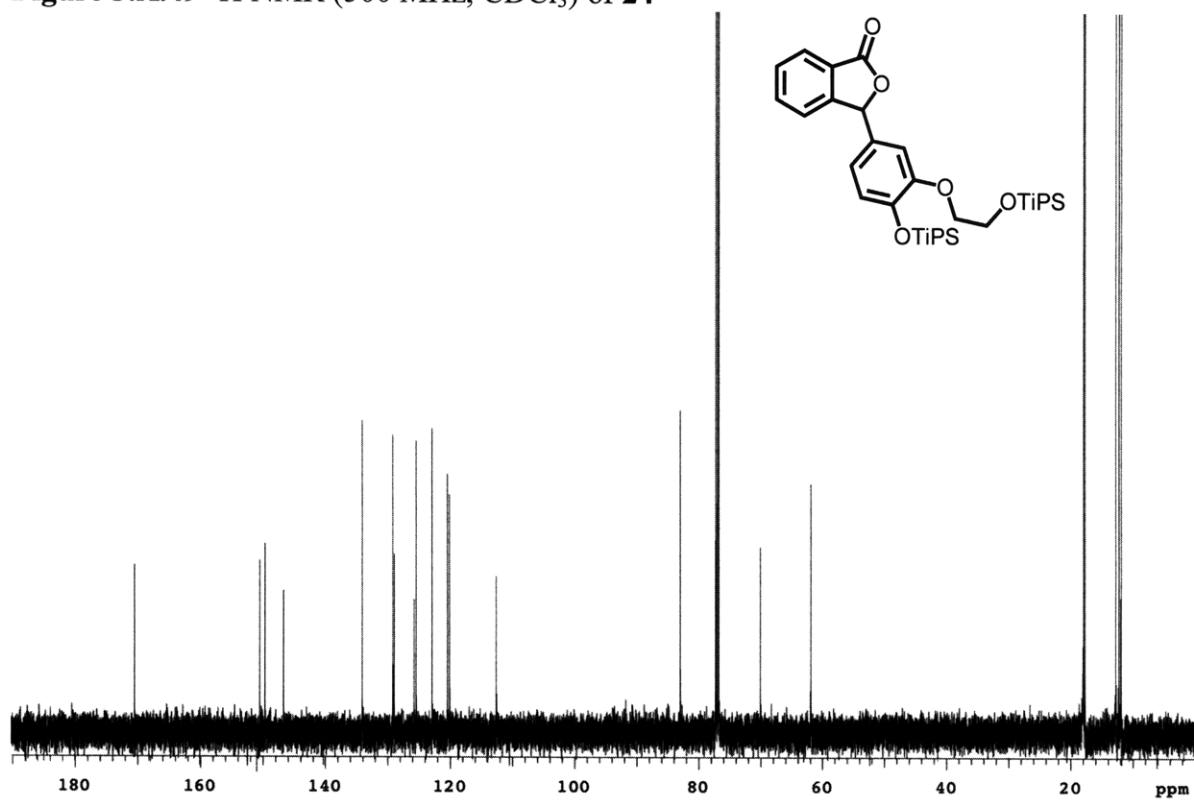

Figure 3.A.50 ^{13}C NMR (125 MHz, CDCl$_3$) of **24**
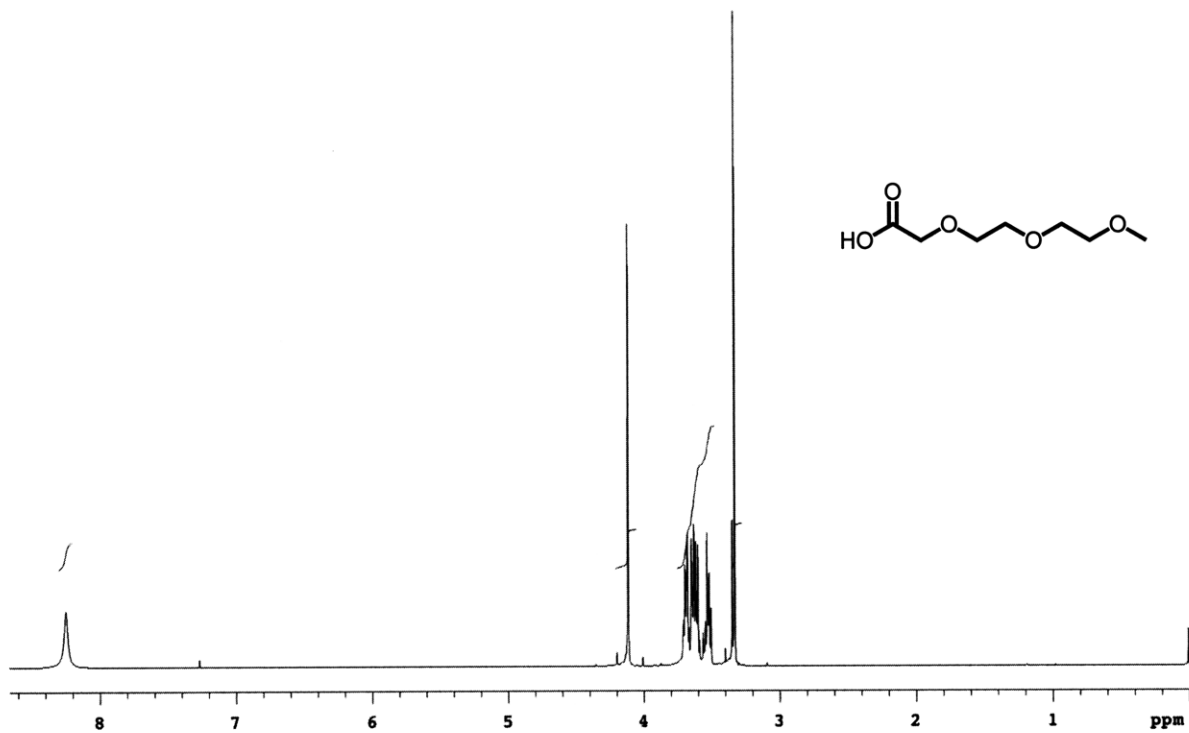
Figure 3.A.51 ^{1}H NMR (300 MHz, CDCl$_3$) of **27**
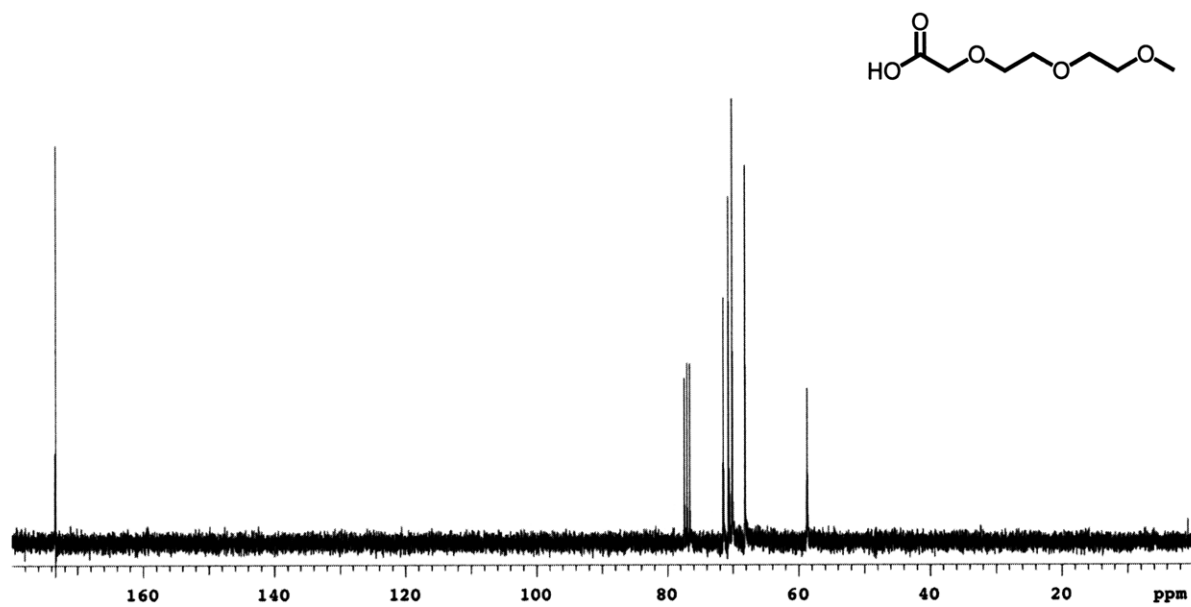
Figure 3.A.52 ^{13}C NMR (75 MHz, CDCl$_3$) of **27**
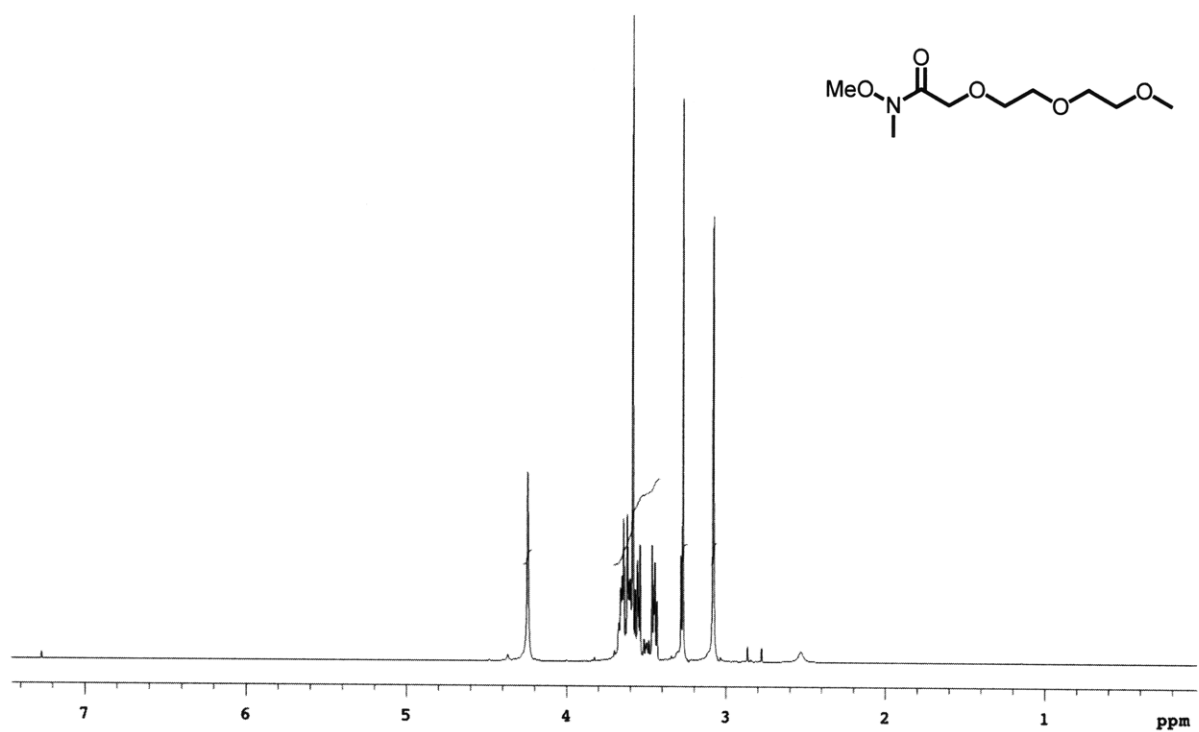
Figure 3.A.53 ^{1}H NMR (300 MHz, CDCl$_3$) of **28**
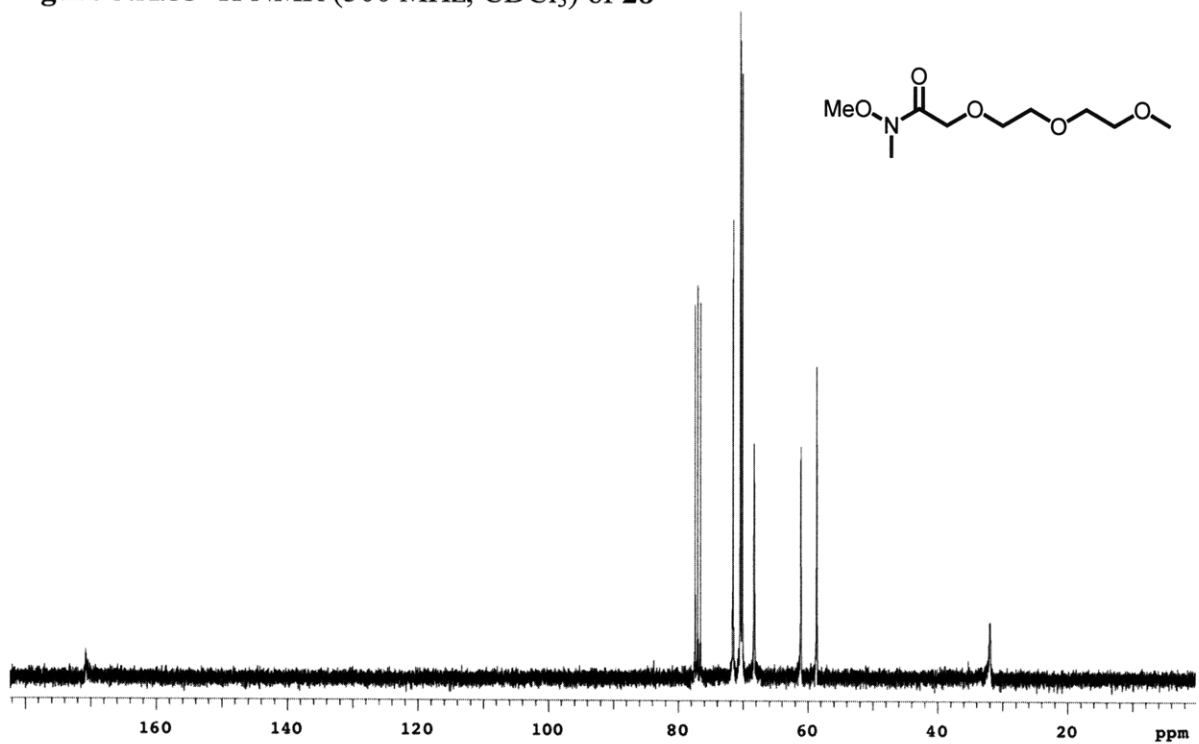
Figure 3.A.54 ^{13}C NMR (75 MHz, CDCl$_3$) of **28**

210
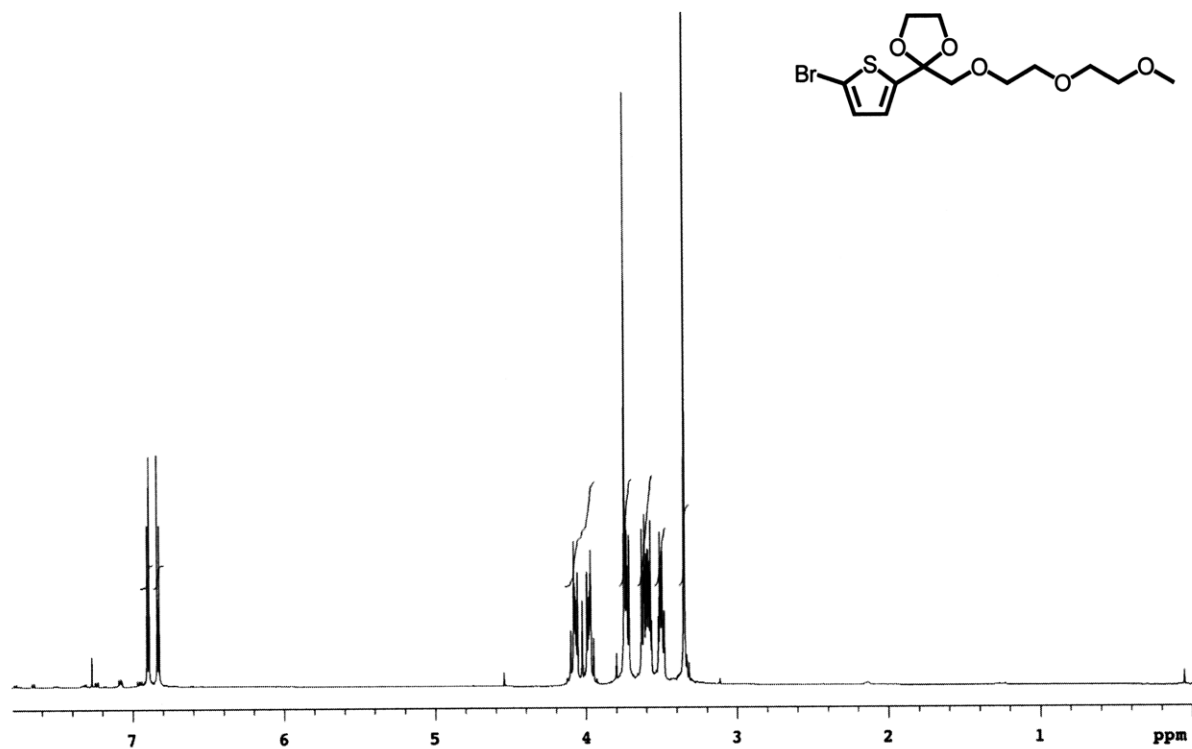
Figure 3.A.55 ^{1}H NMR (300 MHz, CDCl$_3$) of **29**
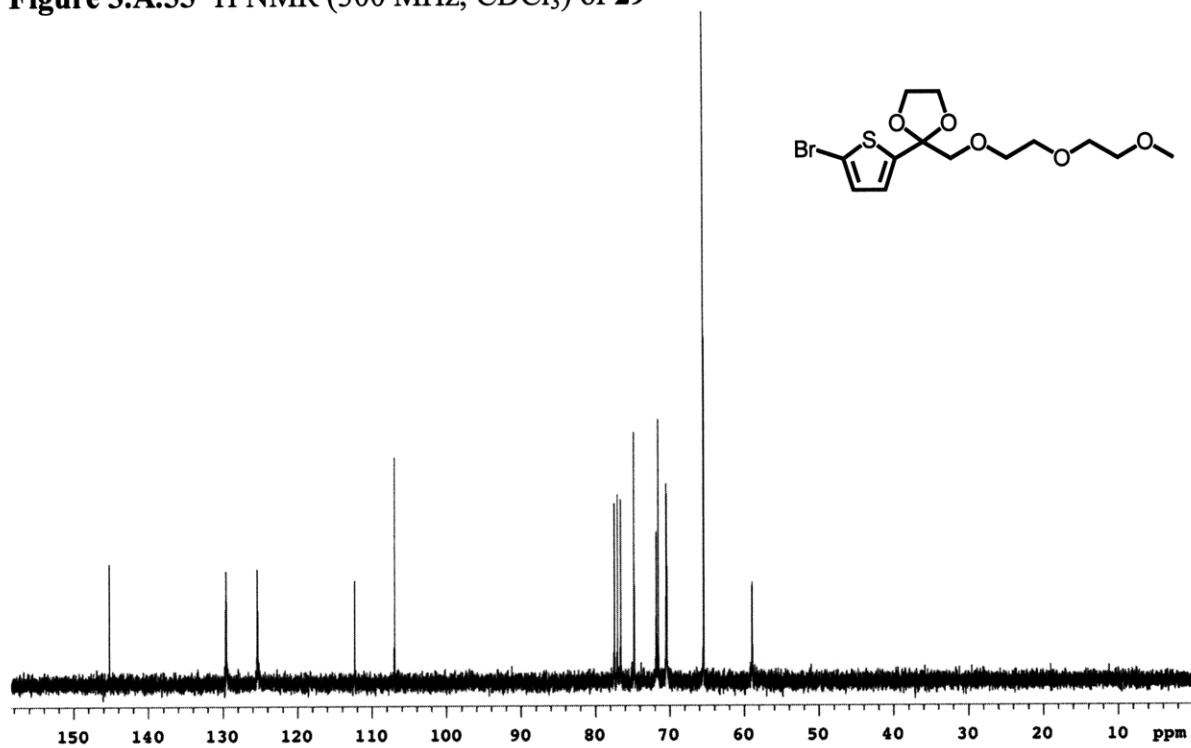
Figure 3.A.56 ^{13}C NMR (75 MHz, CDCl$_3$) of **29**
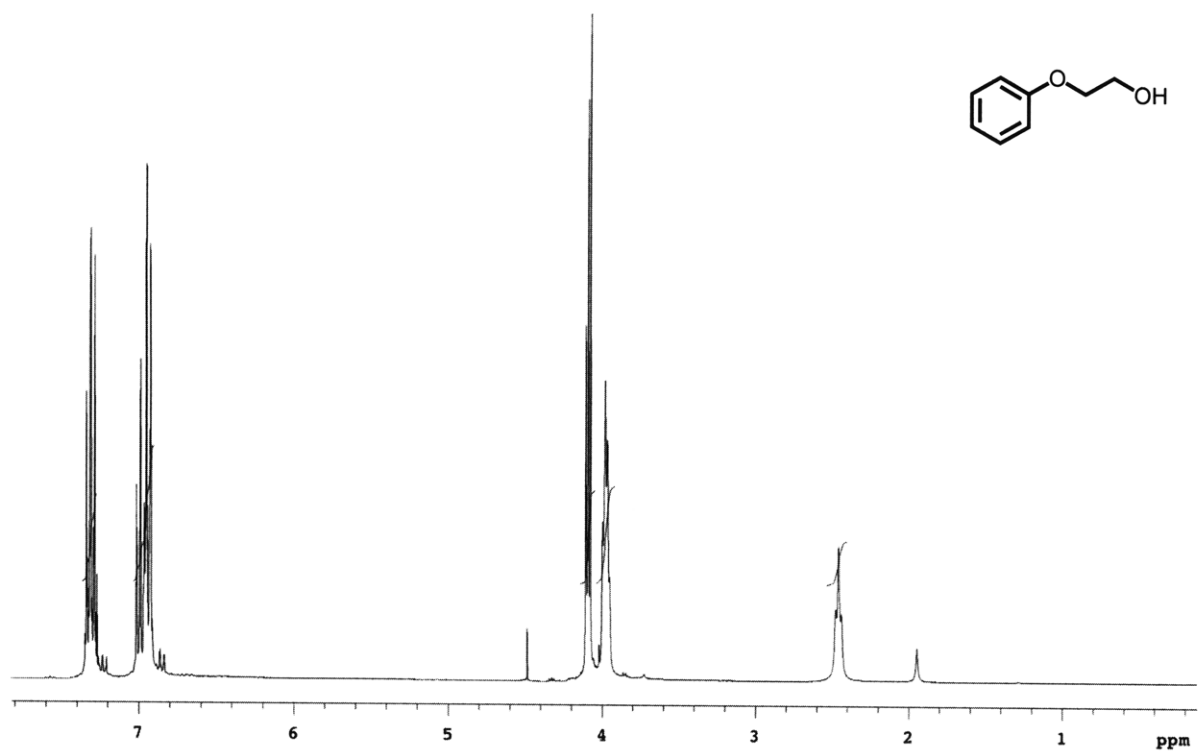
Figure 3.A.57 ^{1}H NMR (300 MHz, CDCl$_3$) of **33**
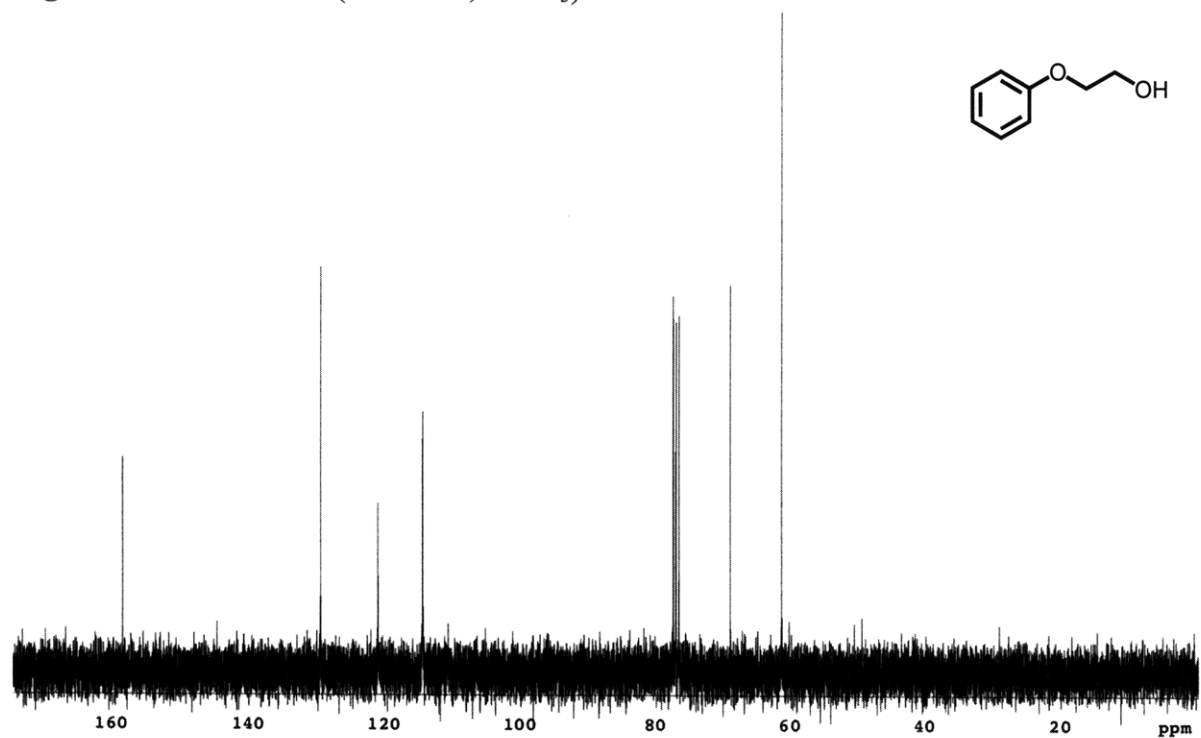
Figure 3.A.58 ^{13}C NMR (75 MHz, CDCl$_3$) of **33**
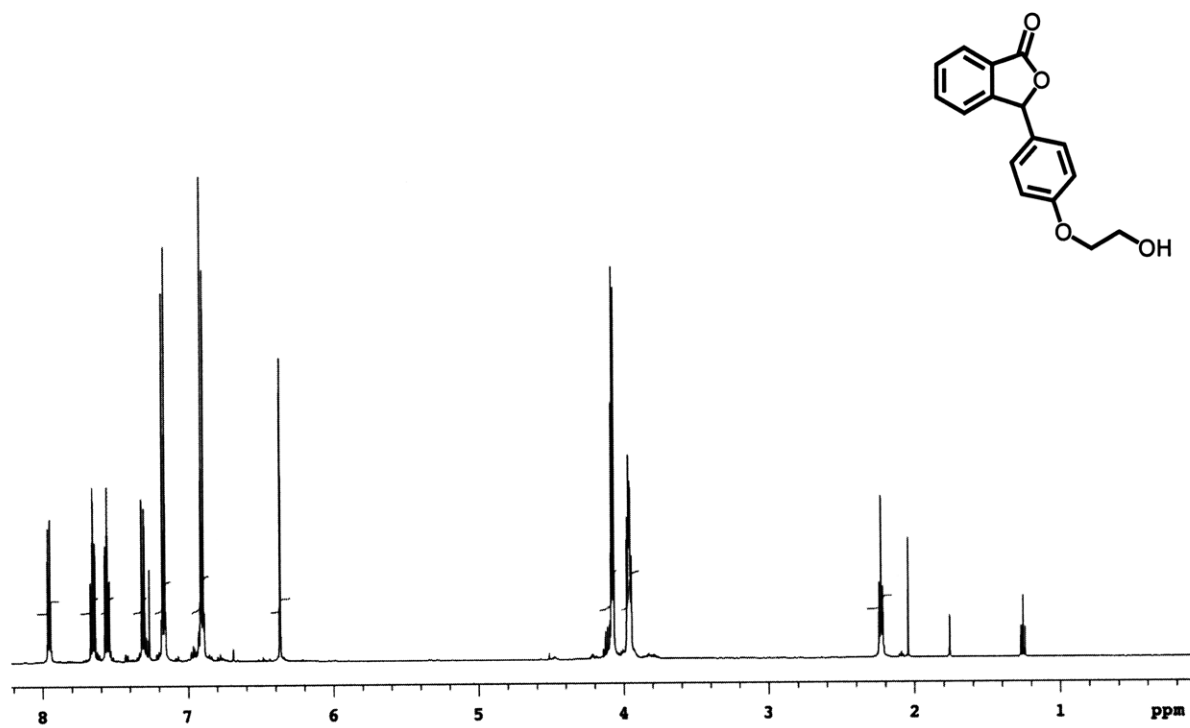
Figure 3.A.59 ^{1}H NMR (500 MHz, CDCl$_3$) of **34**
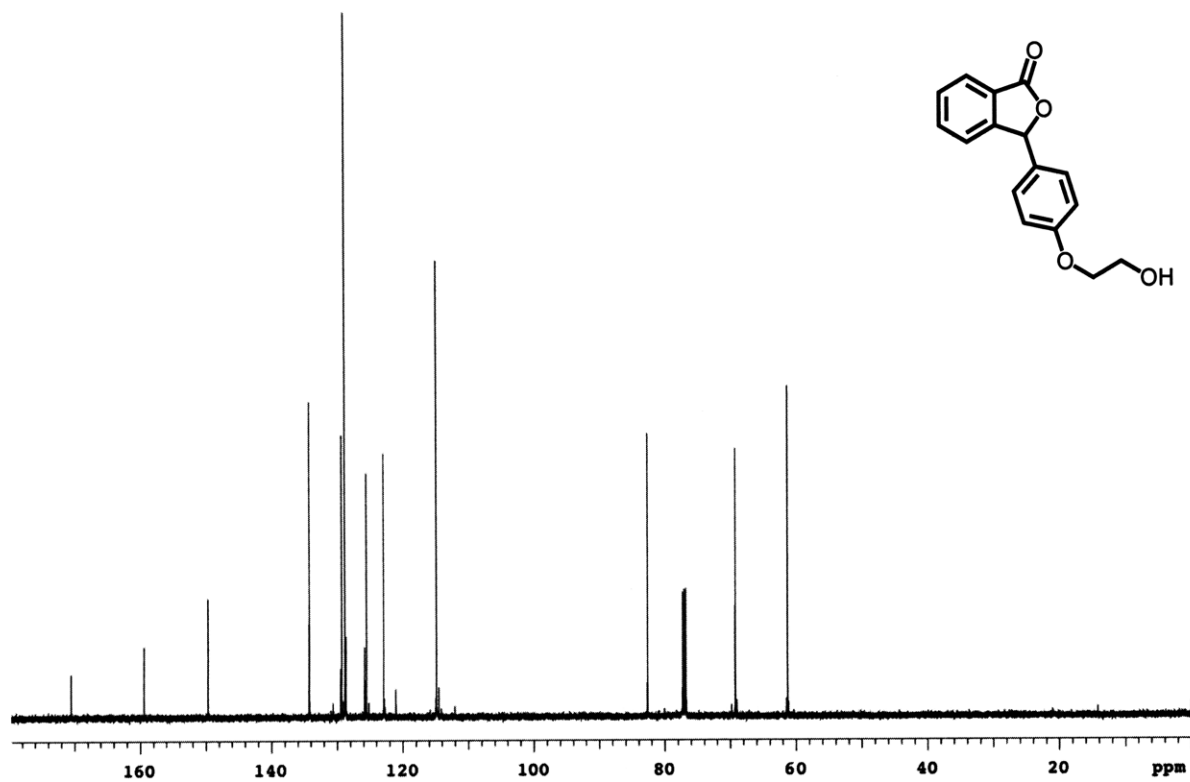
Figure 3.A.60 ^{13}C NMR (125 MHz, CDCl$_3$) of **34**
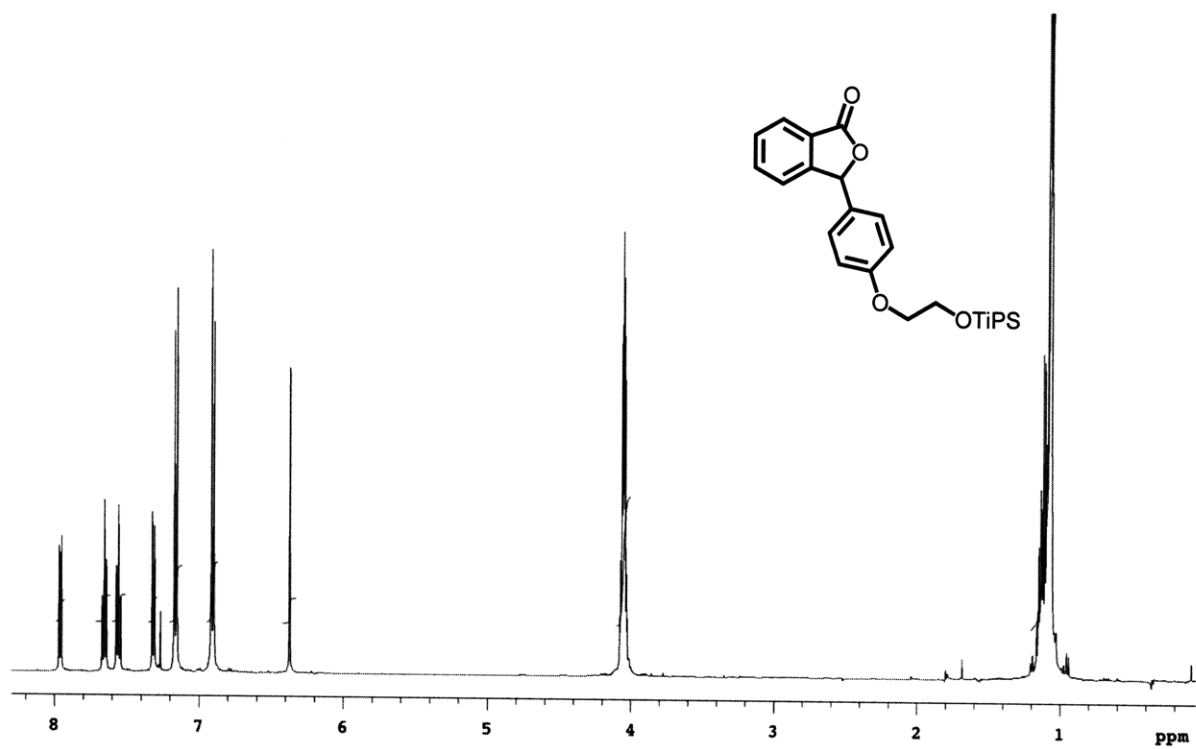
Figure 3.A.61 ^{1}H NMR (500 MHz, CDCl$_3$) of **35**
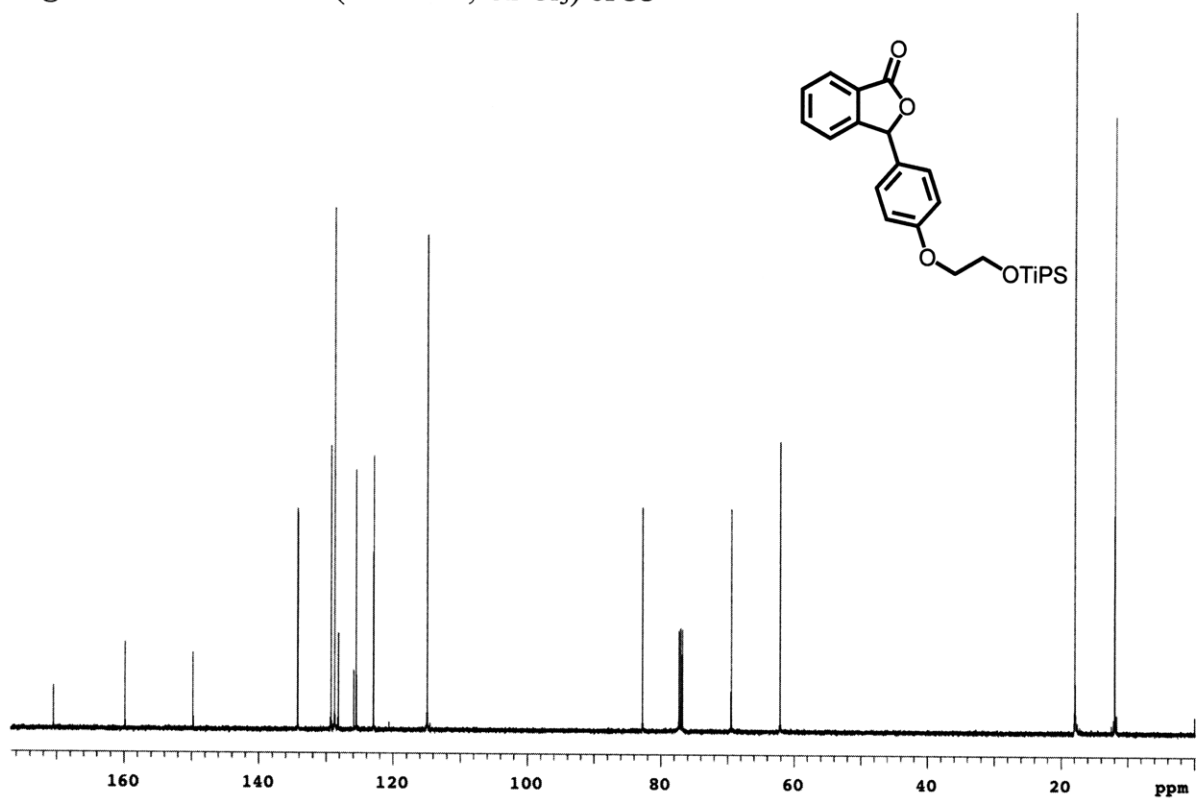
Figure 3.A.62 ^{13}C NMR (125 MHz, CDCl$_3$) of **35**

214
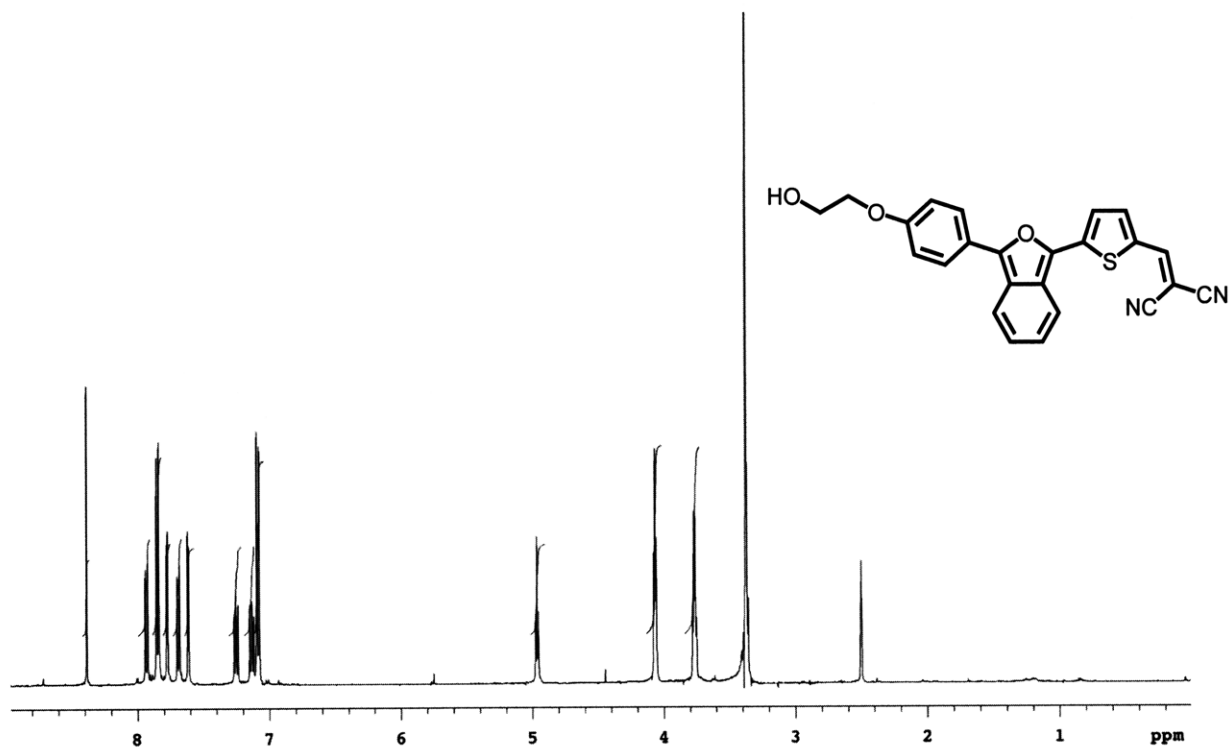
Figure 3.A.63 ^{1}H NMR (500 MHz, DMSO-d$_6$) of **IBF-NIAD 22**
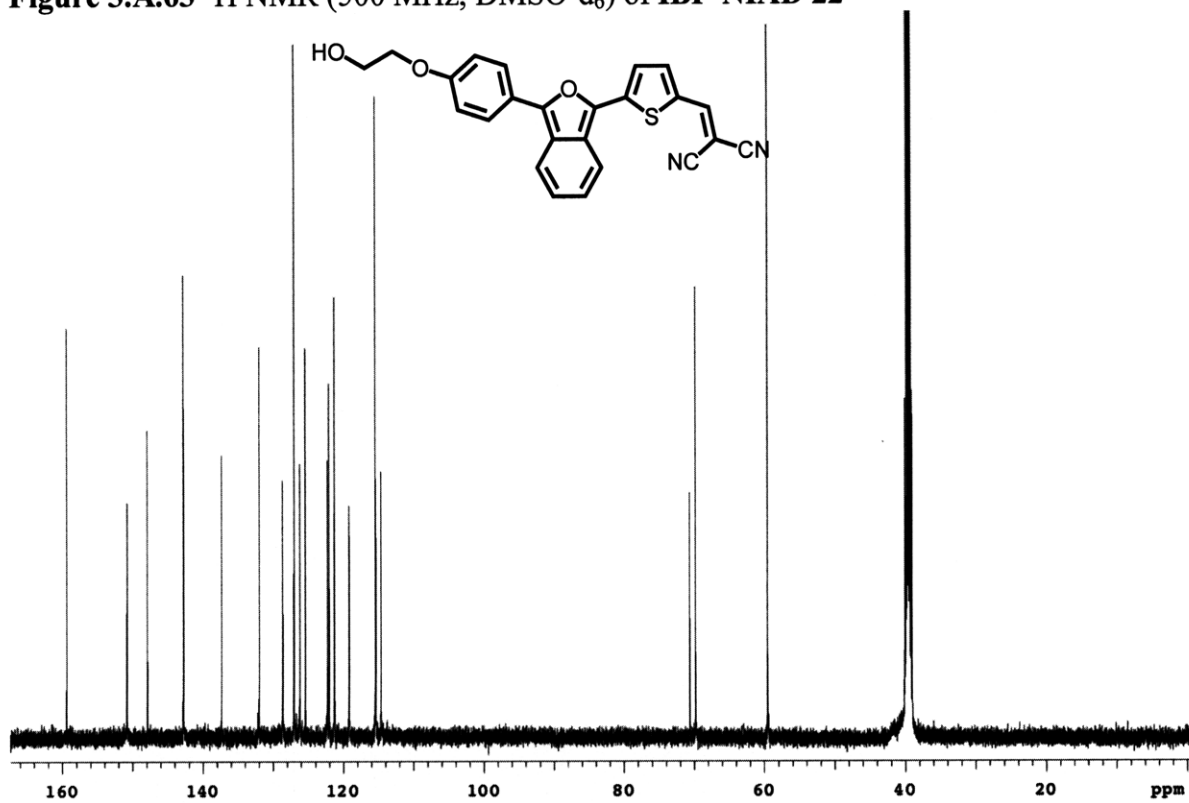
Figure 3.A.64 ^{13}C NMR (125 MHz, DMSO-d$_6$) of **IBF-NIAD 22**
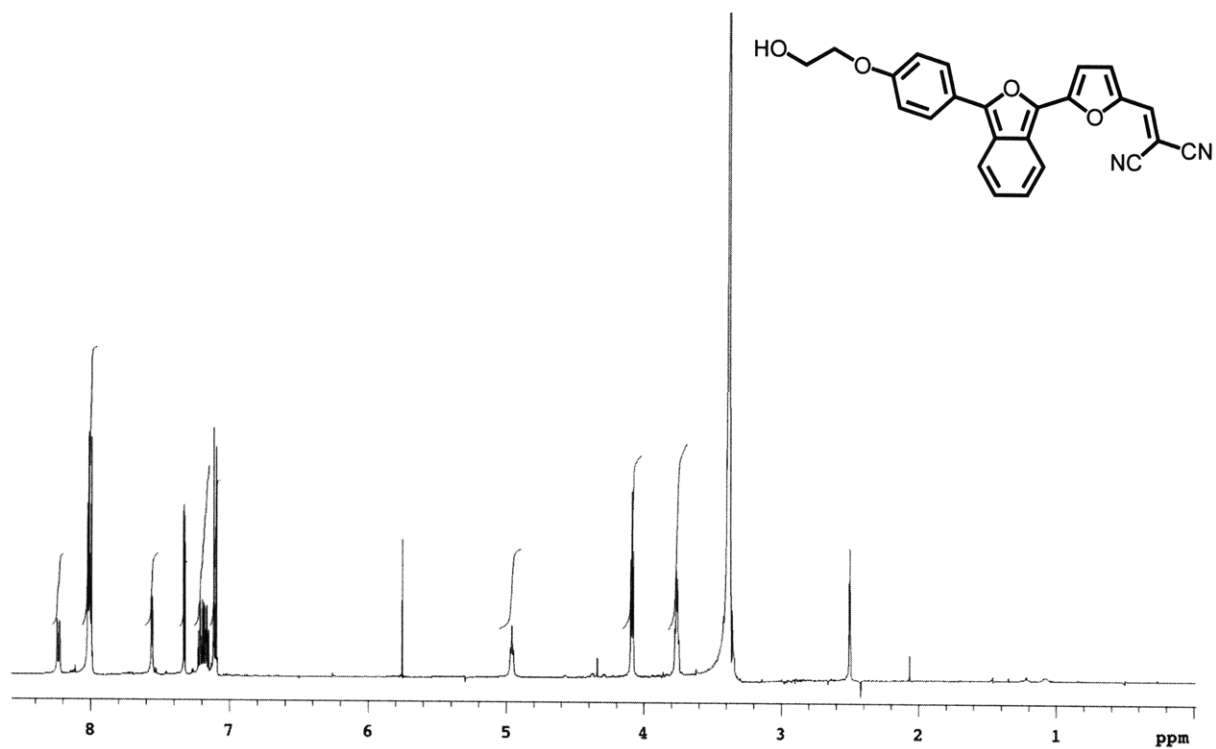
Figure 3.A.65 ^{1}H NMR (500 MHz, DMSO-d$_6$) of **IBF-NIAD 24**
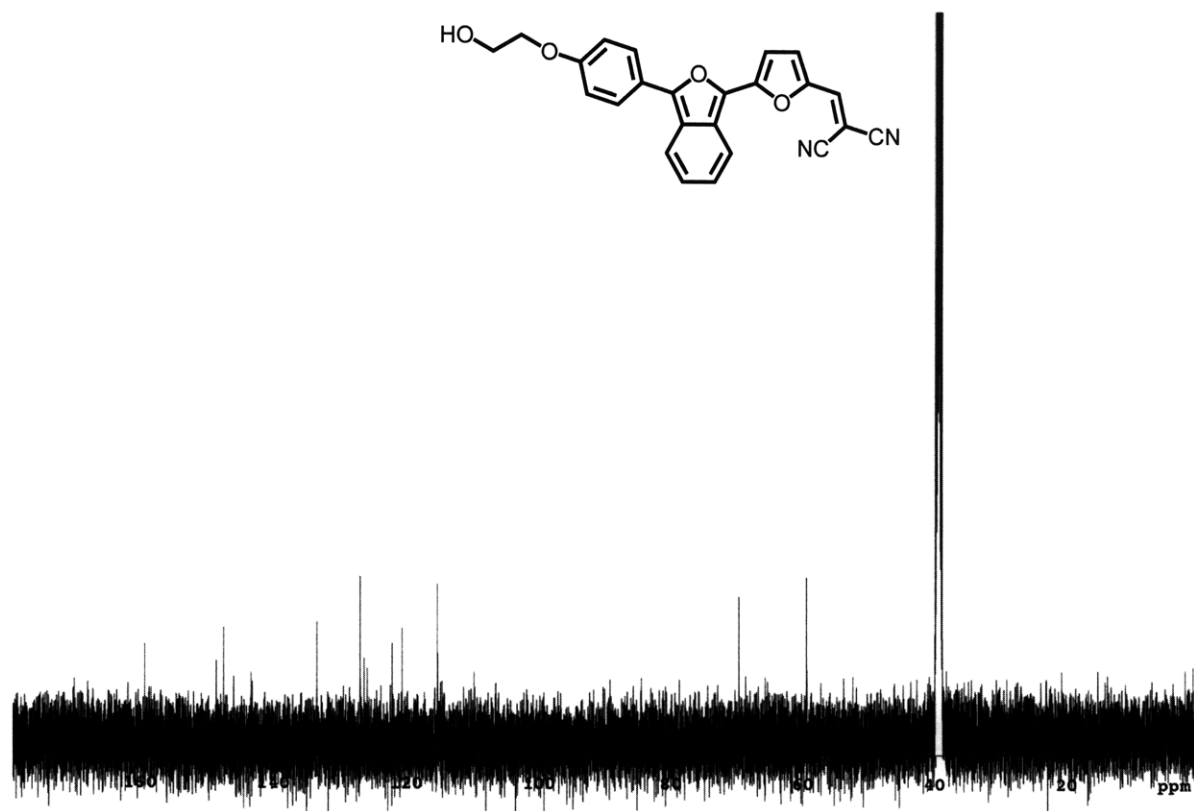
Figure 3.A.66 ^{13}C NMR (125 MHz, DMSO-d$_6$) of **IBF-NIAD 24**
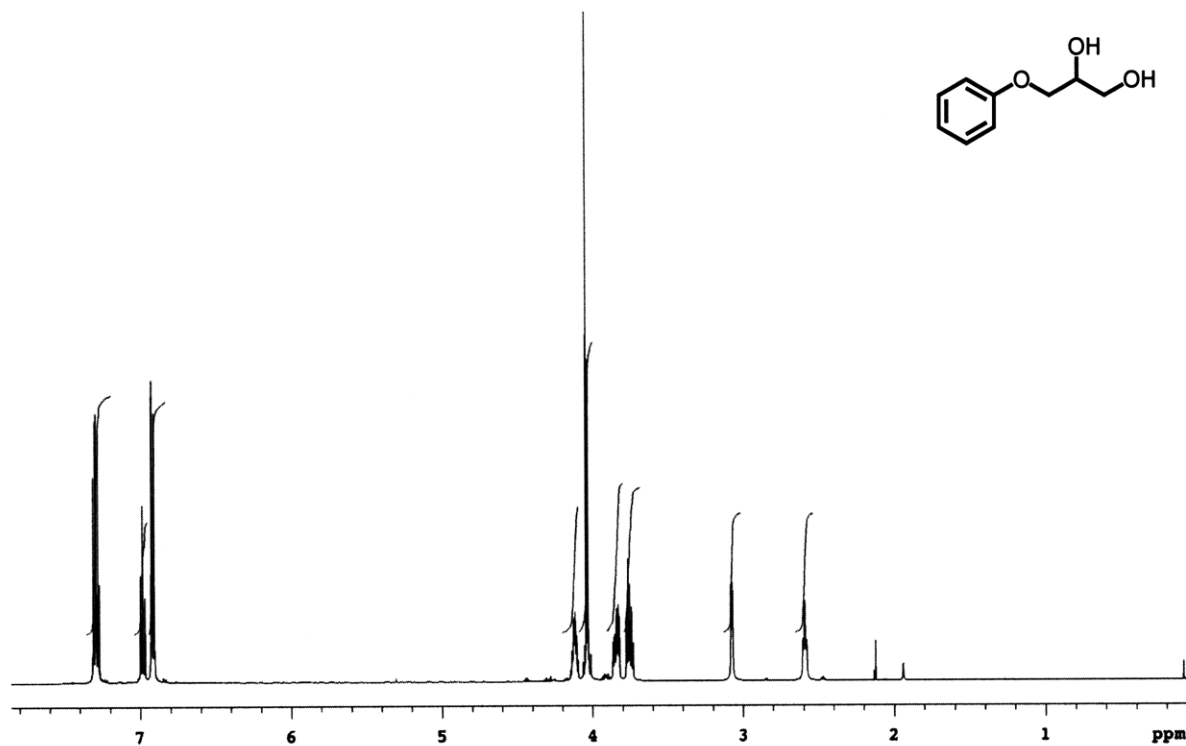
Figure 3.A.67 ^{1}H NMR (500 MHz, CDCl$_3$) of **37**
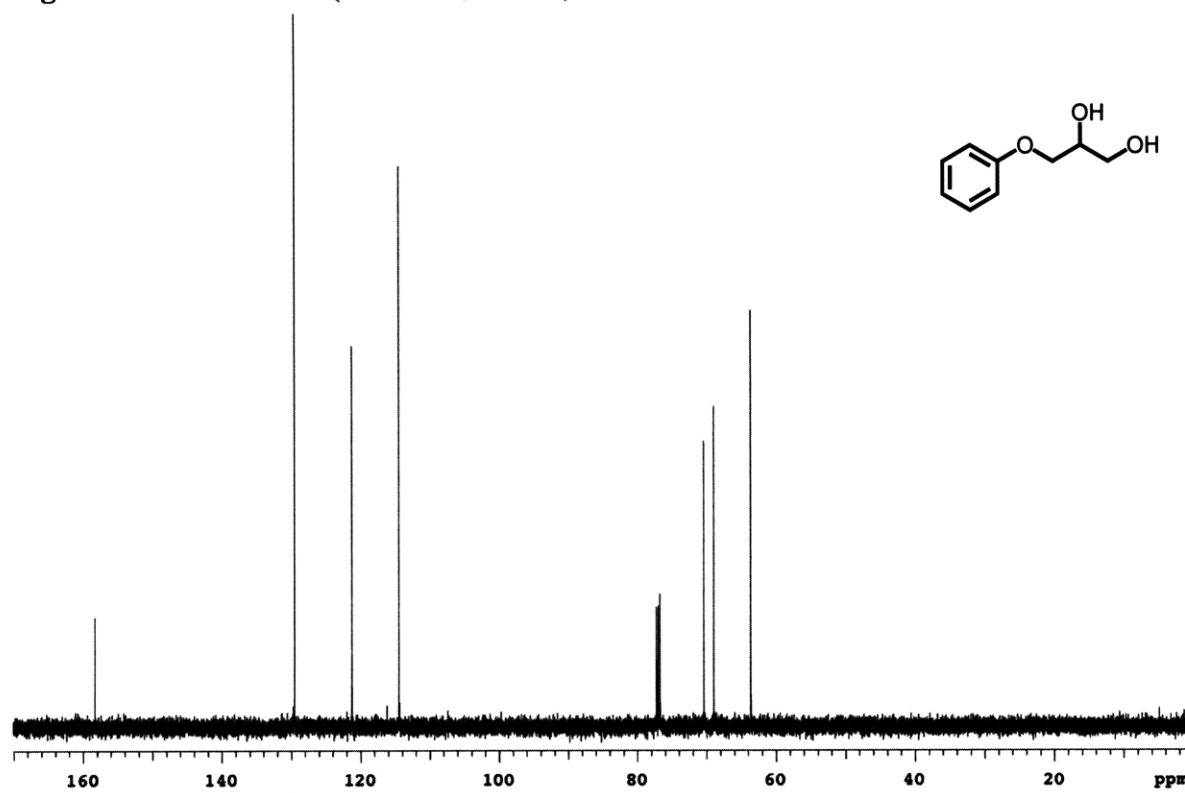
Figure 3.A.68 ^{13}C NMR (125 MHz, CDCl$_3$) of **37**

217
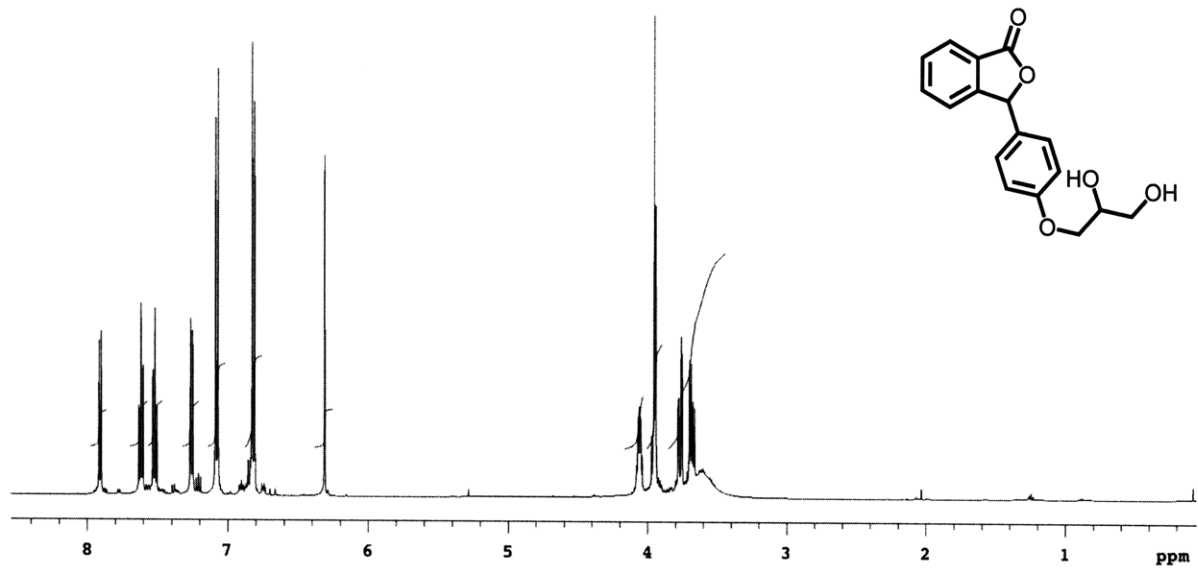
Figure 3.A.69 ^{1}H NMR (500 MHz, CDCl$_3$) of **38**
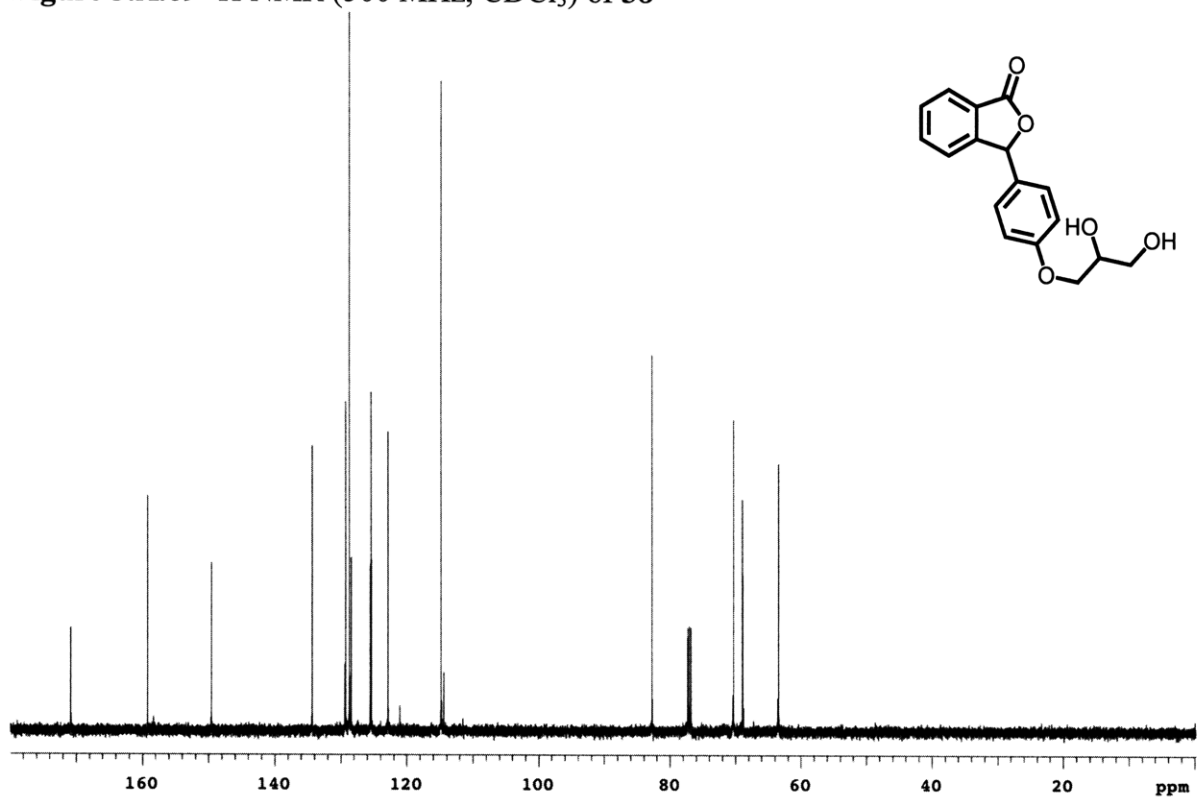
Figure 3.A.70 ^{13}C NMR (125 MHz, CDCl$_3$) of **38**

218
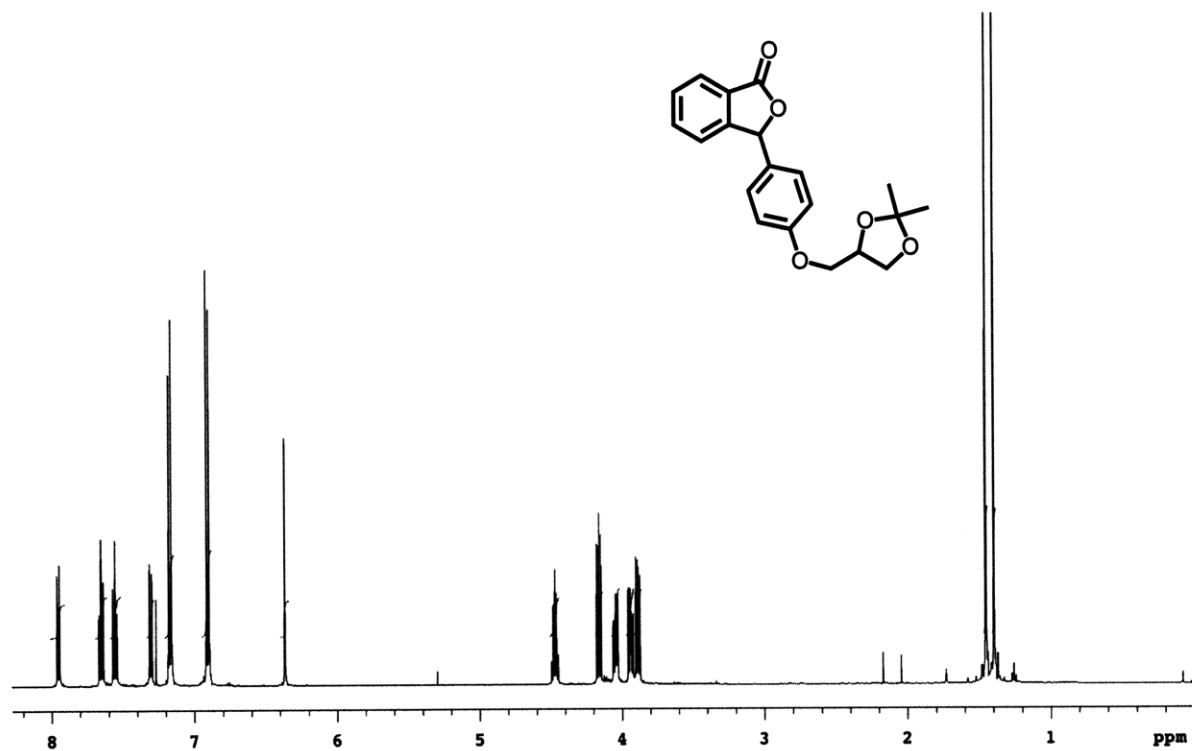
Figure 3.A.71 ^{1}H NMR (500 MHz, CDCl$_3$) of **39**
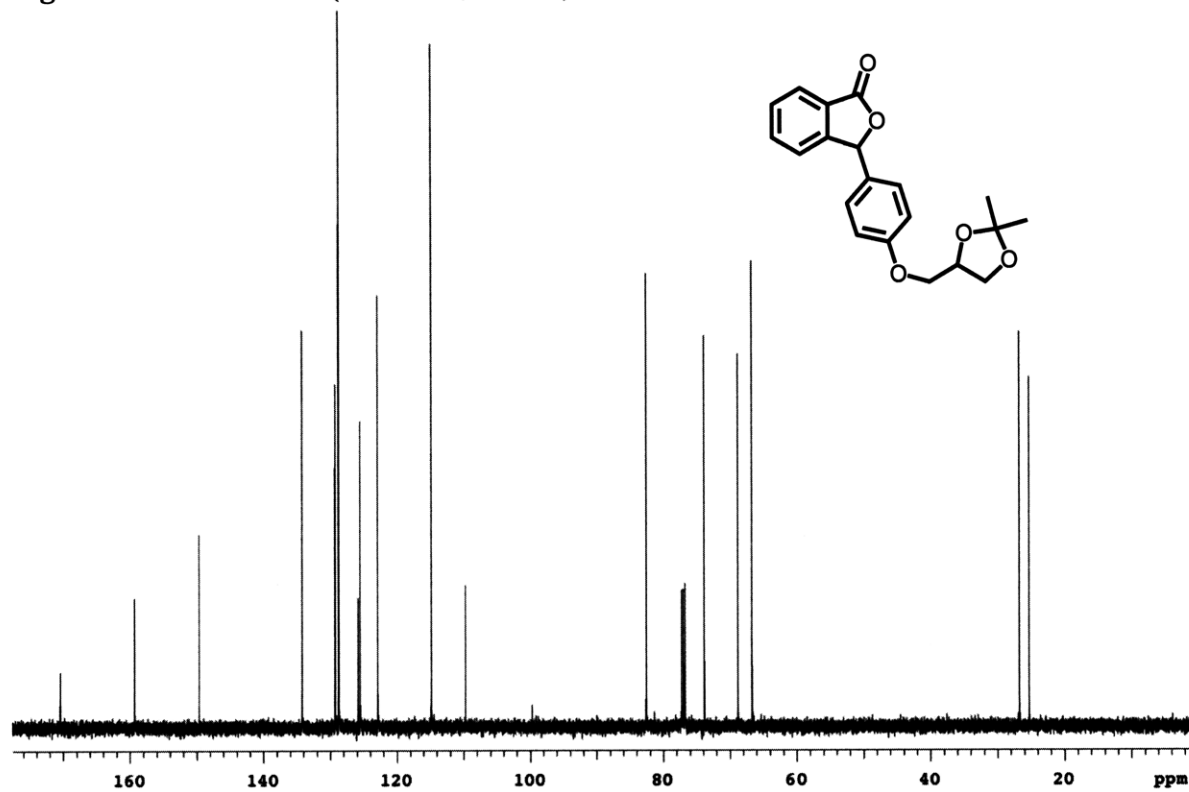
Figure 3.A.72 ^{13}C NMR (125 MHz, CDCl$_3$) of **39**
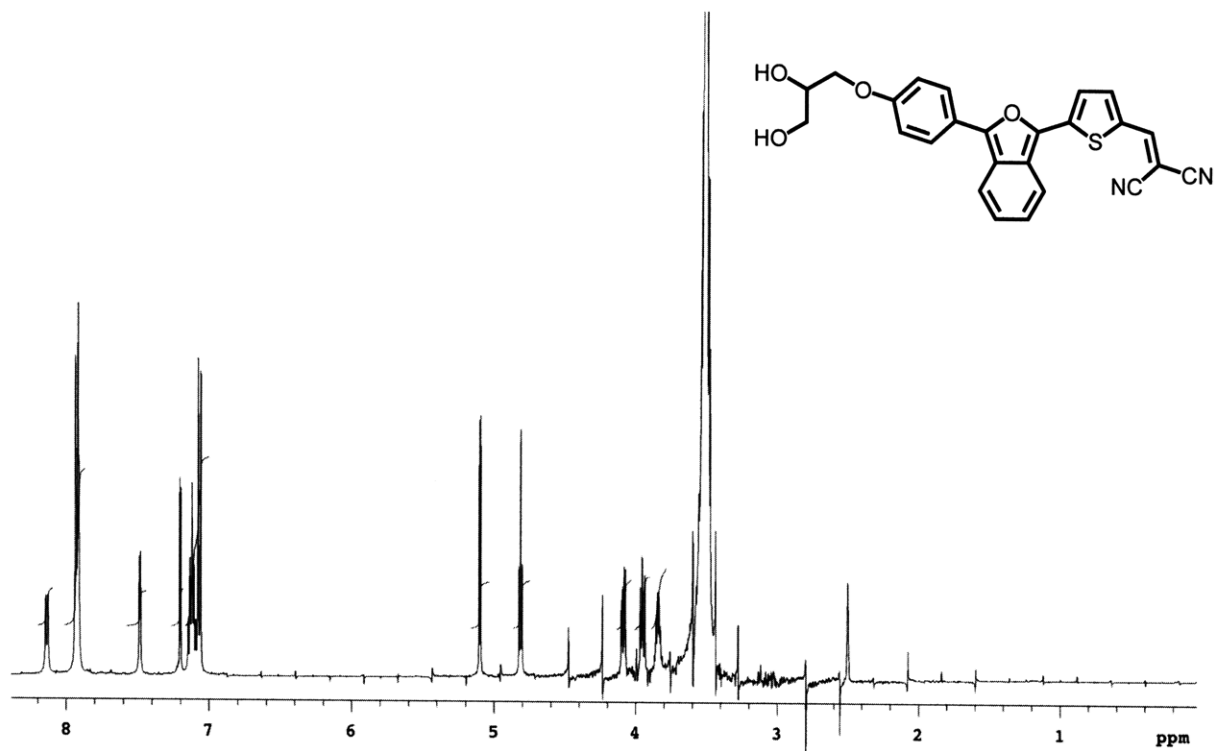
Figure 3.A.73 ^{1}H NMR (500 MHz, DMSO-d$_6$) of **IBF-NIAD 23**
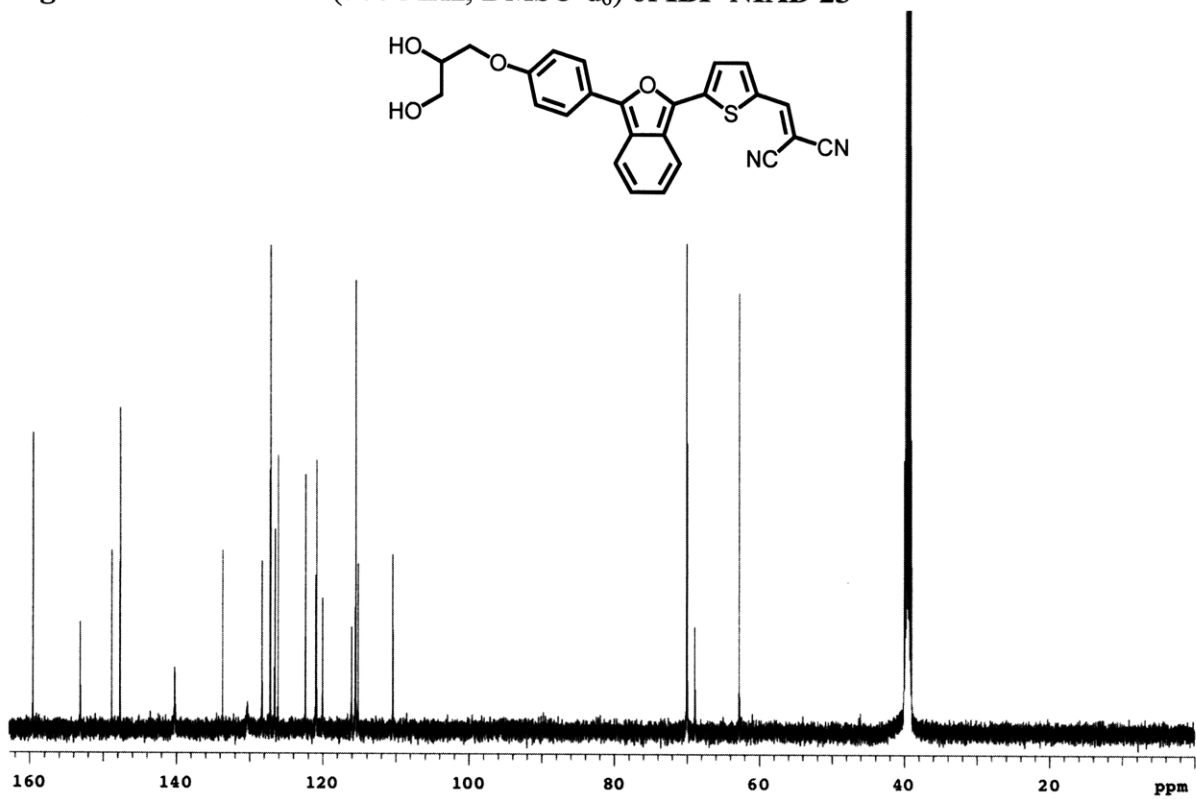
Figure 3.A.74 ^{13}C NMR (125 MHz, DMSO-d$_6$) of **IBF-NIAD 23**

220
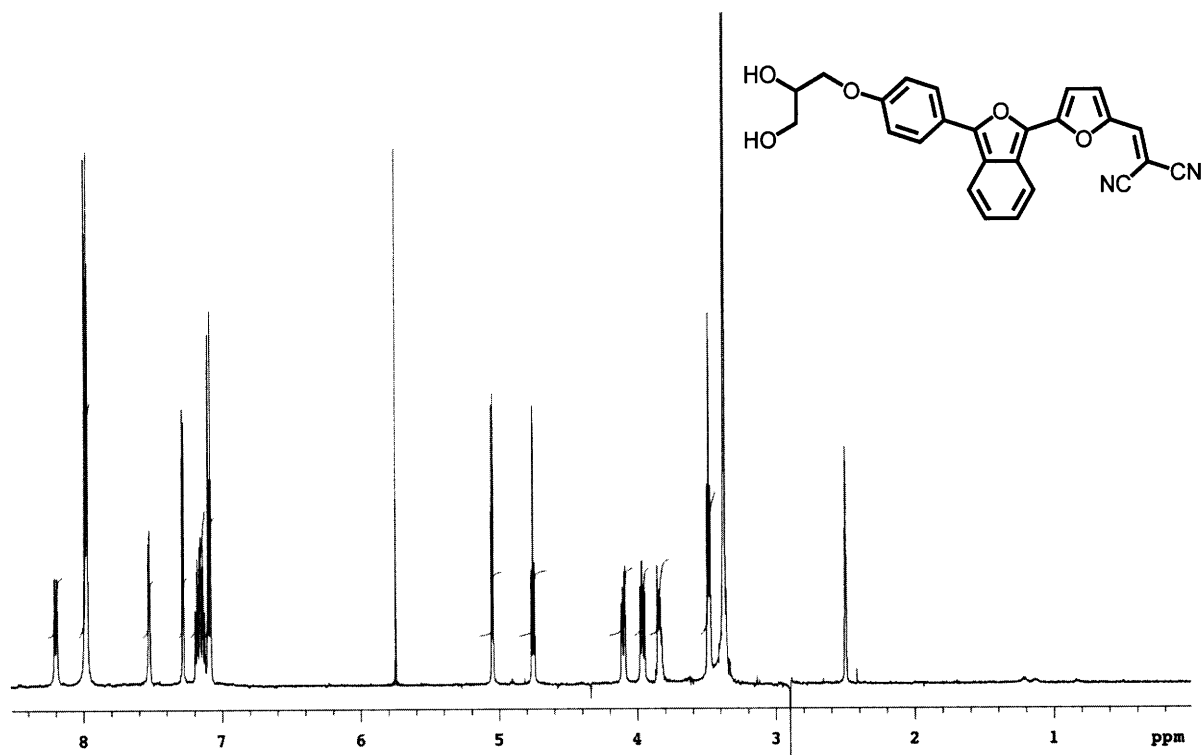
Figure 3.A.75 ^{1}H NMR (500 MHz, DMSO-d$_6$) of **IBF-NIAD 25**
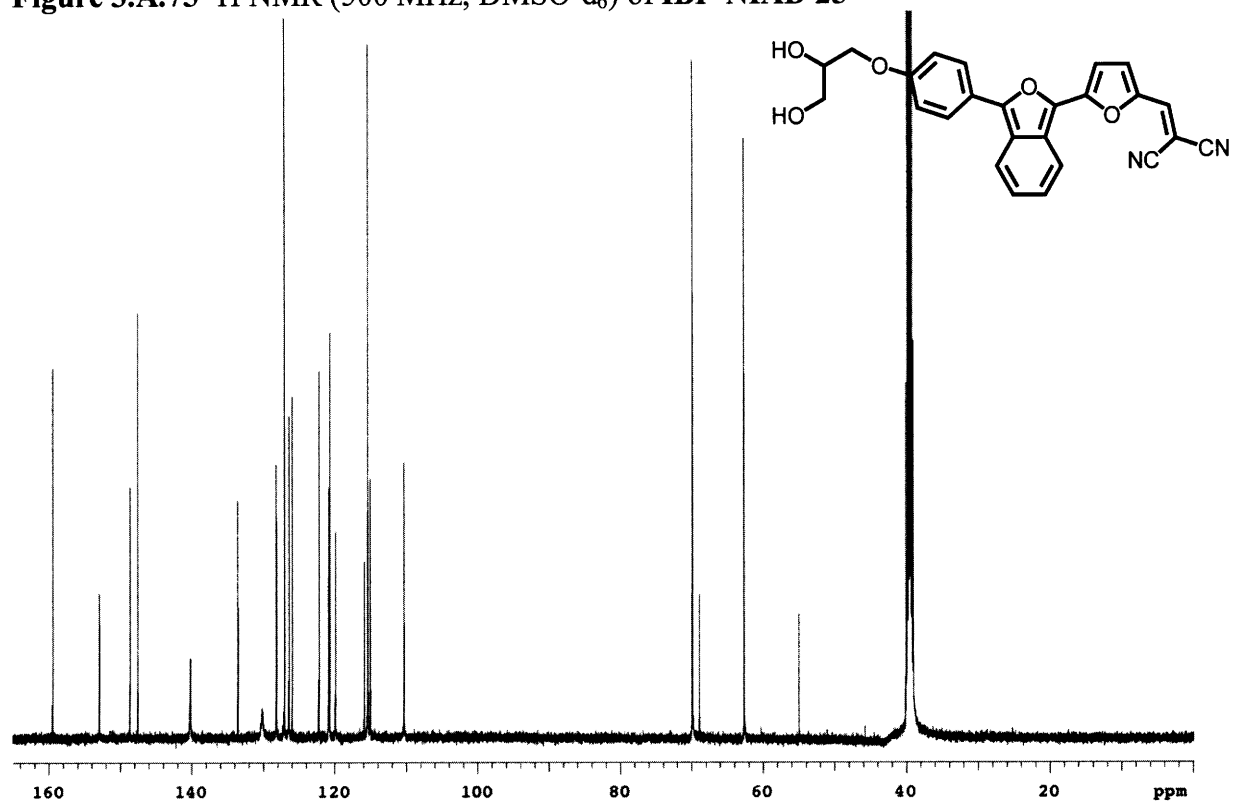
Figure 3.A.76 ^{13}C NMR (125 MHz, DMSO-d$_6$) of **IBF-NIAD 25**

221

Chapter 4

Synthesis of Donor-Acceptor-Donor Chromophores Containing Isobenzofuran

4.1 Introduction

Recent years have seen numerous reports of organic molecules integrated into electronic devices. [1] Their allure is based in part on their modularity; the electronic properties of an organic material, be it a small molecule, oligomer, or polymer, may be controlled synthetically. With possible applications including light emitting diodes,[2] photovoltaics,[3] field effect transistors,[4] sensors,[5] and nonlinear optics,[6] research into new materials with unique electronic properties is continually expanding. In particular, development of novel aromatic systems is of interest, and in this chapter we present an initial synthetic investigation of oligomeric materials containing isobenzofuran.

Under normal conditions, interactions of molecules and light are governed by Beer's law, which shows a linear relationship between the extinction coefficient of a molecule and absorption of light. This same principle applies to other interactions of light and mater, including reflection, diffraction, and refraction which vary linearly with changing light intensity.[7] Under more extreme conditions, such as the high intensity light produced by lasers, this behavior no longer holds true, and many materials exhibit nonlinear optical (NLO) properties. One way to explain this phenomenon is by thinking of matter as combinations of anharmonic oscillators, with electronic transition frequencies corresponding to their resonant frequencies. Light contains an oscillating electric field, and at low field strengths, the resonant excitation of the molecular oscillators is harmonic, and thus polarization of the medium is linear. However, as the electric field strength increases, the anharmonicity begins to take effect, and polarization of the molecule deviates from linearity.[8] Equation 4.1 describes these nonlinear components.

$$P = P_{o} + \chi^{(1)}E + \chi^{(2)}E^2 + \chi^{(3)}E^3 + \dots \tag{4.1}$$

P is the polarization of the medium, E is the electric field component of light, P_o is the intrinsic polarization of the medium and $\chi^{(1)}$, $\chi^{(2)}$, and $\chi^{(3)}$ are the first, second, and third order susceptibilities respectively, and as the second and third susceptibilities are related to E^2 and E^3, they are the nonlinear component. If the medium is a molecule then equation 4.2 describes its dipole moment μ, wherein μ_o is the intrinsic dipole moment of the molecule. The terms β and γ are called the first and second hyperpolarizabilities.

$$\mu = \mu_o + \alpha E + \beta E^2 + \gamma E^3 + ... \tag{4.2}$$

The utility of NLO materials is that they can control light in unique ways. For example, a material with large hyperpolarizability (or $\chi^{(2)}$) can induce second harmonic generation (SHG) on light passing through it, wherein the emerging light is half the wavelength (twice the energy) of the incident light. These materials can also exhibit frequency mixing, in which beams of two different wavelengths of light are focused on the same area and the resulting light has a frequency that is the sum or the difference of the first two.[9] Materials with large second hyperpolarizabilities (third order NLO), can effect third harmonic generation, were the emerging light is a third the wavelength of the incident light and degenerate four-wave mixing, in which three beams of light with different directions combine to generate a fourth beam of the same frequency. Two-photon absorption is also third order NLO process.[10] These properties can be exploited in a variety of ways. SHG can convert the 1064 nm light from a Nd:YAG laser into a green laser (534 nm).[11] Two-photon absorption is a useful property in biological imaging (see Chapter 1 and Chapter 3), and may also be used for optical limiting materials, which selectively absorb high intensity light and can thus be used to protect delicate electronic sensors (and eyes) from its effects.[12]

One particular class of molecules that has generated interest in optical materials is Donor-

acceptor-donor (DAD) compounds. These compounds are composed of two electron-donating groups connected to a central electron-withdrawing group by a polarizable bridges. As with donor-acceptor compounds, changing the donor-acceptor pairing or the nature of the conjugated bridge can modulate their electronic and optical properties. DADs containing proquinoid units such as bisthiadiazoles (1)[13] and thiadiazoloquiloxalines (2),[14] and electron-accepting ketene dithioacetals (3)[15] have been explored as components of NIR OLEDs (Figure 4.1) due to their low bandgaps. With their highly polarizable conjugated backbones, other DADs have been studied as third order nonlinear optical materials, including two-photon chromophore (4)[16] and NLO chromophore tetracyanobutadiene (TCBD) (5).[17] As isobenzofuran's proquinoid nature enhances the polarizability of conjugated systems, we wanted to explore its application in DAD systems, particularly those with TCBD acceptors. Herein we present some initial synthetic efforts toward this goal.
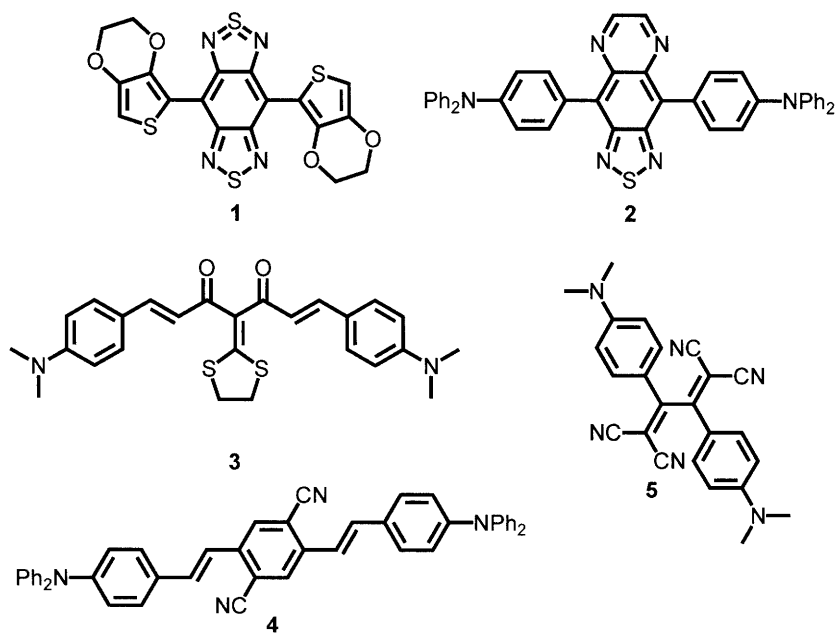
Figure 4.1 Some DAD compounds. See text for discussion.

4.2 Results and Discussion

4.2.1 Synthesis of IBF-DAD 0-2

Scheme 4.1 Synthesis of DAD Components
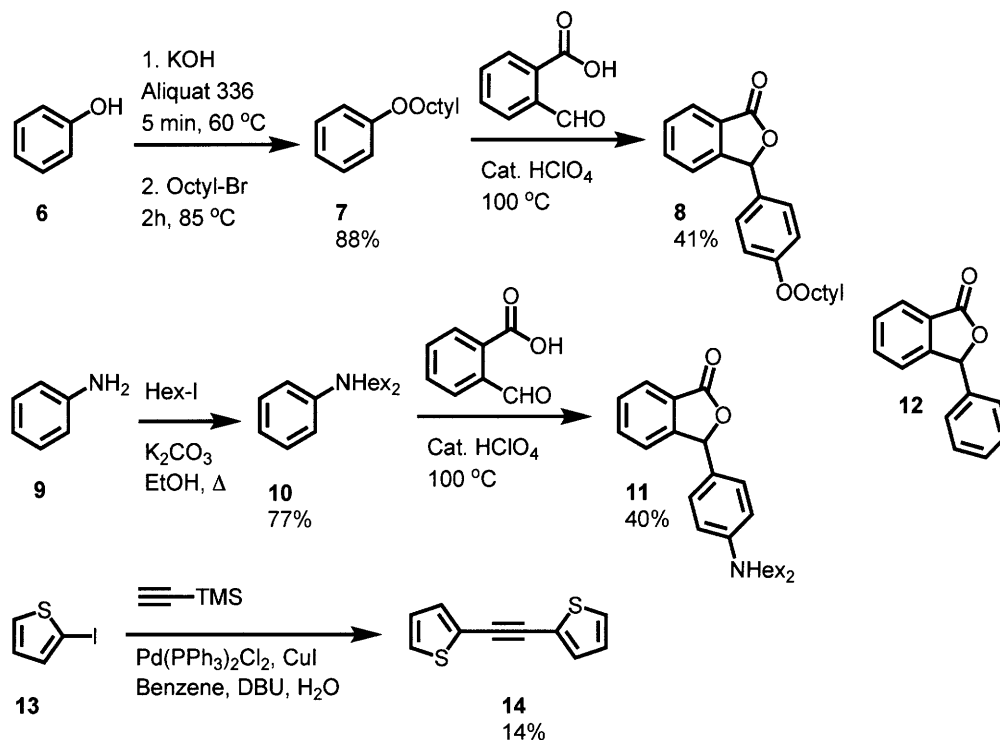
As an investigation into donor-acceptor-donor oligomers containing isobenzofurans, we decided to synthesize symmetrical dimers of the **IBF-NIAD** dyes series with a central TCBD acceptor. The synthesis of **IBF-DAD 0-2** is similar to that of the **IBF-NIAD** series in Chapters 2 and 3. Dithienyl-alkyne **14** was synthesized using the Sonagashira cross coupling with TMS-acetylene. The yield for this reaction was not optimal, but did afford adequate quantities of **14** for the present study. Aryl-phthalides **8** and **11** were synthesized by acid catalyzed condensation of alkyl-benzene **7** and dihexyl-aniline **10** with 2-carboxybenzaldehyde (**12** is commercially available, see Scheme 4.1). Dilithiation of **14**, followed by quenching with a phthalides **8, 11,**

and **12**, and subsequent dehydration with acetic anhydride yielded alkynes **15a-c**, of which only

15a was stable to isolation (Scheme 4.2).

TCBDs are typically formed via reaction of tetracyanoethylene (TCNE) with electron

rich alkynes. The reaction proceeds by a [2+2] cylcoaddition to form a cyclobutene ring, which

then undergoes an electrocyclic ring opening (Figure 4.2) to afford the TCBD unit.[18] Alkynes

15a and **15b** reacted very quickly with TCNE to form the desired **IBF-DAD 1** and **IBF-DAD 2**.

Less electron-rich alkyne **15c** required an excess of TCNE and a longer reaction time. While the

yield for **IBF-DAD 1** was good, low yields were obtained for **IBF-DAD 2** and **IBF-DAD 0**,

presumably due to the instability of alkynes **15b** and **15c**.
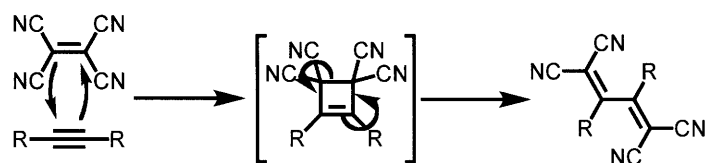
Figure 4.2 Mechanism of TCNE-alkyne interaction

Scheme 4.2 Synthesis of IBF-DAD 0-2

15a: R= OctylO- : 26% (isolated)
15b: R= Hex$_2$N- : 34% (crude)
15c: R= H- : 23% (crude)

15 b: DCM, 30 min, r.t.
15c: DCM, 2h , r.t.

IBF-DAD 1: R= OctylO- : 78%
IBF-DAD 2: R= Hex$_2$N- : 20% (6% over 2 steps)
IBF-DAD 0: R= H- : 11% (3% over 2 steps)
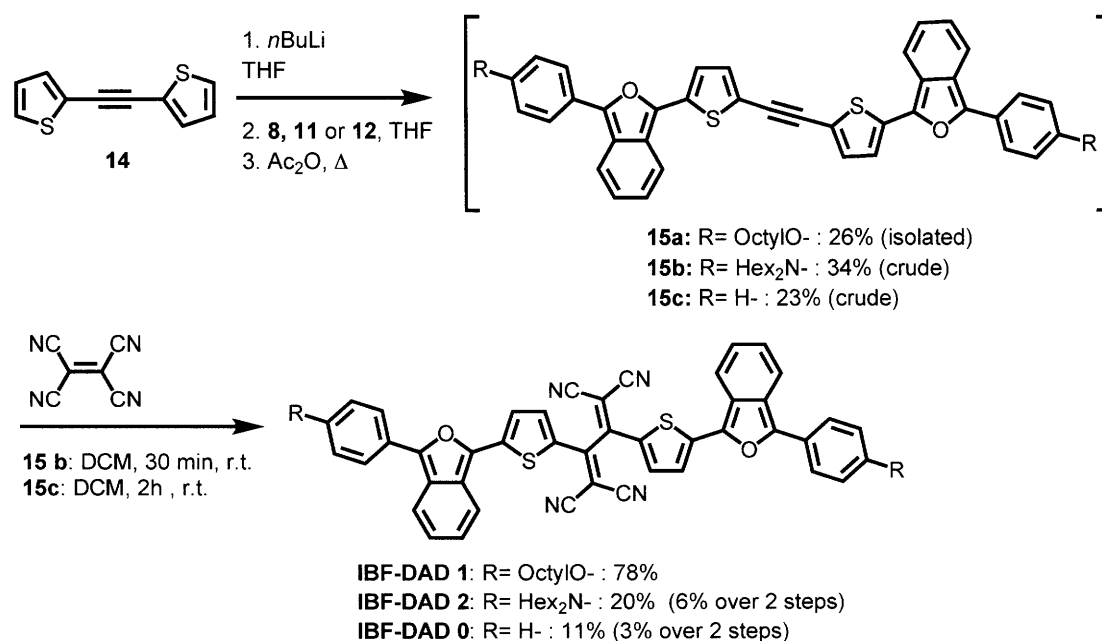
4.2.2 Spectroscopic Properties of IBF-DAD 0-2

The absorption spectra of **IBF-DAD 0-2** are shown in Figure 4.3.

IBF-DAD 0   **IBF-DAD 1**   **IBF-DAD 3**
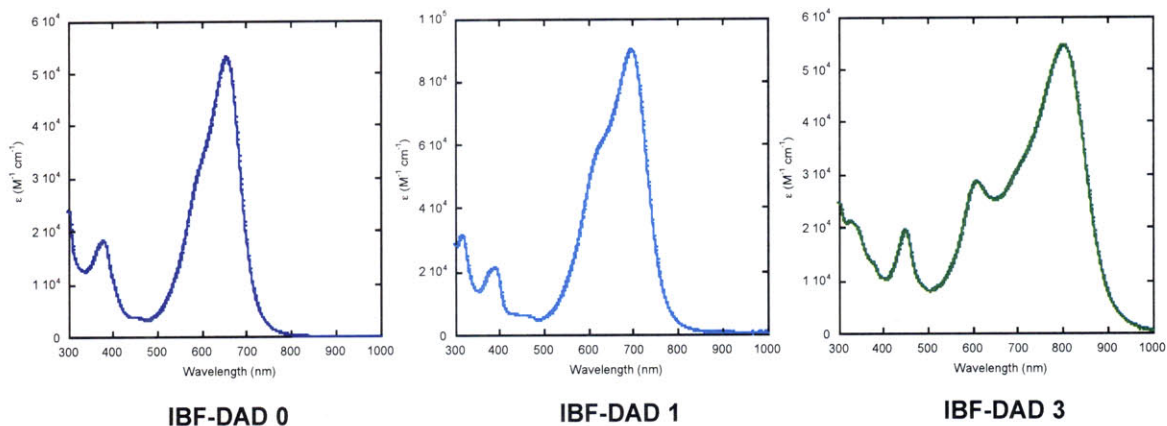
Figure 4.3 Absorption spectra (CHCl$_3$) of (left) **IBF-DAD 0**, λ_{max}= 656 nm, ε= 53300 M^{-1} cm^{-1} (center) **IBF-DAD 1**, λ_{max}= 696 nm, ε= 90400 M^{-1} cm^{-1} (right) **IBF-DAD 2**, λ_{max}= 801 nm, ε= 54800 M^{-1} cm^{-1}

The **IBF-DAD** dyes all have absorption maxima in the NIR region. They also all exhibit a shoulder peak at ~600 nm which becomes more pronounced with red-shifted absorption. As with the **IBF-NIAD** dyes series, increasing the strength of the electron donor from hydrogen to oxygen to nitrogen red shifts the absorption maxima of these chromophores. Compared to their **IBF-NIAD** counter parts, the absorption maxima **IBF-DAD 0**, **IBF-DAD 1**, and **IBF-DAD 2** are red-shifted 78 nm, 97 nm, and 145 nm respectively. The **IBF-DAD** dyes are non-fluorescent in CHCl$_3$, and while this difficiency limits their applicability in NIR two-photon imaging, it does not preclude their use in other third order NLO optical processes.

4.3 Conclusions

In conclusion, we have synthesized a series of tetracyanobutadiene donor-acceptor-donor oligomers containing isobenzofuran. These compounds all absorb in the NIR region, and, while nonfluorescent, may have interesting nonlinear optical properties, which are currently being investigated at the Institute for Soldier Nanotechnology. Depending on the outcome of these studies, these compounds may find utility in NLO material applications such as optical limiting.

4.4 Experimental Section

Materials. Commercial reagents were purchased from Sigma Aldrich, Alfa Aesar, or GFS Chemicals, and used as received. Dry solvents were obtained using a solvent purification system (Innovative Technologies, Inc.), and handled under an argon atmosphere, unless otherwise noted. Flash chromatography was performed using SiliaFlash F60 (230-400 mesh) from Silicycle.

Instrumentation. Melting points were determined in open capillaries using a Mel-Temp II apparatus and are uncorrected. Proton nuclear magnetic resonance (1H NMR) spectra and carbon nuclear magnetic resonance (^{13}C NMR) spectra were recorded on a Varian Mercury-300 (300 MHz) or an Inova-500 (500 MHz) NMR spectrometer. Chemical shifts for protons are reported in parts per million downfield from tetramethylsilane and are referenced to residual protium in the NMR solvent ($CHCl_3$: δ 7.27). Chemical shifts for carbon are reported in parts per million downfield from tetramethylsilane and are referenced to the carbon resonances of the solvent ($CDCl_3$: δ 77.0). Data are represented as follows: chemical shift, integration, multiplicity (br = broad, s = singlet, d = doublet, t = triplet, q = quartet, sp = septet, m = multiplet), and coupling constants in Hertz (Hz). High-resolution mass spectra (HRMS) were obtained at the MIT Department of Chemistry Instrumentation Facility using a peak-matching protocol to determine the mass and error range of the molecular ion, employing either electron impact or electrospray as the ionization technique. Ultraviolet-visible absorption spectra were measured with an Agilent 8453 diode array spectrophotometer and corrected for background signal with a solvent-filled cuvette.
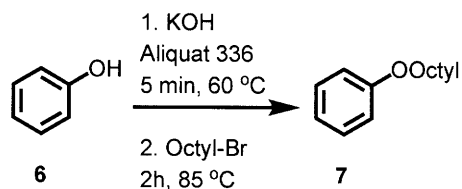
Powdered potassium hydroxide (3.5 g, 0.063 mol) and powdered phenol (4.7 g, 0.050 mol) were added to round bottom flask with Aliquot 336 (0.57 ml), and the reaction mixture was stirred for 5 minutes at 60 °C. 1-Bromooctane (8.6 ml, 0.050 mol) was added, and the reaction mixture was stirred for an additional 2 h at 85 °C. The reaction mixture was then cooled to r.t., diluted with DCM, and filtered through Florisil. The filtrate was concentrated and purified by vacuum distillation (120 °C, 300 mtorr) to afford 7 (9.0 g, 0.044 mol, 88% yield) as a clear liquid.

^{1}H NMR (500 MHz, CDCl$_3$): 9.28-9.24 (2H, m), 8.93-8.87(3H, m), 5.93 (2H, t, 6.6 Hz), 3.76 (2H, quin, 6.6 Hz), 3.44 (2H, quin, 5.6 Hz), 3.32-3.25 (8H, m), 6.37 (1H, s), 2.88 (3H, t, 7.2 Hz)

^{13}C NMR (125 MHz, CDCl$_3$): 159.1, 129.4, 120.4, 114.5, 67.8, 31.8, 29.4, 29.3, 29.2, 26.1, 22.7, 14.1 HRMS (EI): 206.1666 [calc'd for M+: 206.1665] (Adapted from literature procedure)[19]
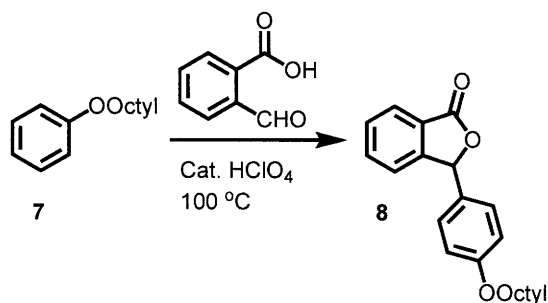
To a mixture of x (1.00 g, 6.67 mmol) in y (3.4 g, 16.5 mmol) were added 2 drops of 70% HClO$_4$, and the solution was stirred at 100 °C for 2 hours. After cooling, the reaction mixture was poured into water and stirred for 30 minutes. The sticky white product was collected by

suction filtration and was washed with water and saturated sodium bicarbonate. Recrystalization

from methanol and then hexane afforded **x** as white crystals (0.933 g, mmol, 41% yield)

^{1}H NMR (500 MHz, CDCl$_3$): 7.96 (1H, d, 7.6 Hz), 7.66 (1H, td, 7.5 Hz, 1.2 Hz), 7.56 (1H, t, 7.5

Hz), 7.32 (1H, dd, 7.6 Hz, 0.9 Hz), 7.16 (2H, dm, 8.5 Hz), 6.88 (2H, dm, 8.7 Hz), 3.95 (2H, t, 6.6

Hz), 1.76 (2H, quin, 6.6 Hz), 1.45 (2H, quin, 7.5 Hz), 1.38-1.25 (8H, m), 0.89 (3H, t, 7.2 Hz) ^{13}C

NMR (125 MHz, CDCl$_3$): 170.5, 160.0, 149.8, 134.2, 129.3, 128.7, 127.9, 125.9, 125.5, 122.9,

114.8, 82.8, 68.1, 31.8, 29.3, 29.2, 29.1, 26.0, 22.6, 14.1 HRMS (ESI): 339.1961 [calc'd for
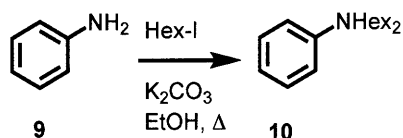
M+H$^+$: 339.1955]

To a solution of aniline (2.0 g, 0.022 mol) in ethanol (20 ml), was added K$_2$CO$_3$ (6.23 g, 0.0459

mol) and 1-iodohexane (9.57 g, 0.0451 mol), and the reaction mixture was refluxed overnight.

The reaction mixture was then cooled to r.t. and filtered, and the collected solid was washed with

DCM. The combined organic layer was dried over MgSO$_4$, concentrated in vacuo, and purified

by flash chromatography (1:1 DCM: petroleum ether (v:v), silica gel) to afford **x** (4.34 g, 0.0166

mol, 76% yield) as a pale yellow oil.

^{1}H NMR (500 MHz, CDCl$_3$): 7.22 (2H, dd, 8.9 Hz, 7.2 Hz), 6.68-6.62 (3H, m), 3.27 (4H, t, 7.8

Hz), 1.64-1.54 (4H, m), 1.38-1.24 (12H, m), 0.93 (6H, t, 6.6 Hz) ^{13}C NMR (125 MHz, CDCl$_3$):

148.1, 129.2, 115.0, 111.6, 51.0, 31.7, 27.2, 26.9, 22.7, 14.1 HRMS (ESI): 262.2532 [calc'd for

M+H$^+$: 262.2529] (Adapted from literature procedure)[20]

To a mixture of **x** (0.75 g, 5.0 mmol) in **y** (3.3 g, 12.6 mmol) were added 2 drops of 70% $HClO_4$, and the solution was stirred at 100 °C for 2 hours. After cooling, the reaction mixture was poured into water and stir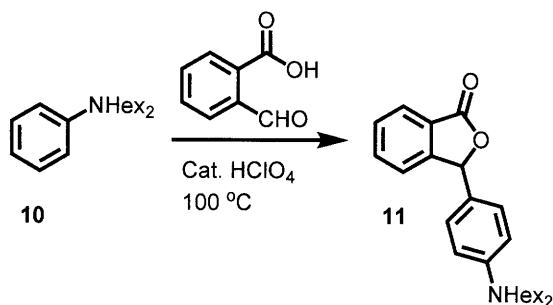red for 30 minutes. The resulting suspension was extracted with DCM, and the combined organic layers were washed with water, saturated sodium bicarbonate, and brine, dried over $MgSO_4$, and concentrated in vacuo. Purification by flash chromatography (1:4 hexane:DCM (v:v), silica gel) afforded phthalide **x** (0.54 g, 1.4 mmol, 27% yield) as a viscous yellow oil.

^{1}H NMR (500 MHz, $CDCl_3$): 7.95 (1H, t, 7.6 Hz), 7.65 (1H, t, 7.5 Hz), 7.55 (1H, t, 7.6 Hz), 7.36 (1H, d, 7.6 Hz), 7.04 (2H, d, 8.9 Hz), 6.57 (2H, d, 9.0 Hz), 6.35 (1H, s), 3.25 (4H, t, 7.8 Hz), 1.56 (4H, quin, 6.0 Hz), 1.38-1.24 (12H, m), 0.90 (6H, t, 6.9 Hz) ^{13}C NMR (125 MHz, $CDCl_3$): 170.7, 149.9, 148.9, 133.9, 129.0, 129.0, 126.4, 125.3, 123.1, 121.5, 111.3, 83.7, 51.0, 31.7, 27.1, 26.8, 22.7, 14.0 HRMS (ESI): 394.2751 [calc'd for M+H$^+$: 394.2741]
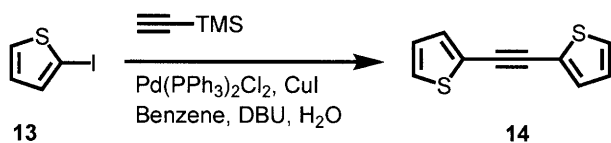
A flame dried, argon purged schlenk flash was charged with 2-iodothiophene (1.05 g, 5.08 mmol), $PdCl_2(PPh_3)_2$ (0.105 g, 0.150 mmol), and CuI (0.095 g, 0.50 mmol), and was then evacuated and purged with argon three times. Dry benzene (25 ml) was added, and the flask was purged with argon. DBU (4.5 ml, 0.030 mol, distilled from CaH_2) was then added, and the flask was purged again with argon. Ice cold TMS-acetylene (0.356 ml, 2.7 mmol) was then added,

followed immediately by water (36 μl). The flask was covered with aluminum foil and the reaction mixture was stirred for 18h at r.t. The reaction mixture was then partitioned between ethyl ether and distilled water, and the organic layer was separated, washed with 10% HCl and brine, dried over $MgSO_4$, and concentrated in vacuo. The residue was taken up in hot hexane and filtered, and then concentrated in vacuo. Recrystallization from hexane afforded **14** (0.13 g, 0.68 mmol, 14% yield) as off-white crystals.

^{1}H NMR (500 MHz, $CDCl_3$): 7.32 (2H, dd, 5.2 Hz, 1.1 Hz), 7.29 (2H, dd, 3.7 Hz, 1.1 Hz), 7.03 (2H, dd, 5.2 Hz, 3.7 Hz) ^{13}C NMR (125 MHz, $CDCl_3$): 132.1, 127.6, 127.1, 122.9, 86.2 HRMS (ESI): 190.9991 [calc'd for M+H$^+$: 190.9984]
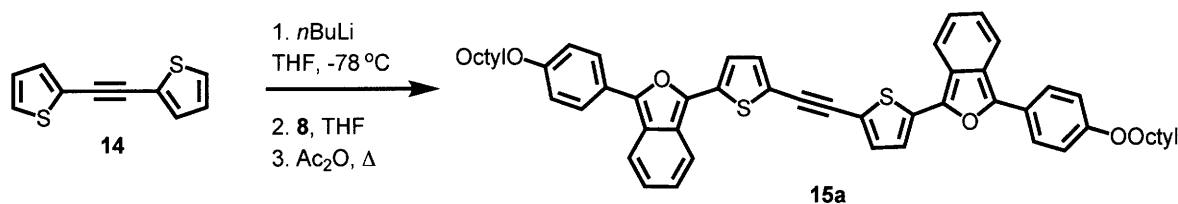
n-BuLi (0.72 ml of 1.6M solution in hexanes, 1.15 mmol) was added to a solution of **14** (0.100 g, 0.526 mmol) in dry THF (4 ml) in a vacuum dried Schlenk flask at -78 °C under argon, and the solution was stirred at -78 °C for 2 h. A solution of phthalide **x** (0.39 g, 1.2 mmol) in dry THF (5 ml) was added dropwise, and the reaction mixture was stirred at -78 °C for an additional hour. Acetic anhydride (0.15 ml, 1.6 mmol) was added, and the solution was warmed to room temperature, and was then refluxed for 10 minutes. The reaction mixture was cooled to room temperature, and was then diluted with ethyl acetate and washed with saturated aqueous sodium bicarbonate and brine. The organic layer was dried over magnesium sulfate and concentrated in vacuo. The residue was taken up in $CHCl_3$ and precipitated from MeOH. The precipitate was

collected by suction filtration and sonicated in MeOH. Recrystallization from cyclohexane afforded **x** (0.113 g, 0.136 mmol, 26% yield) as a purple solid.

^{1}H NMR (500 MHz, CDCl$_3$): 7.84 (2H, dm, 8.9 Hz), 7.76 (1H, dt, 8.9 Hz, 1.1 Hz), 7.68 (1H, dt, 8.7 Hz, 1.1 Hz), 7.34 (1H, d, 4.0 Hz), 7.28 (1H, d, 3.8 Hz), 7.07-6.99 (4H, m), 4.03 (2H, t, 6.7 Hz), 1.83 (2H, quin, 6.7 Hz), 1.50 (2H, quin, 7.6 Hz), 1.51-1.29 (8H, m), 0.92 (3H, t, 7.2 Hz) ^{13}C NMR (125 MHz, CDCl$_3$): 158.6, 144.6, 138.7, 135.3, 132.8, 126.3, 125.7, 125.0, 123.9, 122.4, 121.2, 120.9, 120.4, 120.2, 119.7, 115.1, 88.7, 68.1, 31.8, 29.4, 29.3, 26.0, 22.7, 14.1 HRMS (ESI): 830.3550 [calc'd for M+H$^+$: 830.3536]

15a

IBF-DAD 1
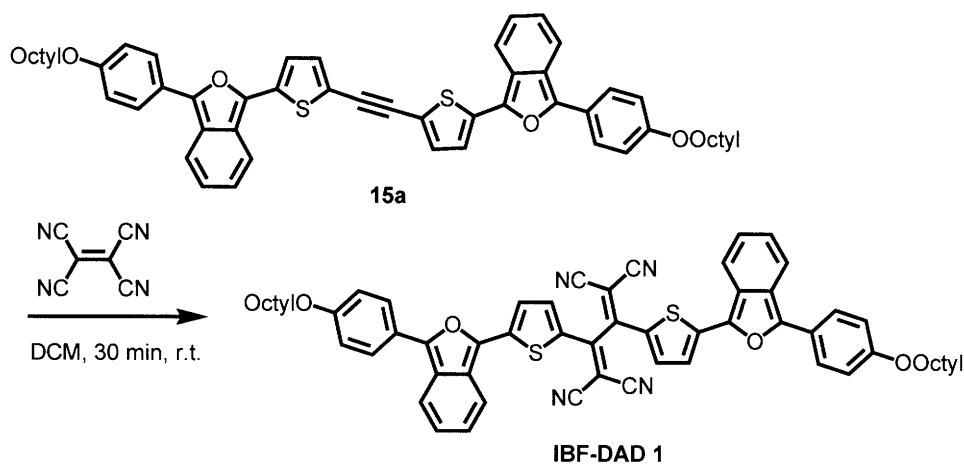
To a stirred solution of **15a** (0.050 g, 0.060 mmol) in 5 ml DCM was added tetracyanoethylene (0.0080 g, 0.063 mmol), and the reaction mixture was stirred for 30 minutes at r.t. The resulting blue solution was purified by flash chromatography (DCM, silica gel) to afford **IBF-DAD 1** (0.045 g, 0.047 mmol, 78% yield) as a dark solid.

^{1}H NMR (500 MHz, CDCl$_3$): 7.88-7.76 (4H, m), 7.61 (2H, d, 8.7 Hz), 7.40 (2H, d, 4.6 Hz), 7.23 (2H, t, 8.0 Hz), 7.11 (2H, t, 8.1 Hz), 6.99 (4H, d, 8.9 Hz), 4.03 (4H, t, 6.6 Hz), 1.83 (4H, quin, 7.6 Hz), 1.48 (4H, quin, 7.6 Hz), 1.42-1.24 (16H, m), 0.90 (6H, t, 6.9 Hz) ^{13}C NMR (125 MHz, CDCl$_3$): 160.4, 154.4, 150.6, 145.5, 139.2, 137.7, 130.7, 129.3, 127.6, 127.4, 126.2, 122.9,

122.2, 122.1, 121.6, 119.5, 115.3, 114.7, 113.6, 72.4, 68.3, 31.8, 29.4, 29.2, 29.1, 26.0, 22.6, 14.1

HRMS (ESI): 959.3659 [calc'd for M+H$^+$: 959.3659] UV-vis λ_{max}: 696 nm (CHCl$_3$, ϵ = 90400 M^{-1} cm^{-1})
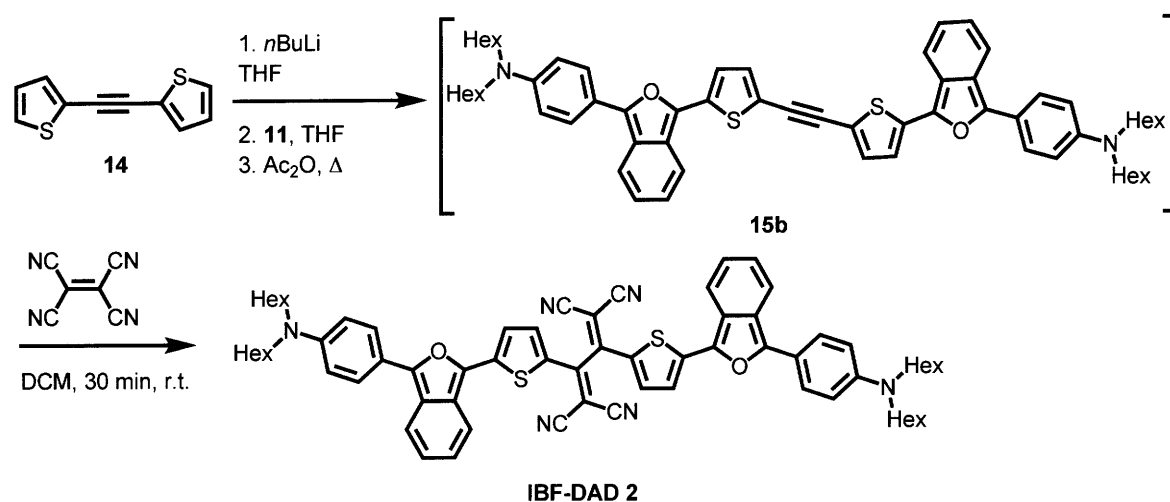
n-BuLi (0.72 ml of 1.6M solution in hexanes, 1.15 mmol) was added to a solution of **14** (0.100 g, 0.526 mmol) in dry THF (5 ml) in a vacuum dried Schlenk flask at -78 °C under argon, and the solution was stirred at -78 °C for 2 h. A solution of phthalide **11** (0.41 g, 1.0 mmol) in dry THF (5 ml) was added dropwise, and the reaction mixture was stirred at -78 °C for an additional hour. Acetic anhydride (0.15 ml, 1.6 mmol) was added, and the solution was warmed to room temperature, and was then refluxed for 10 minutes. The reaction mixture was cooled to room temperature, and was then diluted with ethyl acetate and washed with saturated aqueous sodium bicarbonate and brine. The organic layer was dried over magnesium sulfate and concentrated in vacuo to afford alkyne **15b** (0.166 g, 0.177 mmol, 34%) as a crude product. **15b** (0.085 g, 0.091 mmol) was dissolved in DCM (7 ml) with tetracyanoethylene (0.012 g, 0.094 mmol) and the reaction mixture was stirred for 30 minutes. The reaction mixture was then purified by flash chromatography (DCM, silica gel) to afford **IBF-DAD 2** (0.0178 g, 0.018 mmol, 20% yield, 7%

over 2 steps) ^{1}H NMR (500 MHz, CDCl$_3$): 7.94 (2H, d, 8.9 Hz), 7.90-7.78 (6H, m), 7.72 (2H, d, 8.7 Hz), 7.42 (2H, d, 4.7 Hz), 7.32 (2H, dd, 8.7 Hz, 6.6 Hz), 7.14 (2H, dd, 8.9 Hz, 6.7 Hz), 6.74 (4H, d, 9.3 Hz), 3.37 (8H, t, 7.8 Hz), 1.64 (8H, quin, 7.0 Hz), 1.42-1.30 (24H, m), 0.92 (12H, t, 7.0 Hz) ^{13}C NMR (125 MHz, CDCl$_3$): 153.7, 153.0, 149.2, 145.6, 139.1, 137.1, 129.9, 129.6, 128.5, 128.0, 125.5, 122.4, 122.0, 119.7, 116.4, 115.5, 114.2, 111.9, 69.9, 51.1, 31.7, 27.3, 26.8, 22.7, 14.0 HRMS (ESI): 1069.5301 [calc'd for M+H$^+$: 1069.5231] UV-vis λ_{max}: 801 nm (CHCl$_3$, ε = 54800 M^{-1} cm^{-1})
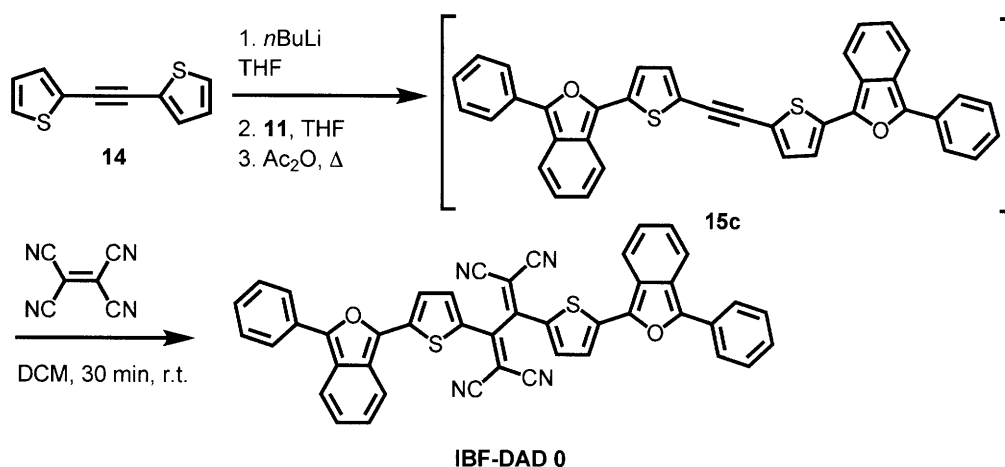
IBF-DAD 0

n-BuLi (0.72 ml of 1.6M *solution* in hexanes, 1.15 mmol) was added to a solution of **14** (0.100 g, 0.526 mmol) in dry THF (5 ml) in a vacuum dried Schlenk flask at -78 °C under argon, and the solution was stirred at -78 °C for 2 h. A solution of phthalide **12** (0.22 g, 1.0 mmol) in dry THF (5 ml) was added dropwise, and the reaction mixture was stirred at -78 °C for an additional hour. Acetic anhydride (0.15 ml, 1.6 mmol) was added, and the solution was warmed to room temperature, and was then refluxed for 10 minutes. The reaction mixture was cooled to room temperature, and was then diluted with ethyl acetate and washed with saturated aqueous sodium bicarbonate and brine. The organic layer was dried over magnesium sulfate and concentrated in vacuo to 5 ml. This solution was added to hexane (15 ml) and **15c** (0.066 g, 0.12 mmol, 23% yield) was collected by suction filtration as a crude product. This solid was dissolved in DCM

(10 ml) with tetracyanoethylene (0.016 g, 0.13 mmol) and the reaction mixture was stirred for 1 hour at r.t., and then additional tetracyanoethylene (0.0115 g, 0.093 mmol) was added and the reaction was stirred for another hour. The reaction mixture was then purified by flash chromatography (DCM, silica gel) to afford **IBF-DAD 0** (0.0095 g, 0.014 mmol, 11% yield, 3% over 2 steps)

^{1}H NMR (500 MHz, CDCl$_3$): 8.03-7.96 (6H, m), 7.92 (4H, 4.6 Hz), 7.82 (2H, d, 8.9 Hz), 7.62 (2H, d, 4.6 Hz), 7.55 (4H, t, 8.1 Hz), 7.44 (2H, t, 7.5 Hz), 7.34 (2H, dd, 8.5 Hz, 6.3 Hz), 7.22 (2H, dd, 9.2 Hz, 6.7 Hz) ^{13}C NMR (125 MHz, CDCl$_3$): 154.8, 149.9, 145.6, 139.1, 138.6, 131.4, 129.8, 129.4, 129.34, 129.25, 127.1, 126.8, 126.1, 123.6, 123.2, 121.4, 119.7, 114.2, 112.9, 74.2 HRMS (ESI): 703.1268 [calc'd for M+H$^+$: 703.1257] UV-vis λ_{max}: 656 nm (CHCl$_3$, ε = 53300 M^{-1} cm^{-1})

4.5 References

(1)   *Organic Electronics*; Klauk, H.; Ed.; Wiley, Weinheim, 2006.

(2)   Mitschke, U.; Bäuerle, P. *J. Mater. Chem.* **2000**, *10*, 1471.

(3)   Roncali, J. *Chem. Soc. Rev.* **2005**, *34*, 483.

(4)   Faccheti, A.; Marks, T. J.; Katz, H. E.; Veinot, J.; Organic Semiconductor Materials. In *Printed Organic and Molecular Electronics*; Gamota, D.; Brazis, P; Kalyanasundaram, K.; Zhang, J.; Eds.; Kluwer Academic Publishers, New York, 2004.

(5)   Thomas, S. W.; Joly, G. D.; Swager, T. M. *Chem. Rev.* **2007**, *107*, 1339.

(6)   Jiang, M.; Fang, Q.; *Adv. Mater.* **1999**, *11*, 1147.

(7)   Anslyn, E. V.; Dougherty, D. A.; *Modern Physical Organic Chemistry*; University Science Books: Sausalito, California, 2006.

(8)   Bredas, J. L.; Adant, C.; Tackx, P. Persoons, A.; Pierce, B. M. *Chem. Rev.* **1994**, *94*, 243.

(9)   Prasad, P. N.; Williams, D. J. *Introduction to Nonlinear Optical Effects in Molecules and Polymers*, Wiley, New York, 1991.

(10)   Bubeck, C. Nonlinear Optical Properties of Oligomers. In *Electronic Materials: The Oligomer Approach*; Mullen, K.; Ed.; Wiley, New York, 1998.

(11)   Gerstenberger, D. C.; Tye, G. E.; Wallace, R. W. *Opt. Lett.* **1991**, *16*, 992.

(12)   Ehrlich, J. E. Wu, X. L.; Lee, I.-Y. S.; Rockel, H.; Marder, S. R.; Perry, J. W. *Opt. Lett.* **1997**, *22*, 1840.

(13)   Yang, Y.; Farley, R. T.; Steckler, T. T.; Eom, S.; Reynolds, J. R.; Schanze, K. S.; Xue, J.; *App. Phys. Lett.* **2008**, *93*, 163305.

(14)   Qian, G.; Zhong, Z.; Luo, M.; Yu, D.; Zhang, Z.; Ma, D.; Wang, Z. Y. *J. Phys. Chem.* **2009**, *113*, 1589.

(15)   Peng, P.; Zhou, Y.; Li, K.; Zhang, H.; Xia, H.; Zhao, Y.; Tian, W. *Synth. Met.* **2009**, *159*, 153.

(16)   Albota, M.; Beljonne, D.; Breda, J.; Ehrlich, J. E.; Fu, J.; Heikal, A. A.; Hess, S. E.; Kogej, T.; Levin, M, D.; Marder, S. R., Mcord-Maughon, D.; Perry, J. W.; Rockel, H.; Rumi, M.; Subramaniam, G.; Webb, W. W.; Wu, X.; Xu, C. *Science* **1998**, *281*, 1653.

(17)   Michinobu, T.; May, J. C.; Lim, J. H.; Boudin, C.; Gisselbrecht, J.; Seiler, P.; Gross, M.; Biaggio, I.; Diederich, F. *Chem. Commun.* **2005**, 737.

(18)   Morioka, Y.; Yoshizawa, N.; Nishida, J.; Yamashita, Y. *Chem. Lett.* **2004**, *33*, 1190.

(19)   Loupy, A.; Sansoulet, J.; Vaziri-Zand, F. *Bull. Soc.Chim. France* **1987**, 1027.

(20)   Raimundo, J.; Blanchard, P.; Gallego-Planas, N.; Mercier, N.; Ledoux-Rak, I.; Hierle, R. Roncali, J. *J. Org. Chem.* **2002**, *67*, 205.
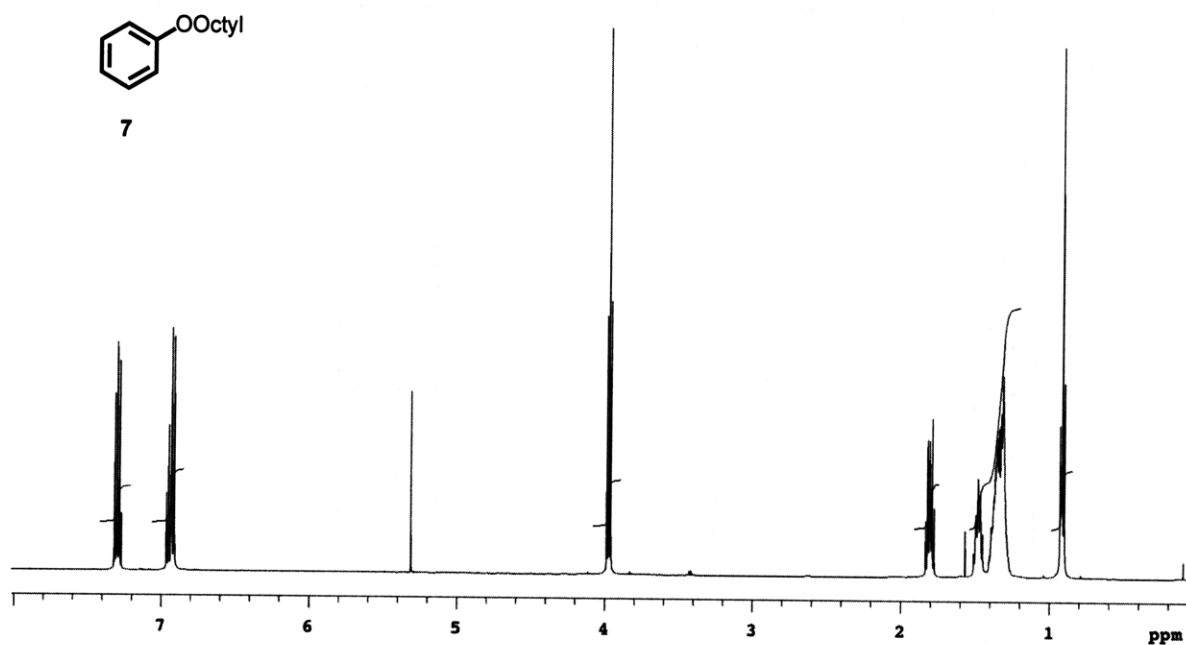
4.A Appendix

^{1}H NMR and ^{13}C NMR Spectra
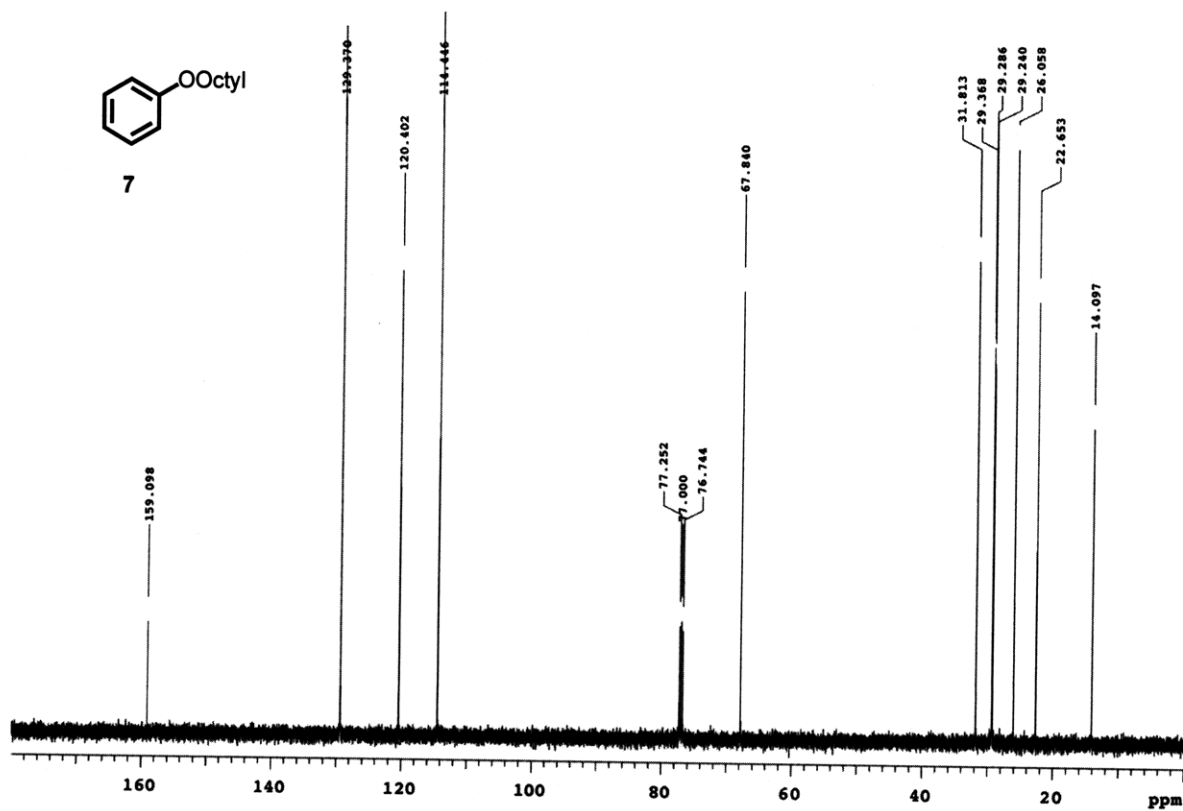
Figure 4.A.1 ^{1}H NMR (500 MHz, CDCl$_3$) of **7**

Figure 4.A.2 ^{13}C NMR (125 MHz, CDCl$_3$) of **7**

242
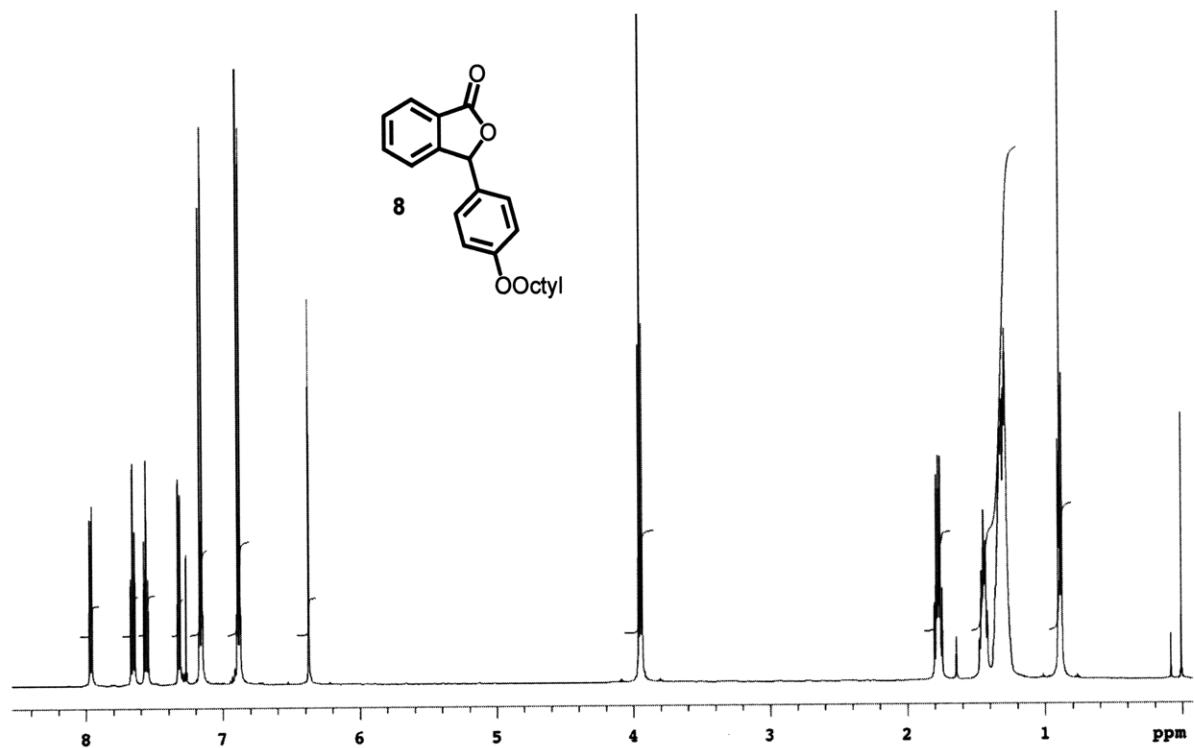
Figure 4.A.3 ^{1}H NMR (500 MHz, CDCl$_3$) of **8**
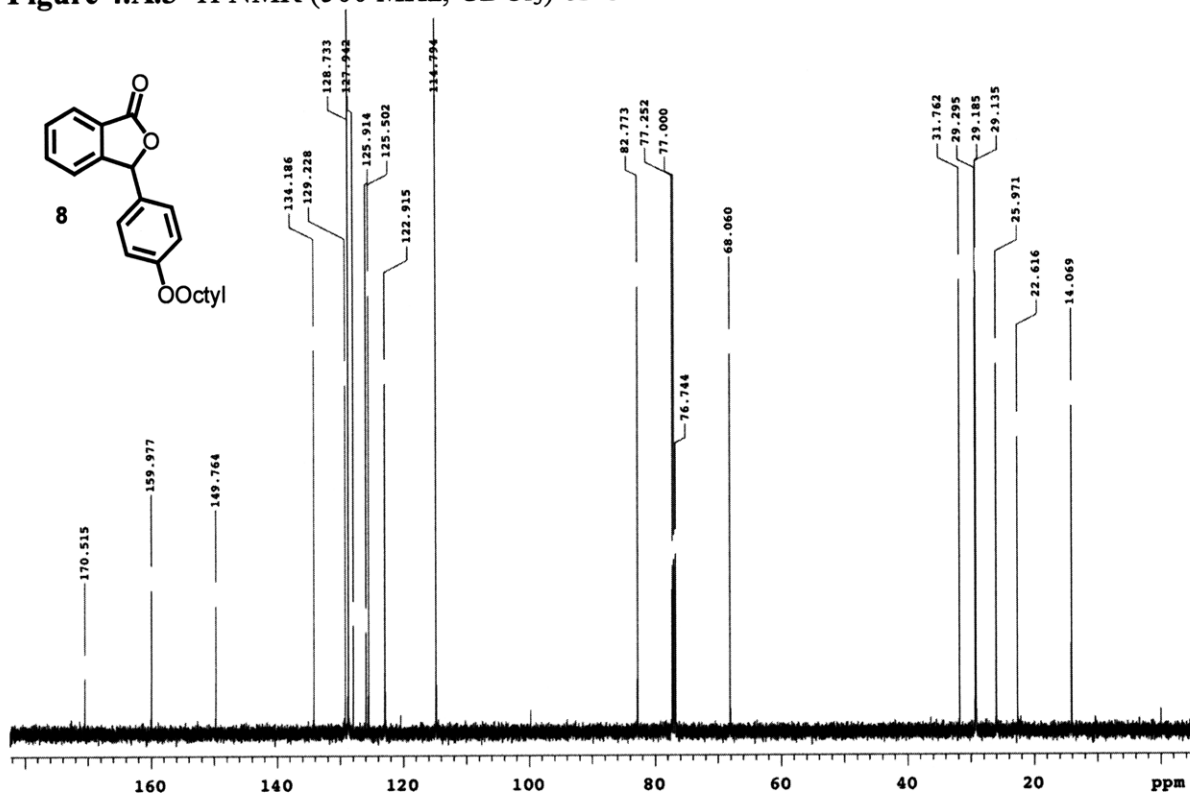
Figure 4.A.4 ^{13}C NMR (125 MHz, CDCl$_3$) of **8**
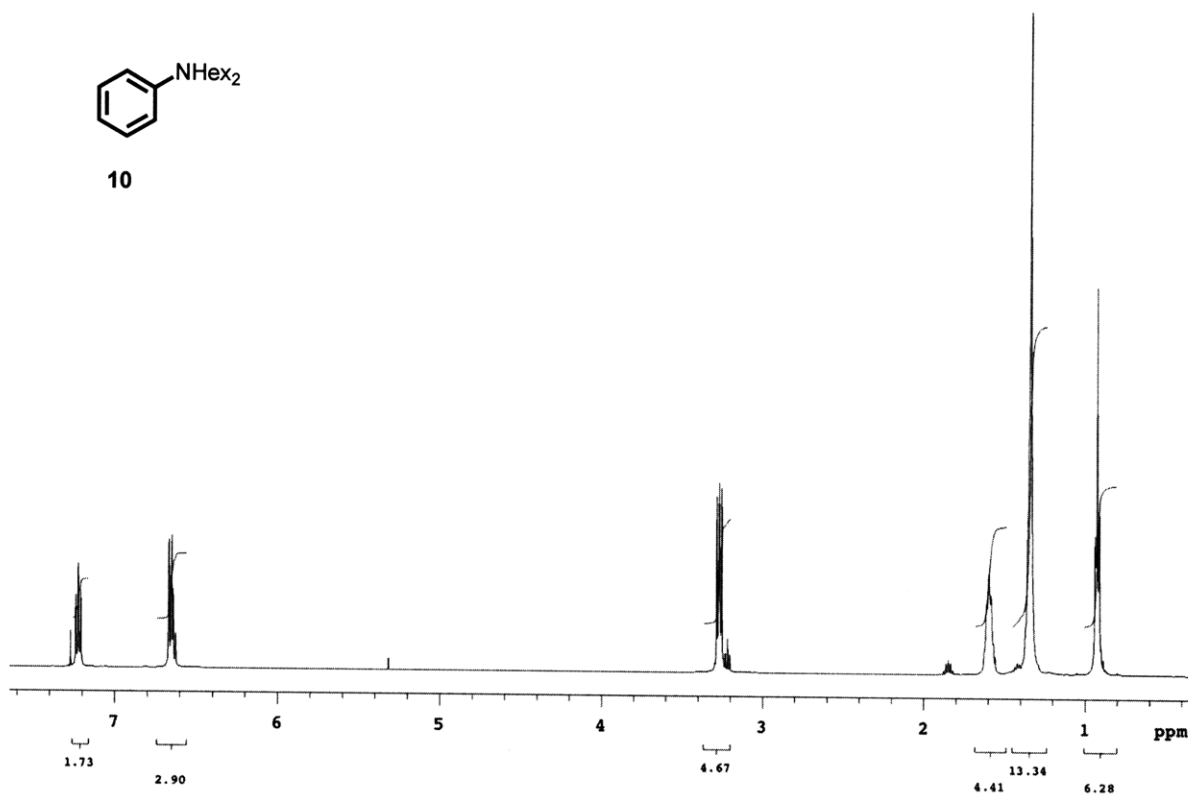
Figure 4.A.5 ^{1}H NMR (500 MHz, CDCl$_3$) of **10**
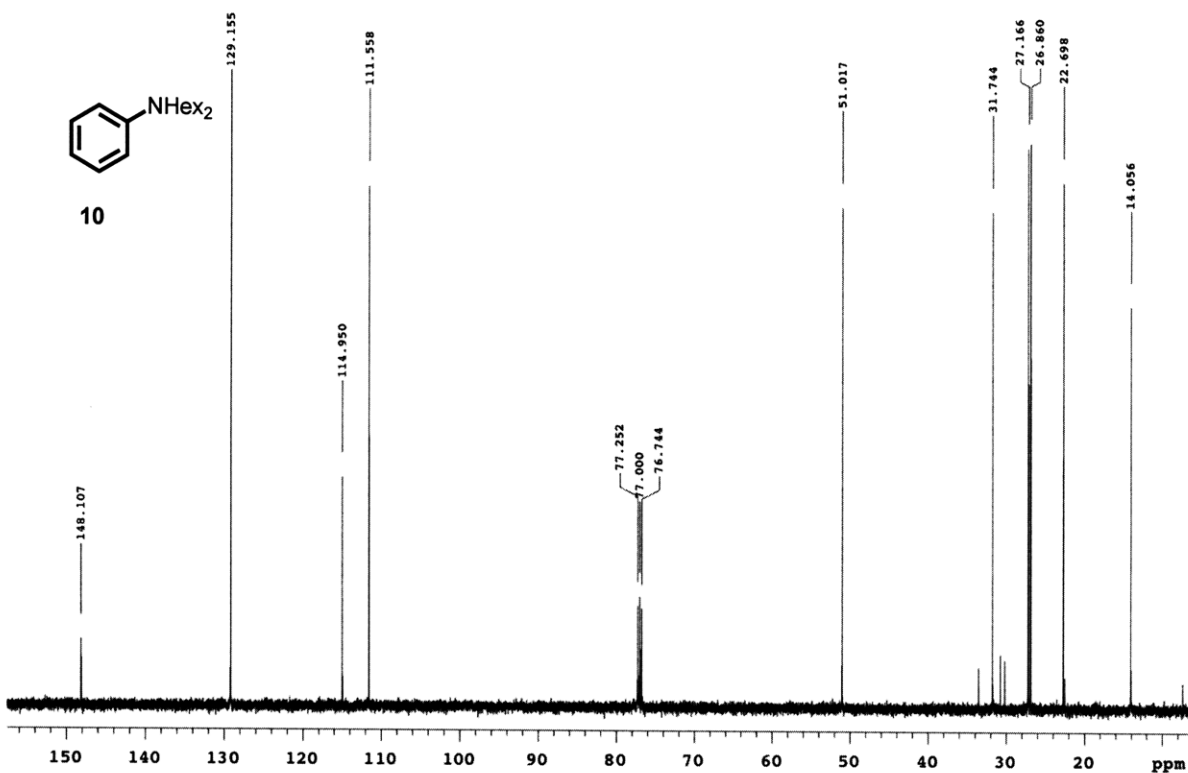
Figure 4.A.6 ^{13}C NMR (125 MHz, CDCl$_3$) of **10**
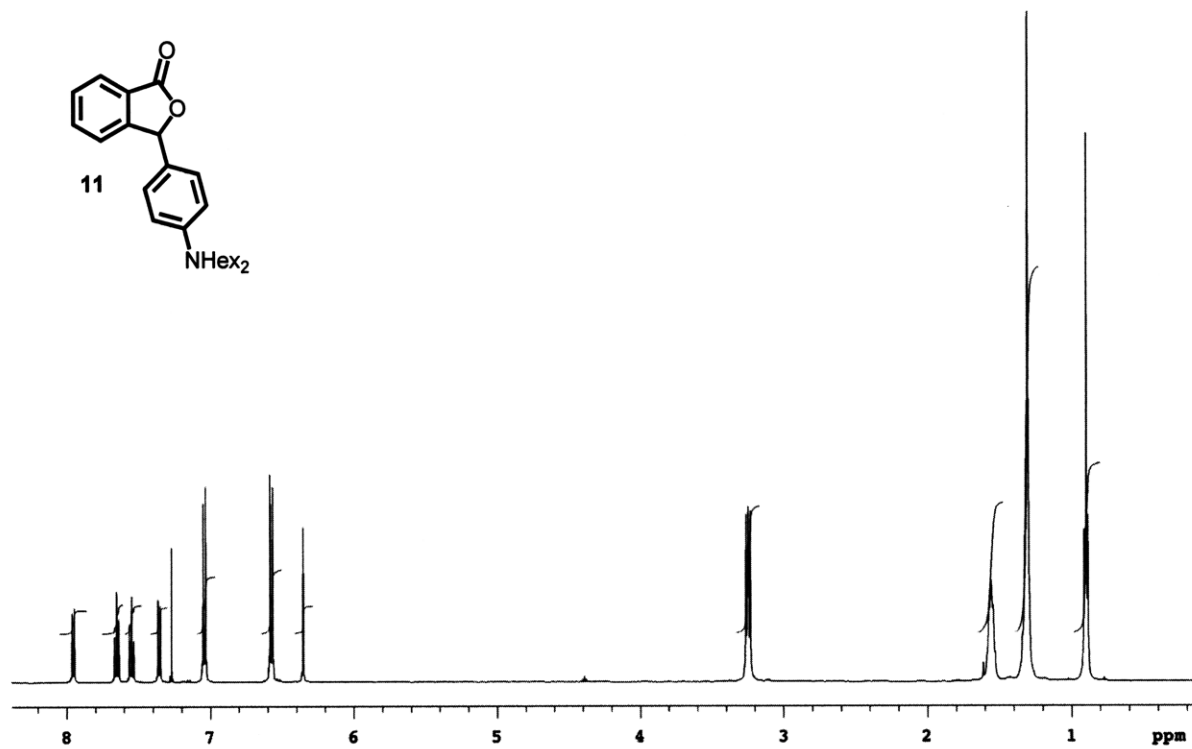
Figure 4.A.7 ^{1}H NMR (500 MHz, CDCl$_3$) of **11**
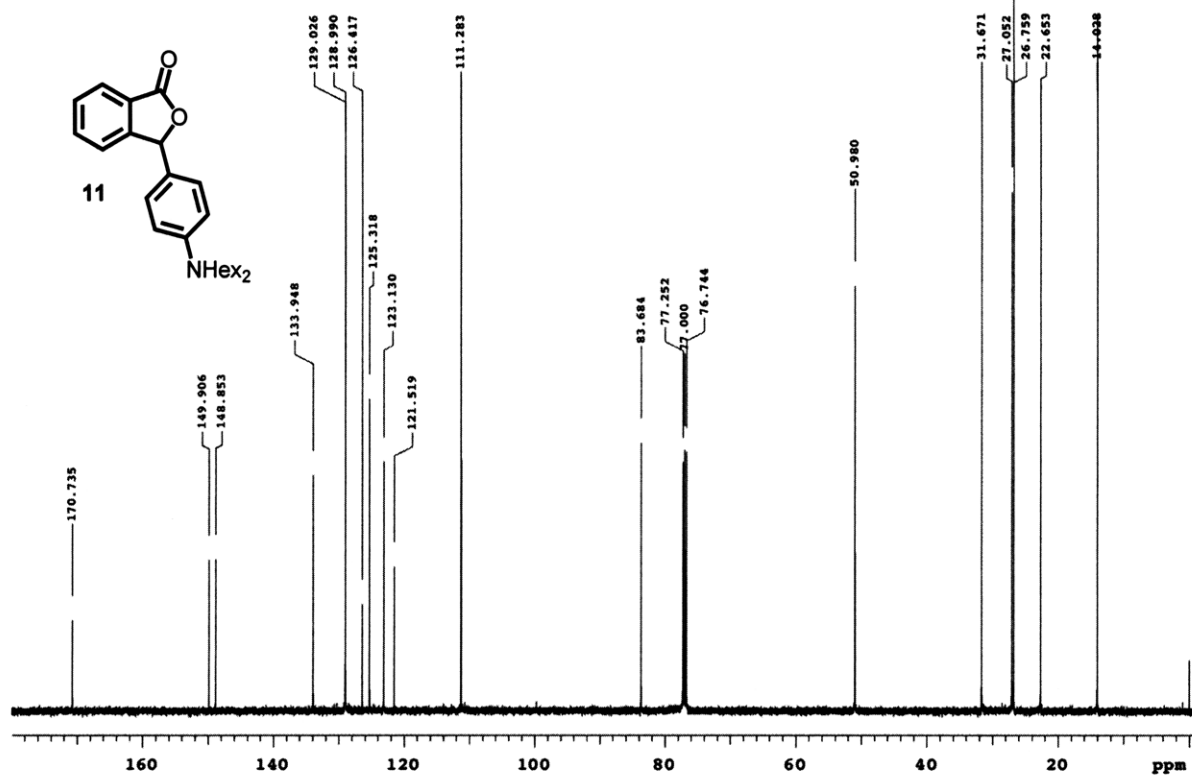
Figure 4.A.8 ^{13}C NMR (125 MHz, CDCl$_3$) of **11**
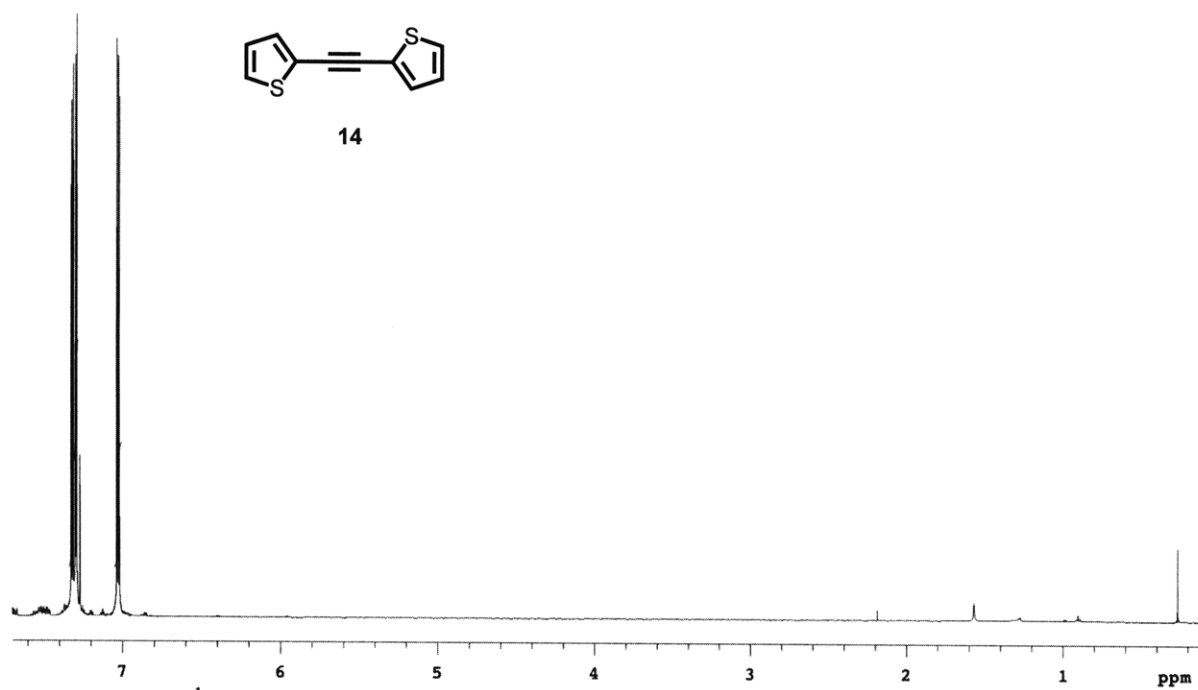
Figure 4.A.9 ^{1}H NMR (500 MHz, CDCl$_3$) of **14**
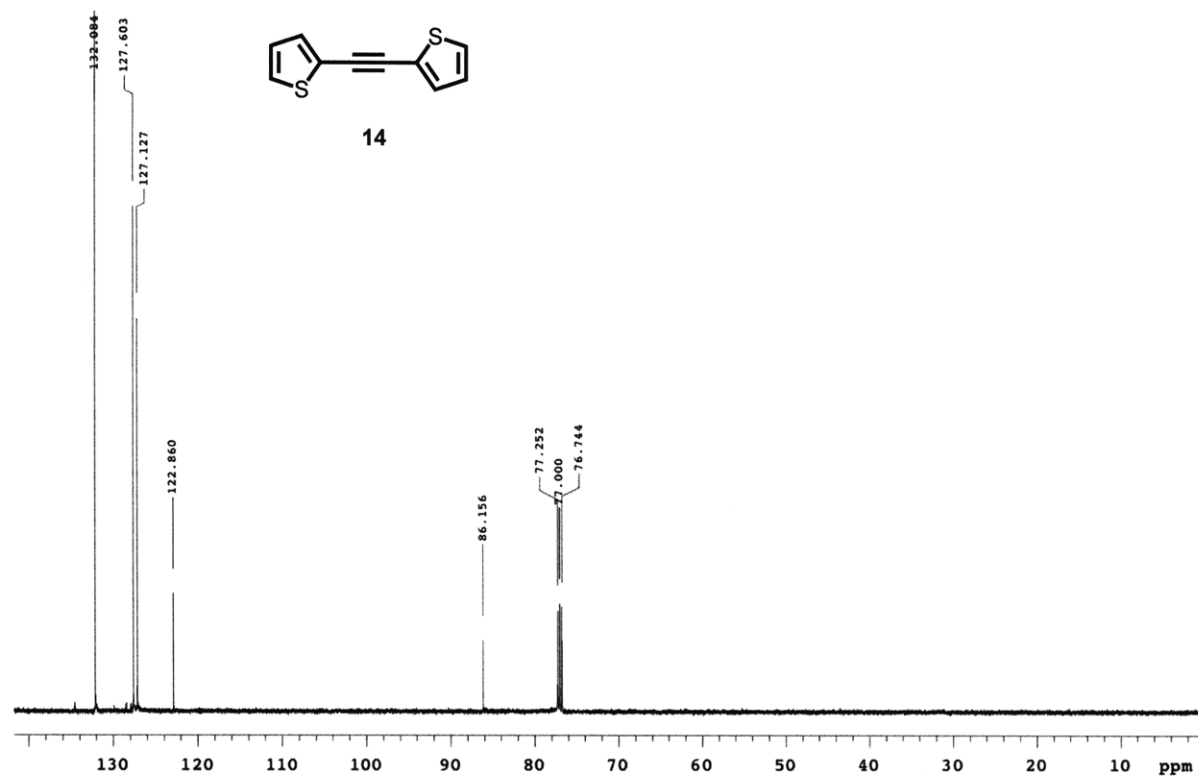
Figure 4.A.10 ^{13}C NMR (125 MHz, CDCl$_3$) of **14**
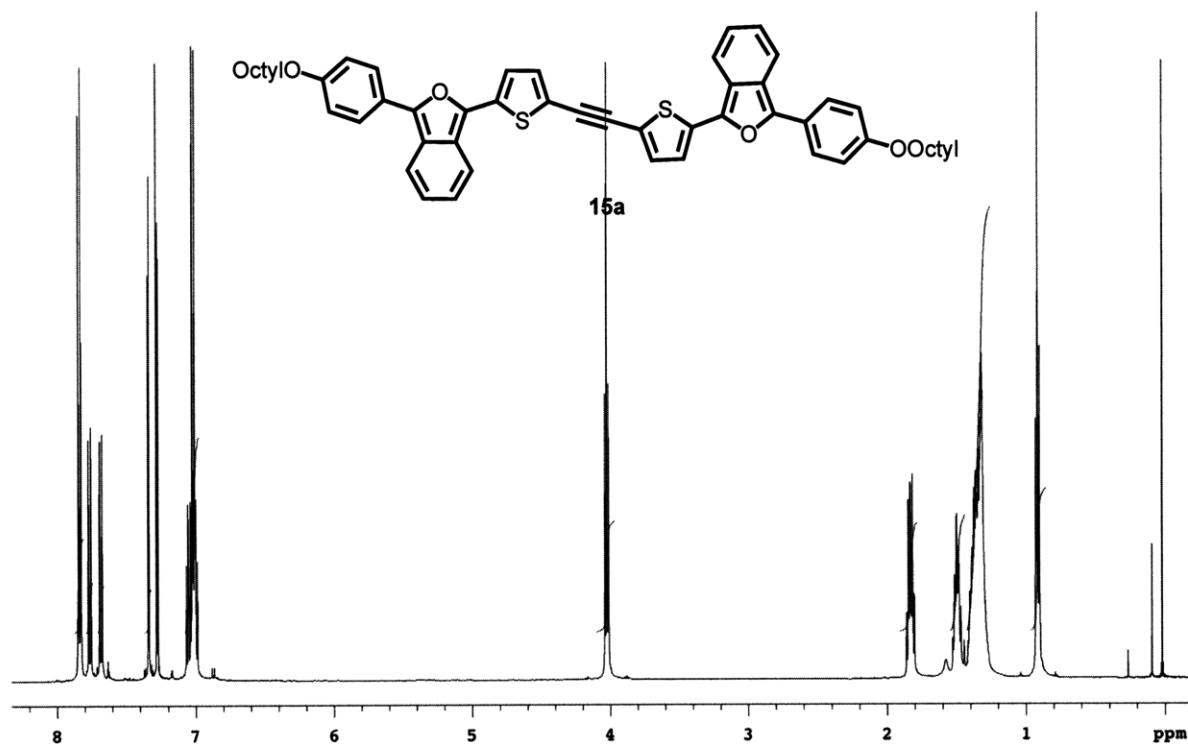
Figure 4.A.11 ^{1}H NMR (500 MHz, CDCl$_3$) of **15a**
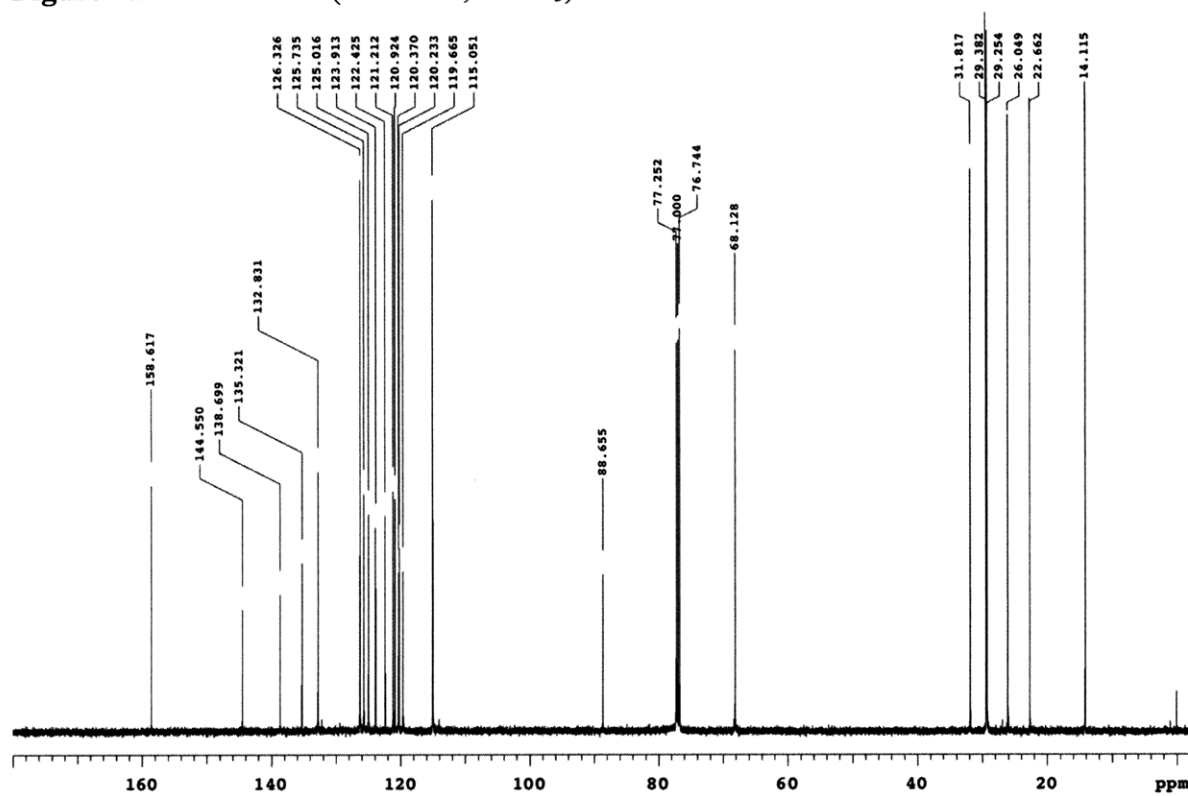
Figure 4.A.12 ^{13}C NMR (125 MHz, CDCl$_3$) of **15a**
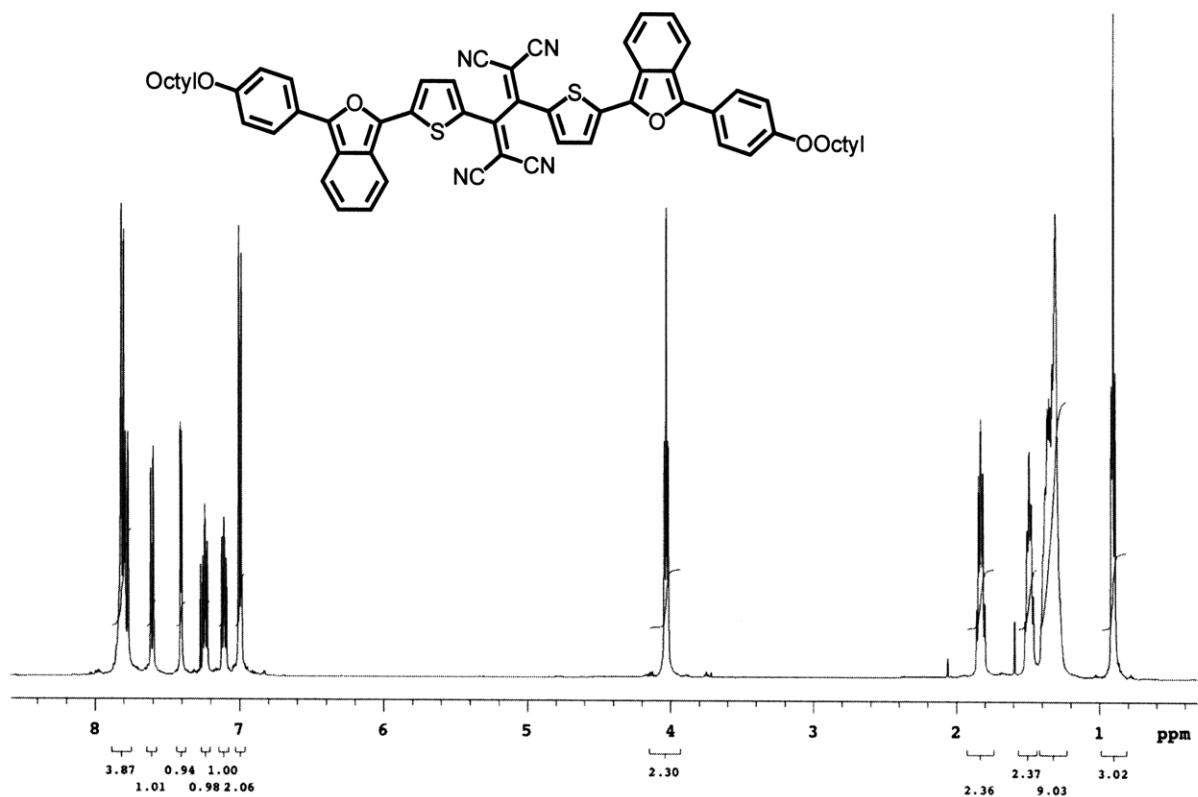
Figure 4.A.13 ^{1}H NMR (500 MHz, CDCl$_3$) of **IBF-DAD 1**
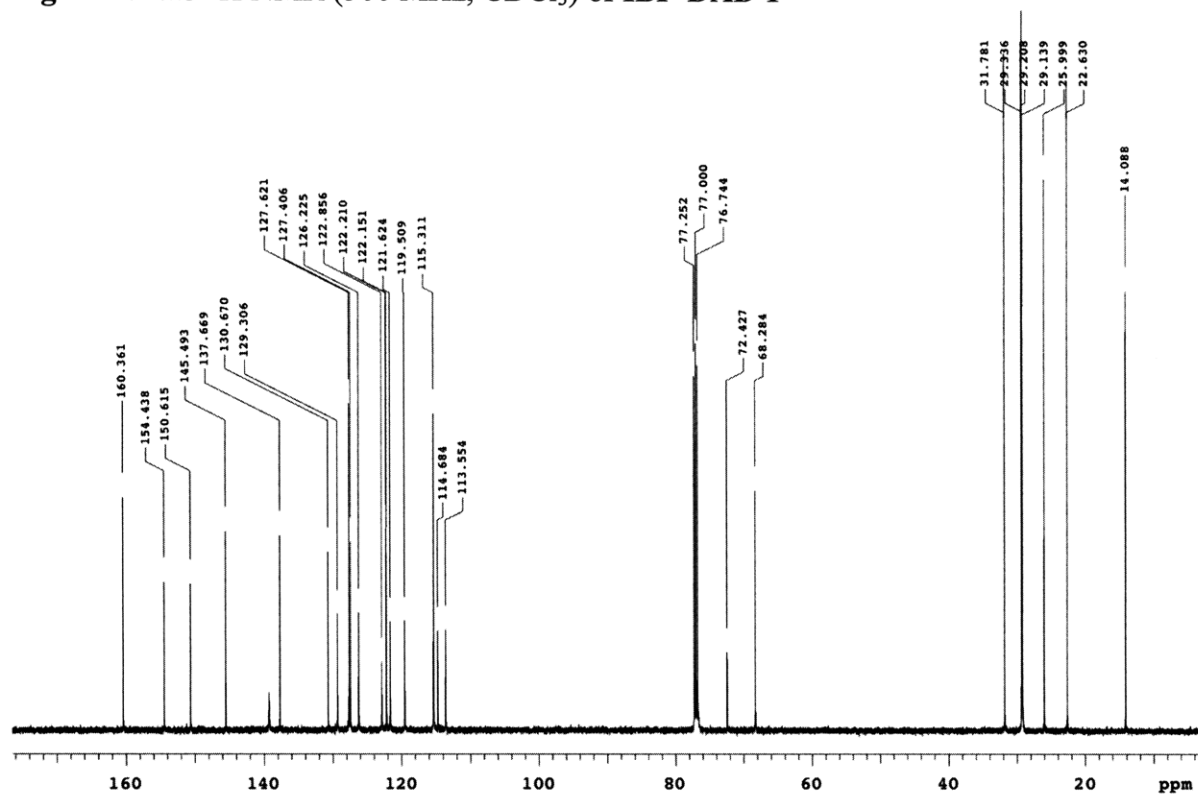
Figure 4.A.14 ^{13}C NMR (125 MHz, CDCl$_3$) of **IBF-DAD 1**
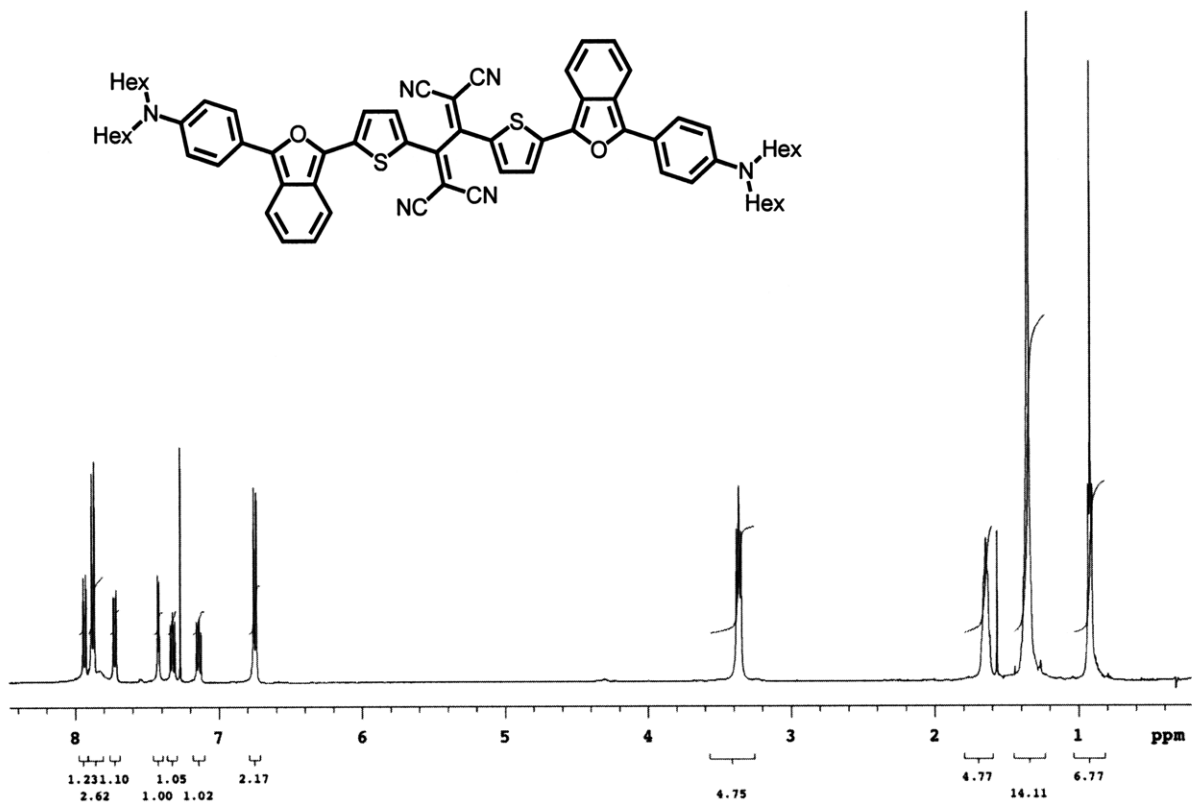
Figure 4.A.15 ^{1}H NMR (500 MHz, CDCl$_3$) of **IBF-DAD 2**
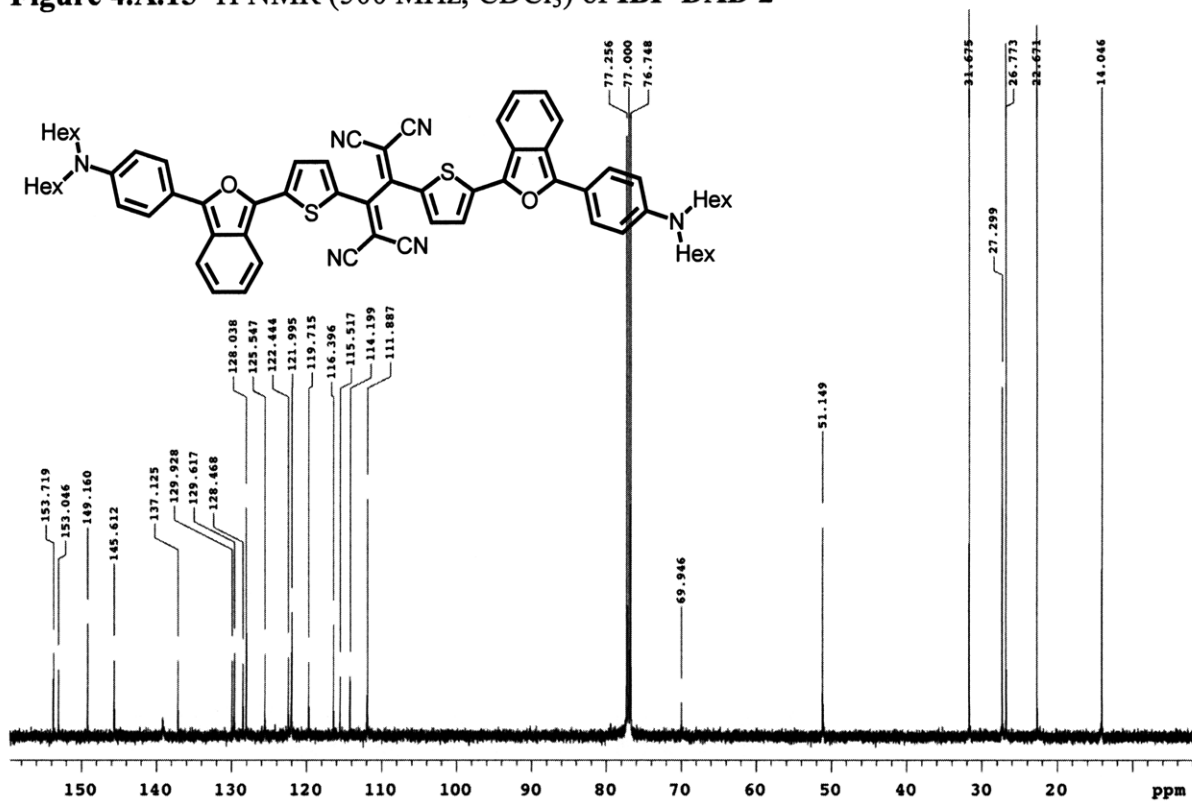
Figure 4.A.16 ^{13}C NMR (125 MHz, CDCl$_3$) of **IBF-DAD 2**

249
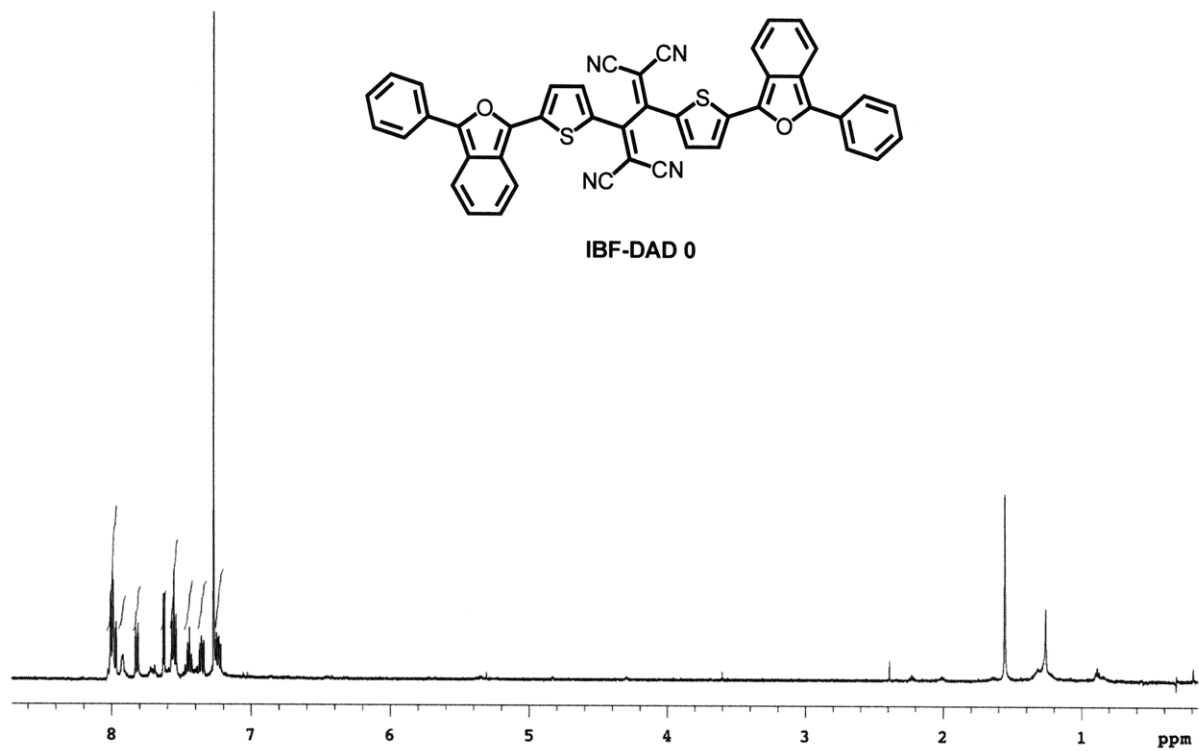
IBF-DAD 0

Figure 4.A.17 ^{1}H NMR (500 MHz, CDCl$_3$) of **IBF-DAD 0**
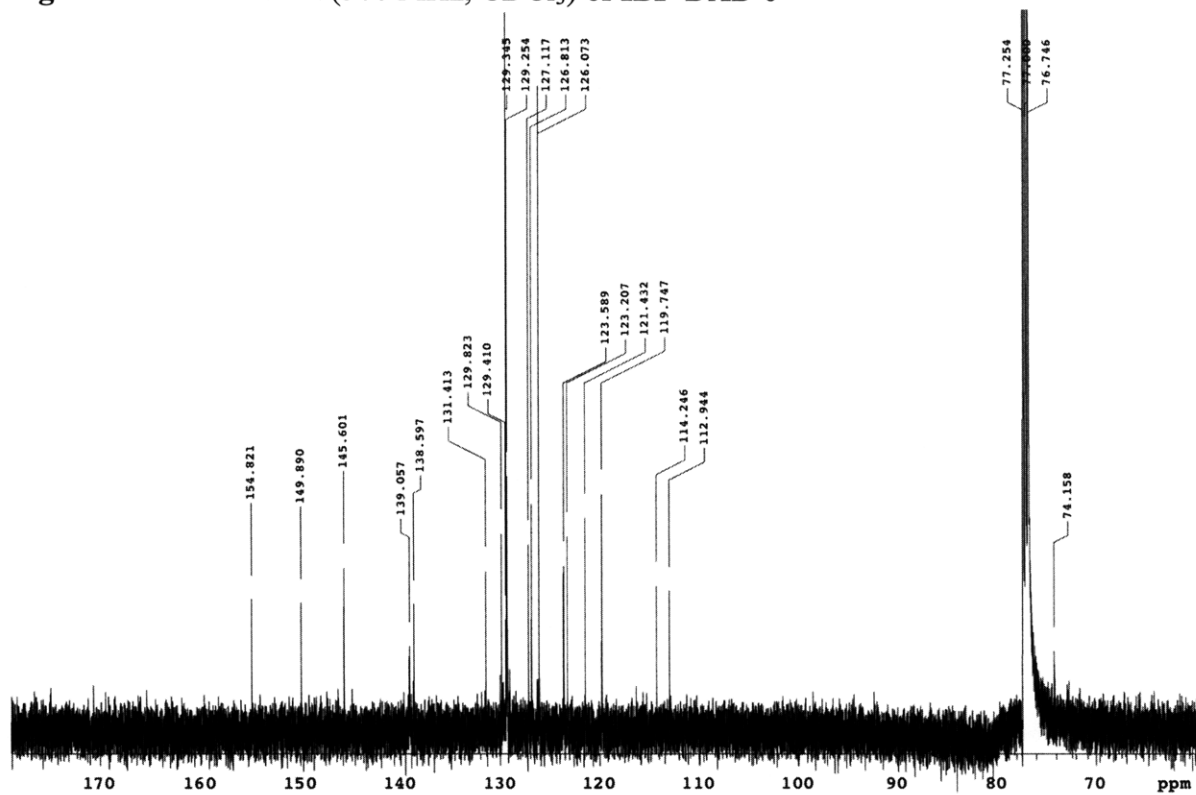
Figure 4.A.18 ^{13}C NMR (125 MHz, CDCl$_3$) of **IBF-DAD 0**

Scott T. Meek

QUALIFICATIONS

- Materials chemist with strong background in organic synthesis
- Design and execution of multi-step syntheses of dyes and monomers
- Characterization of organic small molecules and polymers using a broad spectrum of methods: NMR, FTIR, UV-VIS, fluorescence spectroscopy, GC/MS, GPC, electrochemical analysis, profilometry
- Experience with air-free techniques, chemical and electrochemical polymerization

EDUCATION

Ph.D., Massachusetts Institute of Technology, Cambridge, MA (2003-present)
- Thesis Title: New Optical Materials Containing Isobenzofuran (advisor: Timothy M. Swager, Dept. of Chemistry)
- GPA: 4.0/5.0

B.A., Chemistry with High Honors, Magna Cum Laude, Dartmouth College, Hanover, NH (2003)
- Honors thesis: The synthesis and study of highly fluorinated azulenes (advisor: David Lemal)
- GPA: 3.77/4.00

SCIENTIFIC EXPERIENCE

Ph.D. research, Massachusetts Institute of Technology, Cambridge, MA (2003-present)
- Investigate the incorporation of the heterocycle isobenzofuran into conjugated polymers
- Design and synthesis of a library of novel isobenzofuran based near-infrared dyes for biomedical sensing applications
- Evaluate dyes as contrast agents for the imaging of β-amyloid plaques (Alzheimer's marker) in collaboration with researchers at Massachusetts General Hospital

Synfacts **Journal Contributor**, Thieme Medical Publishers, Inc. (2006)
- Reviewed the organic materials literature for significant synthetic reactions
- Authored one page summaries of reviewed literature for publication

Teaching Assistant, Massachusetts Institute of Technology, Cambridge, MA   (2003-2005)

- Lead undergraduate recitations and designed problem sets to compliment lecture   materials
- Managed an undergraduate laboratory section of 20 students. Instructed students in laboratory techniques and necessary safety protocols

Undergraduate independent research, Dartmouth College, Hanover, NH (2001-2003)
- Synthesized and studied the electronic properties of new pentafluoro, hexafluoro, and heptafluoro azulenes
- Authored proposals for and obtained Dean of the Faculty Grant and Zabriskie Fellowship to financially support the research

Teaching Assistant, Dartmouth College, Hanover, NH (2001-2002)
- Managed an undergraduate laboratory section of 15 students. Instructed students in safety techniques
  and operation of laboratory equipment
- Tested experiments beforehand and ensured the clarity of manual instructions

LEADERSHIP EXPERIENCE

Graduate Resident Tutor, Massachusetts Institute of Technology, Cambridge, MA (2006-present)

- Mentor 30 undergraduates providing in-house support for matters personal and academic
- Create and implement dorm-wide and floor programming (i.e. hiking trip, Wii launch party, dorm pentathlon, fire safety training skit, Resident Scholar lectures)
- Mediate between students and the institute administration
- Interviewing new GRT candidates in order to build the house team
- Led a review panel on GRT training, met with deans to discuss and implement changes

MITOC Adventure Race coordinator, Massachusetts Institute of Technology, Cambridge, MA (2007)
- Devised 10 hour and 12 hour adventure race courses in Franconia Notch, NH
- Organized race entries and travel, obtained necessary race equipment (i.e. maps)
- Acted as safety contact for the race

Freshmen Trip Leader, Dartmouth College, Hanover, NH (2000-2002)
- Guided groups of 10 freshmen on 4 day excursions in the NH wilderness
- Instructed freshmen in relevant Dartmouth traditions

AWARDS AND ACHIEVEMENTS

- Phi Beta Kappa (Dartmouth, 2003)
- Elden Bennett Hartshorn Medal for excellence in chemistry (1 per graduating class) (Dartmouth, 2003)
- Varsity member of Dartmouth XC ski team (Div. I team) (Dartmouth, 2003)
- Zabriskie Fellowship for independent research (2 per year) (Dartmouth, 2002)
- Dean of the Faculty Fellowship for independent research (Dartmouth, 2001)

PUBLICATIONS & PRESENTATIONS

- Meek, S. T, Swager, T. M. Isobenzofuran Fluorophores for β-Amyloid Imaging. *Manuscript in Preparation.*

- Meek, S. T.; Nesterov, E. E.; Swager, T. M. Near-infrared fluorophores containing benzo[c]heterocycle subunits. *Org. Lett.* **2008**, *10*, 2991-2993

- Meek, S. T.; Swager, T. M. Progress toward new isobenzofuran-based polymeric materials. *233rd ACS National Meeting, Chicago, IL.* **2007** (Oral presentation)

- Meek, S. T.; Ferrara, B; Raymond, S; Bacskai, B; Swager, T. M. Isobenzofuran based Near-Infrared Fluorophores for *In vivo* Imaging. *Materials Research Society Nation Meeting, Boston, MA.* **2008** (Oral presentation)

- Meek, S. T.; Ferrara, B; Raymond, S; Bacskai, B; Swager, T. M. Isobenzofuran based Near-Infrared Fluorophores for *In vivo* Imaging. *237^{nth} ACS National Meeting, Salt Lake City, UT.* **2009** (Oral presentation)

INTERESTS

Nordic ski marathons, Alpine skiing, Adventure racing, Triathlons, Cycling, Homebrewing, Tennis, and Bass guitar

Acknowledgements

This has been an incredible journey. My time here at MIT has been an absolutely remarkable experience, one that I will never forget in large part due to the people who I have met along the way. Here I want to recognize their help and support over the last six years.

The first and foremost, I'd like to thank my advisor Professor Tim Swager. He has the rare combination of creativity, passion, charisma, and empathy that makes him one of the best professors to work for. My time here at MIT has had its ups and downs, and Tim has always been incredibly supportive, with good research ideas, good jokes, good advice, and, at his parties, good wine. It has been a real honor to be part of his group.

I'd also like to thank my thesis committee: Professor Tim Jamison and Professor Sarah O'Connor for their guidance. I enjoyed my annual meeting with Tim, and the interesting perspectives he brought to my project. I want to thank Sarah for agreeing to be part of my committee on short notice, and for her insightful comments on my thesis.

The Swager group has been a fantastic place to work. It's a group in which everybody helps everybody else, and that spirit of collaboration makes it a joy to come in to work. In my early days in the lab, I was helped out by many people, including Jordin, who helped me learn calixarene chemistry, John, who taught me electrochemistry, and Karen, Phoebe, and Gigi who provided much needed moral support. Andrew was also a huge help, and provided great instruction on air-free chemistry. Kousik was always there with encouragement, and "kept up the spirit" in tight volleyball matches. Jean provided me with some compounds, and a lot of good synthetic advice. Anne McNeil was a great office-mate, and was always willing to talk. Becky did a great job keeping the lab running smoothly, and I loved talking to her about skiing and cats. The Swager lab has moved to the basement, but that hasn't changed the personality of the group. Brett, and most recently Joel have been great deskmates, and I've enjoyed our discussions on science and life. I'm similarly grateful to Ryan for his encouragement in the final stretch of my Thesis writing. Mindy has been a fantastic collaborator on cyclodextrin chemistry. Caitlyn has been a superb lab coordinator, and I'm indebted to her for ordering so many chemicals for me on short notice. Kathy has also been extraordinarily helpful on the administrative side. Finally, I have to thank Trisha, the Overlord of Fluorescence, for all her help on instrumentation.

Outside of the Swager lab, I've been aided by a few great collaborators. Early on in the isobenzofuran project, Ylva and I worked on some CVD chemistry, which proved a very rewarding experience. More recently I've been working with the Bacskai group at MGH, in particular Scott Raymond and Krista Neal, who have handled the biological part of our amyloid imaging work. I also want to acknowledge Li Li in the DCIF who provided me with my HRMS data, and was willing to run some last minute samples for my thesis.

Over the last six years, I've had a wonderful support system of friends in the Boston area. Colin, Dave, John, Evan, and Alex helped form our "Simsbury Expatriates", and it's been great continuing our fellowship from the old days. Dave helped me win the MITOC adventure race, Evan helped me get a job as a GRT and listened sympathetically to my stories about life in the lab, and Alex, as ever, made sure I got out to socialize and introduced me to the art of homebrewing. Many of my friends from Dartmouth also joined me in Boston, including Cosmo, Jon, Tom, and Courtney, and Tom got to reprise his old role of making sure I got out to have adventures. While I've been here I've made some new friends, Retsina, Reuben, Jon and Keith from Simmons Hall, who helped make being a GRT a really fun and rewarding experience.

Throughout this entire process, my family has been incredibly supportive. My parents have always believed in me, especially during the hard times. Its been great having my sister Jen in Boston, and its been awesome to hang out with her. Uncle Paul and Aunt Barbara helped me move early on in my graduate career, and let me use their house as a staging area. My grandparents have been encouraging throughout the entire process, which has been much appreciated. I should definitely thank Aunt Connie and Uncle Dave for getting me to visit them in Hayward and ski the American Birkebeiner, forcing me to stay in shape.

Finally, I want to thank Liz, the love of my life. I really don't think this thesis would have happened had it not been for her support. She put together the table of contents for the thesis, and helped a lot with editing process, for which I will always be grateful. I'm really looking forward to our continued adventures, starting this summer in California.